T TAURI STARS: MASS ACCRETION AND X-RAY EMISSION

Scott G. Gregory

A Thesis Submitted for the Degree of PhD
at the
University of St Andrews

2007

University of St Andrews

T Tauri Stars: Mass Accretion and X-ray Emission

Scott G. Gregory

May 2007 (In original form December 2006)

Submitted for the degree of Ph.D.

Declarations

I, Scott Gregory, hereby certify that this thesis, which is approximately 50,000 words in length, has been written by me, that it is the record of work carried out by me and that it has not been submitted in any previous application for a higher degree.

Date: 4 May 2007 Signature of candidate:

I was admitted as a research student in September, 2003 and as a candidate for the degree of Ph.D. in September, 2003; the higher study for which this is a record was carried out in the University of St Andrews between 2003 and 2006.

Date: 4 May 2007 Signature of candidate:

In submitting this thesis to the University of St Andrews I understand that I am giving permission for it to be made available for use in accordance with the regulations of the University Library for the time being in force, subject to any copyright vested in the work not being affected thereby. I also understand that the title and abstract will be published, and that a copy of the work may be made and supplied to any bona fide library or research worker, that my thesis will be electronically accessible for personal or research use, and that the library has the right to migrate my thesis into new electronic forms as required to ensure continued access to the thesis. I have obtained any third-party copyright permissions that may be required in order to allow such access and migration.

Date: 4 May 2007 Signature of candidate:

I hereby certify that the candidate has fulfilled the conditions of the Resolution and Regulations appropriate for the degree of Ph.D. in the University of St Andrews and that the candidate is qualified to submit this thesis in application for that degree.

Date: 4 May 2007 Signature of supervisor:

Acknowledgements

My supervisor Moira Jardine has been a source of inspiration for the past three years. This thesis is a product of the many informal chats and discussions we have had. Moira is famous for uttering some of the best one-liners, many of which cannot be put into print. One which can, is [said in Hawai'i] "Scott, I've left your poster back home in St Andrews". Poster transit issues aside, any potential future students contemplating accepting a PhD position at St Andrews will not find a better supervisor than Moira, who attains the perfect balance of kicking you when required, but will also let you get there on your own. I would also recommend that future students sign up to the email listings at phdcomics.com, and on that note I can't help but think of Moira and Andrew when reading this: http://www.phdcomics.com/comics/archive.php?comicid=741, although notice it refers to Daddy's grad students papers! Can I also use this as a forum to admit that I was tempted to obtain a copy of the (alleged) photograph of Moira being dangled by the ankles over Hadrians Wall for use in a future seminar. However, I fear that my funding would suddenly evaporate if such a picture was ever displayed publicly.

As anyone who has ever worked here will testify, St Andrews is a truly special town. However, those that claim it never rains on the east coast have obviously never lived in St Andrews! I hope that in future I will continue to collaborate with the group of people within the department at St Andrews. This will, of course, require trips back to this small town in the middle-of-nowhere. I wonder if the department will still be under its constant state of renovation years from now. I am now immune to the noise of power drills, jigsaws, hammering, roofs being repaired directly above my head, repeated fire alarms and workmen's radios.

I have been incredibly fortunate to have had the chance to travel extensively during the past three years, to Cambridge, Toulouse, Milton Keynes, Edinburgh, Hamburg, Birmingham, Hawai'i, Grenoble, Leicester, Prague, Porto, Pasadena

and Bonn. Throw in a quick trip to Dublin and that makes 37 individual flights in 39 months! Clearly the highlight of my travels was Milton Keynes. Why watch the sunset over the Pacific stretched out on a hammock suspended between palm trees when instead there is the opportunity to study the complex interactions between concrete cows. On a serious note travelling to, and giving talks at, various conferences has afforded a variety of opportunities to interact with many researchers across the fields of low mass star formation and cool stars. They have also provided open forums to advertise the work that we do here within the group at St Andrews.

Of course, the department at St Andrews would be nothing without the many great characters who work here, and I thank them all for creating and maintaining the friendly atmosphere that exists within the group. Although perhaps my own productivity would have increased had the number of (highly competitive) games of snooker decreased.

Finally, Claire, what more can I say that I haven't already. Thanks for your support, love, and understanding when I stagger back through the door after working in the office until late. Together we'll make it.

Contents

List of Figures

List of Tables

Abstract

I develop the first magnetospheric accretion model to take account of the observed complexity of T Tauri magnetic fields, and the influence of stellar coronae. It is now accepted that accretion onto classical T Tauri stars is controlled by the stellar magnetosphere, yet to date the majority of accretion models have assumed that the stellar magnetic field is dipolar. By considering a simple steady state accretion model with both dipolar and complex magnetic fields I find a correlation between mass accretion rate and stellar mass of the form $\dot{M} \propto M_*^{\alpha}$, with my results consistent within observed scatter. For any particular stellar mass there can be several orders of magnitude difference in the mass accretion rate, with accretion filling factors of a few percent. I demonstrate that the field geometry has a significant effect in controlling the location and distribution of hot spots, formed on the stellar surface from the high velocity impact of accreting material. I find that hot spots are often at mid to low latitudes, in contrast to what is expected for accretion to dipolar fields, and that particularly for higher mass stars, accreting material is predominantly carried by open field lines. Material accreting onto stars with fields that have a realistic degree of complexity does so with a distribution of in-fall speeds.

I have also modelled the rotational modulation of X-ray emission from T Tauri stars assuming that they have isothermal, magnetically confined coronae. By extrapolating from surface magnetograms I find that T Tauri coronae are compact and clumpy, such that rotational modulation arises from X-ray emitting regions being eclipsed as the star rotates. Emitting regions are close to the stellar surface and inhomogeneously distributed about the star. However some regions of the stellar surface, which contain wind bearing open field lines, are dark in X-rays. From simulated X-ray light curves, obtained using stellar parameters from the Chandra Orion Ultradeep Project, I calculate X-ray periods and make comparisons with optically determined rotation periods. I find that X-ray periods

are typically equal to, or are half of, the optical periods. Further, I find that X-ray periods are dependent upon the stellar inclination, but that the ratio of X-ray to optical period is independent of stellar mass and radius.

I also present some results that show that the largest flares detected on T Tauri stars may occur inside extended magnetic structures arising from the reconnection of open field lines within the disc. I am currently working to establish whether such large field line loops can remain closed for a long enough time to fill with plasma before being torn open by the differential rotation between the star and the disc. Finally I discuss the current limitations of the model and suggest future developments and new avenues of research.

Chapter 1

Introduction

1.1 Classical and weak line T Tauri stars

Classical T Tauri stars (CTTs) are G-M type low mass, $0.5 - 2\,\mathrm{M}_\odot$, pre-main sequence stars. They are actively accreting from a surrounding dusty disc. The disc will have dispersed before the star arrives on the main sequence, with some of the disc material forming planetary systems. They possess strong magnetic fields, of order a few kG. Average surface fields of this strength disrupt the disc and influence infalling material. Gas is torn from the inner disc and is loaded onto the field lines of the stellar magnetosphere, forming accretion columns. The material essentially free-falls along the field and is channelled onto discrete regions of the stellar photosphere. The accreted material shocks as it impacts the stellar surface and radiates away its kinetic energy in the optical, UV and soft X-ray wave bands. Fig. 1.1 illustrates the magnetic field structure that we believe CTTs may have (Goodson, Winglee & Böhm 1997). Close to the star there are closed field lines that contain the high temperature but low density corona, whilst at larger radii, there are closed field lines which thread the lower temperature but higher density circumstellar disc. It is along this latter set of field lines that accretion may proceed. There are also regions of open field that carry outflows in the form of a

wind, and in some systems, as large collimated bipolar jets.

Weak line T Tauri stars (WTTs) are on average older than CTTs. It is believed that CTTs lose their discs and evolve into WTTs (which are occasionally also refered to as naked T Tauri stars) before arriving on the main sequence. However at any particular stellar age there is observed to be a mixture of the two classes, and the evolutionary link between them is unclear. Traditionally stars have been classified into the two groups based of the equivalent width (EW) of the Hα emission line. CTTs show strong Hα emission and are therefore easy to identify optically. In contrast WTTs have little Hα emission, hence the name "weak line". Stars with EW(Hα)$\leq$10Å are often classified as WTTs (Herbig & Bell 1988). This, however, is a somewhat arbitrary choice and varies with spectral type (see the discussion by Stahler & Palla 2005). There is evidence that some stars which have traditionally been classified as WTTs based on their weak Hα emission, have mass accretion rates which are in fact comparable to those of CTTs (Littlefair et al. 2004). Clearly it is not safe to classify stars as CTTs or WTTs based on the equivalent width of Hα alone. In practice CTTs have other observational characteristics which makes them easy to identify, for example, excess continuum emission in the UV, optical and IR.

In the following sections I discuss the various pieces of observational evidence that CTTs are surrounded by circumstellar discs, and how their variability and excess continuum emission may be interpreted as evidence for magnetically mediated accretion. I then discuss how mass accretion rates can be determined from high resolution spectroscopic observations and the various techniques that have been used to detect magnetic fields. Such measurements give tantalising clues to the magnetic field geometry of young solar-like stars. This provides a basis for discussing magnetospheric accretion models which have been developed to explain the wealth of observational data for CTTs. I further discuss how such models are being extended to incorporate time variable accretion and outflows.

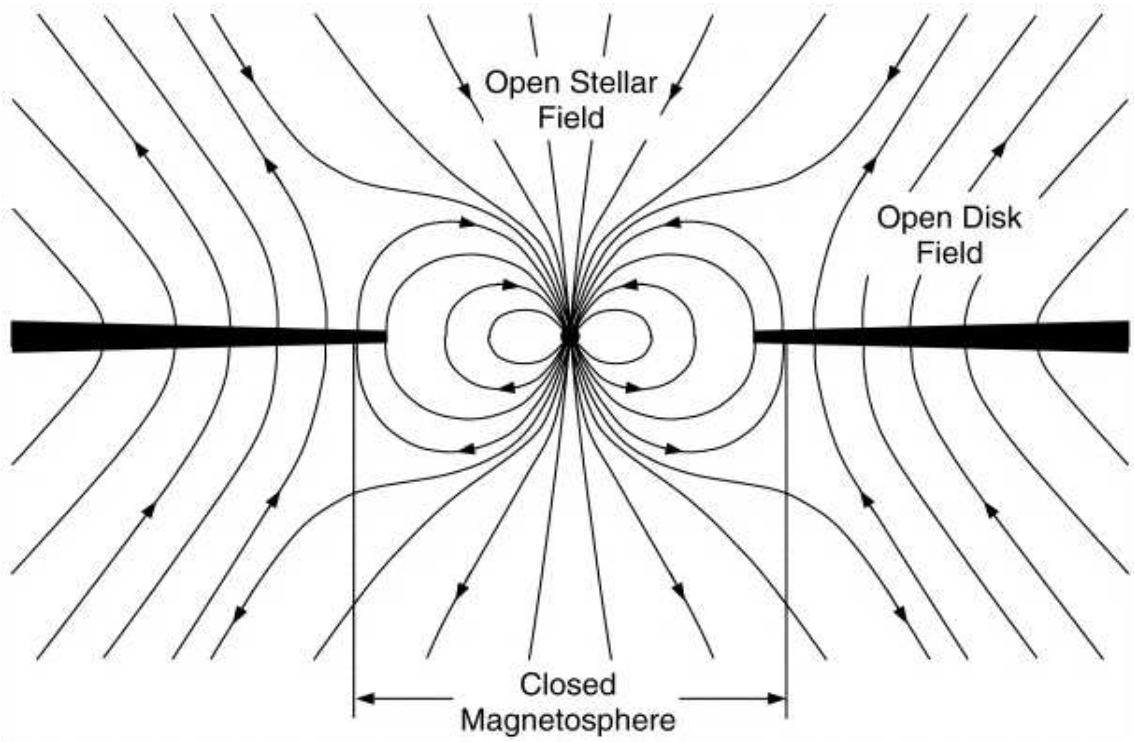

Figure 1.1: An idealised model of the magnetic field structure of a classical T Tauri star, reproduced from Goodson et al. (1997). There are three distinct regions of field (i) the closed field line loops that contain the coronal plasma close to the stellar surface, (ii) closed field lines which thread the circumstellar disc and carry accretion flows and (iii) open field lines which support outflows. Reproduced with permission.

I then present the observed correlation between stellar mass and accretion rate and the various suggestions that have been tabled to explain its existence. The final section of this Chapter discusses the origin of X-ray emission from T Tauri stars and speculates on the reasons why WTTs have been observed to be stronger X-ray emitters than CTTs. Excellent overviews of T Tauri stars and the current outstanding observational and theoretical questions, may be found in the review articles by Ménard & Bertout (1999) and Bouvier et al. (2007a).

1.1.1 Excess continuum emission

CTTs exhibit excess continuum emission most noticeably in the UV and IR wave bands. This excess emission is superimposed upon the stellar photospheric spectrum. Fig. 1.2 is a spectral energy distribution (SED) for the CTTs BP Tau, from Robitaille et al. (2007). The excess continuum emission, referred to as the veiling continuum, reduces the equivalent width of absorption lines, making them appearer shallower than the corresponding lines in the spectra of template stars (see e.g. Hartigan et al. 1991). For the most strongly accreting stars the veiling is large enough that photospheric absorption lines are filled in, while certain lines appear in emission. As I discuss below, measuring the amount of veiling provides a basis for determining the accretion rate onto T Tauri stars. Veiling is also observed to vary with time (e.g. Stempels & Piskunov 2002). Such observations indicate that accretion is not a steady state process, as the UV excess is thought to arise from accretion shocks. Material from the accretion columns rains down onto the photosphere, shocks, and radiates away its kinetic energy, producing excess UV emission. The photometric variability of CTTs is often consistent with the presence of hot spots, which are likely to be associated with accretion shocks (Bertout, Basri & Bouvier 1988; Bouvier et al. 1993; Vrba et al. 1993). This is supported by the detection of a correlation between an increase in both brightness and veiling on a timescale equal to the stellar rotation period (Chelli et al.

1999). The distribution of hot spots on the stellar surface has been modelled by many authors. Mahdavi & Kenyon (1998) find that accretion rings form when considering magnetospheres which are tilted with respect to the stellar rotation axis. The numerical simulations by Romanova et al. (2004a) show that the fractional surface area of the star covered by hot spots (the accretion filling factor) increases for larger mass accretion rates. Recently Long, Romanova & Lovelace (2007) have demonstrated that the geometry of the magnetic field is important in determining the location and distribution of hot spots.

The Hubble Space telescope (HST) has provided direct evidence for circumstellar discs. One of the early high profile HST discoveries was the first direct images of protoplanetary discs around T Tauri stars in Orion (McCaughrean & O'dell 1996). This, combined with the equally dramatic HST images of jets from young stars (e.g. Burrows et al. 1996), define some the most iconic images of star formation ever obtained. The origin of jets is believed to be the star-disc interface, with images of jets often displaying obscuration in the equatorial plane indicating the presence of a dusty disc. Excess IR emission is also indicative of dusty circumstellar material. By fitting the observed shapes of SEDs the excess IR emission is found to be consistent with a disc absorbing stellar radiation and re-emitting it at longer wavelengths. SED shapes are also consistent with the presence of inner disc holes, such as would be expected if the stellar magnetosphere is controlling the infalling disc material close to the star (Bertout et al. 1988 ;Kenyon et al. 1994).

1.1.2 Line profiles and variability

T Tauri stars are highly variable both photometrically and spectroscopically, with line profiles changing irregularly on both long and short timescales. The spectra of CTTs show strong and broad emission lines. Many lines have high excitation potentials such as HeI 5876Å, which is believed to form at the base of accre-

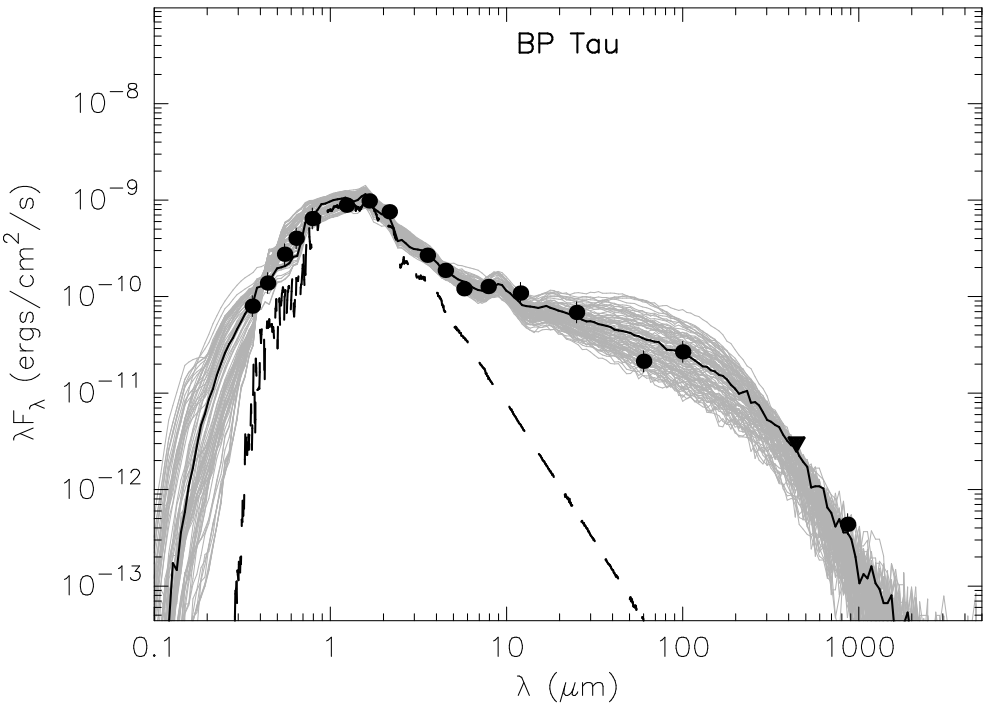

Figure 1.2: The SED of the CTTs BP Tau. The dashed line is the SED we would expect solely from the stellar photospheric emission, which resembles a Planck blackbody distribution function. The observed SED (filled circles) is a combination of the photospheric continuum and the excess veiling continuum emission. Clear excess emission can be seen at UV and IR wavelengths. The solid black line shows the best fit to the data using the models developed by Robitaille et al. (2006), with the grey lines showing models with different parameters. Figure courtesy of T. Robitaille, from Robitaille et al. (2007).

tion columns close to accretion shocks (Valenti, Basri & Johns 1993; Beristain et al. 2001). The spectra of T Tauri stars contain deep Li absorption lines, an indicator of their young age, as Li is destroyed after the onset of convection and once the core temperature of the star exceeds 2.5 MK. Inverse P-Cygni profiles are commonly observed in many lines. Broad redshifted absorption components indicate that material is accreting onto the star at several hundred kms^{-1} (e.g. Edwards et al. 1994). This is consistent with the prediction of accretion models where material essentially free-falls onto the star from a distance of a few stellar radii. The development of a redshifted absorption component was found to coincide with the location of a hot spot on DF Tau, inferred from Doppler imaging by Unruh, Collier Cameron & Guenther (1998). This further supports the idea of a connection between infalling material in accretion columns and the location of hot spots at accretion shocks. Johns-Krull & Hatzes (1997) come to similar conclusions from Doppler images of the CTTs SZ 68, and argue that the Hα line is likely to form predominantly within accretion flows. This is consistent with the predictions of Hartmann, Hewett & Calvet (1994) who constructed a simple magnetospheric accretion model which qualitatively reproduced many of the strong emission line profile variations seen in CTTs. Hartmann et al. (1994) argued that part of the line flux originates within the accretion columns. This model also predicted that a correlation should exist between the received line flux in particular lines and mass accretion rate. Such correlations have since been found for a variety of emission lines (see the discussion and references in the following section and Johns-Krull, Valenti & Linsky 2000; Alencar & Basri 2000; Folha & Emerson 2001). However, this model assumes that the star has a simple dipole field and provides no mechanism for connections between the stellar and disc fields.

Many authors have argued that line profile variations are consistent with accretion along the field lines of a large scale magnetosphere which is tilted with

respect to the stellar rotation axis (e.g. Johns & Basri 1995; Petrov et al. 1996, 2001; Oliveira et al. 2000). Recently the first 3D radiative transfer simulations of line profiles from non-axisymmetric accretion flows have been presented by Symington, Harries & Kurosawa (2005a), who model the Hα, Hγ, Paβ and Brγ lines of hydrogen. They assume a dipolar magnetic field geometry but prescribe the range of azimuths with which accreting material leaves the inner disc, e.g. in two accretion columns carrying material into opposite hemispheres. Their simulated line profiles reproduce the general characteristics of the observed variability, however, the magnitude of variation is too large. In future this may be accounted for by the inclusion of a wind component and a veiling continuum; indeed Alencar et al. (2005) demonstrated that the observed profiles of Hα, Hβ and the NaD line from RW Aur are best explained by a radiative transfer model which includes a collimated disc wind. Building on the work of Symington et al. (2005a), Kurosawa, Harries & Symington (2006) have recently considered how both accretion and outflow processes can effect the Hα emission line. They find that a ratio of mass loss rate to mass accretion rate of between 0.05 and 0.2 produces Hα line profiles which are broadly consistent with observations.

1.1.3 Mass accretion rates

Mass accretion rates are derived from high resolution spectroscopic observations. For CTTs most accretion rate measurements have been inferred from optical and UV veiling measurements, in other words, from the luminosity of the excess continuum emission from the accretion shock (e.g. Hartigan et al. 1991; Valenti et al. 1993; Hartigan, Edwards & Ghandour 1995; Gullbring et al. 1998; White & Basri 2003). The excess (or veiling) continuum is measured by comparing the depths of photospheric features in the spectrum of the CTTs with the depths of the same features in the spectrum of a standard star. From the ratio of excess flux to photospheric flux, and making assumptions about the density and

temperature structure of the accretion shock, an accretion luminosity can be derived (e.g. Calvet & Gullbring 1998). A mass accretion rate $\dot{M}$ can then be calculated from,

$$L_{acc} \approx \frac{GM_*\dot{M}}{R_*}\left(1 - \frac{R_*}{R_t}\right), \tag{1.1}$$

where R_t is the disc truncation radius, often assumed to be $5R_*$ (e.g. Gullbring et al. 1998), comparable to typical corotation radii for CTTs. Veiling measurements have been used extensively to estimate accretion rates in CTTs. However, in young star forming regions such as ρ-Ophiuchus, the extinction is high, making estimates of the veiling difficult (Natta et al. 2004). Furthermore, the accretion rates onto very low mass stars and brown dwarfs are so small that negligible veiling is observed (Muzerolle et al. 2003; Mohanty, Jayawardhana & Basri 2005a; Natta, Testi & Randich 2006). For the higher mass Herbig Ae stars it is difficult to separate the excess UV emission from the hot photospheric continuum (Garcia Lopez et al. 2006). Other techniques have therefore been developed to estimate accretion rates onto low mass and high mass objects, involving detailed modelling of the accretion related Hα emission line profile and by using so-called secondary indicators.

Muzerolle et al. (2003) present accretion rate measurements for very low mass objects ($0.05 - 0.2\,\mathrm{M}_\odot$). They do not detect significant continuum veiling, which would be expected if very low mass accretors have small mass accretion rates (see also White & Basri 2003). In the absence of significant veiling Muzerolle et al. (2003) and Muzerolle et al. (2005) use magnetospheric accretion models to fit Hα emission line profiles in order to estimate accretion rates. This model is discussed in detail by Muzerolle, Calvet & Hartmann (2001) and assumes both dipolar magnetic fields and uses the Sobolev approximation. Despite the many assumptions the Muzerolle model broadly reproduces the observed Hα profiles, and in the absence of significant veiling, provides a useful method for determining mass accretion rates.

Secondary indicators of accretion rates involve searching for a correlation between the luminosity (or flux) of a particular spectral line and accretion rate values which have been derived from veiling measurements or Hα modelling. Once such a correlation has been established mass accretion rate estimates are straightforward. As an example Fig. 1.3 is a plot from Mohanty et al. (2005a) which shows the observed correlation between the CaII 8662Å emission line flux and accretion rate measurements which have been derived using other techniques. The CaII 8662Å line is part of a CaII IR triplet and is seen strongly in emission for accreting objects. The accretion rates in Fig. 1.3 have been estimated from UV and optical veiling measurements for the CTTs and by Hα line modelling for the very low mass accretors and brown dwarfs. The reason for the offset between the two branches in Fig. 1.3 may either be due to systematic differences between estimating accretion rates using veiling measurements or Hα modelling, and/or due to differences in the formation region of the CaII line in the two mass regimes (Mohanty et al. 2005a). The existence of such correlations (stated here without errors),

$$\log \dot{M} = 0.71 \log (F_{CaII}) - 12.66 ... CTTs \tag{1.2}$$

$$\log \dot{M} = 0.93 \log (F_{CaII}) - 15.03 ... VLMs \ and \ BDs, \tag{1.3}$$

(where VLMs = very low mass objects and BDs = brown dwarfs) provides an easy method for determining mass accretion rates, simply by measuring the flux of the CaII line from high resolution spectra. These correlations were used by Mohanty et al. (2005a) to estimate accretion rates for a number of accreting brown dwarfs. Similar correlations have also been found between the luminosities of hydrogen lines and mass accretion rates. Muzerolle, Calvet & Hartmann (1998) discovered an empirical relationship between the luminosity of the Paβ line and the accretion luminosity estimated from veiling measurements for CTTs in Taurus, which was subsequently shown to extend to brown dwarfs by Natta et al. (2004). The

correlation,

$$\log(L_{acc}/L_{\odot}) = 1.36 \log(L(Pa\beta)/L_{\odot}) + 4.0, \tag{1.4}$$

and equation (1.1) were used by Natta et al. (2004) to estimate accretion rates for brown dwarfs in ρ-Ophiuchus and Chamaeleon I. A similar correlation using the luminosity of the Brγ line of hydrogen in CTTs was also found by Muzerolle et al. (1998),

$$\log(L_{acc}/L_{\odot}) = 0.9 \log(L(Br\gamma)/L_{\odot}) + 2.9, \tag{1.5}$$

which was shown by Calvet et al. (2004) to extend to the higher mass intermediate mass T Tauri stars, was used by Natta et al. (2006) to derive accretion rates in ρ-Ophiuchus, and also used by Garcia Lopez et al. (2006) to obtain accretion rates for Herbig Ae stars.

Accretion luminosities and therefore mass accretion rates can also be estimated from broadband photometry. Gullbring et al. (1998) found a strong correlation between de-reddened U-band luminosity and the accretion luminosity,

$$\log(L_{acc}/L_{\odot}) = 1.09 \log(L_U/L_{\odot}) + 0.98. \tag{1.6}$$

This correlation has been exploited by Rebull et al. (2000) and Rebull et al. (2002) to measure accretion rates in the Orion flanking fields and NGC 2264. Robberto et al. (2004) used it to measure accretion rates in the Trapezium cluster, close to the centre of the Orion Nebula, and Romaniello, Robberto & Panagia (2004) used it to estimate accretion rates for stars in the Large Magellanic Cloud from HST observations.

1.1.4 Magnetic field detection

Magnetic fields play a fundamental role in the final stages of low mass star formation. Ever since the seminal papers by Robinson (1980) and Mathys (1988, 1991) measurements of the magnetic field strength have been made on several

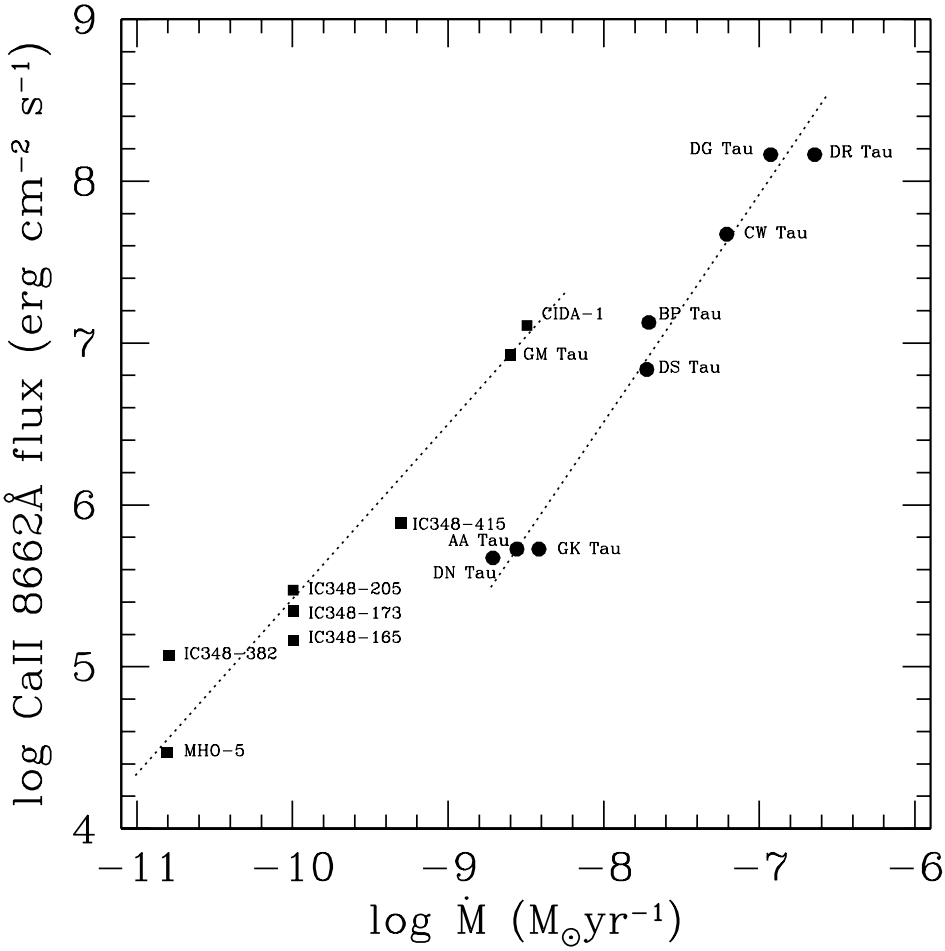

Figure 1.3: The correlations between mass accretion rate and CaII emission line flux for CTTs (filled circles) and very low mass accretors/brown dwarfs (filled squares). Based on a plot from Mohanty et al. (2005a). Note that GM Tau is not an exception, it is of spectral type M6.5 and has a mass of $0.073 M_\odot$.

types of star. Accretion models assume that CTTs have magnetic fields which are strong enough to disrupt the inner disc and channel infalling material onto the stellar surface. It was predicted by Königl (1991) that field strengths of order a kG were sufficient to disrupt the disc at a distance of a few stellar radii, and would explain a number of observations, such as the detection of inverse P-Cygni profiles (Edwards et al. 1994). Average surface fields of $1 - 3\,\mathrm{kG}$ have been detected on a number of T Tauri stars, both classical and weak line, using a variety of techniques. The first field detection on a T Tauri star was made using the optical equivalent width enhancement of spectral lines (Basri, Marcy & Valenti 1992). Guenther et al. (1999) applied the same technique to detect fields on 4 other stars. However, the most successful methods of field detection exploit the Zeeman effect, both through Zeeman broadening itself, and from the circular polarisation of lines which are sensitive to the presence of a magnetic field.

If a stellar atmosphere is permeated by a magnetic field some spectral lines are split into three components. Two components are split from the line centre, called the σ-components, and the third is an unshifted component, called the π-component. The wavelength shift between the two σ-components is,

$$\Delta\lambda = 2\left(\frac{e}{4\pi m_e c^2}\right)\lambda^2 g_{eff} B_z. \tag{1.7}$$

B_z is the field component along the line-of-sight (the longitudinal field component), λ is the wavelength of the transition and g_{eff} is the Landé g-factor which corresponds to the particular atomic transition. An expression for the g-factor was derived empirically by Landé (1923),

$$g_{eff} \approx 1 + \frac{j(j+1) + s(s+1) - l(l+1)}{2j(j+1)}, \tag{1.8}$$

where j, s and l are respectively the total electronic angular momentum, the orbital angular momentum and the spin angular momentum. The g-factor arises in calculations of the effect of a weak (in comparison to the system's internal magnetic field) uniform magnetic field upon the energy levels of an atom. It

is important to note that the wavelength shift in the Zeeman effect is $\Delta\lambda \propto \lambda^2$, whereas for Doppler line broadening mechanisms $\Delta\lambda \propto \lambda$. Therefore IR observations are more sensitive to the presence of magnetic fields than optical observations. Estimating field strengths from high resolution IR spectra has other benefits as well. In calculating field strengths the same atmospheric structure is assumed for both the magnetic and non-magnetic regions of the photosphere, which may lead to inaccuracies in measured field strengths. However this problem is resolved by estimating the broadening measurements in the IR, which have been shown to be insensitive to the assumed model atmosphere (Valenti, Marcy & Basri 1995). When viewed along the axis of a magnetic field the σ-components are circularly polarised, but with opposite helicity (one is left circularly polarised and the other right circularly polarised), with the helicity reversing as the field polarity reverses. If a single magnetic polarity dominates on the surface of a star then a net polarisation signal is detected in magnetically sensitive lines. This results in a wavelength shift when the line is viewed using left and right circular polarisers (see Fig. 1.4). However, if the stellar surface is covered in many regions with opposite polarity, then often no net polarisation signal is detected. The contributions to the net signal from regions of opposite polarity cancel out.

Johns-Krull, Valenti & Koresko (1999b) measured the field strength of BP Tau from the broadening of a magnetically sensitive TiO line, but found that a distribution of field strengths up to 6 kG was required to correctly reproduce the line profile. Zeeman broadening measurements have been used successfully to estimate the average field strengths on a number of stars (e.g. Valenti & Johns-Krull 2004; Johns-Krull, Valenti & Saar 2004; Johns-Krull 2007). Interestingly the average surface field strength does not vary much from star to star (Johns-Krull & Gafford 2002). Measuring the circular polarisation in magnetically sensitive lines is the most direct method of detecting T Tauri magnetic fields. Johns-Krull et al. (1999a) detected strong polarisation in the He I 5876Å emission line from

BP Tau, which forms at the base of accretion columns (Beristain et al. 2001). Symington et al. (2005b) also detected a strong polarisation signal in the same line. Similar spectropolarimetric measurements have since been made to detect fields on a number of T Tauri stars (e.g. TW Hya by Yang, Johns-Krull & Valenti 2005, 2007 and T Tau by Daou, Johns-Krull & Valenti 2006).

A further magnetic field detection has been made on T Tau Sb from electron cylotron maser emission, a coherent emission process from mildly relativistic electrons trapped inside flux tubes close to the star (Smith et al. 2003). New techniques are being developed which in future will allow the detection of magnetic fields on very low mass T Tauri stars and brown dwarfs by measuring the broadening of molecular lines of FeH (Johns-Krull & Valenti 2005; Reiners & Basri 2006).

Fig. 1.5 shows measurements of the line-of-sight field components derived from polarisation detections in photospheric absorption lines, and how this field component changes with rotational phase. The average surface field strength given on each plot is derived from broadening measurements. Furthermore, Valenti & Johns-Krull (2004) have attempted to fit their models with dipolar magnetic fields. Apart from DF Tau, however, none of the polarisation measurements are fitted with the dipole magnetic field model. Despite the surface fields being strong, often no net polarisation signal is detected. This is consistent with the surface fields of T Tauri stars being very complex with many regions of opposite polarity. These observations constitute some of the strongest pieces of evidence for the complex nature of the surface fields of T Tauri stars. However, the accreting field structure may be well ordered. Fig. 1.6 shows the same measurements as in Fig. 1.5 except this time derived from polarisation detections in the HeI 5876Å line. This line forms in accretion shocks and thus traces the structure of the accreting field. Valenti & Johns-Krull (2004) and Johns-Krull & Valenti (2005) find that their data is well fitted by a simple model of a single

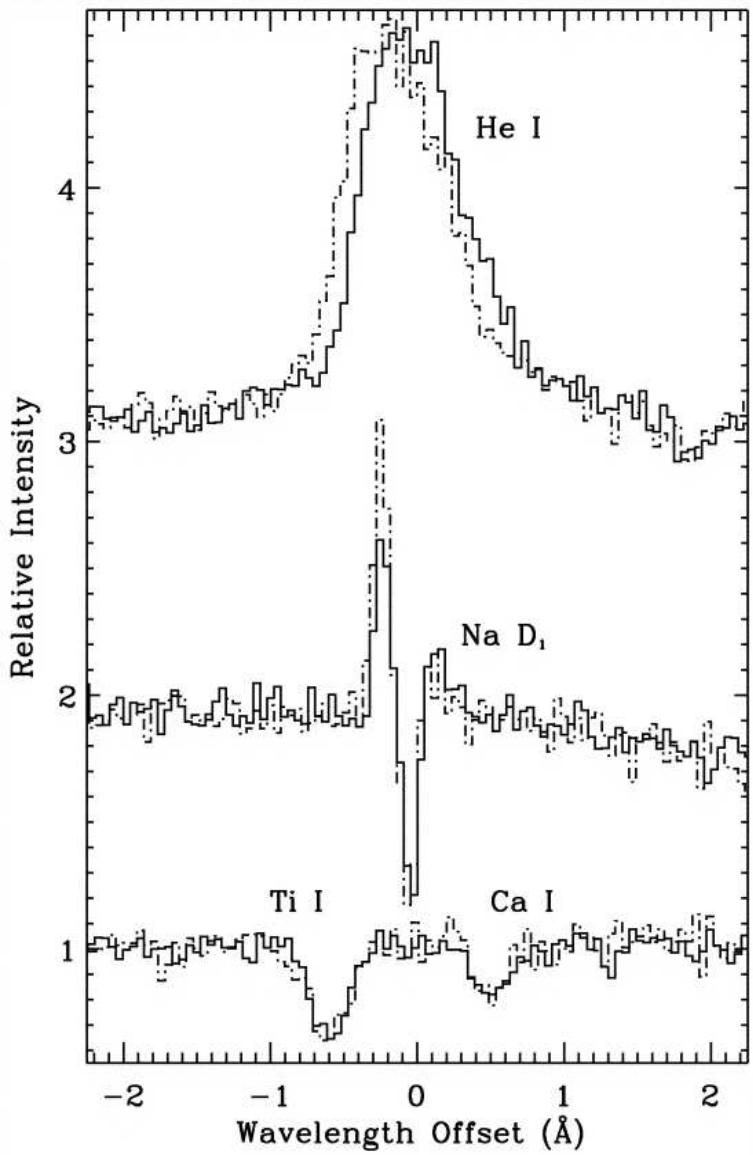

Figure 1.4: Sections of the spectrum of BP Tau, reproduced from Johns-Krull et al. (1999a). There is a clear shift between the left circularly polarised spectrum (solid line) and the right circularly polarised spectrum (dash-dotted line) of the HeI 5876Å line. For clarity the top two lines have been offset by 1.0 and 2.0 in the relative intensity axis. Reproduced with permission.

magnetic spot at some latitude with radial accreting field lines. Therefore although the surface magnetic fields of T Tauri stars are likely to be very complex and multipolar in nature, the accreting field may be well ordered.

1.2 Accretion models

Many observations of CTTs can be explained via the interaction between the central star and a circumstellar disc. Original accretion models assumed that the disc extended to the stellar surface where material decelerated and accreted onto the star through an equatorial boundary layer. This model has since been replaced by magnetospheric accretion models, where a strong stellar magnetic field disrupts the inner accretion disc and controls the infalling material forming accretion columns. Although there are many such accretion models, each differing by how the stellar field interacts with the disc, the basic picture of magnetically mediated accretion is common to all models.

1.2.1 Boundary layer accretion

The first accretion model to explain the excess IR and UV emission observed from T Tauri stars was constructed by Lynden-Bell & Pringle (1974). The star was assumed to be surrounded by a Keplerian disc, where material in the inner disc rotates faster than material in large radius orbits. Any dissipative system evolves into a state of minimum energy. For a star surrounded by a disc, this state would be when most of the mass is concentrated in the star at the centre of the system, with objects in large radius orbits carrying the angular momentum of the system. This condition is almost satisfied in our own Solar System where most of the mass is concentrated in the Sun, with the gas giant planets in large radius orbits carrying the angular momentum. The basis of this model is that shearing

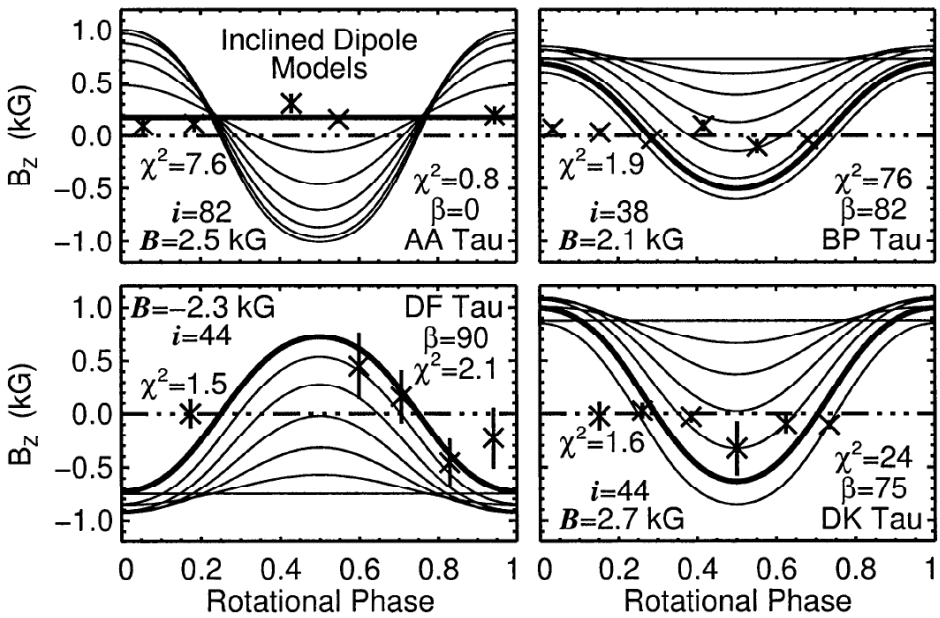

Figure 1.5: The variation in the longitudinal field component B_z with rotational phase for four different stars. Points are derived from polarisation measurements of photospheric absorption lines. Curves represent dipolar magnetic field models, tilted at different angles with respect to the stellar rotation axis. Reproduced from Valenti & Johns-Krull (2004) with kind permission of Springer Science and Business Media.

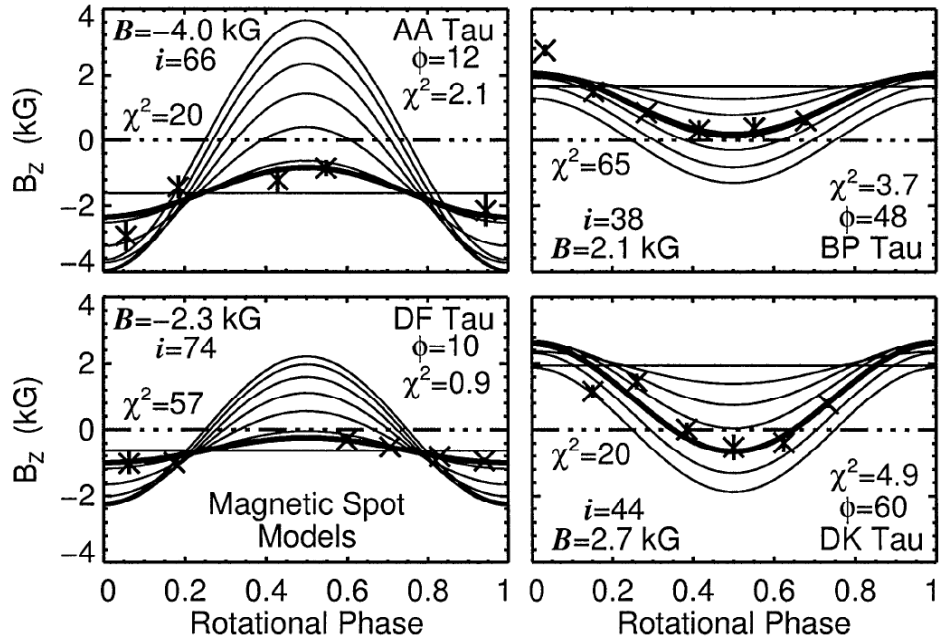

Figure 1.6: Variation in B_z with rotational phase derived from polarisation measurements of the HeI 5876Å emission line. Curves represent a simple model with a single magnetic spot at different latitudes with radially accreting field lines. Reproduced from Valenti & Johns-Krull (2004) with kind permission of Springer Science and Business Media.

between successive disc annuli allows the outward transfer of angular momentum creating an inward flow of material through the disc. This idea was modified so that turbulent mixing of gas between disc annuli generates a kinematic viscosity (Shakura & Sunyaev 1973), giving a more physical accretion process. The disc was assumed to extend to the stellar surface where the high angular momentum material in the inner disc slowed to the stellar rotation rate, accreting onto the star through a complex equatorial boundary layer. The boundary layer accretion model successfully explains the IR and UV excess, with the IR excess arising from the presence of a disc and the UV excess arising from the boundary layer as the high velocity disc material decelerates to the stellar rotation rate (e.g. Adams & Shu 1986; Bertout et al. 1988). However, the process of accreting high angular momentum material from a boundary layer would act to spin-up the star, which would slowly approach break up velocity. This is not observed. CTTs which are actively accreting from circumstellar discs are on average slower rotators than WTTs where the the disc has dispersed (see the discussion by Herbst et al. 2007). It is also difficult to explain the existence of hot spots on the stellar surface with a boundary layer accretion model. In contrast, as I discuss below, hot spots arise naturally in magnetospheric accretion models as the accretion shocks at the base of accretion columns. Magnetospheric accretion models may also explain the observed slow rotation of CTTs.

1.2.2 Magnetospheric accretion models

Uchida & Shibata (1984) and Camenzind (1990) suggested that the magnetic field of a CTTs disrupts the inner disc. However, it was not until the early 1990s that several magnetospheric accretion models were developed, after the realisation that models in which the inner disc is disrupted by the stellar magnetosphere may explain the observed slow rotation of CTTs. Königl (1991) applied the Ghosh and Lamb model of accretion onto neutron stars (Ghosh, Pethick & Lamb 1977;

Ghosh & Lamb 1979a,b) to accreting T Tauri stars and argued that the observed slow rotation rates of CTTs could be accounted for if they possessed magnetic fields which were strong enough to disrupt the inner disc. He predicted that CTTs would have field strengths of order a kG, and that provided the stellar magnetic field could couple effectively to the gas in the inner disc, then the stellar field would control infalling material. Königl (1991) argued that shocks were produced where accretion columns reached the star giving rise to the observed UV excess emission. He also argued that the emergence of inverse P-Cygni profiles could be explained by the alignment between an accretion column and the observer's line-of-sight.

An important point in magnetospheric accretion models is the location of the corotation radius R_{co},

$$R_{co} = \left(\frac{GM_*}{\omega^2}\right)^{1/3}, \tag{1.9}$$

which is radius at which the Keplerian rotation rate of the disc is equal to that of the star. A field line threading the disc at the corotation radius would corotate with the star, and would not be stretched due to differential rotation. Magnetospheric accretion models, such as that proposed by Königl (1991), Collier Cameron & Campbell (1993) and Paatz & Camenzind (1996), provide magnetic links between the star and regions of the disc which are beyond R_{co} and are therefore rotating more slowly than the star. Thus by having field lines threading the disc at a range of radii the star is able to accrete material without spinning up, as happens in boundary layer accretion models. However in such models field lines threading the disc beyond the corotation radius quickly become wrapped up and would be torn open after only a few rotation periods (see e.g. Aly & Kuijpers 1990; van Ballegooijen 1994). The Shu X-wind model gets around this problem, and was developed through a series of papers (Shu et al. 1994a,b; Najita & Shu 1994; Ostriker & Shu 1995; Shu et al. 1995). This model introduces the idea of trapped flux, where the closed field lines connecting the star and the disc are

pinched together in a small interaction region about the corotation radius (called the X-region). In such a way the strong dipolar field of the star rotates as a solid body with material from the inner part of the X-region accreting onto the star. Torques in the funnel flow deposit excess angular momentum into the X-region which is then removed by a wind which carries material away from the outer portion of the X-region. Thus the Shu X-wind model allows accretion to occur without spinning up the star, whilst also providing a connection between the accretion process and outflows. Models which combine accretion and outflows often predict a correlation between the mass accretion and mass outflow rates (e.g. Ostriker & Shu 1995; Ferreira 1997), which have been observed (e.g. Ardila et al. 2002).

Models have also been produced of accretion flows. Martin (1996) derives the density and temperature structure of accretion flows and concludes that accreting material consists solely of gas and not dust. This gas is heated primarily by compression as a result of field line convergence as the flow approaches the stellar surface. However the temperature profiles derived by Martin (1996) do not agree with those successfully used to reproduce observed line profiles (Hartmann et al. 1994). Li, Wickramasinghe & Ruediger (1996) consider how angular momentum may be exchanged through an accretion column between the star and the disc, and argue that the transfer is primarily from the star to the disc, lending support to the Shu model. More recent MHD simulations by Romanova et al. (2002) suggest that up to a third of the magnetic flux responsible for the exchange of angular momentum actively carries accreting material from the disc to the star. Using the same model Koldoba et al. (2002a) argues that the rotation and twisting of accretion columns is an important effect which should be incorporated into models of emission line profiles.

The accretion shock which develops at the base of accretion columns has been modelled by Lamzin (1995), Calvet & Gullbring (1998) and Gullbring et al.

(2000). Such models reproduce the excess UV continuum emission responsible for line veiling and demonstrate that the accretion luminosity is a function of the surface area of the star covered in accretion shocks, the accretion filling factor, and the energy flux of the accretion flows. However, such models predict that some UV lines are shallower than is observed (Ardila et al. 2002). It has been suggested that this issue may be resolved by including the effects of turbulent accretion flows, which would result in broader line profiles (Alencar & Basri 2000). Vasconcelos, Jatenco-Pereira & Opher (2002) have investigated the effects of Alfvén waves generated from both the stellar surface and within turbulent accretion flows, and how they may heat the material in accretion columns.

The currently accepted model of magnetospheric accretion is that CTTs possess strong dipolar magnetic fields which truncate the disc at, or close to, the corotation radius. Material is loaded onto the stellar field forming accretion columns as it flows onto the star. Upon impact with the photospheric the material shocks, producing hot spots, as the kinetic energy of the flow is radiated away. As I have discussed in the previous sections there are a number of observations which support this basic picture. The variations in system brightness are well explained by hot spots on the stellar surface (e.g. Bouvier et al. 1993), with hot continuum emission periodically increasing on timescales that are comparable to the stellar rotation period (Bertout et al. 1988). Also, the UV excess emission can be explained naturally as the reemission of incident photons within the accretion shock (e.g. Gullbring et al. 1998). Average surface field strengths of order a few kG have been detected on a number of CTTs, which are strong enough to disrupt the disc at a distance of a few stellar radii (e.g. Valenti & Johns-Krull 2004). The shapes of SEDs are best explained by models with a hole in the inner disc (e.g. Kenyon et al. 1994), suggesting that the magnetosphere is disrupting the disc and controlling the infalling material in the regions closest to the star. The widths of redshifted absorption components of inverse P-Cygni profiles can

reach several hundred kms^{-1}, consistent with material free-falling from the inner disc at a distance of a few stellar radii (e.g. Edwards et al. 1994). Further, the shapes and variability of line profiles can be readily explained by magnetospheric accretion models (e.g. Hartmann et al. 1994; Muzerolle et al. 1998). There is also direct evidence (discussed below) for magnetic links between the star and the disc. Favata et al. (2005) found that the brightest flares seen on CTTs appear to occur inside magnetic loops which extend to perhaps $5R_*$ or larger. Such large magnetic loops would be unstable and quickly torn open if their foot points were anchored solely on the star (see e.g. Jardine & Unruh 1999), and have thus been interpreted as the field lines which connect stars to their accretion discs.

However, despite the success of the magnetospheric accretion scenario, there are observations which it cannot explain. Some of these are related to time variable accretion; below I discuss accretion models which have been developed that can account for unsteady accretion flows and variations in the magnetic field structure. To date the majority of accretion models assume that CTTs have dipolar magnetic fields and neglect the effects of a stellar corona. Safier (1998) provided critical arguments against current models and suggested that if a realistic hot stellar coronae was incorporated into such models then many field lines would be blown open. The disc would then extend in closer to the star, well within the corotation radius. This would of course mean that accretion would inherently act to increase the rotation rate of the star and that another mechanism must be responsible for the removal of excess angular momentum from CTTs systems (see the discussion in the next section). In the following Chapters I consider how a stellar corona may effect the structure of T Tauri magnetic fields. The magnetic fields of T Tauri stars are almost certainly non-dipolar in nature. There is strong evidence that their magnetic fields are more complex with the detection of rotationally modulated X-ray emission (Flaccomio et al. 2005), and the often net zero polarisation signal detected from photospheric

absorption lines (Valenti & Johns-Krull 2004). Furthermore, accretion filling factors (f_{acc} - the fractional surface area of the star covered in accretion hot spots) are inferred from observations to be small, of order 1% (e.g. Johns-Krull & Gafford 2002; Valenti & Johns-Krull 2004). Also, current dipolar accretion models cannot explain observed correlations between mass accretion rate and the inferred size of hot spots (Ardila & Basri 2000). Dipolar accretion models predict accretion filling factors which are too large. Also, there is the result that the average surface field strength detected does not vary much from star to star, suggesting that observed differences and variability may in some way be related to variations in the magnetic field geometry from star to star (Johns-Krull & Gafford 2002). There is also now direct evidence for the complex nature of T Tauri magnetic fields from Zeeman-Doppler imaging (Donati et al. 2007).

Johns-Krull & Gafford (2002) took the first steps towards investigating accretion models with non-dipolar magnetic fields. They demonstrated that if the dipolar magnetic field assumption is removed from the Shu X-wind model, and under the assumption that the field strength does not vary from star to star, then there should be a correlation between the stellar and accretion parameters (that is between M_*, R_*, P_{rot}, $\dot{M}$ and f_{acc}). Johns-Krull & Gafford (2002) found that such a correlation, $R_*^2 f_{acc} \propto (M_* \dot{M} P_{rot})^{1/2}$, agrees reasonably well with observations. Recent accretion models have also dropped the dipolar field assumption. von Rekowski et al. (2004b) and von Rekowski & Piskunov (2006b) consider the effects of the interaction between a stellar and disc field which are both dynamo generated and maintained; whilst Long et al. (2007) consider more complex field structures such as a quadrupole and a dipole/quadrupole composite. The field resembles a dipole in one hemisphere and a quadrupole in the other. Mohanty & Shu (2007) have further developed the Shu X-wind model to incorporate axisymmetric multipolar magnetic fields. They find that the X-wind portion of the model remains unaffected, but that accretion filling factors are smaller. In

the following Chapters I develop models of accretion to stars with generalised non-axisymmetric magnetic fields.

1.2.3 Rotation and magnetic braking

T Tauri stars are highly variable, a feature which lead to their discovery by Joy (1945). The variability of WTTs is primarily attributed to the presence of cool spots on the stellar surface. This leads to brightness variations as the star rotates. In the mid-1980s techniques were developed to use the observed brightness modulations to estimate stellar rotation periods (e.g. Rydgren & Vrba 1983; Herbst et al. 1986; Bouvier & Bertout 1989). Recent advances in wide-field imaging has allowed rotation periods to be derived for young stars in various star forming regions. There are now 1700 stars with rotation period estimates which are believed to be accurate to within 1% (Herbst et al. 2007). Observations taken years apart yield the same rotation periods for various WTTs. (e.g the photometric studies of the ONC by Stassun et al. 1999, Herbst et al. 2000 and Herbst et al. 2002). Therefore cool spots, which are associated with magnetic activity, perhaps remain stable for many hundreds if not thousands of rotation periods. However, it would only be possible to tell if cool spots remain stable by tracking individual spots. It could be the case that the surfaces of T Tauri stars are undergoing differential rotation but that spots typically appear at the same latitude. However, there is no evidence for surface differential rotation on T Tauri stars, unlike the Sun, where lower latitudes rotate faster than latitudes towards the poles. There is a single exception of one star in NGC 1333 which showed a 20% change in it's rotation period, however, such objects are extremely rare (Herbst et al. 2006).

Photometric variability from cool surface spots has also been detected on CTTs (e.g. Bouvier et al. 1995), however, the variability of CTTs is more strongly influenced by the presence of accretion hot spots. Variability from hot spots leads

to irregular brightness variations, indicative of the time variable nature of the accretion process, and/or changes in the field structure which is carrying accreting material (Bouvier et al. 1995). In contrast to cool spots which (perhaps) remain stable for hundred or thousands of rotation periods, hot spots appear to remain stable for only a few rotation periods (Herbst et al. 2007). The amplitude of variations seen in V-band observations of CTTs can be a factor of 2-3 larger than that seen for WTTs, making variability from hot spots easy to distinguish from variability from cool spots. This also suggests that the contrast in temperature between the photosphere and the spot is larger for hot spots than for cool spots.

By studying the brightness modulations arising from cool and hot spots it has been found that CTTs are more slowly rotating than WTTs, suggesting that the presence of a disc is somehow responsible for the slow rotation rate of CTTs (e.g. Bouvier et al. 1995). Magnetospheric accretion models provide a mechanism to explain the slow rotation of CTTs. Magnetic links between the star and regions of disc beyond the corotation radius which are more slowly rotating than the star can explain their slow rotation rates (Collier Cameron & Campbell 1993; Armitage & Clarke 1996; Shu et al. 1994a). Such models therefore allow the transfer of angular momentum from the star to the disc, and in the case of the Shu X-wind model, it is then carried away from the system in a wind originating from close to the corotation radius (Ostriker & Shu 1995). There is evidence for such a disc-locking scenario by, for example, the discovery of an anti-correlation between stellar angular velocity and disc indicators, such as excess IR emission (e.g. Herbst et al. 2002). Despite such observations, disc-locking models remain controversial. A number of authors detail problems with such models, such as Stassun et al. (1999) and Herbst et al. (2000) who find no correlation between stars with low rotation rates and disc accretion for the lowest T Tauri masses. Also, disc-locking models require field strengths of a few kG. Such strong average fields have been found on a number of T Tauri stars (Johns-

Krull et al. 1999b; Johns-Krull et al. 2004; Yang et al. 2005). Models assume that T Tauri stars have dipolar magnetic fields, however, current observations have shown that the dipole magnetic field component is at least a factor of 10 weaker than such models require (Valenti & Johns-Krull 2004; Daou et al. 2006; Yang et al. 2007). As a result it is unclear whether the real (non-dipolar) magnetic field geometries of T Tauri stars can enforce corotation between the star and the disc. Further, Johns-Krull & Gafford (2002) found that current magnetospheric accretion models do not provide a reasonable fit to observed parameters, and instead found that better fits were obtained when the dipolar magnetic field assumption was dropped. However, models of CTTs must still try to explain how high angular momentum material can be accreted from inside of corotation without spinning up the star; indeed CTTs have been observed to evolve towards the main sequence without increasing their rotation rates (Rebull et al. 2002).

Alternative models have been developed with tend to differ by how the stellar magnetic field interacts with the disc. In the next section I consider some time-dependent accretion models which consider the complex interaction between accretion and outflow processes. One such model is the reconnection X-wind (Ferreira, Pelletier & Appl 2000; Ferreira, Dougados & Cabrit 2006). In this model a disc wind carries away excess angular momentum, which allows the contracting protostar to spin-down despite accreting material from the disc. This appears to be one of the most efficient mechanisms in braking the stellar rotation rate (Ferreira et al. 2000). Another model argues that there is nothing special about the location of the corotation radius, and that the disc extends to well within corotation (Matt & Pudritz 2004, 2005a,b). This is exactly what was argued by Safier (1998). In the model by Matt & Pudritz (2004, 2005a,b) the process of accretion alone would act to increase the rotation rate of the star, however, this is prevented by angular momentum being removed by a stellar wind. They argue that the slow spin rate of CTTs can be explained if at least 10% of the energy

from accretion powers a stellar wind. However, there remain many avenues of research with standard disc-locking models, with new numerical simulation being performed (Long, Romanova & Lovelace 2005). Also, disc-locking models have yet to take account of the true complexity of CTTs magnetic fields, although initial work modelling accretion to a quadrupole stellar field appears to indicate that the transfer of angular momentum from the star back to the disc is less efficient than for a dipole field (Long et al. 2007). Another new model described by von Rekowski & Piskunov (2006b) assumes that both the star and the disc have magnetic fields which are dynamo generated and maintained, leading to aperiodic episodes of stellar spin-up and spin-down.

1.2.4 Time dependent accretion and outflows

Many observations indicate that accretion is highly time dependent, and is not the steady state process assumed by the most accepted magnetospheric accretion models. Stempels & Piskunov (2002) find that their veiling measurements vary with time, indicating a variable mass accretion rate. The time variations in line fluxes expected as accretion columns cross the line-of-sight, and excess continuum emission, are not always detected (Ardila & Basri 2000; Batalha et al. 2002). The observations of TW Hya by Alencar & Batalha (2002) show that line profiles vary substantially, despite the inclination of TW Hya being such that the system is seen nearly pole-on. Therefore the line profiles should not be affected by accretion columns rotating across the line-of-sight, or by a warped inner disc occulting the star (unless the large scale magnetosphere of TW Hya is tilted significantly with respect to the stellar rotation axis). However, the line profiles remain highly variable, suggesting that either the accretion rate is varying, or that the magnetic field structure is changing significantly with time. Other IR observations appear to show evidence for warped inner discs, or accretion columns, periodically occulting the star (Johns-Krull & Valenti 2001).

Bouvier et al. (1999) present observations of AA Tau which exhibits deep photometric eclipses on a timescale equal to the stellar rotation period. Given the large inclination of AA Tau, $i \approx 75\,^{\circ}$, the eclipses were attributed to a warped inner disc perhaps generated by a stellar magnetic field which is inclined to the stellar rotation axis. It was demonstrated by Terquem & Papaloizou (2000) that a tilted stellar dipole field interacting with a Keplerian accretion disc could indeed explain the deep eclipses observed in the light curve of AA Tau. Ménard et al. (2003), O'Sullivan et al. (2005) and Pinte & Ménard (2005) have since derived parameters for the geometry of the disc warp and the inner disc. Follow up observations, combining medium term simultaneous photometric and spectroscopic monitoring of AA Tau, again indicated cyclic eclipses of the star by an inner disc warp (Bouvier et al. 2003). However, the warp appeared to disperse for one rotation period, only to return. During this missing eclipse both the line fluxes and veiling were strongly reduced and the variability was less, indicating that not only had the inner disc warp vanished, but at the same time the accretion process appeared to have switched off. There is evidence that this event may be part of a magnetospheric cycle, as I discuss below, where accretion occurs periodically. This suggestion is supported by an observed correlation between the radial velocity of the redshifted absorption component (an accretion indicator) and the blueshifted absorption component (an outflow indicator) of the Hα line. Such anti-correlations between inflow and outflow signatures have been observed before, e.g. in SU Aur by Johns & Basri (1995). Bouvier et al. (2003) interpret this as direct evidence of the magnetospheric inflation model of Goodson & Winglee (1999). In this model the magnetosphere inflates over a timescale of several rotation periods, due to the differential rotation of field lines between the star and the disc, and is then disrupted, before returning to the initial field configuration. This interpretation is strengthened by more observations of AA Tau by Bouvier et al. (2007b), again combining long term photometric and high resolution spectroscopic data. There is evidence for variability on timescales of

days to months. They further demonstrate that during the deep photometric eclipses, attributed to the warped inner disc, the veiling and HeI 5876Å line flux reach a maximum. At the same time large redshifted absorption components appear in the Balmer lines of hydrogen. Putting the pieces of evidence together this suggests that the accretion shock, the accretion column and the inner disc warp are at the same rotational phase. Furthermore, Bouvier et al. (2007b) find that the mass accretion rate varies over several rotation periods, with evidence for strong accretion rates coinciding with a weak hot wind, and weak accretion rates when a strong hot wind is observed. Again this has been interpreted as evidence for magnetospheric inflation, although it should be stressed, that this has only been observed on one star, and more long term monitoring campaigns are required (e.g. the initial results presented by Grankin et al. 2007). It is also worth noting that the dataset for AA Tau now spans a decade and it has been found that as well as the short term variability attributed to magnetospheric inflation, there is tentative evidence for a magnetic cycle. Although deep eclipses have been observed consistently for many years on a timescale of AA Tau's rotation period, the shape and depth of such eclipses have changed over the years, perhaps indicating the presence of a magnetic cycle (Bouvier et al. 2007b).

The observed correlation in AA Tau between signatures of accretion and outflow has been interpreted as evidence for magnetospheric inflation. This refers to a class of models which predict cyclic changes in the structure of the magnetosphere with alternating episodes of accretion and outflow (Aly & Kuijpers 1990; Bardou & Heyvaerts 1996; Goodson et al. 1997; Goodson, Böhm & Winglee 1999; Goodson & Winglee 1999; Agapitou & Papaloizou 2000; Matt et al. 2002). The basis for such time dependent models is that the differential rotation between the foot points of field lines connecting the star to the disc, causes the field lines to expand (see Fig. 1.7). After a few rotation periods the twisted field lines are torn open, ejecting material from the system. The open field lines then recon-

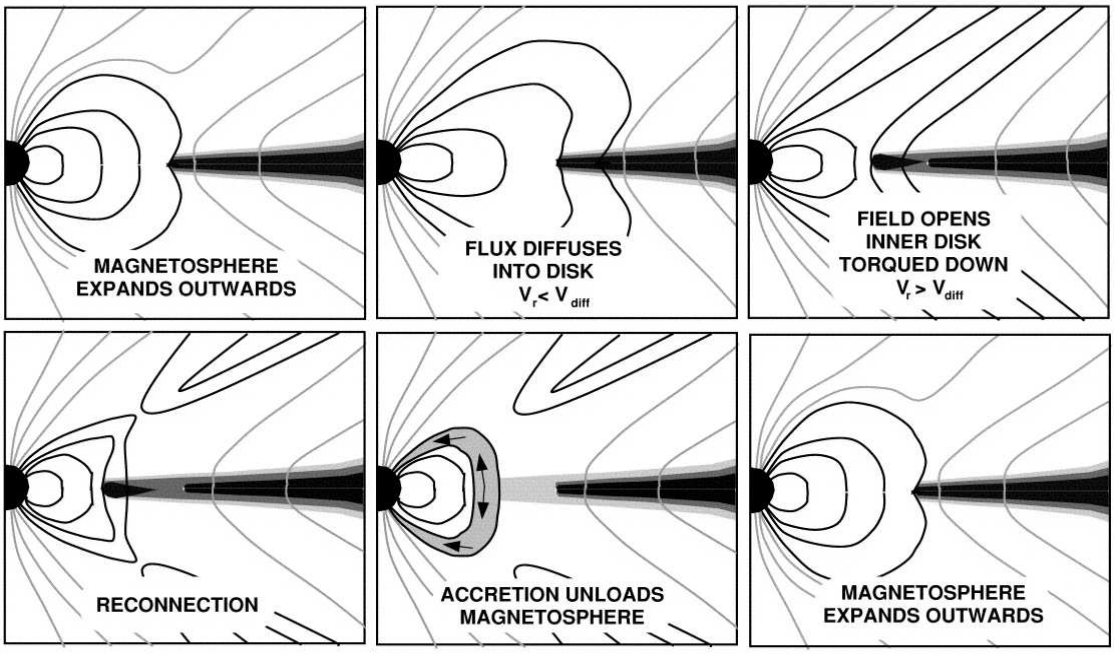

Figure 1.7: An illustration of magnetospheric inflation, reproduced from Goodson & Winglee (1999). The solid black lines are field lines that constitute the original stellar magnetosphere. Such a model is believed to explain the observed correlation between accretion and outflow signatures in AA Tau (Bouvier et al. 2003, 2007b). Reproduced with permission.

nect, uploading disc material onto the stellar magnetosphere (Hayashi, Shibata & Matsumoto 1996; Romanova et al. 2002). After the accretion episode the initial field configuration is restored. In such a way the accretion process is periodic, and intimately connected to ejection processes. There are further observations which suggest that the magnetosphere is dynamic and is strongly influenced via the interaction with the disc. Oliveira et al. (2000) present observations of SU Aur which indicate that field lines are being twisted by differential rotation. Alencar, Johns-Krull & Basri (2001) and Ardila et al. (2002) find evidence for reconnection events, with periodic high velocity outbursts identified via the blueshifted absorption components of emission line profiles.

Highly time variable accretion is a feature of other accretion models as well (e.g. Miller & Stone 1997), however, the most comprehensive numerical modelling of the star-disc interaction are the 3D simulations being carried out as part of the US-Russian collaboration on plasma physics. Koldoba et al. (2002b) and Romanova et al. (2003) demonstrated that the interaction between the inner disc and an inclined dipolar magnetosphere often leads to the creation of a disc warp as well as another secondary warp created by the tendency of matter within the magnetospheric cavity to corotate with the stellar magnetosphere. They predict the existence of many accretion columns connecting the star to the disc, whose geometry changes in time. They argue that such accreting structures may be responsible for the large variability seen in accreting T Tauri stars. This work was extended to determine the distribution and shapes of accretion hot spots and the resulting photometric variability (Romanova et al. 2004a). Furthermore, they have also considered field geometries which are more complex than a dipole (Long et al. 2007); however their initial field configurations are still axisymmetric. Long et al. (2007) do find that the location and distribution of hot spots is strongly dependent upon the geometry of the magnetic field; this is also a prediction of my complex field accretion model discussed in Chapter 4, and published in Gregory

et al. (2005, 2006a).

Many accretion models have been developed that attempt to combine accretion with ejection processes (stellar winds, disc winds, X-winds and bipolar jets). The Shu model, discussed in the previous section, was one of the first models to attempt to combine accretion with disc winds and jets. In the Shu model an accretion powered disc wind, originating from a small region close to the corotation radius, carries away angular momentum from accreting material, preventing the star from spinning up (Shu et al. 1994a; Ostriker & Shu 1995). Various other models have been proposed studying the connections between accretion and ejection processes, which tend to differ on exactly how the field interacts with the disc. Goodson et al. (1997) show that field lines threading the disc can drive winds and jets, whilst Hirose et al. (1997) argue that reconnection events can drive jets and explain the slow rotation of CTTs. Such accretion-ejection models often provide very efficient spin down mechanisms (e.g. Ferreira et al. 2000; Romanova et al. 2005). One of the most efficient such models is the Reconnection X-wind model (Ferreira et al. 2000), which is compared to other outflow models and their observable predictions by Ferreira et al. (2006). In this model a dynamo generated stellar magnetosphere reconnects with the remnant disc field, deflecting the disc material away from the disc plane. A fraction of the material is accreted with the rest emerging as an MHD jet, the reconnection X-wind. Such outflows are fed with disc material, but are powered by the stellar rotational energy. Thus unlike the Shu X-wind model, the reconnection X-wind provides a torque that brakes the star efficiently.

An alternative accretion model is being developed which does not assume that material is mass loaded onto field lines (von Rekowski & Brandenburg 2004a; von Rekowski et al. 2004b; von Rekowski & Brandenburg 2006a; von Rekowski & Piskunov 2006b). The basis of this accretion model is that the both the stellar and the disc magnetic fields are dynamo generated and maintained. Material

accreting from the disc is in constant competition with the outflowing stellar wind from the star. Accretion is episodic, with material only able to accrete onto the star into regions where, and at times when, it is able to overcome the stellar wind (von Rekowski & Piskunov 2006b). There is of course a lot of evidence that accretion is a highly time dependent process, however, in this model accretion only occurs onto the star's equator; it therefore remains to be seen if such a model can explain the level of photometric variability which is often attributed to the presence of hot spots at higher latitudes. Furthermore, von Rekowski & Piskunov (2006b) argue that although material may reach several hundred kms^{-1} in the gap between the star and the inner disc edge (consistent with the large redshifted absorption components of inverse in P-Cygni profiles), it slows to only a few tens of kms^{-1} before accreting onto the star. This raises the question as to whether hot spots can be explained at all by this model. Of course, this model, as with the many others which are attempting to explain the deep connections between time dependent accretion and outflows processes, will continue to develop in the future. Reconciling the wealth of observational data of the highly variable and complex CTTs systems is truly a difficult task, however, much progress is likely to be made over the coming years.

1.3 Mass accretion and stellar mass

Hillenbrand et al. (1992) calculated mass accretion rates for both T Tauri stars and higher mass Herbig Ae/Be stars. They found that $\dot{M}$ values were highest for the largest mass stars, and suggested that $\dot{M} \propto M_*^{2.2}$. They commented that "This result may be of fundamental importance not only to our understanding of the factors which influence accretion disk physics around stars of differing mass but also to our ultimate understanding of how stars are assembled from protostellar core and disk material". However, it is only in recent years that the

apparent correlation between $\dot{M}$ and M_* has sparked interest amongst a number of authors.

Rebull et al. (2000) noted that the apparent increase in mass accretion rate with stellar mass and that the lack of low mass stars with high $\dot{M}$ was a real effect for stars in the Orion flanking fields. The authors argued that although there were various selection effects which influenced the overall trend in $\dot{M}$ values with stellar mass, their methods would have been able to detect lower mass stars with large mass accretion rates, if they had existed. White & Ghez (2001) also noted an apparent $\dot{M} - M_*$ correlation for stars in Taurus-Auriga, with a large scatter in $\dot{M}$ values, with Rebull et al. (2002) reporting that the correlation also existed for stars in NGC 2264. White & Basri (2003) demonstrated that the correlation extended across several orders of magnitude in mass with the detection of accretion in low mass T Tauri stars and brown dwarfs. However, they caution that any correlation between extinction and accretion would leave high accretion rate, but low mass, stars below detection limits, introducing a false dependence on $\dot{M}$ with M_*. Muzerolle et al. (2003) measured accretion rates in low mass objects and suggested that $\dot{M} \propto M_*^2$. Subsequent observations by Calvet et al. (2004) indicated that this correlation extended to the higher mass, intermediate mass T Tauri stars with several authors adding data at lower masses from various star forming regions (Natta et al. 2004; Mohanty et al. 2005a; Muzerolle et al. 2005). Natta et al. (2006) added data across a range of mass from the ρ-Ophiuchus star forming region. Further data has been obtained from some of the youngest stars in Taurus-Auriga by White & Hillenbrand (2004), with data for some of the highest mass objects, Herbig Ae stars, being added by Garcia Lopez et al. (2006). Further accretion rate estimates for mainly brown dwarfs have been published by Gatti et al. (2006). There can be as much as three orders of magnitude scatter in the measured mass accretion rate at any particular stellar mass. Fig. 1.8 shows the observed correlation between stellar

mass and mass accretion rate which extends through the lowest mass accreting brown dwarfs, very low mass T Tauri stars, classical T Tauri stars, intermediate mass T Tauri stars and Herbig Ae/Be stars.

It should also be noted that mass accretion rate measurements for stars in the Trapezium cluster are not consistent with the $\dot{M}$-M_* correlation. Robberto et al. (2004) report $\dot{M}$ values for the Trapezium cluster which are significantly lower than those obtained for stars in Taurus, the Orion flanking fields and ρ-Ophiuchus, and suggest that the probable cause is that the discs of lower mass stars are being disrupted by UV radiation from the Trapezium OB stars. This causes a large drop in mass accretion rates. Also, Calvet et al. (2004) point out that there is a strong bias against the detection of intermediate mass T Tauri stars ($M_* = 1.5 - 4\,\mathrm{M}_\odot$) with lower mass accretion rates, therefore the exponent of the $\dot{M} - M_*$ correlation may be less that 2. Further, Clarke & Pringle (2006) demonstrate that currently available data may be limited by selection effects at high $\dot{M}$ values (whereby accretion rates cannot be determined when the accretion luminosity is greater than the stellar luminosity) and also by a lower bound defined by the upper limits of non-detections. Their work therefore suggests that the steep correlation between $\dot{M}$ and M_* is a natural consequence of detection/selection limitations, and that the true $\dot{M} - M_*$ correlation may be different. Hartmann et al. (2006) argue that the bulk of the data follows $\dot{M} \propto M_*^2$, but there could be an upper envelope of accretion rates which follow a different relation of $\dot{M} \propto M_*$.

The physical origin of the correlation between M_* and $\dot{M}$, and the large scatter in measured $\dot{M}$ values, is not clear; however several ideas have been put forward, which are discussed in detail in the following sections. First, increased X-ray emission in higher mass T Tauri stars (Preibisch et al. 2005; Jardine et al. 2006) may cause an increase in disc ionisation, leading to a more efficient magnetorotational instability and therefore a higher mass accretion rate (Glassgold, Najita

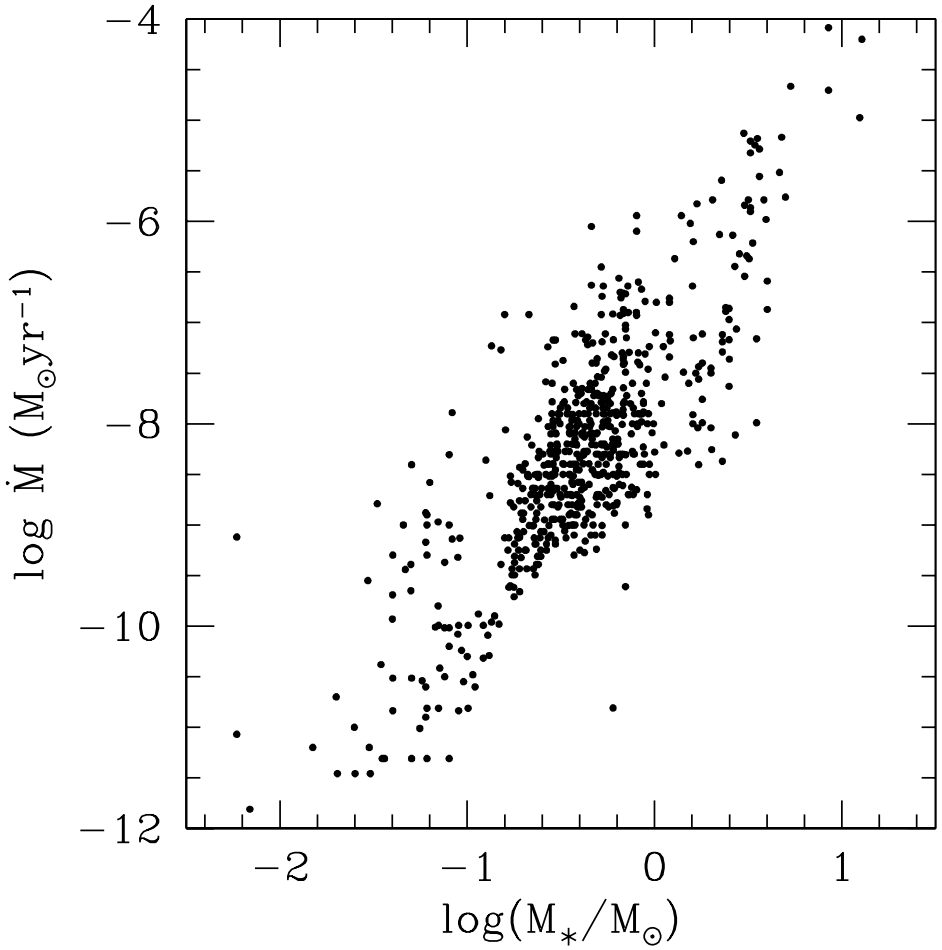

Figure 1.8: The correlation between mass accretion rate and stellar mass. Previously published values are taken from Hillenbrand et al. (1992), Rebull et al. (2000); Rebull et al. (2002), White & Hillenbrand (2004), Mohanty et al. (2005a), Natta et al. (2006), Garcia Lopez et al. (2006) [which includes data from Rodgers (2001)], Gatti et al. (2006) and Muzerolle et al. (2005) [which is a collection of data from Gullbring et al. (1998), White & Ghez (2001), White & Basri (2003), Muzerolle et al. (2003), Calvet et al. (2004) and Natta et al. (2004)].

& Igea 1997; Muzerolle et al. 2003; Hartmann et al. 2006). Second, Padoan et al. (2005) argue that the correlation $\dot{M} \propto M_*^2$ arises from Bondi-Hoyle accretion, with the star-disc system gathering mass as it moves through the parent cloud. In their model the observed scatter in $\dot{M}$ arises from variations in stellar velocities, gas densities and sound speeds. Third, Alexander & Armitage (2006) suggest that the correlation may arise from variations in the disc initial conditions combined with the resulting viscous evolution of the disc. The model that they develop makes the prediction that brown dwarfs (the lowest mass accretors) have discs which are larger than those of the higher mass accretors. Thus the Alexander & Armitage (2006) suggestion, if correct, will soon be directly verifiable by observations. Fourth, Dullemond, Natta & Testi (2006) argue that the initial conditions during the formation of the star-disc system are responsible for the correlation between $\dot{M}$ and M_*. The rotation rate of the parent core sets the radius at which infalling material is loaded onto the surface of the disc. Consequently the accretion rate measured long after the dispersal of the parent core bears the imprint of the initial conditions during the formation of the star-disc system. Fifth, Scholz & Jayawardhana (2006) and Natta et al. (2006) suggest that the large scatter in the correlation between $\dot{M}$ and M_* may arise from time variable accretion or by the influence of close companion stars. Sixth, Hartmann et al. (2006) suggest that the stellar mass-accretion rate correlation arises from the combination of many processes, including the gravitational instability for the highest mass accreting stars.

1.3.1 X-ray irradiation of the disc

Muzerolle et al. (2003) suggest that the increase in $\dot{M}$ with M_* arises from X-ray emission from the central star increasing the disc ionisation and therefore angular momentum transfer. Higher mass pre-main sequence (PMS) stars have been observed to be more active in X-rays than lower mass PMS stars, with several

authors reporting a strong correlation between X-ray luminosity and stellar mass (Preibisch & Zinnecker 2002; Mokler & Stelzer 2002; Feigelson et al. 2003; Flaccomio et al. 2003a; Preibisch et al. 2005; Telleschi et al. 2007a). However, there is also several orders of magnitude difference in L_X values at any given stellar mass (see Fig. 1.9). Increased X-ray emission in higher mass stars may increase the ionisation of gas in their circumstellar discs (Glassgold et al. 1997). Increased disc ionisation leads to a more efficient magnetorotational instability (MRI), believed to be the viscosity mechanism in accretion discs which allows the inward transfer of mass via the outward transfer of angular momentum (Balbus & Hawley 1991). Thus, higher mass T Tauri stars, with their increased X-ray emission, are likely to have higher mass accretion rates. Conversely, lower mass stars with their lower levels of disc ionisation are likely to have lower mass accretion rates. However, Muzerolle et al. (2003) and Natta et al. (2006) point out that it is not clear whether the observed increase in X-ray luminosity with stellar mass is large enough to explain a correlation as steep as $\dot{M} \propto M_*^2$. Mohanty et al. (2005a) also comment that an increase in ionising flux with stellar mass does not explain the particular functional form of the correlation. Other authors claim that although X-ray emission from the central star may influence the calculated value of $\dot{M}$, it does not influence the observed trend with stellar mass (Alexander & Armitage 2006; Dullemond et al. 2006). However, it may be the case that the large scatter in L_X values (see Fig. 1.9) could account for the large scatter in $\dot{M}$ for a given M_* (Natta et al. 2006).

The roll of the MRI as it relates to the $\dot{M} - M_*$ correlation is discussed in detail by Hartmann et al. (2006), who suggest that different disc processes may be dominant depending on the mass of the star. The basic idea is that layered MRI accretion combined with the gravitational instability governs the mass accretion rate in the highest mass stars, with full viscous MRI accretion occurring in the lowest mass stars. In order for the MRI to operate the disc must

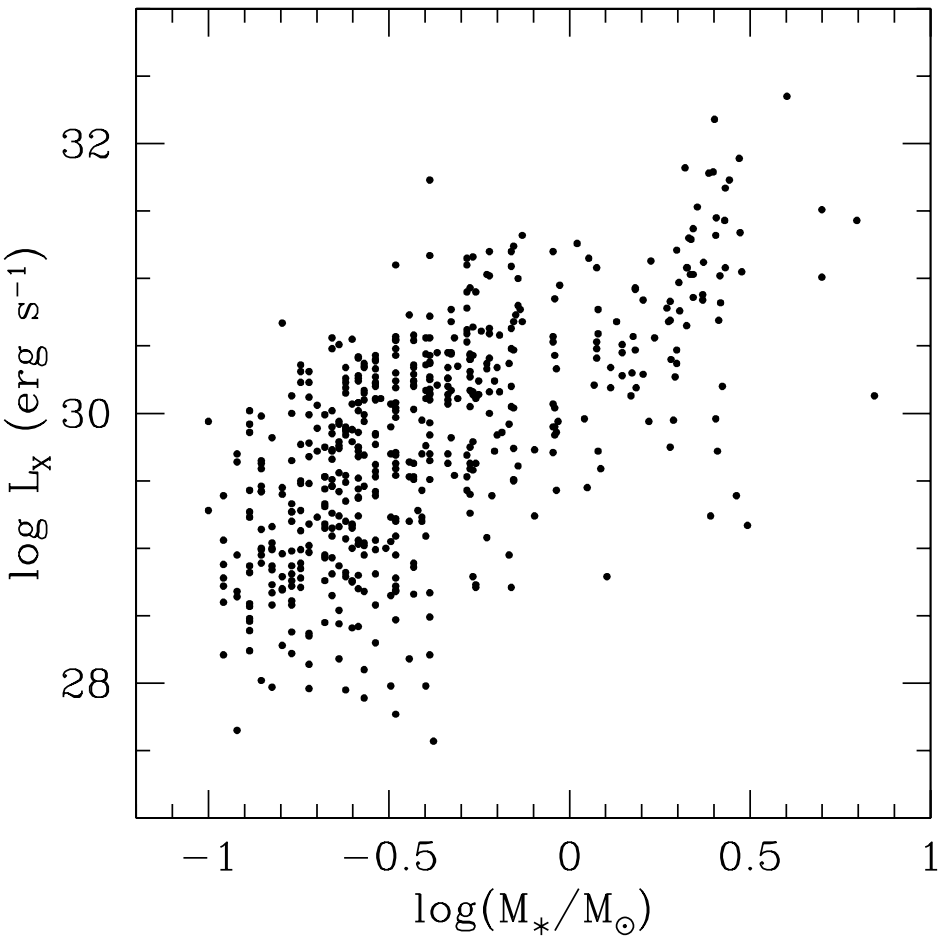

Figure 1.9: The increase in X-ray luminosity with stellar mass illustrated with data from the Chandra Orion Ultradeep Project. Based on a plot from Preibisch et al. (2005).

be highly ionised, but T Tauri discs are typically cold and thus have a low level of ionisation. A layered accretion model was proposed by Gammie (1996), where cosmic rays ionise the outermost layers of the disc, leaving a dead zone (a non-turbulent region) in the disc midplane. Further, as discussed above, X-rays from the central star can increase the level of disc ionisation (Glassgold et al. 1997). A layered disc model whereby the outer layers accrete material onto the star, with little contribution from regions in the disc midplane, may neither account for the large accretion rates derived for T Tauri stars, nor explain the observed correlation with stellar mass. However, Hartmann et al. (2006) demonstrate that the layered accretion model of Gammie (1996), where $\dot{M}$ is independent of stellar mass, can be modified to include the effect of disc heating by irradiation from the central star, leading to a moderate dependence of $\dot{M}$ on M_*, with $\dot{M} \propto M_*$. A relation of this form is consistent with the upper envelope of observations (Clarke & Pringle 2006; Hartmann et al. 2006). Accreting brown dwarfs, the lowest mass accretors, are found well below this upper envelope. Hartmann et al. (2006) argues that the discs of brown dwarfs are likely to be fully MRI-active. Since brown dwarfs have smaller accretion rates the layered accretion model of Gammie (1996) predicts that their disc surface densities are much lower that those of T Tauri discs. This leads to brown dwarfs having completely viscous discs (without non-accreting dead zones) as the disc material can be completely ionised by cosmic rays/X-rays. Thus full viscous MRI accretion may operate in brown dwarf discs. Accretion through the discs of higher mass stars may be somewhat different. Although the MRI may operate in the inner disc of higher mass stars, where thermal ionisation is high, there may be a dead zone at larger radii. The continuous accumulation of material from the outer disc may force the dead zone into gravitational instability (Hartmann et al. 2006). However a disc mass of at least $0.1M_*$ is required for gravitational instabilities to operate (Pringle 1981). Andrews & Williams (2005) derived a median disc-to-star mass ratio of 0.5% from a comprehensive survey of the Taurus-Auriga star forming

region, suggesting that the typical masses of T Tauri discs are too low for any gravitational instabilities to develop. Hartmann et al. (2006) argues, however, that disc masses are likely to be underestimated and that perhaps more massive discs which are close to the limit for gravitational instability exist in at least the most massive T Tauri star systems.

1.3.2 Bondi-Hoyle accretion

Padoan et al. (2005) argue that the stellar mass - accretion rate correlation may be explained by star-disc systems gathering mass via Bondi-Hoyle accretion from the large scale gas distributions within parent clouds. They argue that this large scale accretion constitutes the majority of the estimated accretion rates for pre-main sequence stars. The Bondi-Hoyle accretion rate is

$$\dot{M}_{BH} = \frac{4\pi G^2 \rho_\infty}{\left(c_\infty^2 + v_\infty^2\right)^{3/2}} M^2 \tag{1.10}$$

(Bondi 1952), where M is the combined mass of the star and the disc, G is the gravitational constant, and ρ_∞, c_∞ and v_∞ are the gas density, sound speed and velocity of the surrounding medium relative to the star-disc system, at a large distance from the star. The mass of a typical circumstellar disc is much less than that of the central star and therefore $M \approx M_*$. The Bondi-Hoyle accretion rate $\dot{M}_{BH}$ is the amount of mass accreted onto the entire star-disc system and provided that this is equal to the disc accretion rate $\dot{M}$, then the correlation $\dot{M} \propto M_*^2$ follows directly from (1.10). However, as is discussed by Mohanty et al. (2005a) and Mohanty, Basri & Jayawardhana (2005b), Bondi-Hoyle accretion may not be relevant in explaining the $\dot{M} - M_*$ correlation, and the observed large scatter in $\dot{M}$ values. It is unlikely that the Bondi-Hoyle accretion rate is equal to the disc accretion rate at all times. Instead mass may build up in the disc before being accreted onto the star in bursts, meaning that $\dot{M}$ is equal to $\dot{M}_{BH}$ only in a time-averaged sense. Furthermore, from equation (1.10) ρ_∞, c_∞ and

v_∞ are characteristic properties of molecular cloud filaments within star forming regions, which are independent of stellar mass. Padoan et al. (2005) argue that variation of these quantities over a large cloud volume could explain the large scatter in calculated $\dot{M}$ values (see Fig. 1.8). Mohanty et al. (2005a) are critical of this suggestion, pointing out that objects in Taurus (which account for data across most of the mass range covered in Fig. 1.8) appear to be lined up along dense gas filaments - their likely birthplace (Hartmann 2002; Briceño et al. 2002). Also, their observed low extinctions suggest that such stars are no longer buried within the filaments but are still unlikely to have moved far from their birthplace. There is likely to be less variation in the physical conditions close to the filaments when compared to the cloud as a whole, making it difficult to account for the large scatter in $\dot{M}$ values (which can be up to three orders of magnitude). Hartmann et al. (2006) are also critical of the Bondi-Hoyle accretion argument, pointing out that in order to demonstrate that equation (1.10) yields a typical T Tauri mass accretion rate of $10^{-8}\,\mathrm{M}_\odot yr^{-1}$, Padoan et al. (2005) assumed a value of $v_\infty = 1\,\mathrm{kms}^{-1}$, which is much larger than the value obtained by Hartmann (2002). Also, Hartmann et al. (2006) demonstrate that the sound speeds and densities attributed to the young cluster Trumpler 37 gives a Bondi-Hoyle accretion rate that is five orders of magnitude smaller than observed accretion rates. Thus, Bondi-Hoyle accretion is unlikely to be responsible for the observed $\dot{M} - M_*$ correlation.

1.3.3 Initial conditions

Several authors have suggested that the stellar mass - accretion rate correlation is an imprint of the physical conditions in the molecular cores from which the star-disc systems form (Alexander & Armitage 2006; Dullemond et al. 2006; Natta et al. 2006; Hartmann et al. 2006). The initial conditions may also explain the large spread in $\dot{M}$ values. Hueso & Guillot (2005) present a model which

follows the formation and evolution of circumstellar discs with different initial core properties, in particular different rotation velocities, which gives rise to a large spread in $\dot{M}$ values.

Dullemond et al. (2006) expand upon the ideas of Hueso & Guillot (2005) and suggest that initial core rotation may explain the $\dot{M} - M_*$ correlation. In their model the rotation rate of the parent core sets the radius at which material is loaded onto the surface of the disc, and in such a way the accretion rate measured after the dispersal of the parent core bears an imprint of the initial conditions. By assuming that cores of different mass have similar rotation rates measured in units of their breakup rate, a trend of $\dot{M} \propto M_*^{1.8\pm0.2}$ is found, agreeing with observations. However, the Dullemond et al. (2006) model also predicts a correlation between $\dot{M}$ and disc mass, which is not reproduced by available data. Although the concerns of Hartmann et al. (2006), discussed above, that disc masses may be underestimated should be kept in mind.

Alexander & Armitage (2006) demonstrate that the $\dot{M} - M_*$ correlation can be accounted for by viscous disc evolution if the ratio of disc-to-stellar mass is fixed at the end of core collapse. This model produces the correlation $\dot{M} \propto M_*^2$ by assuming that the initial disc size increases with decreasing stellar mass. Thus Alexander & Armitage (2006) predict that discs around brown dwarfs will be large and typically 50-100AU in radius, a prediction which will be testable in future.

1.3.4 Other suggestions

Time variable accretion has been suggested as an explanation for the large scatter in calculated $\dot{M}$ values at fixed M_* (Scholz & Jayawardhana 2006; Natta et al. 2006). The accretion rate for a couple of brown dwarfs targeted by Scholz & Jayawardhana (2006) was found to vary by an order of magnitude over the course

of their observations. The authors argue that this level of variability is likely to be a lower limit and larger changes in $\dot{M}$ may occur over longer timescales. Evidence for a variable mass accretion rate was found for another brown dwarf as part of the XEST (XMM-Newton Extended Survey of the Taurus Molecular Cloud; Grosso et al. 2007). However, by comparing archival data of the same stars in their sample from ρ-Ophiuchus, Natta et al. (2006) caution that the variability in $\dot{M}$ values may not be large enough to account for the amount of scatter seen in the $\dot{M} - M_*$ correlation.

Natta et al. (2006) also discuss how the presence of close companion stars could lead to a spread in $\dot{M}$ values, and provide a summary of the arguments of Calvet et al. (2000). Companion stars disrupt the circumstellar disc at a radius that depends on the binary separation. This leads to a rapid drop in the disc mass and the mass accretion rate, as material expands outside the truncation radius with time. Although this may be a possible explanation for the large scatter in $\dot{M}$ values there is no observational evidence to date to support this suggestion. Indeed White & Ghez (2001) find that accretion rates in Taurus are similar for both single stars and the primary companions of binary systems.

The scatter in calculated mass accretion rates may be due to age differences (Muzerolle et al. 2003; Muzerolle et al. 2005; Alexander & Armitage 2006). The mass accretion rate is expected to decrease with time, $\dot{M} \propto t^{-\gamma}$, where for viscous discs with a constant α, $\gamma = 3/2$ (Hartmann et al. 1998). Such a model is broadly supported by observation, with Fig. 1.10 showing the observed decrease in accretion rates with age for stars in various clusters (Sicilia-Aguilar et al. 2004; Sicilia-Aguilar et al. 2006). Discs become depleted with age and consequently it is natural to expect that older stars should have smaller mass accretion rates. This effect is likely to contribute to the large scatter in accretion rates at any particular stellar mass. It is also worth noting that at the highest mass range Garcia Lopez et al. (2006) find that there is a lack of very strong accretors amongst Herbig Ae

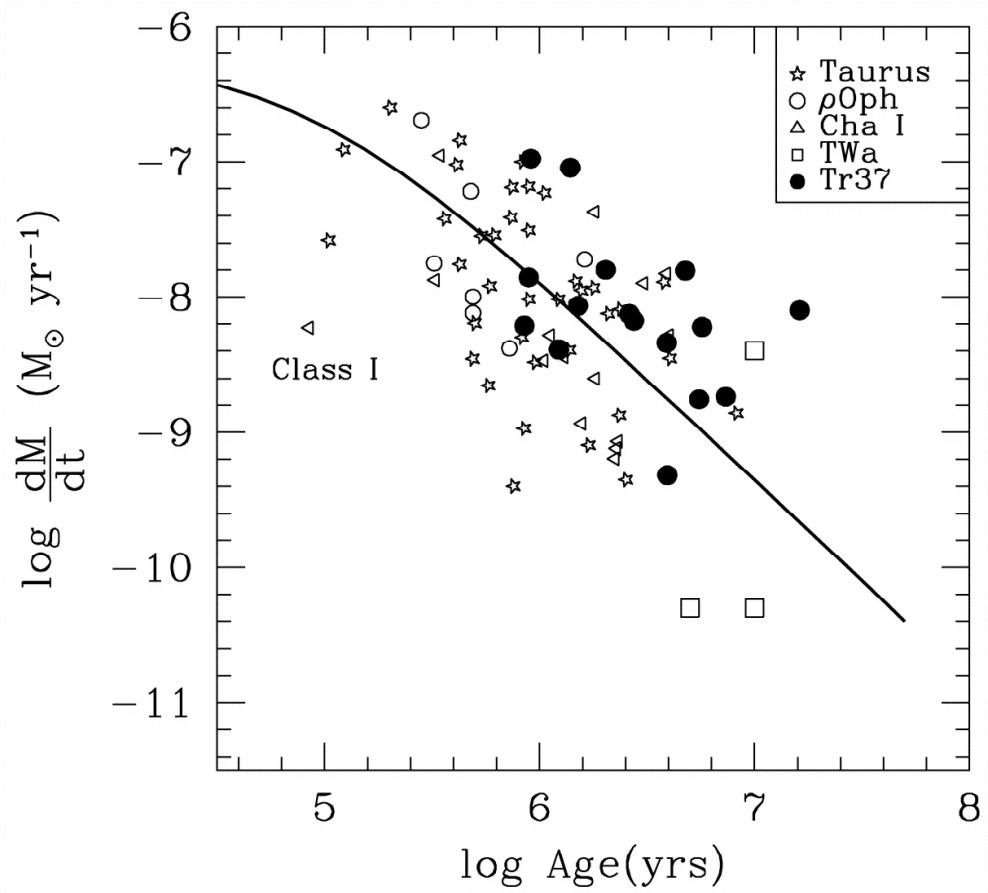

Figure 1.10: The decrease in mass accretion rate with age for stars in various clusters, reproduced from Sicilia-Aguilar et al. (2004). The solid line is the behaviour predicted by the viscous disc evolution model of Hartmann et al. (1998). Reproduced with permission.

stars which is probably due to the fact that they are on average older than T Tauri stars.

1.3.5 Detection and selection limitations

The correlation between mass accretion rate and stellar mass may be strongly influenced by selection/detection limitations. The published mass accretion rates from Natta et al. (2006) for stars in ρ-Ophiuchus provide a homogeneous data set where $\dot{M}$ values have been measured in a uniform manner. Clarke & Pringle (2006) used this data set to demonstrate that the lower bound to accretion rates is dominated by sensitivity limits. In other words the lower bound of the $\dot{M} - M_*$ correlation appears to be set by the upper limits of non-detections. Furthermore, as Clarke & Pringle (2006) point out, the upper bound of the $\dot{M} - M_*$ correlation appears to corresponds to the condition that the accretion luminosity equals the stellar luminosity. This is perhaps suspicious and likely arises as mass accretion rates cannot easily be determined when the accretion luminosity exceeds the stellar luminosity (Hartmann et al. 1998). It therefore appears that data is almost uniformly spaced between the upper and lower bounds on the $\dot{M} - M_*$ plane. Clarke & Pringle (2006) suggest that the correlation $\dot{M} \propto M_*^2$ simply arises as a result of the detection/selection limitations. They further demonstrate that a correlation of the form $\dot{M} \propto M_*$ is also consistent with the available data, and thus the true correlation between mass accretion rate and stellar mass may be somewhat different than the observed $\dot{M} \propto M_*^2$; if it genuinely exists at all.

1.4 X-ray emission

T Tauri stars can be up to ten thousand times more active in X-rays than the Sun (e.g. Feigelson et al. 2002). Typical X-ray luminosities are $L_X \sim$

$10^{28} - 10^{32}\,\mathrm{ergs}^{-1}$. This compares to the solar value of $L_X \sim 10^{27}\,\mathrm{ergs}^{-1}$, with T Tauri coronae being significantly hotter than what is observed on the Sun ($5 - 50\,\mathrm{MK}$ are typical temperatures for T Tauri coronae, with temperatures in excess of $100\,\mathrm{MK}$ during flares; compared to the solar corona at $2\,\mathrm{MK}$ and temperatures of less than $10\,\mathrm{MK}$ during flares). The origin of their X-ray emission and how it is affected by the process of accretion has been the subject of open debate for many years. However, recent large X-ray surveys of star forming regions have provided a wealth of X-ray data which have helped address many of the outstanding questions but created many more. There is no X-ray quiet population amongst pre-main sequence stars with almost every object being variable in X-rays (Preibisch et al. 2005). Many flares have been detected on T Tauri stars with length scales that are comparable to flares seen on the Sun and other main-sequence stars (Favata, Micela & Reale 2001). This had lead to suggestions that the origin of X-ray emission from T Tauri stars is similar to that from the Sun, with hot plasma confined within compact magnetic structures heated by violent magnetic reconnection events. High resolution X-ray spectroscopic measurements indicate contributions to the (softer) X-ray emission from accretion shocks, whilst the shearing open and periodic reconnection of field lines which interact with circumstellar discs may provide an additional X-ray emission mechanism. However, as I discuss below, the dominant X-ray emission mechanism in T Tauri stars is likely to be coronal in nature. Interestingly the presence or absence of a disc does not appear to influence the amount of X-ray emission that is detected, however, active accretion does. Stars which show evidence for accretion typically have observed X-ray luminosities which are a factor of 2-3 lower than those which are not accreting. The origin of this difference is not clear, and although it is small, it has now been found consistently in various star forming regions. Below I discuss these points in detail.

1.4.1 COUP, XEST and DROXO

The Chandra Orion Ultradeep Project (COUP) has provided a remarkable dataset of X-ray properties of young stellar objects (Getman et al. 2005). COUP was a 13 day continuous Chandra observation of the Orion Nebula Cluster (ONC), the deepest X-ray observation ever taken of any star forming region. Without new X-ray satellites the community will never again obtain such a data set, due to degradation of components within the Chandra satellite. Over 1600 X-ray sources were detected during COUP with approximately 1400 sources being identified as young stars in the cluster (most of the other sources were identified as either background AGNs seen through the cluster, or foreground stars). COUP found that there is no X-ray quiet population in the ONC with almost every source being observed to vary in X-rays during the observation time. Many flares were detected, most occurring inside compact magnetic structures which are comparable to the flaring loop lengths seen on the Sun (Wolk et al. 2005). However, some extremely large flares were also detected with flaring loop lengths which are comparable to the typical corotation radii for classical T Tauri stars (Favata et al. 2005). It should be noted that the loop lengths are derived from modelling the flare profiles from X-ray light curves and are not directly observed (see the discussion in Chapter 6). Such large magnetic structures have been interpreted as direct evidence of magnetic links between stars and their discs. COUP also found that higher mass stars were more active in X-rays than lower mass stars, albeit with a large scatter in X-ray luminosities at any particular stellar mass (Preibisch et al. 2005). Rotational modulation of X-ray emission was observed from a number of COUP sources, suggesting that the dominant X-ray emitting regions on T Tauri stars are confined within magnetic structures which are close to the stellar surface, and inhomogeneously distributed about the star. In such a way the dominant emitting regions enter eclipse as the star rotates (Flaccomio et al. 2005). COUP sources represent the largest sample of stars of any type with

evidence for rotationally modulated X-ray emission. It was found that the presence of a disc does not affect the amount X-ray emission, but that active accretion does (Preibisch et al. 2005). Accreting T Tauri stars were observed to be less luminous in X-rays than non-accreting stars, an effect which is not yet understood, but may be related to the attenuation of coronal X-rays by the dense material in accretion columns (Preibisch et al. 2005; Flaccomio et al. 2003a; Stassun et al. 2004a; Güdel et al. 2007b; Gregory, Wood & Jardine 2007). Interestingly the detection of rotationally modulated X-ray emission appears to be the same for both accreting and non-accreting stars suggesting that the coronal structure is similar for both weak line and classical T Tauri stars (Flaccomio et al. 2005).

The XMM-Newton Extended Survey of the Taurus Molecular Cloud (XEST) is another recent X-ray project which monitored young stars in the most populated region of the Taurus star forming region (Güdel et al. 2007a). The first results from XEST are currently appearing in the literature but so far there appears to be excellent agreement between the X-ray properties of stars in Taurus and those in Orion observed during COUP. XEST found an increase in X-ray luminosity with stellar mass and accreting T Tauri stars were observed to be less luminous in X-rays than non-accreting objects, exactly as was found during COUP (Telleschi et al. 2007a).

Another large X-ray study of young stellar objects is the Deep ρ-Ophiuchi XMM Observation (DROXO; Sciortino et al. 2006). This project consists of six observations taken over a time span of 10 days, with a total observing time of $\sim$500 ks (about 8 d) taken in March 2005. Sadly only about 50% of the total observing time has a low enough background level to be useful, as after only a few hours of observing a micro-meteorite struck one of the three XMM-Newton mirrors, causing one of the CCDs to die. The DROXO results have not yet been published, however, preliminary analysis of the brightest observed flares indicate that some may occur inside large magnetic structure with lengths of several stellar

radii (Flaccomio et al. 2007). Such large flaring loops where also found in COUP and are perhaps direct evidence for magnetic links between stars and their discs (Favata et al. 2005).

1.4.2 X-rays from accretion shocks

High resolution X-ray spectroscopy of some T Tauri stars appears to show evidence for X-ray emission from accretion shocks (e.g. Telleschi et al. 2007b; Günther et al. 2007). Accreting material shocks and radiates away its kinetic energy when it impacts the stellar photosphere, producing excess optical and UV emission, as well as some soft X-rays (Lamzin et al. 1996; Calvet & Gullbring 1998). High resolution X-ray spectroscopy of TW Hya, XZ Tau, BP Tau and V4046 Sgr yield plasma densities and temperatures which would be expected from an accretion shock (Kastner et al. 2002; Favata et al. 2003; Stelzer & Schmitt 2004; Schmitt et al. 2005; Günther et al. 2006). Accretion shock temperatures are at most a few MK which would give rise to soft X-ray emission. Thus the temperatures in accretion shocks are an order of magnitude lower than typical coronal temperatures, which show a cool component of $\approx 10\,\mathrm{MK}$ and a hot component in excess of $20\,\mathrm{MK}$ (Preibisch et al. 2005). This suggests that coronal (harder) X-ray emission dominates the X-ray spectrum of T Tauri stars. Also, if the X-ray emission comes exclusively from accretion shocks one may expect to see simultaneous brightness variations at optical/UV wavelengths and in X-rays. However, this is not found. Stassun et al. (2006) have compared X-ray light curves from COUP with simultaneous optical light curves for 800 stars and find little evidence for any correlation between X-ray and optical variability. This is strong evidence that accretion is not the primary source of X-ray emission from T Tauri stars.

Furthermore, stars in the COUP sample for which Robberto et al. (2004) have estimates of mass accretion rates, have X-ray luminosities which are compara-

ble or larger than the accretion luminosity. This strongly suggests that X-ray emission from accretion shocks does not dominate the X-ray spectrum of T Tauri stars. Although X-ray emission from accretion shocks may contribute some fraction of the soft X-ray emission detected from T Tauri stars it is not responsible for the bulk of X-ray emission, which is likely to be coronal in origin (Preibisch et al. 2005). This view point is supported by the high resolution spectroscopic X-ray observation of BP Tau by Schmitt et al. (2005) who find evidence for the coexistence of cool plasma with an unusually high density, attributed to emission from accretion shocks, and plasma which is too hot to have been shock produced and is therefore likely to be contained and heated in some form of coronal structure.

1.4.3 X-rays from star-disc interactions

Large magnetic loops which connect the star with the disc may also contribute to T Tauri X-ray emission. Differential rotation between the star and the disc twists such field lines which are torn open and then reconnect. Plasma trapped in the field lines may be heated to a high enough temperature to emit in X-rays by the energy release from magnetic reconnection events - as predicted by a number of models (Hayashi et al. 1996; Montmerle et al. 2000; Isobe et al. 2003; Romanova et al. 2004b). Favata et al. (2005) have found evidence during the COUP for large flares apparently occurring inside large extended magnetic structures connecting the star to the surrounding disc. However, such large flares were found to be rare, with the majority of flaring loop lengths derived for T Tauri stars being compact and only a few tenths of a stellar radius. This suggests that contributions to the X-ray emission from star-disc interactions only occurs during the most intense flares, which do not contribute to the bulk of X-ray emission. Also, Preibisch et al. (2005) demonstrate that the X-ray luminosity is independent of the presence or absence of a disc, again suggesting that solar-like coronal emission is the dominant X-ray emitting mechanism in young pre-main sequence stars.

1.4.4 Solar-like coronal X-ray emission

T Tauri stars exhibit enhanced solar-like coronal activity. The X-ray emission is most likely to originate in solar-like coronal structures (see Preibisch et al. (2005); and the comprehensive reviews by Feigelson et al. (2003) and Favata & Micela (2003)). The detection of rotationally modulated X-ray emission suggests that the dominant X-ray emitting regions are confined within magnetic structures which are close to the stellar surface. Such magnetic structures are compact with length scales of less than a stellar radius. Thousands of flares were detected during COUP. The typical flaring loop lengths (a few tenths of R_*), and the temporal behaviour of flares, are comparable to those seen on the Sun and other main-sequence stars (Wolk et al. 2005). Plasma temperatures and X-ray luminosities derived for T Tauri stars are comparable to the most active main-sequence stars; in particular X-ray luminosities can be up to 10000 times larger that the solar values (Feigelson et al. 2002). Such large luminosities cannot be reproduced by filling the stellar surface with solar-like active regions, but can be explained if coronal structures have higher plasma densities. This is consistent with coronal densities derived from the modelling of individual flares (Wolk et al. 2005).

1.4.5 X-rays from CTTs and WTTs

It is now clear that accreting T Tauri stars are observed to be less active in X-rays than non-accretors (Stelzer & Neuhäuser 2001; Flaccomio et al. 2003a; Stassun et al. 2004a; Flaccomio, Micela & Sciortino 2006). This result was also found by COUP and XEST (Preibisch et al. 2005; Telleschi et al. 2007a). However, it is only in recent years that this result has become clear; previously there was apparently conflicting evidence with some studies claiming that there was no difference in X-ray luminosities between accreting and non-accreting stars, and others claiming that accreting stars were less luminous in X-rays.

Table 1.1: Summary of recent studies of large surveys of star forming regions, modified from Rebull et al. (2006).

Work	Instrument	Cluster	Range of L_X/L_{bol}[a]	Disc Indicator	Conclusions on Discs[b]	Conclusion on Rotation
Bouvier (1990)	Einstein	Taurus-Auriga	$\log L_X = 27-32$	Hα >10Å	no diff.	anti-correl.
Feigelson et al. (1993)	ROSAT/PSPC	Cham I	-2 to -5	EW(Hα)>10Å	L_X(C)<L_X(W) but no diff. within sel. eff.	no correl.
Gagne & Caillault (1994)	Einstein	ONC	-2 to -7	$H-K$, Hα	no difference	no correl.
			(-2 to -4.5)			
Damiani & Micela (1995)	Einstein	Taurus-Auriga	-3 to -5	IRAS-25	WTTS fainter	weak anti-correl. with scatter
Gagne et al. (1995)	ROSAT/HRI	ONC	-2 to -7	$\Delta(H-K) > 0.1$	L_x, L_X/L_{bol}(C)<L_X, L_X/L_{bol}(W)	no correl.
			(-2 to -5)			
Casanova et al. (1995)	ROSAT/PSPC	ρ Oph	-2 to -5	Class 0-3	L_X(embedded)$\sim L_X$(less embedded), no diff.	N/A
Neuhäuser et al. (1995)	RASS	Taurus-Auriga	-4 to -7	EW(Hα)> 5-15Å	L_X(C)<L_X(W)	correl.
					L_X(C) harder than W	
Lawson et al. (1996)	ROSAT/PSPC	Cham I	-2 to -5	Hα	no difference	N/A
Preibisch (1997)	ROSAT/PSPC	several	$\log L_X$=27-32	N/A	N/A	anti-correl.
Alcalá et al. (2000)	RASS	Orion	$\log L_X \sim 31$	N/A	N/A	no correl. for K stars
Wichmann et al. (2000)	RASS	Taurus-Auriga	-2.5 to -5	N/A	N/A	correl.
Flaccomio et al. (2000)	ROSAT/HRI	NGC 2264	-2 to -5	Hα	no difference, but C more variable	N/A
			(-2 to -4)			
Grosso et al. (2000)	ROSAT/HRI	ρ Oph	-2 to -4	ISO data	no difference	N/A
Stelzer et al. (2000)	ROSAT/PSPC	Taurus-Auriga		HBC listing W/C	L_X(C)<L_X(W) but stronger flares,	anti-correl.
					& C more variable	
Imanishi et al. (2001)	Chandra/ACIS	ρ Oph		Class 0-3	L_X/L_{bol}(Class I)<L_X/L_{bol}(Class II & III)	N/A
Stelzer & Neuhäuser (2001)	ROSAT/PSPC	Taurus-Auriga	-3 to -6	EW(Hα)> 10Å	L_X(C)<L_X(W)	correl.
Preibisch & Zinnecker (2002)	Chandra/ACIS	IC 348	-2 to -6	EW(Hα)$\geq$ 10Å,	L_X(C)<L_X(W), but likely to be sel. eff.	N/A
			(-2 to -4.5)	$\Delta(K-L) > 0.17$	(goes away for $\Delta(K-L)$	
Feigelson et al. (2002, 2003)	Chandra/ACIS	Orion (ONC)	-2.5 to -6	$\Delta(I-K) > 0.3$	no difference	weak correl.
Getman et al. (2002)	Chandra/ACIS	NGC 1333		JHK	no difference	N/A
Tsujimoto et al. (2002)	Chandra/ACIS	OMC-2, OMC-3		Class 0-3	kT of C higher than W, but poss. sel. eff.	N/A
Flaccomio et al. (2003a)	ROSAT/HRI	NGC 2264,	-2 to -7.8	$\Delta(I-K) > 0.8$	L_X, L_X/L_{bol}(C)<L_X, L_X/L_{bol}(W)	N/A
		Cham I	(-2 to -5)			
Flaccomio et al. (2003b)	Chandra/HRC	ONC	-2 to -7.8	EW(Ca II)> 1Å	L_X, L_X/L_{bol}(C)<L_X, L_X/L_{bol}(W)	no correl.; stars with P high L_X
			(-2 to -5)			
Stassun et al. (2004a)	Chandra/ACIS	ONC	-2 to -6	EW(Ca II)> 1Å	L_X, L_X/L_{bol}(C)<L_X, L_X/L_{bol}(W)	$\log L_X/L_{bol}$ correl. with P, but not
						$v \sin i$; stars with P high L_X
Feigelson & Lawson (2004)	Chandra/ACIS	Cham I	L_x=28-31	various	L_X(C)<L_X(W) (slightly)	N/A
Preibisch (2004)	XMM/EPIC	Serpens	~ -3	literature	Class I more variable than Class II+III	N/A
Ozawa et al. (2005)	XMM/EPIC	ρ Oph	-2 to -5	literature	Class I higher T, absorp. than II+III	N/A
Preibisch et al. (2005)	Chandra/ACIS	ONC (COUP)	-1 to -6	$\Delta(I-K)$,	accretors less active	weak correl.
				$\Delta(K-L)$, EW(Ca II)		

[a]Value in parentheses are for the low-mass stars in the sample.

[b]"C"= CTTs; "W" = WTTs.

Results from X-ray surveys of various star forming regions are presented in Table 1.1, which is reproduced from Rebull et al. (2006). Early studies of star forming regions showed conflicting results, with Feigelson et al. (1993), Gagne, Caillault & Stauffer (1995), Casanova et al. (1995), Lawson, Feigelson & Huenemoerder (1996) and Preibisch & Zinnecker (2002) reporting that there were no significant differences between the X-ray luminosity functions (XLFs - the cumulative distribution of L_X values; see Fig. 1.11) of CTTs and WTTs. However, other studies such as that of Taurus-Auriga by Stelzer & Neuhäuser (2001) found that WTTs were stronger X-ray emitters than CTTs. There was even conflicting results between observations of the same star forming region taken with the same X-ray satellite! Feigelson et al. (2003) found no difference in X-ray activity between stars in the Orion Nebula Cluster with and without discs, whilst Flaccomio, Micela & Sciortino (2003b) argued that their Chandra observations revealed that accreting stars were less active in X-rays than non-accretors. The reasons for the different conclusions arose from how stars were classified as CTTs or WTTs, and also to a lesser extent, selection effects. Some studies used the strength of the Hα or CaII emission lines to identify CTTs, whereas other studies used the presence or absence of excess IR emission (see Table 1.1 for a summary). However, the different indicators actually measure different things. Hα or CaII emission indicates that accretion is taking place; excess IR emission indicates the presence of a disc. In this sense it is perhaps better to think of T Tauri stars as accretors or non-accretors, rather than as classical or weak-line. Clearly a disc is a necessary requirement for accretion to take place, however, simply having a disc does not mean that accretion is taking place. Many stars show evidence for circumstellar discs without evidence for accretion (e.g. Lada et al. 2006). Therefore studies which relied solely on the presence discs, determined from excess IR emission, as being indicative of a CTTs, misclassified some stars as accretors. Some stars, for whatever reason, are not actively accreting from their discs. Furthermore, the issue of searching for differences in the X-ray emission of CTTs (actively accret-

ing stars) and WTTs (non-accreting stars) is affected by selection effects. This arises depending on whether the sample of stars has been chosen using X-ray or optical data. Samples chosen optically, by e.g. the equivalent width of the Hα line, are likely to more complete for CTTs and incomplete for WTTs. This arises as CTTs are easy to identify optically due to the strength of their Hα emission, even if they are very faint, whereas WTTs of the same brightness are much harder to identify (see e.g. Preibisch & Zinnecker 2002). The opposite is true of X-ray selected samples, as many more WTTs have been found through X-ray observations (Neuhäuser 1997).

Large surveys such as COUP provide a statistically complete sample of the X-ray luminosities for all optically visible stars in a particular region. Thus such datasets do not suffer from selection bias. It is now clear that stars which show evidence for accretion are observed to be less luminous in X-rays than those which are not accreting (Stelzer & Neuhäuser 2001; Flaccomio et al. 2003b; Stassun et al. 2006; Preibisch et al. 2005; Flaccomio et al. 2006; Telleschi et al. 2007a). However, the presence or absence of a disc does not affect the X-ray luminosity. Fig. 1.11 shows a cumulative distribution of the ratio of X-ray to bolometric luminosity for stars in NGC 2264 (Flaccomio et al. 2006). Accreting stars are clearly less luminous in X-rays than the non-accretors. Although the difference is small (accreting stars are typically a factor of 2-3 less luminous in X-rays than non-accretors) it has been found consistently in various star forming regions. This suppression of X-ray emission by accretion is not yet understood, although a few qualitative ideas have been put forward (for a discussion see Preibisch et al. 2005).

1.4.6 Suppression of X-ray Emission by accretion

Several ideas have been put forward to explain why accreting T Tauri stars are less active in X-rays than non-accretors. It has been suggested that the weaker

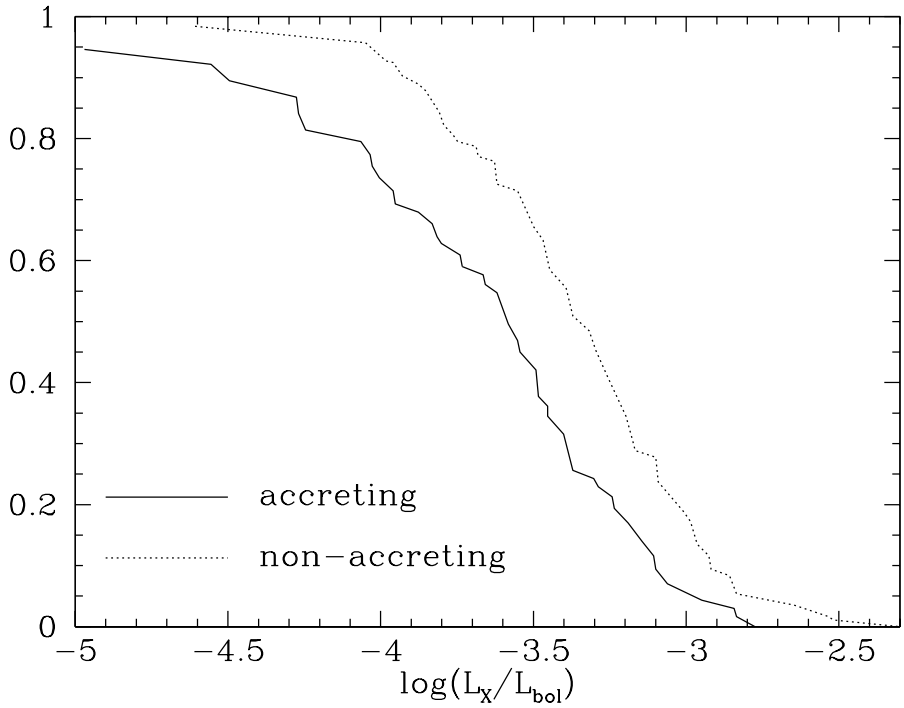

Figure 1.11: Cumulative distributions of the ratio of X-ray to bolometric luminosity for accreting and non-accreting T Tauri stars in the star forming region NGC 2264, modified from Flaccomio et al. (2006). Accreting stars are observed to be less luminous in X-rays than non-accretors, a trend which has been observed in various star forming regions, but which is not yet understood.

observed X-ray emission from CTTs could be caused by the higher extinction due to absorption by accretion discs (Stassun et al. 2004a). However, the COUP results do not support this suggestion. X-ray luminosities measured during COUP were corrected for extinction in a self-consistent way by fitting individual X-ray spectra, and it is argued that such techniques should not lead to a difference in X-ray luminosities due to extinction differences between accreting and non-accreting stars (Preibisch et al. 2005). Another idea is that accretion may alter the stellar structure, and in such a way influence the magnetic field generation process (Preibisch et al. 2005). Siess, Forestini & Bertout (1999) found suggestions from stellar evolution models that accretion reduces the efficiency of convection, a suggestion that is supported by Stassun et al. (2004b). This leads to a weaker dynamo action, and therefore a reduction in X-ray emission for accreting stars. A third suggestion is that accreting T Tauri stars are weaker X-rays emitters because of magnetic braking via the interaction with a disc. This would lead to a weaker dynamo action and therefore less X-ray emission than the non-braked WTTs. Although the lack of any rotation activity relation for T Tauri stars has ruled out this idea (Flaccomio et al. 2003a; Preibisch et al. 2005; Briggs et al. 2007). The most plausible suggestion is that the suppression of X-ray emission in accreting stars is related to the geometry of the accretion columns. Accretion columns rotating across an observer's line-of-sight may attenuate the coronal X-rays reducing the observed X-ray emission in accreting stars (Flaccomio et al. 2003a; Stassun et al. 2004a; Preibisch et al. 2005; Güdel et al. 2007b). I have recently demonstrated that this effect can provide a reduction in X-ray emission of roughly a factor of 2, in good agreement with the observations (Gregory et al. 2007). In such a way magnetic reconnection events within the underlying corona may not be able to heat the dense accreting material to a high enough temperature to emit in X-rays. This may explain why accreting stars show lower levels of X-ray activity compared with non-accreting stars. A final suggestion is that the process of mass-loading of field line with disc material reduces the

available coronal volume, making accreting stars appear to be less luminous in X-rays (Preibisch et al. 2005; Telleschi et al. 2007a).

1.5 Summary

T Tauri stars represent a key transitional period in the life of a star, between the embedded protostellar phase of spherical accretion and the main sequence stage where accretion has ceased. They are low mass pre-main sequence stars, the youngest of which accrete material from dusty circumstellar discs. They possess strong magnetic fields, of order a few kG (e.g. Johns-Krull 2007), which truncate the disc and force in-falling gas to flow along the field lines of the stellar magnetosphere. It is this crucial time, lasting only about 10 Myr, which sets the challengingly brief window in which planets may form (Hartmann et al. 1998). The duration of this period is set by the lifetime of the disc, which in turn depends on the mass accretion rate. It is therefore important to understand how the magnetic field of the central star disrupts the disc and influences the accretion process. In doing so, we gain insight into the formation of all planetary systems including our own.

Previous accretion models assume that T Tauri stars have dipolar magnetic fields. However, recent observational results demonstrate that their fields are much more complex. First, strong fields have been detected from Zeeman broadening of photospheric lines, but often with no net circular polarization signal (Valenti & Johns-Krull 2004). This indicates that the stellar surface is covered in many regions of opposite polarity. Second, the detection of rotational modulation of X-ray emission cannot be explained in the framework of dipolar magnetic fields (Flaccomio et al. 2005).

In the following Chapters I develop models of the magnetospheres of T Tauri stars using powerful numerical techniques to extrapolate 3D magnetic field struc-

tures from Zeeman-Doppler images. I am currently working with surface maps of T Tauri stars, which have recently become available (Donati et al. 2007), but to date I have used magnetograms of young main sequence stars. In Chapter 2 I describe a method for extrapolating magnetic fields from surface magnetograms, and how observed X-ray emission measures may be used to put constraints on the coronal structure of T Tauri stars. I then go on to develop a simple steady state isothermal accretion model in Chapters 3 and 4, by first considering accretion to dipolar fields, then using fields with a realistic degree of complexity. By calculating mass accretion accretion rates I demonstrate that my model produces results which are consistent with the observed correlation between accretion rate and stellar mass. In Chapter 5 I demonstrate that my model reproduces the observed rotational modulation of X-ray emission, and in Chapter 6 I argue that the largest flares detected on T Tauri stars (which have been interpreted as direct evidence for magnetic links between stars and their discs) may arise from the reconnection of large extended open field lines within the disc. I summarise the main results from my thesis work in Chapter 7 and discuss future directions for my own research and for the field of low mass star formation as a whole.

Chapter 2

Realistic Magnetic Fields

Parts of the discussion in this chapter are based on the published papers Gregory, Jardine, Simpson, Donati, 2006, MNRAS, 371, 999 and Jardine, Collier Cameron, Donati, Gregory, Wood, MNRAS, 2006, 367, 917. Sections 2.3.1 and 2.3.2 summarise the discussion contained within the latter paper.

2.1 Zeeman-Doppler imaging

Zeeman-Doppler imaging (ZDI) is a tomographic technique that uses high resolution spectropolometric observations to reconstruct stellar surface magnetic fields. It was introduced by Semel (1989) and further developed by Donati, Semel & Praderie (1989), Brown et al. (1991), Semel, Donati & Rees (1993) and Donati & Brown (1997). ZDI recovers the shape and distribution of surface magnetic regions and also, to some extent, the orientation of field lines within those magnetic regions. Surface maps have been obtained for various types of star from young rapid rotators, a wholly convective M-dwarf, a massive B-type star and a star at the red giant phase (e.g. Donati 1999; Donati et al. 2003; Donati et al. 2006a; Donati et al. 2006b). Recently ZDI has been performed on the CTTs V2129 Oph

and BP Tau, which will for the first time allow the magnetic field geometry of CTTs to be determined (Donati et al. 2007).

ZDI combines Doppler imaging with circular polarimetry, and is reviewed in detail by Hussain (1999) and Berdyugina (2005); for our purposes it is sufficient to briefly outline the technique and to highlight some limitations. ZDI is an advancement of conventional polarimetric techniques, which involve measuring the projected line-of-sight field component averaged over an entire visible hemisphere, for it allows the magnetic polarity distribution across the stellar surface to be determined. Fig. 2.1 shows an example of what can be determined from ZDI. Note that the meridional component of the field is so small it is not displayed. The magnetic field components can be determined at the stellar surface by analysing the Doppler shifts of Zeeman split spectral line profiles (see Fig. 2.2). In order for the technique to work, sufficient resolution is required in the line profiles; therefore the star must be sufficiently rapidly rotating so that rotational broadening makes a significant contribution to the line profiles

Typical circular polarisation signatures due to star spots can be extremely small. Zeeman signatures have relative amplitudes of 0.1% with noise levels of order 10^{-3} in a single line, making the polarisation signal difficult to detect (Donati, Semel & Rees 1992). Multi-line approaches have therefore been developed to increase the signal-to-noise ratio for the measured polarisation. The technique called least squares deconvolution (LSD) was developed by Semel (1989) and Semel & Li (1996) and involves combining the Stokes V profiles (the measurement of circular polarisation) for thousands of magnetically sensitive lines. Such a method significantly increases the signal-to-noise ratio.

The radial, azimuthal and meridional field components at the stellar surface are then determined by applying an inversion technique to the Stokes parameters (I, Q, U and V; which measure the intensity of the received signal in unpolarised light, the amount of linear polarisation present determined using filters at $0\,^{\circ}$

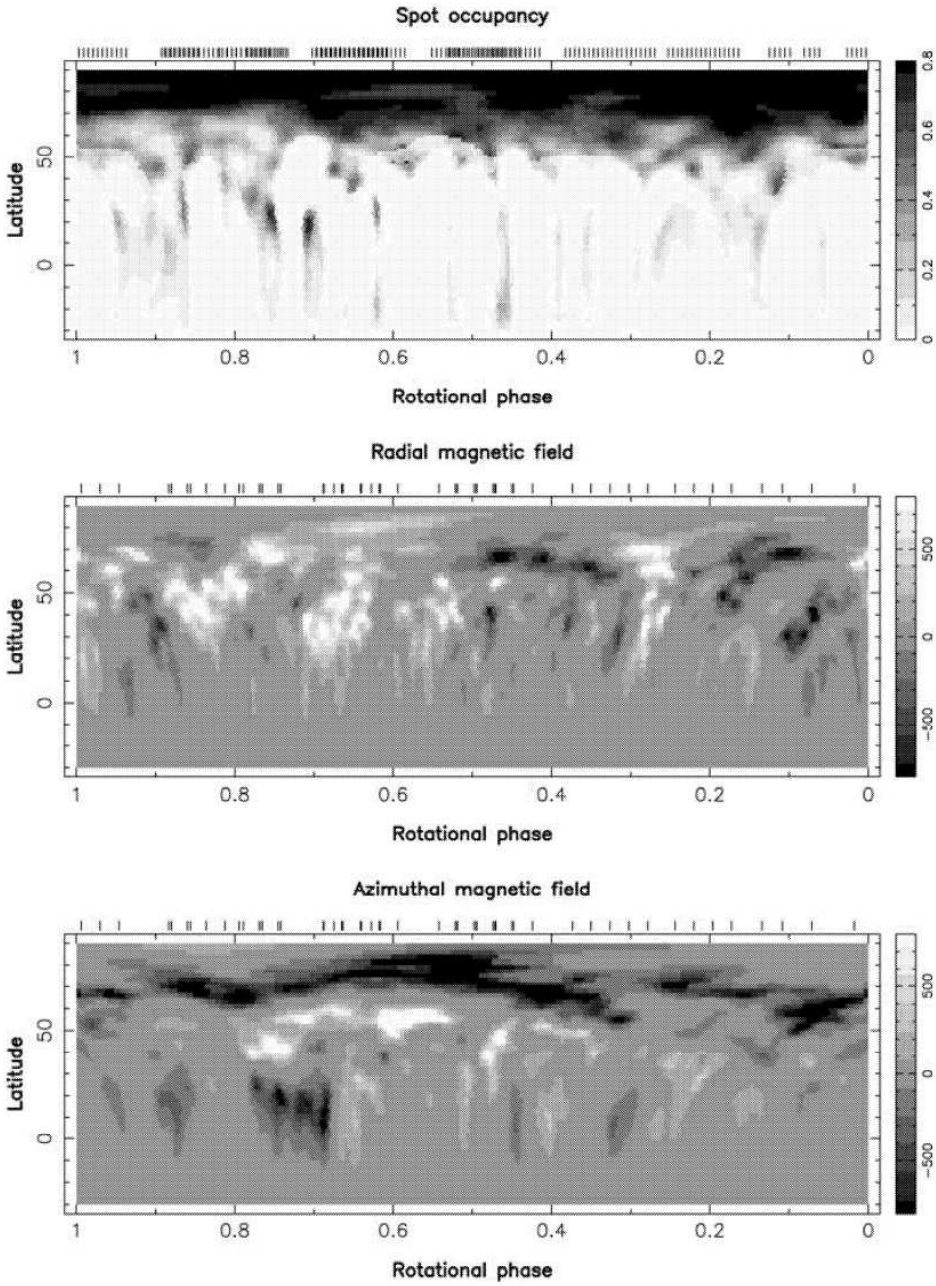

Figure 2.1: Brightness map of the K0 dwarf star AB Dor (upper panel), with the corresponding magnetic maps (lower panels) reconstructed from Zeeman-Doppler imaging. Field strengths are labelled in G, with positive values corresponding to field vectors directed outward and eastward for the radial and azimuthal maps respectively. The tick marks indicate the phases of observation; reproduced with permission from Donati et al. (2003).

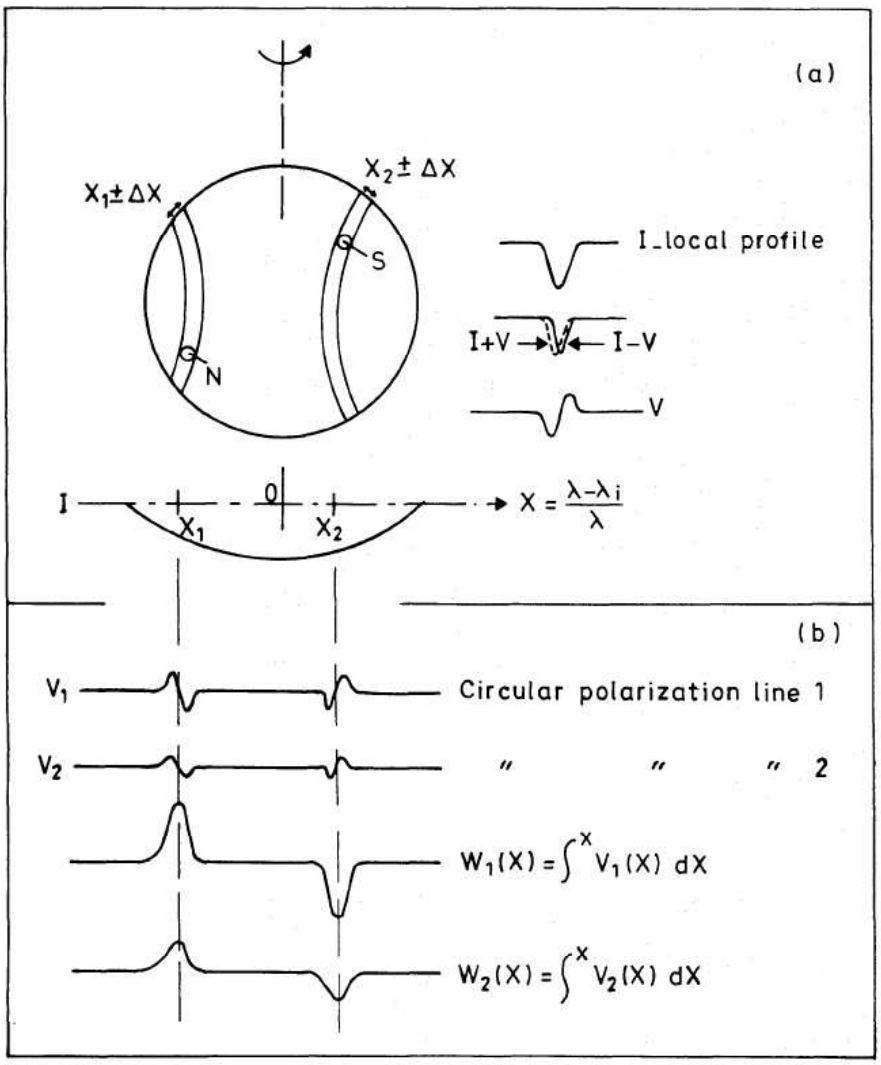

Figure 2.2: The observed circular polarisation signal (b) is the sum of opposite polarity Stokes V profiles due to spots at different Doppler shifts (a). Reproduced with permission from Semel (1989).

and 45 °, and the amount circular polarisation respectively - see Tinbergen 1996 for details and for the relationships between the different parameters). Several such inversion techniques have been developed (e.g. Brown et al. 1991; Hussain et al. 2000; Piskunov & Kochukhov 2002), although Zeeman-Doppler images are typically constructed using only the Stokes V and I profiles as the magnetic signatures detected in Stokes Q and U are too small to be of use. This lose of information can be accounted for by assuming relationships between the different field components, allowing fields to be reconstructed (e.g. Hussain, Jardine & Collier Cameron 2001).

There are several limitations to ZDI. As was noted above you need enough rotational broadening to get decent resolution in individual lines, but not as much as is required for traditional Doppler imaging. Further, as with all circular polarisation techniques, the measurements are sensitive to the line-of-sight component of the magnetic field. Circularly polarisation measurements thus suffer from flux cancellation (see the discussion in Hussain 1999), a combined effect of having a low signal from azimuthal fields and poor surface resolution at high latitudes. Hence the overall level of flux received is suppressed. ZDI therefore provides limited information about the field strength, but does provide the best method for detecting changes in field polarity. Another limitation is that one pole of the star is inclined towards the observer, permanently obscuring much of one hemisphere. Thus the polarity distribution may only be determined across the visible hemisphere, and a small portion of the other.

2.2 Magnetic fields of T Tauri stars

Magnetic field detections have now been made on many T Tauri stars, both classical and weak line. In Chapter 1 I discussed the various methods that have been used to measure surface averaged magnetic field strengths. From Zeeman

broadening measurements average surface fields of 2 to 3 kG are detected (e.g. Johns-Krull et al. 1999b, 2004). Measurements of the net polarisation signal detected in the HeI 5876Å line indicate that accretion streams impact the stellar surface in regions where the field strength may be of the order 3 to 4.5 kG (e.g. Johns-Krull et al. 1999a; Symington et al. 2005b). In contrast to this, as is discussed in Valenti & Johns-Krull (2004), often no net circular polarisation signal is detected in photospheric lines. This suggests that T Tauri stars have complex surface fields. However, such measurements do not yield information about the magnetic polarity distribution across the surface of a star. ZDI does give information about the magnetic polarity distribution, however it does not give as accurate field strength measurements at the level of the photosphere that can be gained from Zeeman broadening measurements.

ZDI, as with any technique which measures circular polarisation signals, suffers from flux cancellation from small scale field concentrations on the stellar surface of opposite polarity. On length scales smaller than a resolution element signals of opposite polarity cancel. Due to this cancellation effect the field strengths determined from Zeeman-Doppler images are always lower than those derived from Zeeman broadening measurements, which are made in unpolarised light and therefore do not suffer from cancellation effects. The field strengths in Zeeman-Doppler images are actually flux densities averaged over a surface resolution element (Donati & Collier Cameron 1997), and are therefore always lower than the values derived from broadening measurements. However, potential field extrapolations from surface magnetograms obtained through Zeeman-Doppler imaging should accurately reproduce the drop off in field strength at heights above a few tenths of a stellar radius.

2.3 Potential field extrapolations

In order to model the coronae of T Tauri stars something must be assumed about the form of their magnetic fields. Observations suggest that their fields are compact and inhomogeneous and may vary not only with time on each star, but also from one star to the next. To capture this behaviour, we use as examples the field structures of two different main sequence stars, LQ Hya and AB Dor determined using Zeeman-Doppler imaging (Donati & Collier Cameron 1997; Donati et al. 1997; Donati 1999; Donati et al. 1999; Donati et al. 2003; McIvor et al. 2003; McIvor et al. 2004). By using both stars, we can assess the degree to which variations in the detailed structure of a star's corona may affect its X-ray emission, and ultimately the accretion process. We extrapolate stellar magnetic fields by assuming that the field is potential. Using the field structures of LQ Hya and AB Dor as examples we can adjust the stellar parameters (mass, radius and rotation period) to construct a simple model of a CTTs, surrounded by a thin accretion disc.

The method for extrapolating magnetic fields follows that employed by Jardine, Collier Cameron & Donati (2002a). Assuming the magnetic field $\boldsymbol{B}$ is potential, or current-free, then $\nabla \times \boldsymbol{B} = 0$. This condition is satisfied by writing the field in terms of a scalar flux function Ψ, such that $\boldsymbol{B} = -\nabla\Psi$. Thus in order to ensure that the field is divergence-free ($\nabla \cdot \boldsymbol{B} = 0$), Ψ must satisfy Laplace's equation, $\nabla^2\Psi = 0$; the solution of which is a linear combination of spherical harmonics,

$$\Psi = \sum_{l=1}^{N} \sum_{m=-l}^{l} \left[a_{lm} r^{l} + b_{lm} r^{-(l+1)}\right] P_{lm}(\theta) \mathrm{e}^{\mathrm{i}m\phi}, \tag{2.1}$$

where P_{lm} denote the associated Legendre functions. It then follows that the magnetic field components at any point (r, θ, ϕ) are,

$$B_r = -\frac{\partial \Psi}{\partial r} = -\sum_{l=1}^{N} \sum_{m=-l}^{l} [l a_{lm} r^{l-1} - (l+1) b_{lm} r^{-(l+2)}] P_{lm}(\theta) \mathrm{e}^{\mathrm{i}m\phi} \tag{2.2}$$

$$B_\theta = -\frac{1}{r}\frac{\partial \Psi}{\partial \theta} = -\sum_{l=1}^{N}\sum_{m=-l}^{l}[a_{lm}r^{l-1} + b_{lm}r^{-(l+2)}]\frac{d}{d\theta}P_{lm}(\theta)\mathrm{e}^{\mathrm{i}m\phi} \tag{2.3}$$

$$B_\phi = -\frac{1}{r\sin\theta}\frac{\partial \Psi}{\partial \phi} = -\sum_{l=1}^{N}\sum_{m=-l}^{l}[a_{lm}r^{l-1} + b_{lm}r^{-(l+2)}]\frac{P_{lm}(\theta)}{\sin\theta}\mathrm{i}m\mathrm{e}^{\mathrm{i}m\phi}. \tag{2.4}$$

The coefficients a_{lm} and b_{lm} are determined from the radial field at the stellar surface obtained from Zeeman-Doppler maps and also by assuming that at some height R_s above the surface (known as the source surface) the field becomes radial and hence $B_\theta(R_s) = 0$, emulating the effect of a corona blowing open field lines to form a stellar wind (Altschuler & Newkirk 1969). In order to extrapolate the field we use a modified version of a code originally developed by van Ballegooijen, Cartledge & Priest (1998).

2.3.1 Coronal extent

We determine the maximum possible extent of the corona (which is the extent of the source surface) by determining the maximum radius at which a magnetic field could contain the coronal gas. Since a dipole field falls off with radius most slowly, we use this to set the source surface. For a given surface magnetogram we consider a dipole field that has the same average field strength. We then calculate the hydrostatic pressure along each field line. For an isothermal corona and assuming that the plasma along the field is in hydrostatic equilibrium then,

$$p = p_0 \exp\left(\frac{1}{c_s^2}\oint_s g_s ds\right), \tag{2.5}$$

where c_s is the isothermal sound speed and g_s the component of the effective gravity along the field line such that, $g_s = \boldsymbol{g}\cdot\boldsymbol{B}/|\boldsymbol{B}|$, p_0 is the gas pressure at a field line foot point and p the pressure at some point along the field line. The effective gravity in spherical coordinates for a star with rotation rate ω is,

$$\boldsymbol{g}\,(r,\theta,\phi) = \left(-\frac{GM_*}{r^2} + \omega^2 r\sin^2\theta, \omega^2 r\sin\theta\cos\theta, 0\right). \tag{2.6}$$

We can then calculate how the plasma β, the ratio of gas to magnetic pressure, changes along each field line. If at any point along a field line $\beta > 1$ then we assume that the field line is blown open. This effect is incorporated into the model by setting the coronal (gas) pressure to zero whenever it exceeds the magnetic pressure ($\beta > 1$). We also set the coronal pressure to zero for open field lines, which have one foot point on the star and one at infinity. The gas pressure, and therefore the plasma β, is dependent upon the choice of p_0 which is a free parameter of the model. Jardine et al. (2006) provide a detailed explanation of how p_0, the coronal base (gas) pressure, can be scaled to the magnetic pressure at a field line foot point. We assume that the base pressure is proportional to the magnetic pressure, $p_0 = KB_0^2$, a technique which has been used successfully to calculate mean coronal densities and X-ray emission measures for the Sun and other main sequence stars (Jardine et al. 2002a,b). By varying the constant K we can raise or lower the overall gas pressure along field line loops. If the value of K is large many field lines would be blown open and the corona would be compact, whilst if the value of K is small then the magnetic field is able to contain more of the coronal gas. The extent of the corona therefore depends both on the value of K and also on B_0 which is determined directly from surface magnetograms. For an observed surface magnetogram the base magnetic pressure B_0 varies across the stellar surface, and as such so does the base pressure p_0 at field line foot points. By considering stars from the COUP dataset Jardine et al. (2006) obtain the value of K which results in the best fit to observed X-ray emission measures, for a given surface magnetogram. Below it is discussed in detail how the values of K may be calculated, by first considering how X-ray emission measures can be estimated. For a prescribed value of K we then make a conservative estimate of the size of a star's corona by calculating the largest radial distance at which a dipole field line would remain closed, which we refer to as the *source surface* R_s.

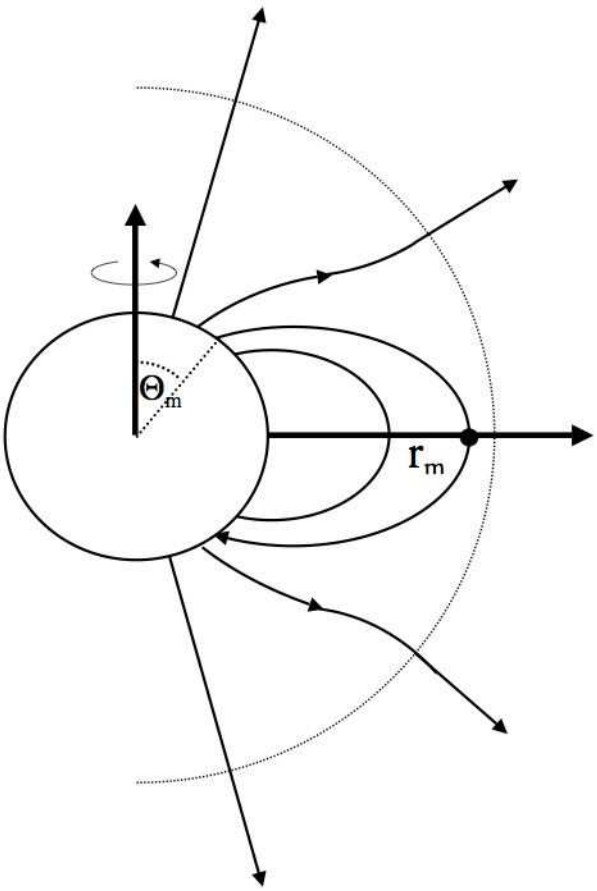

Figure 2.3: A dipole magnetic field with a source surface (the dotted line). The field is distorted by the pressure of the hot coronal gas trapped on field lines, which are forced open by the gas pressure beyond the radius of the source surface. An example is shown of the last closed field line that intersects the equatorial plane at a radial distance of r_m and emerges from the stellar surface at a co-latitude of Θ_m. If the coronal temperature and hence pressure is increased, or the stellar field strength is decreased, then r_m moves inwards and the angle Θ_m increases. As a result the fraction of the stellar surface that is covered in closed field capable of confining X-ray emitting plasma decreases; reproduced from Jardine et al. (2006).

We first consider the case of a dipolar magnetic field (see Fig. 2.3) for which

$$\boldsymbol{B} = (B_r, B_\theta, B_\phi) = \left(\frac{2\mu}{r^3}\cos\theta, \frac{\mu}{r^3}\sin\theta, 0\right). \tag{2.7}$$

The path of the field line may be described by

$$\frac{B_r}{dr} = \frac{B_\theta}{rd\theta} = \frac{B_\phi}{r\sin\theta d\phi}, \tag{2.8}$$

from which an expression for the flux function Ψ can be established,

$$\Psi = \frac{\sin^2\theta}{r}, \tag{2.9}$$

which is a constant denoting different field lines. Different values of Ψ correspond to different field lines. The gas pressure at the foot point of the field line p_0 is a free parameter of this model, which we choose to scale to the magnetic pressure. At the base of field lines $p_0 = KB_0^2$ where $B_0 =< |B| >$ is the average surface field strength and K is a constant that is the same for every field line. The value of K is crucial in controlling the extent of the corona, and hence also the X-ray emission measure and coronal density. If the value of K is small then the corona is large, whilst for large values of K the corona will be more compact, with the increased gas pressure overcoming the magnetic field closer to the stellar surface. Beginning with (2.5) we can derive an expression for the variation of X-ray emission measure with radial distance from the star. If we scale all distances to a stellar radius, and make use of the metric of spherical polars to convert from ds to dr, then equations (2.9), (2.7) and (2.6) can be combined to re-express (2.5) as,

$$p(r,\theta) = p_*(1,\theta)\exp\left[\Phi_g\left(\frac{1}{r}-1\right) + \Phi_c\sin^2\theta(r^2-1)\right]. \tag{2.10}$$

$p_*(1,\theta)$ is the pressure distribution across the stellar surface and

$$\Phi_g = \frac{GM_*/R_*}{k_BT/m} = \frac{GM_*}{R_*c_s^2} \tag{2.11}$$

$$\Phi_c = \frac{\omega^2R_*^2/2}{k_BT/m} = \frac{1}{2}\left(\frac{\omega R_*}{c_s}\right)^2 \tag{2.12}$$

are the surface ratios of gravitational and centrifugal energies to the thermal energy. The emission measure $EM = \int n_e^2 dV$ is then

$$\begin{aligned} EM &= \frac{4\pi R_*^3}{(k_B T)^2} \\ & \int_{\theta_m}^{\pi/2} p_*^2(1,\theta) \exp\left[-2\Phi_c \cos^2\theta (r^2-1)\right] \sin\theta d\theta \\ & \int_1^{r_m} r^2 \exp\left[2\Phi_g\left(\frac{1}{r}-1\right) + 2\Phi_c(r^2-1)\right] dr. \end{aligned} \tag{2.13}$$

With the substitution $\mu = \cos\theta$ such that $\mu_m = \cos\theta_m = (1 - r/r_m)^{1/2}$, the θ-integral can be written as

$$\int_0^{\mu_m} p_*^2(1,\theta) \exp\left[-2\Phi_c \mu^2 (r^2-1)\right] d\mu \tag{2.14}$$

which, on using the substitution $t = [2\Phi_c(r^2-1)]^{1/2}\mu$, gives

$$\frac{1}{[2\Phi_c(r^2-1)]^{1/2}} \int_0^{t_m} p_*^2(1,\theta) e^{-t^2} dt \tag{2.15}$$

where $t_m = [2\Phi_c(r^2-1)]^{1/2}[1 - r/r_m]^{1/2}$. Assuming that the pressure is uniform over the stellar surface we obtain the following expression for the emission measure as a function of r:

$$\begin{aligned} EM(r) &= \sqrt{\frac{2\pi^3}{\Phi_c}} \frac{R_*^3 p_*^2}{(k_B T)^2} \\ & \int_1^{r_m} \frac{r^2}{(r^2-1)^{1/2}} \mathrm{erf}\left[2\Phi_c(r^2-1)\left(1-\frac{r}{r_m}\right)\right]^{1/2} \\ & \exp\left[2\Phi_g\left(\frac{1}{r}-1\right) + 2\Phi_c(r^2-1)\right] dr. \end{aligned} \tag{2.16}$$

The total observed X-ray emission measure accounts for the contributions from each emitting region projected onto the observer's line-of-sight. In a similar way an expression for the emission measure weighted density $\bar{n}_e(r) = \int n_e^3 dV / \int n_e^2 dV$ can be obtained,

$$\bar{n}_e(r) = \frac{1}{EM(r)} \sqrt{\frac{\pi^3}{3\Phi_c}} \frac{2R_*^3 p_*^3}{(k_B T)^3} \tag{2.17}$$

$$\int_1^{r_m} \frac{r^2}{(r^2-1)^{1/2}} \mathrm{erf}\left[3\Phi_c(r^2-1)\left(1-\frac{r}{r_m}\right)\right]^{1/2}$$
$$\exp\left[3\Phi_g\left(\frac{1}{r}-1\right)+3\Phi_c(r^2-1)\right]dr$$

where I remind the reader that all distances r have been scaled to a stellar radius.

For each value of K we can determine the maximum radial extent of the last closed field line by calculating the radius at which the gas pressure overcomes the magnetic pressure. If the field strength is decreased, or if the coronal temperature is increased, then this radius also decreases. The COUP data set provides estimates of stellar masses, radii, rotation periods, and from a two-temperature fit to X-ray spectra, X-ray emission measures and coronal temperatures (Getman et al. 2005). All that remains to be constrained is the base gas and magnetic pressures. We have chosen to scale the gas pressure at field line foot points to the magnetic pressure, as this gives good agreement between predicted and observed emission measures and coronal densities for the Sun and other rapidly rotating main sequence stars (Jardine et al. 2002a,b). By comparing the calculated X-ray emission measures with the observed values from COUP we can determine the best values of p_0 and B_0 to use. For the N stars in the COUP database, and for particular combinations of p_0 and B_0 we calculate,

$$D = \sum_{i=1}^{N} \frac{(\log(EM_{\mathrm{obs,i}}) - \log(EM_{\mathrm{calc,i}}))^2}{\sigma_i^2}, \tag{2.18}$$

where the σ_i are the errors in the $\log(EM_{\mathrm{obs,i}})$ values. Figs. 2.4 and 2.5 show contours of D for a range of values of (p_0, B_0), with Table 2.1 showing the values which give the best fit to the COUP data; more details and in-depth discussion can be found in Jardine et al. (2006).

Once the values of p_0 and B_0 which give the best fit to the observed X-ray emission measures have been obtained we calculate the coronal extent relative to the position of the corotation radius. Fig. 2.6 is a plot of this ratio as a function

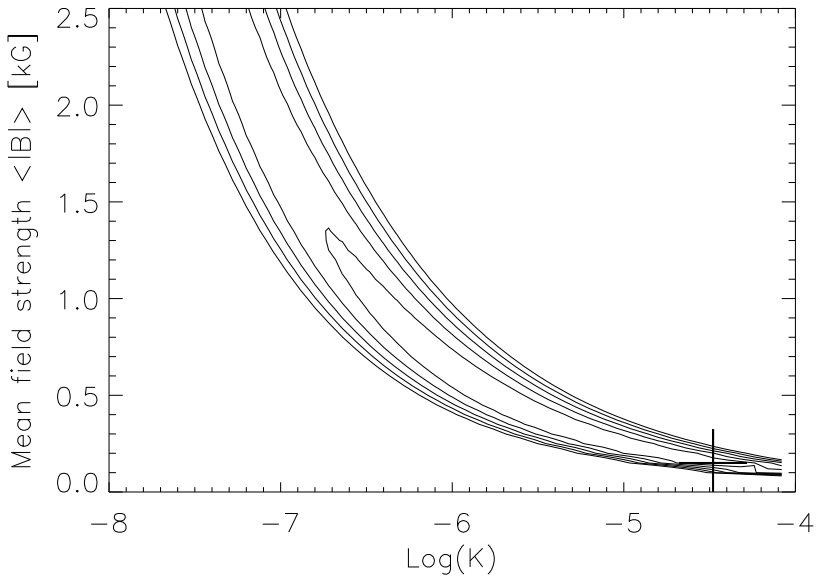

Figure 2.4: Contours of D (a measure of the goodness of fit to the COUP emission measures) as a function of the average value of the magnitude of the surface field strength and the constant of proportionality K which determines the pressure p_0 at the base of the corona since $p_0 = KB_0^2$. The cross marks the position of the minimum value of D. The plot is shown for models of the higher temperature emission measures. A plot for the lower temperature emission measures is qualitatively similar; from Jardine et al. (2006).

Table 2.1: The values of the average field strength $B_0 =< |B| >$ at the base of the corona and the corresponding gas pressure $p_0 = KB_0^2$ that give the best fit to the observed emission measures from the COUP sample, for a dipolar magnetic field; from Jardine et al. (2006).

	Passive disc		Active Disc	
T	*High*	*Low*	*High*	*Low*
$< \|B\| >$ [G]	100	50	150	50
p_0 [dyne cm^{-2}]	1.9	1.2	7.5	1.4

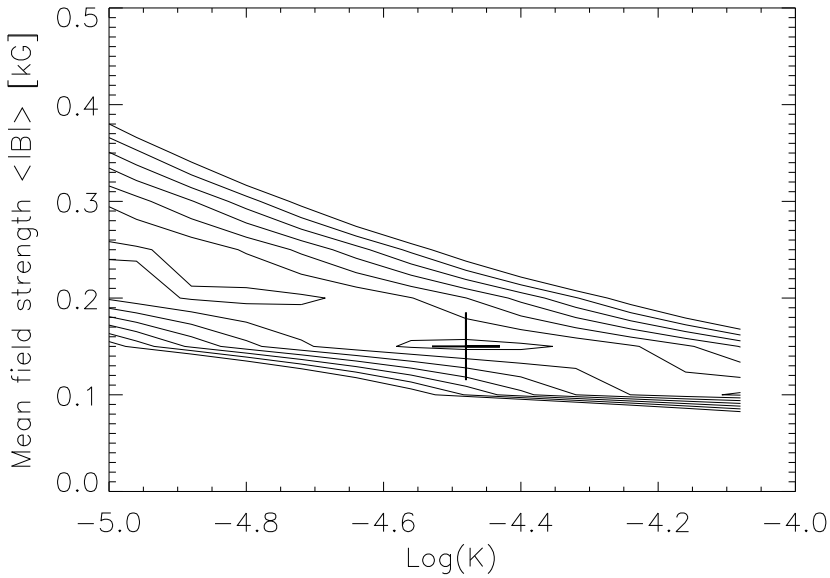

Figure 2.5: As Fig. 2.4 but for a smaller range of $\log(K)$ values, to illustrate in greater detail the region around the minimum value of D, from Jardine et al. (2006).

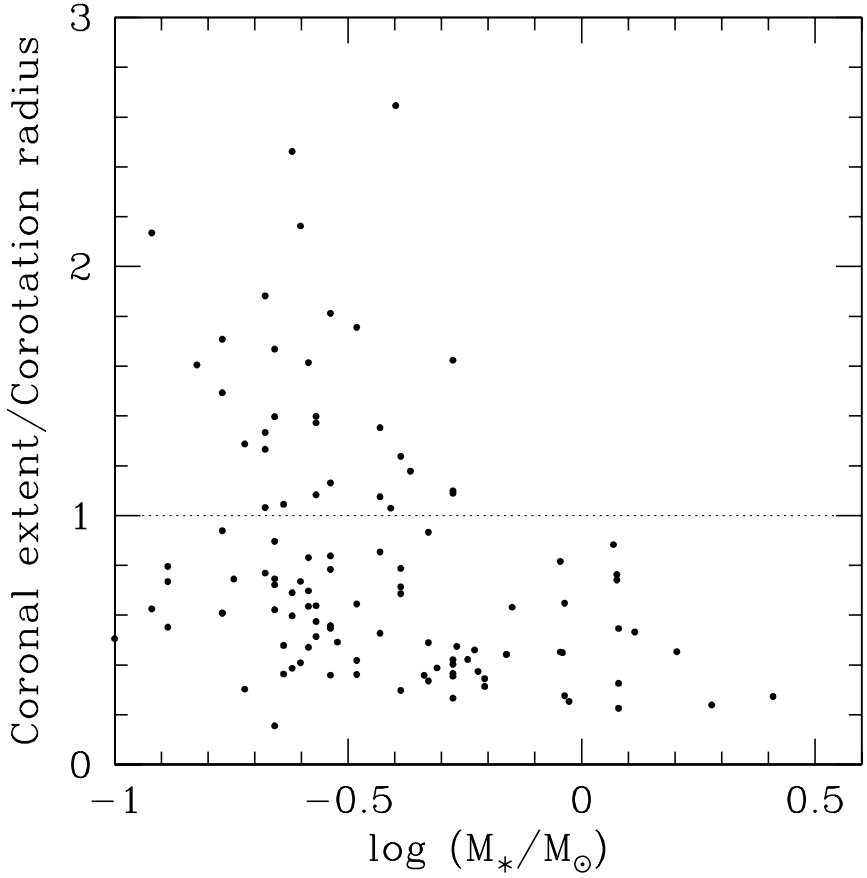

Figure 2.6: Coronal extent (in units of the Keplerian corotation radius) as a function of stellar mass for stars in the COUP sample. For stars where the natural coronal extent is beyond the corotation radius, the coronal extent is instead set to be the corotation radius.

of stellar mass. None of the more massive stars have coronae which naturally extend to beyond the corotation radius. This is because more massive stars have large surface gravities and therefore small pressure scale heights. As such they tend to have compact coronae well within the corotation radius (of course the position of corotation itself is larger the more massive the star). In contrast to this some of the lower mass stars have coronae whose natural extent is well beyond the corotation radius. The coronae of such stars are therefore likely to be affected by the presence of circumstellar discs.

2.3.2 Coronal stripping

We have not yet considered how a circumstellar disc would affect the structure of the corona. Above we discussed the situation where each star had a *passive* disc, where the coronae extends out until the field is no longer strong enough to contain the coronal gas. When the gas pressure exceeds the magnetic pressure the field is opened up and the gas released into the stellar wind. For some of the lower mass stars, however, the presence of a disc may significantly alter the structure of their coronae. Many lower mass stars have natural coronal extents which are beyond the corotation radius (see Fig. 2.6). Field lines which pass through the disc beyond corotation will be sheared open due to the differential rotation between the star and the disc (e.g. Lynden-Bell & Boily 1994; Lovelace, Romanova & Bisnovatyi-Kogan 1995). We refer to this as an *active* disc. This process reduces the overall X-ray emission measure, as closed field lines which would have otherwise contained the hot coronal gas, are converted to open field lines - reducing the size of the X-ray emitting corona. Lower mass stars, whose coronae are naturally more extended due their smaller surface gravities and therefore larger pressure scale heights, are therefore more affected by this coronal stripping mechanism. In contrast to this, higher mass stars with their higher surface gravities and therefore smaller pressure scale heights, have compact coronae that typically do not

extend to beyond the corotation radius. The X-ray emission from such stars is therefore less affected by the presence of a disc.

We therefore consider the maximum extent of a stars corona to be either its natural height limited only by the gas pressure, provided this is within the corotation radius. Or, for stars whose natural coronal extent would be beyond corotation, we set the coronal extent to be the corotation radius itself. For each set of stellar parameters from the COUP data set we calculate the X-ray emission measure of the coronal gas within each stellar corona for a range of mean magnetic field strengths and base gas pressures of the corona. Table 2.1 lists the values of the base gas and magnetic pressures, determined by Jardine et al. (2006), which yield the minimum value of D (as defined by (2.18)). Jardine et al. (2006) provide a discussion about the extent of T Tauri coronae relative to corotation radii, and demonstrate that an active disc is required to give the best fit to the observed increase in X-ray emission measure with stellar mass. It is also worth noting that Safier (1998) criticises current magnetospheric accretion models for not including the effects of a stellar corona. He argues that the inclusion of a realistic corona blows open most of the closed field with the eventual net effect being that the disc would extend closer to the star. However, in our model there are open field lines threading the disc at corotation and it is therefore reasonable to assume that they are able to carry accretion flows.

2.3.3 Realistic magnetic fields

In Chapter 1 I discussed the observations which demonstrate that T Tauri stars do not have simple dipolar magnetic fields. The detection of rotationally modulated X-ray emission from many of the stars in the COUP data set indicates that their fields are more complex, with the dominant X-ray emitting regions confined within compact magnetic structures (Flaccomio et al. 2005). Often no net circular polarisation signal is detected in photospheric absorption lines, suggesting that

the stellar surface is covered in many regions with opposite polarity (e.g. Valenti & Johns-Krull 2004). Together these results suggest that the magnetic field close to the surface of a CTTs is very complex, and non-dipolar. The detection of strong polarisation in the HeI 5876Å emission line, however, suggests that the large scale field is well-ordered. We therefore explore the impact on accretion models that magnetic fields with a realistic degree of complexity might have.

In the absence of magnetic surface maps of CTTs (which have only recently become available; Donati et al. 2007) we extrapolate magnetic fields from surface magnetograms of LQ Hya and AB Dor, using the techniques discussed above. We can estimate the extent of the corona for young rapid rotators such as AB Dor from the observed location of slingshot prominences, however we do not have this option for models of T Tauri stars. To determine the coronal extent for T Tauri stars (the radius of the source surface) we determine the largest radius at which a dipolar field (of the same average field strength) would remain closed. This gives the most extended possible corona since of all the multipolar field components the dipole component drops most slowly with radius. In such a way the source surface is set to be the maximum possible radial extent of a dipolar field line. If this radius exceeds the corotation radius then field lines threading the disc beyond R_{co} would be quickly wrapped up and torn open. In such cases we instead set the maximum coronal extent to be the corotation radius.

We again assume that the gas pressure at field line foot points scales with the magnetic pressure. However, from the surface magnetograms the field strength varies across the stellar surface, and therefore so does the base magnetic pressure and consequently the gas pressure. We determine the gas pressure at every point by calculating the path of the field line through that point and by assuming that the plasma along the field line is in hydrostatic equilibrium. Again the free parameter is the constant of proportionality K which when varied will increase or decrease the overall gas pressure everywhere within the corona. If at any point

along a field line the gas pressure exceeds the magnetic pressure then that field line should have been opened up and so the pressure is set to be zero. For the dipole field, we chose for simplicity to have a uniform p_0 based on the average field strength $< |B| >$. However for the complex fields the gas pressure changes across the stellar surface. In Table 2.2 therefore it should be noted that the value of $p_0 = K < |B| >^2$ is just the value based on the average value of $< |B| >$. For each given field structure we again determine which value of K gives the best fit to the X-ray emission measure from the COUP survey. It has been demonstrated by Jardine et al. (2006) that this model can reproduce the observed increase in X-ray emission with stellar mass.

The initial field extrapolation yields regions of open and closed field lines. Of these, some intersect the disc and may be accreting. The disc is assumed to occupy a range of latitudes extending 10° above and below the equator. The location of the inner edge of the disc is allowed to adjust locally to the structure of the magnetic field at each latitude and longitude. For closed field lines which do not intersect the disc we calculate the X-ray emission measure in the same way as discussed above. To determine if a field line can accrete we find where it threads the disc and calculate if the effective gravity along the path of the field line points inwards, towards the star. From this subset of field lines we select those which have $\beta < 1$ along their length. In other words, for any given azimuthal element we assume that accretion can occur along the first field line within the corotation radius which is able to contain the coronal plasma. We assume that the loading of disc material onto the field lines is infinitely efficient, such that the first field line at any azimuth which satisfies the accretion conditions will accrete, and that field lines interior to this are shielded from the accretion flow. We also assume that the accreting field is static and is therefore not distorted by the disc or by the process of accretion. In the following chapters we consider in more detail how to determine which field lines are able to support accretion flows, in order

Table 2.2: The values of the average field strength $B_0 =< |B| >$ at the base of the corona and the corresponding gas pressure $p_0 = KB_0^2$ that give the best fit to the observed emission measures from the COUP sample, for the realistic magnetic fields; from Jardine et al. (2006).

	Passive disc		Active Disc	
T	$High$	Low	$High$	Low
$< \|B\| >$ [G]	143	143	143	143
p_0 [dyne cm^{-2}]	3.6	0.2	13.2	0.9

Table 2.3: Data for CTTs from Valenti & Johns-Krull (2004)

$Star$	$M_*(M_\odot)$	$R_*(R_\odot)$	$P_{rot}(d)$	$R_{co}(R_*)$
DF Tau	0.17	3.9	8.5	2.47
CY Tau	0.58	1.4	7.5	9.55

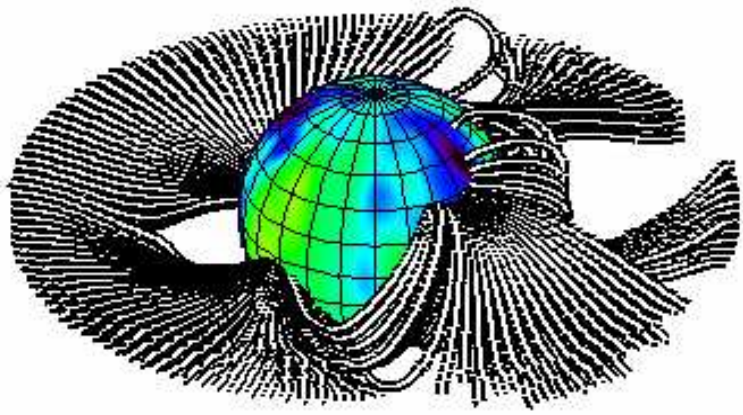

Figure 2.7: Field lines which could support accretion flows for a model of a CTTs with a field topology that resembles LQ Hya, obtained using the DF Tau parameters from Table 2.3. The stellar surface is coloured to show the strength of the radial component of the field, with red representing 1 kG and black −1 kG. Field lines have been drawn from the corotation radius. The natural extent of the corona of DF Tau, a lower mass CTTs, would be beyond corotation and therefore there is a mixture of open and closed field lines threading the disc at R_{co}; reproduced from Gregory et al. (2006a).

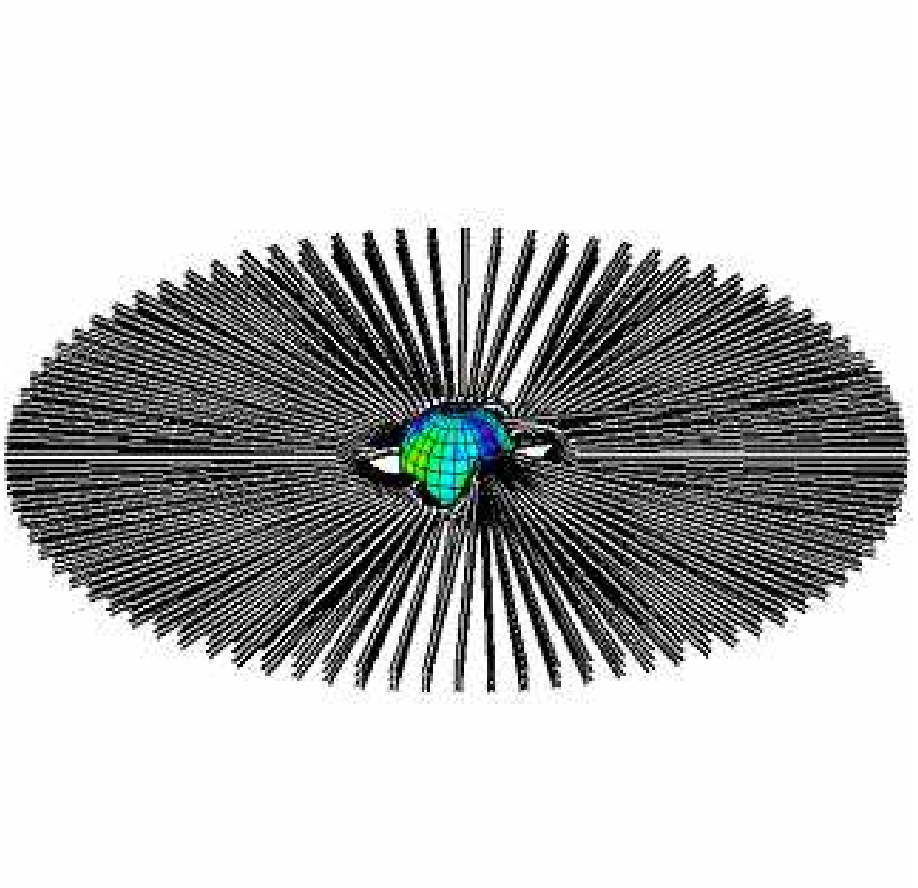

Figure 2.8: As Fig. 2.7, but with a field topology that resembles AB Dor, obtained using the CY Tau parameter from Table 2.3. The corona of CY Tau, a higher mass CTTs, is more compact than that of DF Tau and material flows along open field lines from corotation; reproduced from Gregory et al. (2006a).

to calculate mass accretion rates and accretion filling factors.

Figs. 2.7 and 2.8 show the first set of field lines which may be accreting, obtained by surrounding the field extrapolations of LQ Hya and AB Dor with a thin wedge-shaped accretion disc, with an opening angle of approximately $10\,^{\circ}$. In the following chapter we develop a model for isothermal accretion flows where material leaves the disc at a low subsonic speed, but arrives at the star with a large supersonic speed. Not all of the field lines in Figs. 2.7 and 2.8 are capable of supporting such accretion flows, and instead represent the maximum possible set of field lines which may be accreting. We assume a coronal temperature of 10 MK and obtain the gas pressure at the base of each field line as discussed above. When using the DF Tau parameters from Table 2.3, the natural extent of the corona would be beyond the corotation radius and therefore accretion occurs along a mixture of closed and open field lines from corotation. One suggestion for how accretion may proceed along open field lines is that an open field line which stretches out into the disc, may reconnect with another open field line for long enough for accretion to occur, only to be sheared open once again. This is of particular importance for the higher mass stars, such as CY Tau, where in some cases we find that the inner edge of the disc is sitting in a reservoir of radial open field lines. This may have important implications for the transfer of torques between the disc and star. However more work is needed here in order to develop models for accretion along open field lines.

The field extrapolations suggest that accretion may occur along field lines that have very different geometries. Indeed, a substantial fraction of the total mass accretion rate may be carried by open field lines. Before developing a detailed model of the mass accretion process, however, we first consider the simple case of a tilted dipole. While this is an idealisation of the true stellar field it allows us to clarify the role that the geometry of the field may have in governing the mass accretion process.

Chapter 3

Mass Accretion I: Dipole Magnetic Fields

This work has been published in Gregory, Jardine, Simpson & Donati, 2006, MNRAS, 371, 999.

3.1 Introduction

Classical T Tauri stars (CTTs) are young, low mass, pre-main sequence stars that are actively accreting from a surrounding disc which is the eventual birth-place of planets. Uchida & Shibata (1984) suggested that the magnetic field of a CTTs disrupts the inner disc. In the early 1990s several magnetospheric accretion models were developed (Königl 1991; Collier Cameron & Campbell 1993; Shu et al. 1994a) where material is lifted from the disc plane and is channelled along dipolar magnetic field lines onto the star, terminating in a shock at the photosphere. In an idealised model of a CTTs magnetic field there are closed field lines close to the star that contain the X-ray emitting corona, whilst at larger radii, there are closed field lines which thread the circumstellar disc. It is along this latter

set of field lines that accretion may proceed. There are also regions of open field which carry outflows in the form of a wind, and in some cases, as large collimated bipolar jets.

Magnetospheric accretion models assume that CTTs possess magnetic fields that are strong enough to disrupt the disc at a distance of a few stellar radii. Such strong fields have been detected in a number of systems using a variety of techniques. Average surface fields of $1-3$ kG have been detected most successfully by exploiting the Zeeman effect, both through Zeeman broadening (e.g. Johns-Krull, Valenti & Koresko 1999b) and from the circular polarisation of lines which are sensitive to the presence of a magnetic field (e.g. Johns-Krull et al. 1999a; Symington et al. 2005b; Daou, Johns-Krull & Valenti 2006). Field detections have also been made from the increase in line equivalent width (Basri, Marcy & Valenti 1992; Guenther et al. 1999) and also from electron cyclotron maser emission, a coherent emission process from mildly relativistic electrons trapped inside flux tubes close to the star (Smith et al. 2003). The mean magnetic field strengths detected so far appear to be roughly constant across all stars (Valenti & Johns-Krull 2004).

Traditionally magnetospheric accretion models have assumed the CTTs have dipolar magnetic fields. Dipole fields (or inclined dipole fields) have been used successfully to explain some of the observations of CTTs (e.g. the photopolarimetric variability of AA Tau, O'Sullivan et al. 2005), but fail to account for others. Valenti & Johns-Krull (2004) present magnetic field measurements for a number of stars, and despite detecting strong average surface fields from Zeeman broadening, often measurements of the longitudinal (line-of-sight) field component (obtained from photospheric lines) are consistent with no net circular polarisation signal. This can be interpreted as there being many regions of opposite polarity on the stellar surface, giving rise to oppositely polarised signals which cancel each other out giving a net polarisation signal of zero. This suggests

that CTTs have magnetic fields which are highly complex, particularly close to the stellar surface; however, as Valenti & Johns-Krull (2004) point out, as the higher order multipolar field components will drop off quickly with distance from the star, the dipole component may still remain dominant at the inner edge of the disc. Also their measurements of the circular polarisation of the HeI 5876Å emission line (believed to form at the base of accretion columns) are well fitted by a simple model with a single magnetic spot on the surface of the star with radially accreting field lines. This suggests that the accreting field may be well ordered, despite the surface field being complex.

The fractional surface area of a CTTs which is covered in hot spots, the accretion filling factor f_{acc}, is inferred from observations to be small; typically of order one percent (Muzerolle et al. 2003; Calvet et al. 2004; Valenti & Johns-Krull 2004; Symington et al. 2005b; Muzerolle et al. 2005). Dipolar magnetic field models predict accretion filling factors which are too large. This, combined with the polarisation results, led Johns-Krull & Gafford (2002) to generalise the Shu X-wind model (Shu et al. 1994a) to include multipolar, rather than dipolar, magnetic fields. With the assumption that the average surface field strength does not vary much from star to star the generalised Shu X-wind model predicts a correlation between the stellar and accretion parameters of the form $R_*^2 f_{acc} \propto (M_* \dot{M} P_{rot})^{1/2}$, a prediction that matches observations reasonably well.

In this Chapter I consider accretion onto an aligned, and then tilted dipole fields, in order to develop a simple steady state accretion model and to investigate how tilting the field affects the mass accretion rate, and accretion filling factors. In the next Chapter these ideas are extended by considering magnetic fields with a realistic degree of complexity and I apply the accretion model to study the correlation between mass accretion rate and stellar mass.

3.2 Accretion to a dipole

We have constructed two simple analytic models as sketched in Fig. 3.1. The first case is for a star with a dipolar field with the dipole moment $\boldsymbol{\mu}$ aligned with the stellar rotation axis $\boldsymbol{\Omega}$. In standard spherical coordinates this field may be described as,

$$\boldsymbol{B} = \left(\frac{2\mu}{r^3}\cos\theta, \frac{\mu}{r^3}\sin\theta, 0\right), \tag{3.1}$$

a scenario that allows us to model accretion flows along field lines in the star's meridional plane. If we then take this field structure and tilt it by $\pi/2$ radians such that $\boldsymbol{\mu}$ now lies in the star's equatorial plane, perpendicular to $\boldsymbol{\Omega}$, then those field lines which ran north-south in the meridional plane, now lie east-west in the equatorial plane, with,

$$\boldsymbol{B} = \left(\frac{2\mu}{r^3}\cos\phi, 0, \frac{\mu}{r^3}\sin\phi\right). \tag{3.2}$$

Throughout we shall refer to these cases as the *perpendicular dipole* for the tilted dipole field and the *aligned dipole* for the aligned dipole field. We consider steady isothermal accretion flows from a thin accretion disc oriented such that the disc normal is parallel to the stellar rotation axis. An initial sonic Mach number, $\mathcal{M}$, is prescribed to the accreting material. We then calculate the pressure and velocity profiles, relative to arbitrary initial conditions defined at the disc plane. We calculate the ratio of pressure p at each point along a field line, relative to that at the disc, p_d; and then from this we calculate how the Mach number of the flow changes along the field.

The path of a field line may be described by

$$\frac{B_r}{dr} = \frac{B_\theta}{rd\theta} = \frac{B_\phi}{r\sin\theta d\phi}. \tag{3.3}$$

For the perpendicular dipole, where $\theta = \pi/2$ for all field lines that pass through the disc, it is quickly established that,

$$\sin^2\phi = \Psi r, \tag{3.4}$$

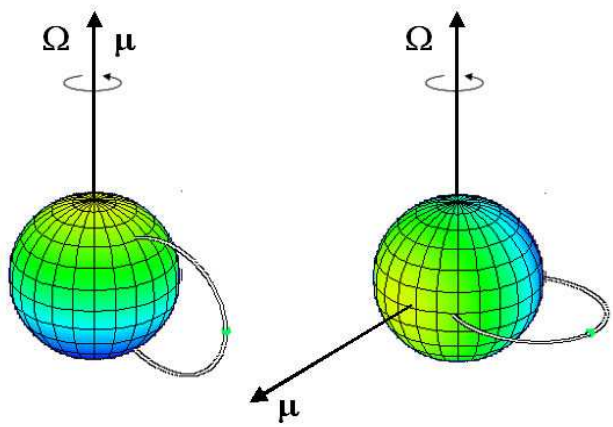

Figure 3.1: An aligned and tilted dipole field geometry. The aligned dipole (left) with a field line in the star's meridional plane, with the dipole moment $\boldsymbol{\mu}$ aligned with the stellar rotation axis $\boldsymbol{\Omega}$, and the perpendicular dipole (right) with a field line in the star's equatorial plane, with $\boldsymbol{\mu}$ perpendicular to $\boldsymbol{\Omega}$. The average surface field strength matches that considered by Jardine et al. (2006) with yellow (blue) representing the positive (negative) magnetic pole.

where Ψ is a constant along a particular field line, such that different values of Ψ correspond to different field lines. For the perpendicular dipole case, at $r = R_d$, the maximum radial extent of the field line, $\phi = \pi/2$; thus, $\Psi = 1/R_d$. Using this result the magnitude of the magnetic field at a point along a field line a distance r from the centre of the star, relative to that at the disc, may be obtained from (3.2),

$$\frac{B}{B_d} = \left(\frac{R_d}{r}\right)^3 \sqrt{\left(4 - \frac{3r}{R_d}\right)}, \tag{3.5}$$

where $B_d = B\,(r = R_d)$. An identical expression can be derived for the aligned dipole case. We determine the location of the source surface, the maximum radius at which a dipolar field line could contain a 10 MK corona, using the techniques discussed in Chapter 2.

3.2.1 Steady isothermal accretion flows

The momentum equation for a steady inviscid flow along a flux tube is

$$\rho\,(\boldsymbol{v}\cdot\nabla)\,\boldsymbol{v} = -\nabla\left(p + \frac{B^2}{8\pi}\right) + \frac{1}{4\pi}\,(\boldsymbol{B}\cdot\nabla)\,\boldsymbol{B} + \rho\boldsymbol{g}_{eff} - 2\rho\boldsymbol{\omega}\times\boldsymbol{v}, \tag{3.6}$$

where the symbols have their usual meaning with $\boldsymbol{g}_{eff}$ being the sum of the gravitational and centrifugal accelerations. In a frame of reference rotating with the the star the effective gravity is,

$$\boldsymbol{g}_{eff} = \boldsymbol{g} - \boldsymbol{\omega}\times(\boldsymbol{\omega}\times\boldsymbol{r})\,. \tag{3.7}$$

The component of the momentum equation along a field line is then,

$$\rho\frac{d}{ds}\left(\frac{v^2}{2}\right) = -\frac{dp}{ds} + \rho\boldsymbol{g}_{eff}\cdot\hat{\boldsymbol{s}}, \tag{3.8}$$

since the Coriolis term $(-2\rho\boldsymbol{\omega}\times\boldsymbol{v})$ does not contribute for flows along the field, and where $\hat{\boldsymbol{s}}(\boldsymbol{r})$ is a unit vector along the path of the field line. Throughout terms with a subscript d will denote quantities defined at the disc; for example

ρ_d, p_d, v_d and B_d are respectively the density, pressure, velocity along the field and the magnetic field strength as defined at the plane of the disc, a radial distance R_d from the centre of the star. Integrating equation (3.8) from the disc plane to some position along the field line at a distance r from the stellar centre, and using the isothermal equation of state for an ideal gas, $p = \rho c_s^2$, gives,

$$\ln\left(\frac{p}{p_d}\right) = \frac{1}{c_s^2}\left[-\frac{1}{2}\left(v^2 - v_d^2\right) + \int \boldsymbol{g}_{eff} \cdot \hat{\boldsymbol{s}} ds\right], \tag{3.9}$$

where c_s is the isothermal sound speed. If we assume that both mass and magnetic flux are conserved along each flux tube (of cross-sectional area A), then the flow must satisfy

$$\frac{d}{ds}(\rho v A) = 0 \tag{3.10}$$

$$\frac{d}{ds}(BA) = 0, \tag{3.11}$$

which may be expressed equivalently as,

$$\frac{pv}{B} = \frac{p_d v_d}{B_d} = const. \tag{3.12}$$

By combining (3.9) with (3.12) a relation for the pressure structure along an accreting field line can be established,

$$\ln\left(\frac{p}{p_d}\right) + \frac{1}{2}\mathcal{M}^2\left(\frac{p_d}{p}\frac{B}{B_d}\right)^2 - \frac{1}{2}\mathcal{M}^2 - \frac{1}{c_s^2}\int \boldsymbol{g}_{eff} \cdot \hat{\boldsymbol{s}} ds = 0, \tag{3.13}$$

and also directly from (3.12) an expression for the velocity structure,

$$\frac{v}{c_s} = \mathcal{M}\frac{p_d}{p}\frac{B}{B_d}, \tag{3.14}$$

where in both cases $\mathcal{M} = v_d/c_s$ denotes the initial sonic Mach number at which the accretion flow leaves the plane of the disc. It is then possible to find the pressure at each point along a field line, relative to the pressure at the disc (p/p_d), by finding the roots of (3.13). Once these roots have been found the velocity profile can be obtained from (3.14) by calculating how the Mach number of the flow varies as material moves from the disc to the star.

3.2.2 Pressure and velocity profiles

For the perpendicular dipole, in the star's equatorial plane, the effective gravity has only a radial component,

$$\boldsymbol{g}_{eff} = \left(-\frac{GM_*}{r^2} + \omega^2 r\right)\hat{\boldsymbol{r}}. \tag{3.15}$$

Taking the component of the effective gravity along the field, that is along a path parameterised by $\hat{\boldsymbol{s}} = \boldsymbol{B}/B$, substituting into (3.13), and using (3.5) gives an expression for the pressure structure along equatorial field lines,

$$\begin{aligned}\ln\left(\frac{p}{p_d}\right) + \frac{1}{2}\mathcal{M}^2\left(\frac{R_d}{r}\right)^6\left(4 - \frac{3r}{R_d}\right)\left(\frac{p_d}{p}\right)^2 - \frac{1}{2}\mathcal{M}^2 \\ +\Phi_g\left(\frac{1}{R_d} - \frac{1}{r}\right) + \Phi_c\left(R_d^2 - r^2\right) = 0,\end{aligned} \tag{3.16}$$

where both r and R_d are measured in units of the stellar radius R_* and Φ_g and Φ_c are the surface ratios of the gravitational and centrifugal energies to the thermal energies,

$$\Phi_g = \frac{GM_*}{R_* c_s^2} \tag{3.17}$$

$$\Phi_c = \frac{1}{2}\left(\frac{\omega R_*}{c_s}\right)^2. \tag{3.18}$$

The roots of (3.16) give the pressure at some point along a field line loop which is a radial distance r from the stellar centre.

For the aligned dipole, in the star's meridional plane, the effective gravity has both an r and θ component,

$$\boldsymbol{g}_{eff} = \left(-\frac{GM_*}{r^2} + \omega^2 r \sin^2\theta\right)\hat{\boldsymbol{r}} + \left(\omega^2 r \sin\theta\cos\theta\right)\hat{\boldsymbol{\theta}}. \tag{3.19}$$

Following an identical argument to that above it can be established that for accretion in the star's meridional plane, the pressure function (3.13) becomes,

$$\begin{aligned}\ln\left(\frac{p}{p_d}\right) + \frac{1}{2}\mathcal{M}^2\left(\frac{R_d}{r}\right)^6\left(4 - \frac{3r}{R_d}\right)\left(\frac{p_d}{p}\right)^2 - \frac{1}{2}\mathcal{M}^2 \\ +\Phi_g\left(\frac{1}{R_d} - \frac{1}{r}\right) + \Phi_c\left(R_d^2 - \frac{r^3}{R_d}\right) = 0.\end{aligned} \tag{3.20}$$

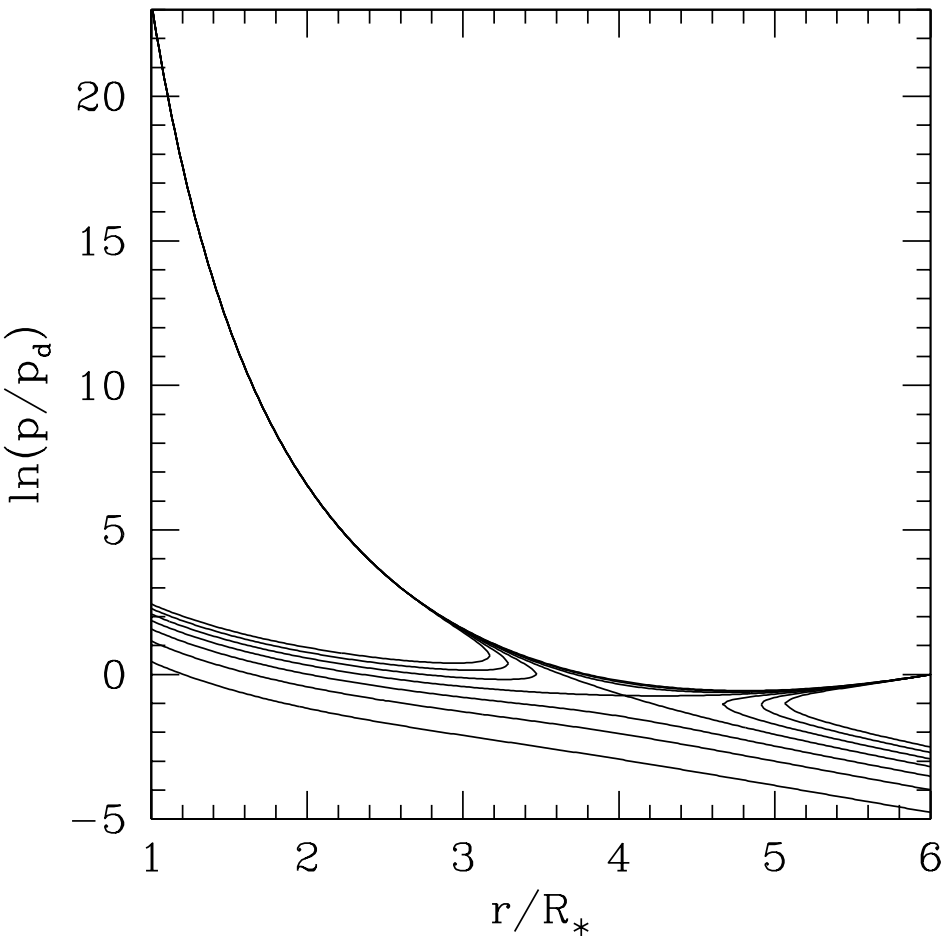

Figure 3.2: The resulting pressure profiles for accretion along equatorial dipole field lines. The inner edge of the disc is at $R_d = 6.0R_*$ which is approximately the corotation radius. Different lines represent different initial velocities.

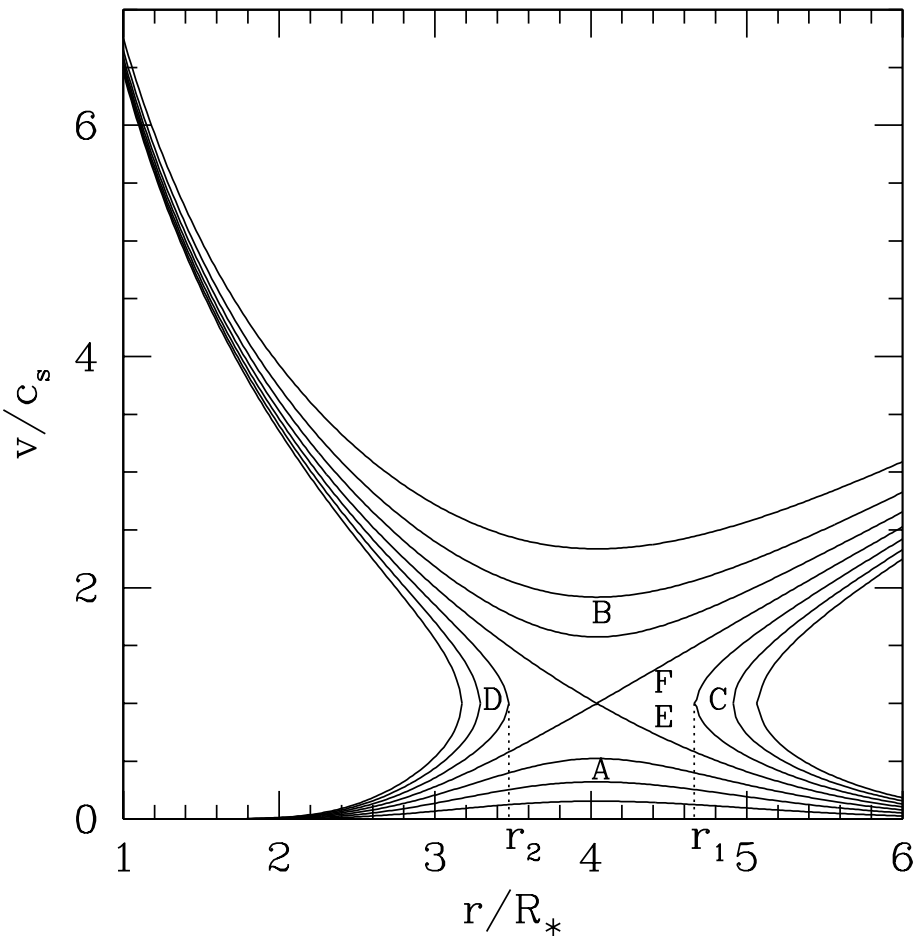

Figure 3.3: The resulting velocity profiles for accretion along equatorial dipole field lines. The inner edge of the disc is at $R_d = 6.0R_*$ which is approximately the corotation radius. Different lines represent different initial velocities.

The only difference from the perpendicular dipole is in the final term.

For a CTTs with a mass of $0.5\,\mathrm{M}_\odot$, radius $2\,\mathrm{R}_\odot$ and a rotation period of 7 d we have calculated the pressure and velocity structure along accreting dipole field lines, for a range of accretion flow temperatures, starting radii and initial sonic Mach numbers. Figs. 3.2 and 3.3 show a typical pressure and velocity profile for the perpendicular dipole, whilst those for the aligned dipole are qualitatively similar. The pressure profile shows how the ratio p/p_d, where p is the pressure along the field line and p_d the pressure at the disc, varies as the flow moves from the disc to the star (plotted logarithmically for clarity). The velocity profile shows how the Mach number of the flow changes along the field line. For different accretion flow temperatures and starting radii the resulting profiles are similar, except in a few select cases, as discussed in the next section. Figs. 3.2 and 3.3 are for an accretion flow leaving the disc at $R_d = 6.0R_*$, which is approximately the equatorial corotation radius R_{co} where,

$$R_{co} = \left(\frac{GM_*}{\omega^2}\right)^{1/3}, \tag{3.21}$$

and for an accretion flow temperature of $10^5\,\mathrm{K}$. This is at least one order of magnitude higher than what is believed to be typical for accretion in CTTs, but a higher temperature has been selected here in order to clearly illustrate the various types of solutions labelled in Fig. 3.3. At lower temperatures the form of the velocity solutions is similar.

At the critical radius r_c either the flow velocity equals the sound speed, $v = c_s$, or $dv/ds = 0$. There are several distinct velocity solutions labelled in Fig. 3.3. For very small subsonic initial Mach numbers (curve A) the flow remains subsonic all the way to the star, and for large supersonic initial Mach numbers, it remains supersonic from the disc to the star (curve B). There is also a range of initial Mach numbers (curves C) where the flow will not reach the star, and one value of $\mathcal{M}$ that results in a transonic solution where the flow leaves the

disc at a subsonic speed and accelerates hitting the star at a supersonic speed (curve E). Measurements of the widths of the redshifted absorption components of line profiles suggests that accreting material reaches the stellar surface at several hundred kms^{-1}, certainly at supersonic speeds (e.g. Edwards et al. 1994). The velocity profiles indicate that it is possible to have accretion flows which leave the disc at a low subsonic velocity but which arrive at the star with a large supersonic velocity. In Fig. 3.3 the transonic solution arrives at the star with a Mach number of 6.54, which at a temperature of 10^5 K corresponds to an in-fall velocity of $243\,\mathrm{kms}^{-1}$. For a realistic accretion temperature of 10^4 K the in-fall velocity is $259\,\mathrm{kms}^{-1}$.

Models of funnel flows have been studied using an isothermal equation of state (Li & Wilson 1999) and for a polytropic flow (Koldoba et al. 2002a), with the latter demonstrating that transonic accretion flows are only possible for a range of starting radii around the corotation radius. MHD simulations by Romanova et al. (2002) also indicate that accretion flows can arrive at the star with large supersonic velocities. However, our aim here is to determine whether or not the magnetic field geometry has any affect on accretion; in particular how the field structure affects the mass accretion rate, rather than to discuss the types of velocity solutions that we would expect to observe. In Appendix A we discuss an efficient algorithm which allows us to determine both the location of the sonic point on a field line and the initial Mach number required to give a smooth transonic solution. This algorithm may be applied to accretion flows along field lines of any size, shape and inclination, even in the absence of analytic descriptions of the magnetic field and effective gravity.

3.2.3 Mass accretion rates and filling factors

For accretion to occur the effective gravity at the point where a field line threads the disc must point inwards towards the star. From this subset of field lines we

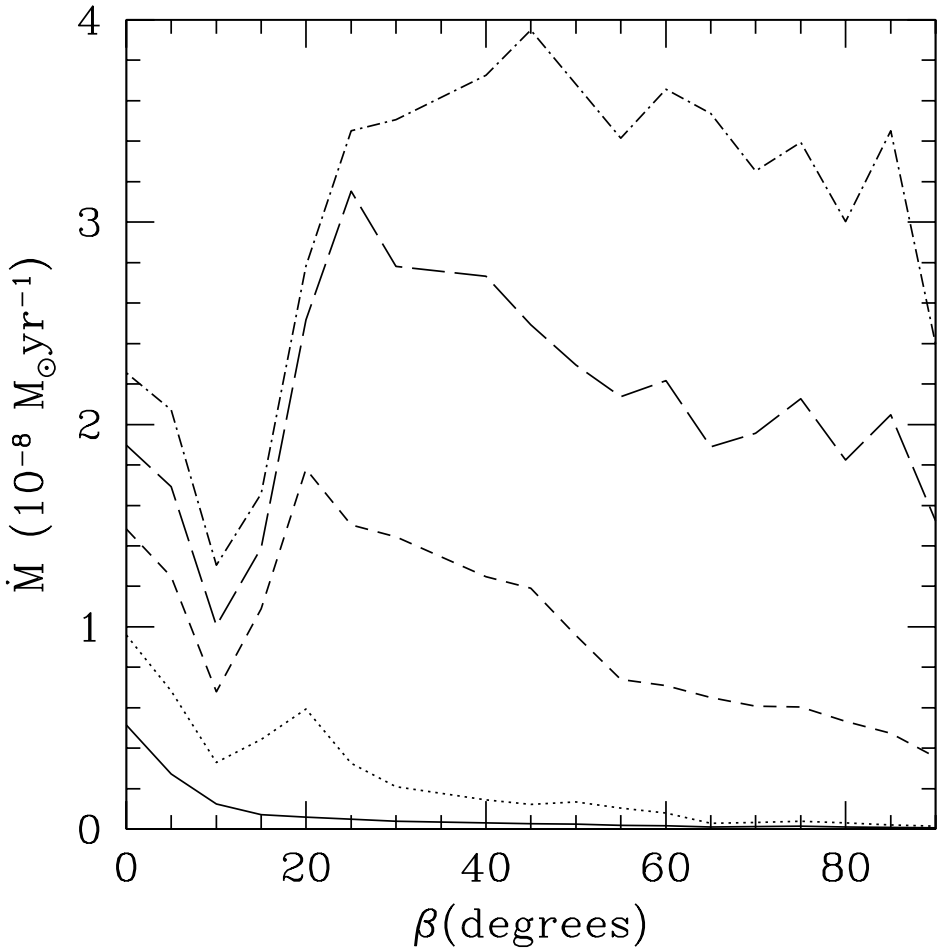

Figure 3.4: The change in mass accretion rate and as a function of β, for accretion to dipole fields where β is the obliquity - the angle between the rotation and magnetic poles, for accretion flow temperatures of 1000 K (*solid*), 2500 K (*dotted*), 5000 K (*short dash*), 7500 K (*long dash*) and 10000 K (*dash-dot*). The DF Tau parameters from Table 2.3 have been used.

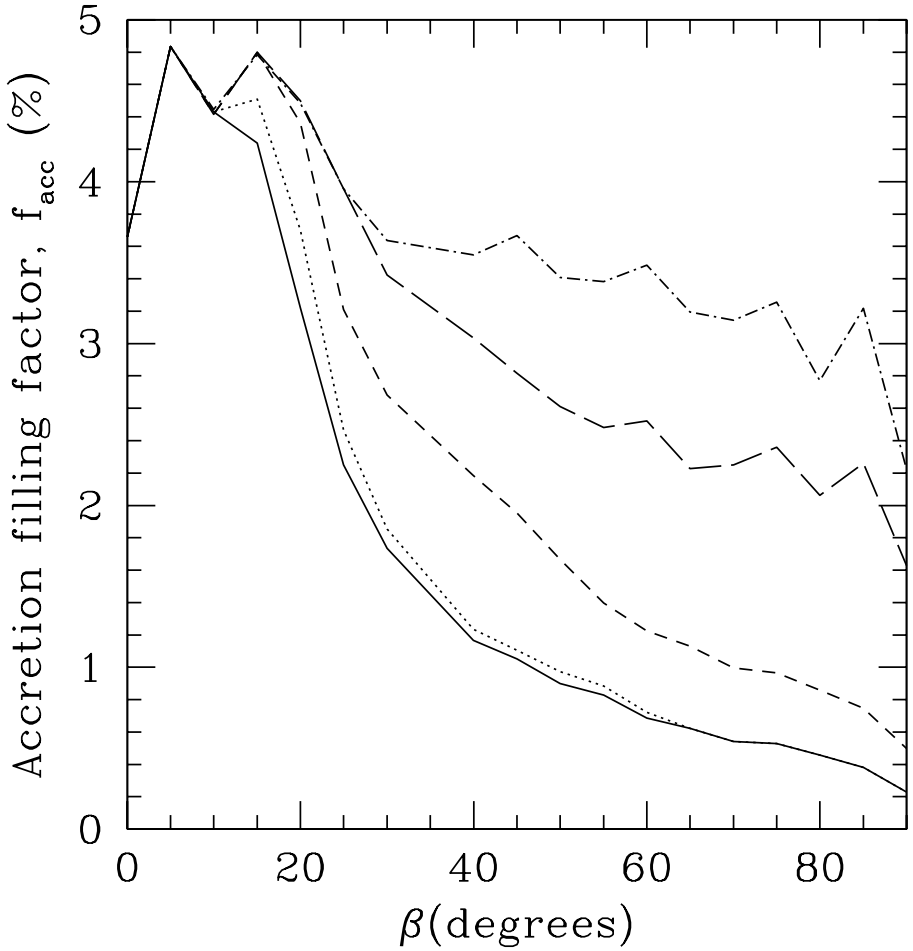

Figure 3.5: The change in accretion filling factor and as a function of β, for accretion to dipole fields where β is the obliquity - the angle between the rotation and magnetic poles, for accretion flow temperatures of 1000 K (*solid*), 2500 K (*dotted*), 5000 K (*short dash*), 7500 K (*long dash*) and 10000 K (*dash-dot*). The DF Tau parameters from Table 2.3 have been used.

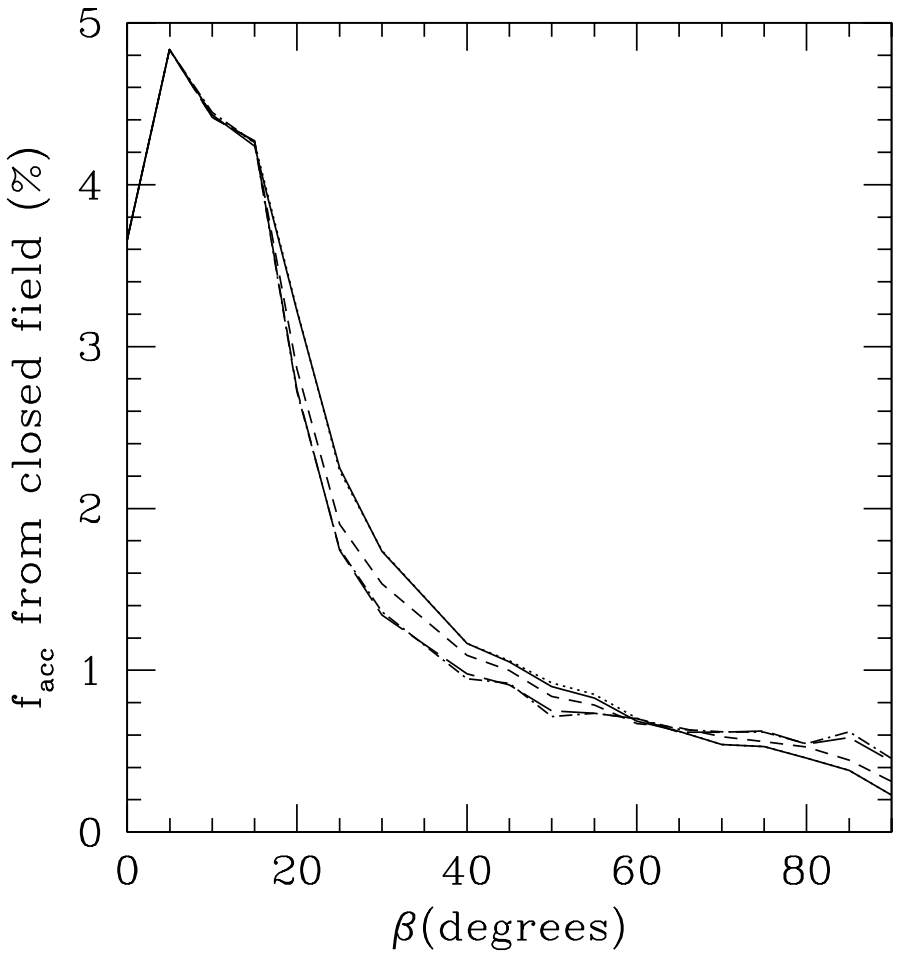

Figure 3.6: The contribution to the accretion filling factors plotted in Fig. 3.5 from accreting closed field lines as a function of β, for accretion flow temperatures of 1000 K (*solid*), 2500 K (*dotted*), 5000 K (*short dash*), 7500 K (*long dash*) and 10000 K (*dash-dot*).

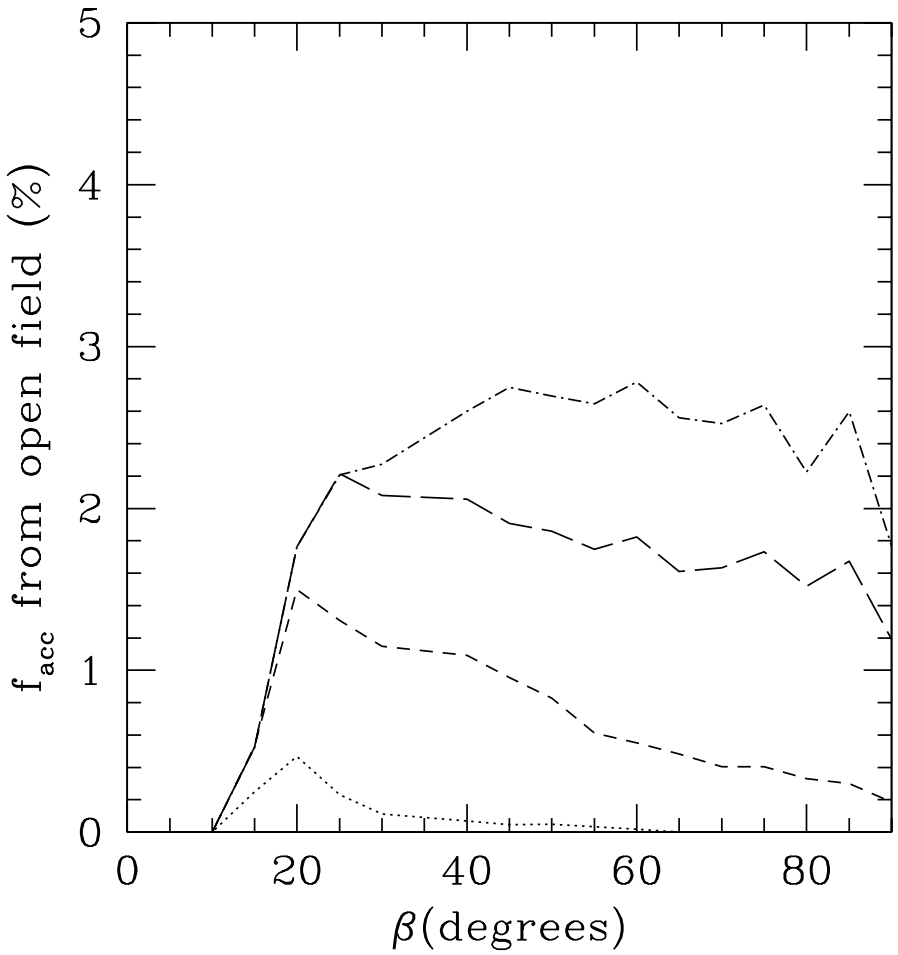

Figure 3.7: The contribution to the accretion filling factors plotted in Fig. 3.5 from accreting open field lines as a function of β, for accretion flow temperatures of 2500 K (*dotted*), 5000 K (*short dash*), 7500 K (*long dash*) and 10000 K (*dash-dot*). There are no open accreting field lines for the $T_{acc} = 1000$ K case.

select those which are able to contain the corona and support transonic accretion flows. We further check to ensure that the plasma beta resulting from accretion remains < 1 along their length. Therefore, at any particular azimuth, accretion occurs along the first field line at, or slightly within, the corotation radius; the field line must be able to contain the coronal plasma and have a sonic point along its length. In order to determine if a field line can support a transonic accretion flow, the first step is to find the pressure and velocity structure its length, which will be similar to those described above. To do this we need to determine the initial Mach number that would produce an accretion flow. We can achieve this by determining if a field line has a sonic point as discussed in Appendix A.

To calculate a mass accretion rate we require the velocity and density of each accretion flow at the stellar surface, and also the surface area of the star covered in hot spots. For an assumed accretion flow temperature we determine the initial Mach number required to generate a transonic velocity profile, along each field line, and determine the in-fall velocity from (3.14). At every point along a field line we know the ratio of pressure at that point, to that at the disc, p/p_d. For an isothermal equation of state $p \propto \rho$, so we also know the ratio of densities ρ/ρ_d at every point along the accreting field line. Thus for a given disc midplane density ρ_d, we can estimate the density at the stellar surface ρ_*. Throughout we assume a constant disc midplane density of $\rho_d = 5.0 \times 10^{-9}\,\mathrm{gcm}^{-3}$, a reasonable value at the corotation radius for T Tauri stars (e.g. Boss 1996). The mass accretion rate may be expressed in terms of quantities defined at the disc plane, with $\dot{M} \propto \rho_d$. Therefore raising or lowering ρ_d directly increases or decreases $\dot{M}$. We estimate the total surface area of the star covered in accretion hot spots by summing the area of individual grid cells which contain accreting field line foot points. For each grid cell i (of area A_i) on the stellar surface we obtain the average in-fall velocity $\bar{v}_*$ and average density $\bar{\rho}_*$ of material accreting into that cell. Most grid cells do not contain any accreting field line foot points and therefore do not contribute

to the mass accretion rate. The mass accretion rate is then the sum over all cells i containing accreting field line foot points,

$$\dot{M} = \sum_i \dot{M}_i = \sum_i \left[A\bar{v}_*\bar{\rho}_*\right]_i . \tag{3.22}$$

The mass accretion rate can be expressed equivalently as $\dot{M} = \rho_d v_d A_d$, where A_d is the surface area of the disc that contributes to accretion (which depends on the radial extent of accreting field lines within the disc). Using the surface area of grid cells within the disc which contain accreting field lines to estimate A_d, we obtain $\dot{M}$ values that are comparable to those calculated from (3.22). Therefore it makes little difference which formulation for $\dot{M}$ is used. The accretion filling factor f_{acc}, the fractional surface area of the star covered in hot spots, is then calculated from,

$$f_{acc} = \frac{\sum_i A_i}{4\pi R_*^2} \tag{3.23}$$

We have calculated the total mass accretion rate that dipole fields can support for isothermal accretion flow temperatures of between 10^3 K and 10^4 K; for values of β from $0\,^\circ$ to $90\,^\circ$, where β is the obliquity of the dipole (the angle between the dipole moment and the stellar rotation axis); for the DF Tau parameters in Table 2.3 and for a coronal temperature of 10 MK (see Fig. 3.4). $\beta = 0\,^\circ$ and $\beta = 90\,^\circ$ correspond to the aligned and perpendicular dipoles respectively.

For dipolar accretion we obtain typical mass accretion rates of $\dot{M} \approx 10^{-9} - 10^{-8}\,\mathrm{M_\odot\,yr^{-1}}$. The mass accretion rate increases with temperature in all cases, but at low accretion temperatures T_{acc}, there is little difference in $\dot{M}$ for all values of β (see Fig. 3.4). For higher T_{acc} values, the aligned dipole field can support mass accretion rates which are a factor of two times less than those fields with large values of β. This, in part, can be attributed to the increase in the amount of open field lines which thread the disc, and are able to support accretion as β is increased (see Fig. 3.7). As the dipole is tilted from $\beta = 0\,^\circ$ to $10\,^\circ$ the mass accretion rate is reduced (see Fig. 3.4). This can be understood by the

changing shape of the closed field lines as β is increased. For accretion along aligned dipole field lines, accreting material may flow along two identical paths from the disc to the star; that is it may accrete either on to the northern, or the southern hemisphere. Once the dipole has been tilted through a small angle, the path along the field into each hemisphere changes, with one segment of the closed field line loop being shallower than before and curved towards the star, and the other being longer. This longer segment bulges out slightly, so that material flowing along such field lines follows a path which initially curves away from the star, before looping back around to the stellar surface. This creates a difference in initial Mach numbers necessary to create transonic accretion flows along the different field line segments, with the net result that some closed field line segments are no longer able to accrete transonically when $\beta = 10\,^\circ$ (see Fig. 3.6). As the dipole is tilted further from $\beta = 10\,^\circ$ to $\approx 30\,^\circ - 40\,^\circ$ the mass accretion rate increases in all but the lowest T_{acc} cases. This is because once the dipole has been tilted far enough the open field lines (those that have foot points at latitudes closer to the magnetic axis) begin to intersect the disc (see Fig. 3.7). There are therefore more possible paths that material can take from the disc to the star, causing an increase in $\dot{M}$ (again in all but the lower T_{acc} cases). As β is further increased the amount of accreting closed field lines continues to reduce, while the amount of open field lines threading the disc reaches a maximum, and we therefore see a trend of falling mass accretion rates towards the largest values of β.

The accretion flow temperature is important in determining whether open field lines are able to support transonic accretion flows. From Figs. 3.6 and 3.7 it is clear that the contribution to accretion from the closed field is constant for all values of T_{acc}, whereas the contribution from the open field depends strongly on T_{acc}, with more open field lines accreting at higher accretion flow temperatures. At the lowest accretion flow temperature which we consider (1000 K), there are

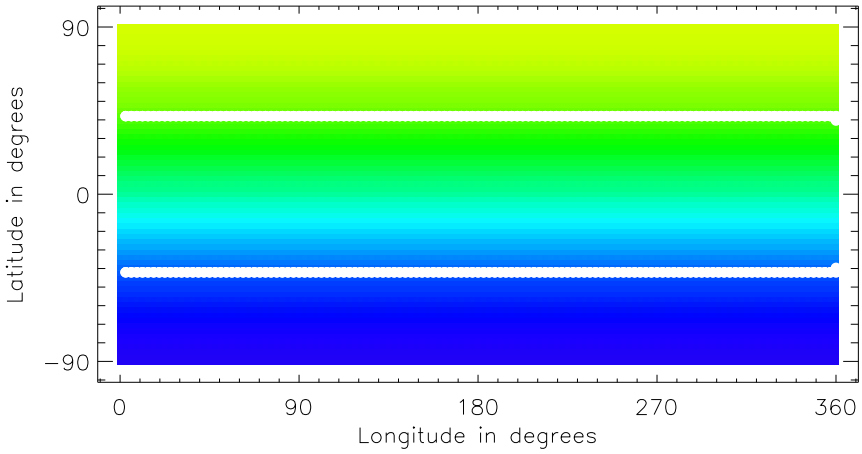

Figure 3.8: The stellar surface with white (black) points indicating the closed (open) accreting field line foot points for accretion to a dipole with obliquity $\beta = 0\,^{\circ}$, the aligned dipole, where accretion proceeds into two rings in opposite hemispheres. The accretion flow temperature is $10^4\,\mathrm{K}$ and the average surface field strength matches that considered by Jardine et al. (2006) with yellow (blue) representing the positive (negative) magnetic pole.

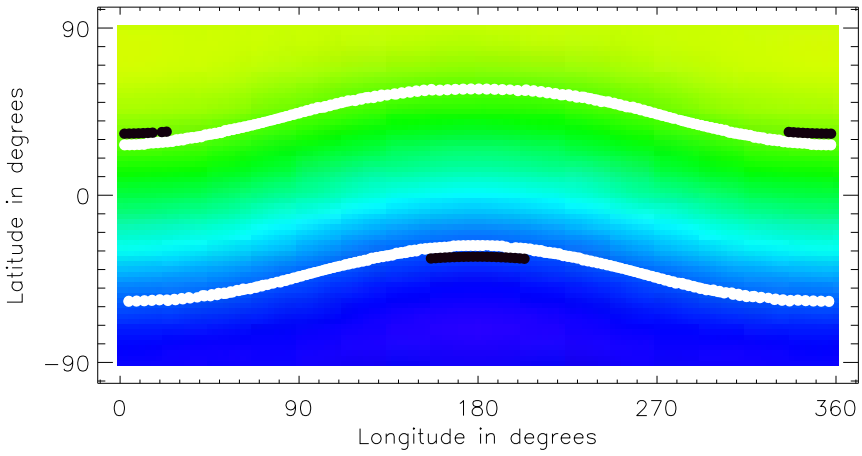

Figure 3.9: As Fig. 3.8 but for a dipole with obliquity $\beta = 15\,^{\circ}$ where the accretion rings have been distorted and open field lines produce the small bands centred on $180\,^{\circ}$ and $360\,^{\circ}$ longitude.

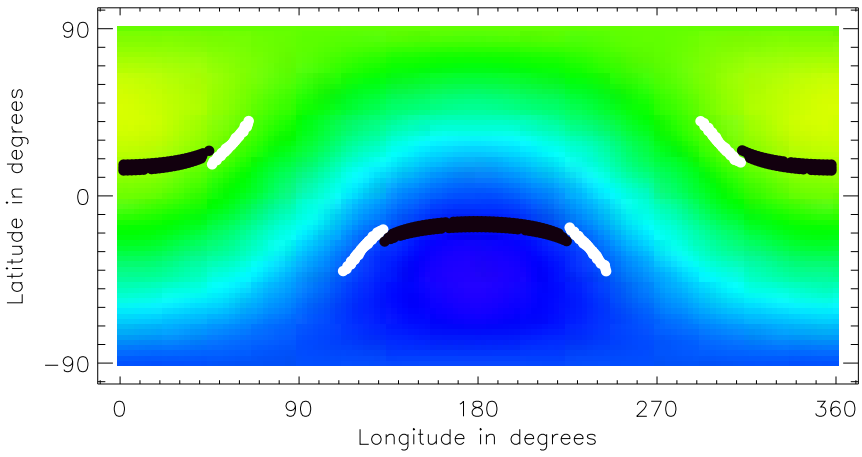

Figure 3.10: As Fig. 3.8 but for a dipole with obliquity $\beta = 45\,^\circ$ where accretion occurs predominantly along the open field lines.

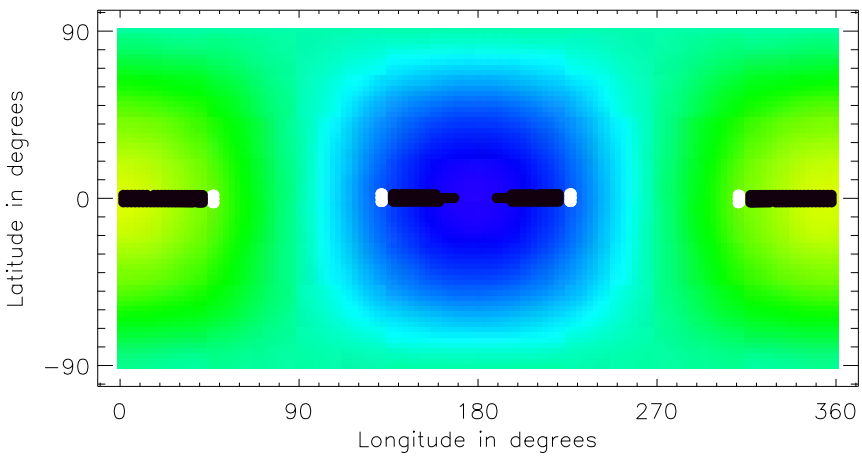

Figure 3.11: As Fig. 3.8 but for a dipole with obliquity $\beta = 90\,^\circ$, the perpendicular dipole, where accretion occurs in bars around the star's equator.

no open field lines able to support transonic accretion, even for large values of β where there are many such field lines passing through the disc. This can be understood as follows. For transonic accretion a sonic point must exist on a field line. At a sonic point $v = c_s$; applying this to (3.14), substituting into (3.13) and rearranging gives,

$$\frac{1}{v}\frac{dv}{ds}\left(v^2 - c_s^2\right) = \boldsymbol{g}_{eff} \cdot \hat{\boldsymbol{s}} - \frac{c_s^2}{B}\frac{dB}{ds}, \tag{3.24}$$

from which it can be seen that there exists some critical radius r_c where either $v = c_s$ or $dv/ds = 0$. Clearly at this critical radius the two terms on the RHS of (3.24) must be equal,

$$\frac{c_s^2}{B}\frac{dB}{ds} = \boldsymbol{g}_{eff} \cdot \hat{\boldsymbol{s}}, \tag{3.25}$$

where all the terms are evaluated at r_c. It should be noted that (3.25) may also be obtained by finding the maximum turning point of (7.5), consistent with the argument in Appendix A.

The condition for a sonic point to exist on any field line, open or closed, may be expressed as equation (3.25). $\hat{\boldsymbol{s}}$ is a unit vector along the path of the field which may be written as $\hat{\boldsymbol{s}} = \boldsymbol{B}/B$, which can be used to rewrite (3.25) as,

$$c_s^2\frac{dB}{ds} = \boldsymbol{g}_{eff} \cdot \boldsymbol{B}. \tag{3.26}$$

From this it can be seen that the condition for a sonic point to exist depends on three things: first, the path that a field line takes through the star's gravitational potential well; second, how quickly the strength of the magnetic field varies as the flow moves along the field line and third, the accretion flow temperature which enters through the sound speed, where for isothermal accretion $c_s^2 \propto T_{acc}$. It is the interplay between all three of these factors which determines if a sonic point exists.

For low accretion temperatures the sound speed c_s is small, whilst for open field lines the $\boldsymbol{g}_{eff} \cdot \boldsymbol{B}$ on the RHS of (3.26) is usually larger than for closed field lines. This can be seen by considering the simple example of a closed dipolar

field line and a radial open field line threading the disc at the same point R_d. For both field lines the effective gravity vector $\boldsymbol{g}_{eff}$ at R_d is the same. For the radial open field line the magnetic field vector $\boldsymbol{B}$ is aligned with $\boldsymbol{g}_{eff}$, whereas for the closed dipolar field line, which threads the disc at a large angle, there is some angle θ between it and $\boldsymbol{B}$. Hence the scalar product $\boldsymbol{g}_{eff} \cdot \boldsymbol{B} = gB\cos\theta$ is larger for the open field line. Thus for open field lines the RHS of (3.26) is larger compared to closed field lines, and therefore a higher accretion flow temperature is required to create the necessary high value of c_s in order to balance the two sides of equation (3.26). Of course, for reasons discussed above, dB/ds is larger for the radial field line, but it is not large enough to compensate for the $\boldsymbol{g}_{eff} \cdot \boldsymbol{B}$ term being so small. At higher values of the accretion flow temperature more open field lines are able to accrete, thus helping to increase the mass accretion rate even though the number of closed accreting field lines are significantly less compared to an aligned dipole field.

The aligned dipole field has an accretion filling factor of just under 4% (see Fig. 3.5), with the $\beta = 15\,^\circ$ case having the largest filling factor due to the shape of the closed field lines threading the disc, which allows material to be channelled onto a larger area of the stellar surface. More accreting open field lines mean a larger fraction of the star is covered in accreting field line foot points thus increasing the f_{acc} at large accretion flow temperatures. However, when β becomes larger as we tilt the dipole further onto its side, f_{acc} decreases. As the field is tilted fewer closed field lines are available for accretion as they no longer intersect the disc (see Fig. 3.6), leading to a decrease in the filling factor (see Fig. 3.5). The accretion filling factor is smallest for the perpendicular dipole where material is accreted onto bars about the star's equator (see Fig. 3.11), compared to the accretion rings about the poles obtained with the aligned dipole.

We therefore conclude that by considering accretion to tilted dipolar magnetic fields that both the mass accretion accretion rate and the accretion filling factor

are dependent on the balance between the number of closed and open field lines threading the disc. If there are many open field lines threading the disc, then a higher accretion flow temperature is required in order for the open field to contribute to $\dot{M}$. At high accretion flow temperatures there is at most a factor of two difference between the mass accretion rate that the aligned dipole can support compared to the tilted dipoles with large values of β. It appears as though the structure of the magnetic field has only a small role to play in determining the mass accretion rate, at least for purely dipolar fields, however, as is discussed in the next Chapter, the magnetic field geometry is of crucial importance in controlling the location and distribution of hot spots.

3.3 Summary

By considering accretion to dipolar magnetic fields we have constructed a steady state isothermal accretion flow model were material leaves the disc at low subsonic speeds, but arrives at the star at large supersonic speeds. We find that in-fall velocities of a few hundred kms^{-1} are possible which is consistent with measurements of the redshifted absorption components of inverse P-Cygni profiles (e.g. Edwards et al. 1994). We found that for accretion along aligned and perpendicular closed dipole field lines that there was little difference in in-fall speeds between the two cases. However, for tilted dipole fields in general (rather than just considering a single closed field line loop) there are many open and closed field lines threading the disc providing different paths that material could flow along from the disc to the star. The path that a particular field line takes through the star's gravitational potential combined with the strength of magnetic field and how that changes along the field line path, are all important in determining whether or not a field line can support transonic accretion. At low accretion flow temperatures open field lines are typically not able to support

transonic accretion, but at higher accretion flow temperatures they can accrete transonically and consequently there is an increase in the mass accretion rate. We only find a factor of two to three difference in $\dot{M}$ values for accretion to tilted dipolar magnetic fields suggesting that the geometry of the field itself is not as significant as the stellar parameters (which control the position of corotation) in controlling the mass accretion rate.

Chapter 4

Mass Accretion II: Complex Magnetic Fields

This work has been published in Gregory, Jardine, Simpson & Donati, 2006, MNRAS, 371, 999.

4.1 Introduction

In this Chapter I present a model of the accretion process using complex magnetic fields extrapolated from surface magnetograms. I apply my model to a large sample of pre-main sequence stars obtained from the Chandra Orion Ultradeep Project (COUP; Getman et al. 2005), in order to test if the model can reproduce the observed correlation between mass accretion rate and stellar mass. An increase in $\dot{M}$ with M_* was originally noted by Hillenbrand et al. (1992) and subsequently by Rebull et al. (2000); Rebull et al. (2002) and White & Ghez (2001). The correlation was then found to extend to very low mass objects and accreting brown dwarfs by White & Basri (2003) and Muzerolle et al. (2003), and to the higher mass, intermediate mass T Tauri stars, by Calvet et al. (2004).

Further low mass data has recently been added by Natta et al. (2004), Mohanty, Jayawardhana & Basri (2005a) and by Muzerolle et al. (2005) who obtain a correlation of the form $\dot{M} \propto M_*^{2.1}$, with as much as three orders of magnitude scatter in the measured mass accretion rate at any particular stellar mass. However, Calvet et al. (2004) point out that due to a bias against the detection of higher mass stars with lower mass accretion rates, the power may be less than 2.1. Further data for accreting stars in the $\rho-$Ophiuchus star forming region has recently been added by Natta et al. (2006), Gatti et al. (2006) and Garcia Lopez et al. (2006).

The physical origin of the correlation between M_* and $\dot{M}$, and the large scatter in measured $\dot{M}$ values, is not clear; however several ideas have been put forward. First, increased X-ray emission in higher mass T Tauri stars (Preibisch et al. 2005; Jardine et al. 2006) may cause an increase in disc ionisation, leading to a more efficient magnetorotational instability and therefore a higher mass accretion rate (Calvet et al. 2004). Second, Padoan et al. (2005) argue that the correlation $\dot{M} \propto M_*^2$ arises from Bondi-Hoyle accretion, with the star-disc system gathering mass as it moves through the parent cloud. In their model the observed scatter in $\dot{M}$ arises from variations in stellar velocities, gas densities and sound speeds. Mohanty et al. (2005a) provide a detailed discussion of both of these suggestions. Third, Alexander & Armitage (2006) suggest that the correlation may arise from variations in the disc initial conditions combined with the resulting viscous evolution of the disc. In their model they assume that the initial disc mass scales linearly with the stellar mass, $M_d \propto M_*$, which, upon making this assumption, eventually leads them to the conclusion that brown dwarfs (the lowest mass accretors) should have discs which are larger than higher mass accretors. Thus the Alexander & Armitage (2006) suggestion, if correct, will soon be directly verifiable by observations. Fourth, Natta et al. (2006) suggest that the large scatter in the correlation between $\dot{M}$ and M_* may arise from the influence of close compan-

ion stars, or by time variable accretion. It should however be noted that Clarke & Pringle (2006) take a more conservative view by demonstrating that a steep correlation between $\dot{M}$ and M_* may arise as a consequence of detection/selection limitations, and as such $\dot{M} \propto M_*^2$ is perhaps not a true representation of the correlation between $\dot{M}$ and M_*.

4.2 Realistic magnetic fields

From Zeeman-Doppler images it is possible to extrapolate stellar magnetic fields by assuming that the field is potential. At the moment we do not have the necessary observations of CTTs, but we do have for the young main sequence stars LQ Hya and AB Dor (Donati & Collier Cameron 1997; Donati et al. 1997; Donati 1999; Donati et al. 1999; Donati et al. 2003), which have different field topologies (Jardine et al. 2002a; Hussain et al. 2002; McIvor et al. 2003; McIvor et al. 2004). Using their field structures as an example we can adjust the stellar parameters (mass, radius and rotation period) to construct a simple model of a CTTs, surrounded by a thin accretion disc. The method for extrapolating magnetic fields was described in detail in Chapter 2.

4.2.1 Field extrapolations

The initial field extrapolation yields regions of open and closed field lines. Of these, some intersect the disc and may be actively accreting. For closed field lines which do not intersect the disc it is possible to calculate the X-ray emission measure in the same way as Jardine et al. (2006). To determine if a field line can accrete we find where it threads the disc and calculate if the effective gravity along the path of the field line points inwards, towards the star. From this subset of field lines we select those which have $\beta < 1$ along their length. In

Figure 4.1: Field lines which could support accretion flows for a model of a CTTs with a field topology that resembles LQ Hya, obtained using the DF Tau parameters from Table 4.1. The stellar surface is coloured to show the strength of the radial component of the field, with red representing 1 kG and black −1 kG. Field lines have been drawn from the corotation radius. The natural extent of the corona of DF Tau, a lower mass CTTs, would be beyond corotation and therefore there is a mixture of open and closed field lines threading the disc at R_{co}.

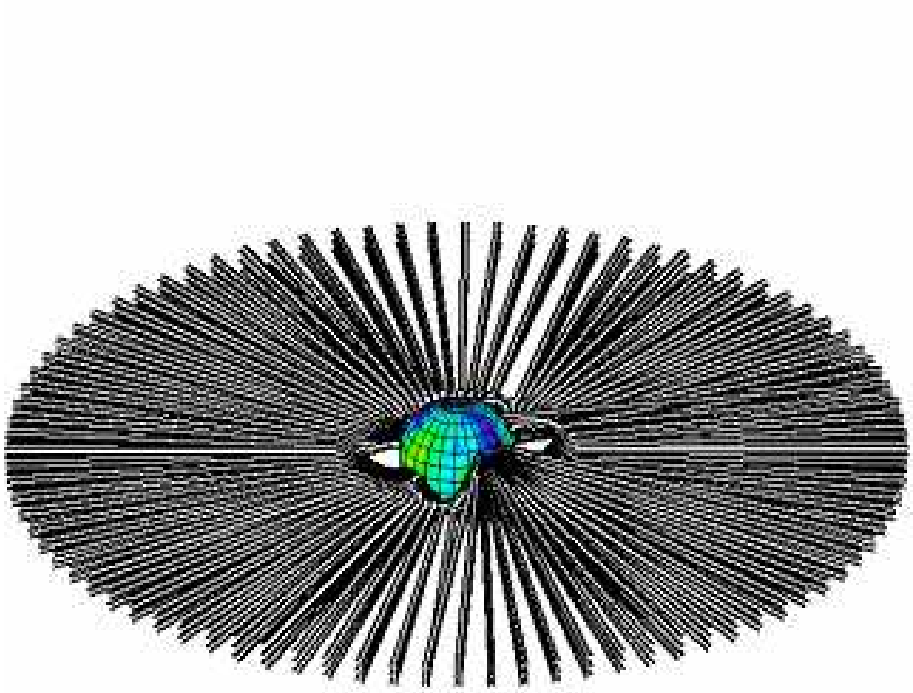

Figure 4.2: As Fig. 4.1, but with a field topology that resembles AB Dor, obtained using the CY Tau parameters from Table 4.1. The corona of CY Tau, a higher mass CTTs, is more compact than that of DF Tau and material flows along open field lines from corotation.

Table 4.1: Data for CTTs from Valenti & Johns-Krull (2004)

Star	$M_*(M_\odot)$	$R_*(R_\odot)$	$P_{rot}(d)$	$R_{co}(R_*)$
DF Tau	0.17	3.9	8.5	2.47
CY Tau	0.58	1.4	7.5	9.55

other words, for any given azimuthal extent we assume that accretion can occur along the first field line within the corotation radius which is able to contain the coronal plasma. We assume that the loading of disc material onto the field lines is infinitely efficient, such that the first field line at any azimuth which satisfies the accretion conditions will accrete, and that field lines interior to this are shielded from the accretion flow. We also assume that the accreting field is static and is therefore not distorted by the disc or by the process of accretion. Below we consider in more detail how to determine which field lines are able to support accretion flows, in order to calculate mass accretion rates and accretion filling factors.

Figs. 4.1 and 4.2 show the first set of field lines which may be accreting, obtained by surrounding the field extrapolations of LQ Hya and AB Dor with a thin wedge-shaped accretion disc, with an opening angle of approximately $10\,^{\circ}$. Below we apply our model for isothermal accretion flows where material leaves the disc at a low subsonic speed, but arrives at the star with a large supersonic speed. Not all of the field lines in Figs. 4.1 and 4.2 are capable of supporting such accretion flows, and instead represent the maximum possible set of field lines which may be accreting. We assume a coronal temperature of 10 MK and obtain the gas pressure at the base of each field line as discussed in Chapter 2 and by Jardine et al. (2006). The natural extent of the corona of DF Tau would be beyond the corotation radius and therefore accretion occurs along a mixture of closed and open field lines from corotation. One suggestion for how accretion may proceed along open field lines is that an open field line which stretches out into the disc, may reconnect with another open field line for long enough for accretion to occur, only to be sheared open once again. This is of particular importance for the higher mass stars, such as CY Tau, where in some cases we find that the inner edge of the disc is sitting in a reservoir of radial open field lines. This may have important implications for the transfer of torques between

the disc and star. However more work is needed here in order to develop models for accretion along open field lines.

4.3 Accretion to complex magnetic fields

4.3.1 Distribution of hot spots

Brightness modulations have long been interpreted as evidence for hot spots on CTTs (e.g. Bouvier et al. 1995). Hot spots are a prediction of magnetospheric accretion models and arise from channelled in-falling material impacting the star at large velocity. The distribution of accretion hot spots and their subsequent effects on photometric variability have been studied by several authors, however, only with dipolar magnetic fields (Wood et al. 1996; Mahdavi & Kenyon 1998; Stassun et al. 1999; Romanova et al. 2004a). We find that complex magnetic field geometries have a large effect on the location of hot spots. The accreting field line foot points are shown in Figs. 4.3 and 4.4, which represent those field lines in Figs. 4.1 and 4.2 which satisfy the accretion conditions discussed below. These give an indication of how different field geometries control the shape, location and distribution of hot spots. We find a series of discrete hot spots which span a range of latitudes and longitudes with typical accretion filling factors of around 2%. This is quite different to what would be expected for accretion to an aligned dipole field, where the accreting field line foot points would be at high latitudes, towards the poles. With the complex magnetic fields presented here hot spots can be at high latitudes, but also often at low latitudes close to the star's equator. The existence of low latitude hot spots has also been predicted by von Rekowski & Brandenburg (2006a) who assume that both the stellar and disc fields are dynamo generated and maintained. It is worth noting that the line-of-sight field magnetic components inferred from polarisation measurements made using the HeI 5876Å emission line by Valenti & Johns-Krull (2004), are well matched by a simple

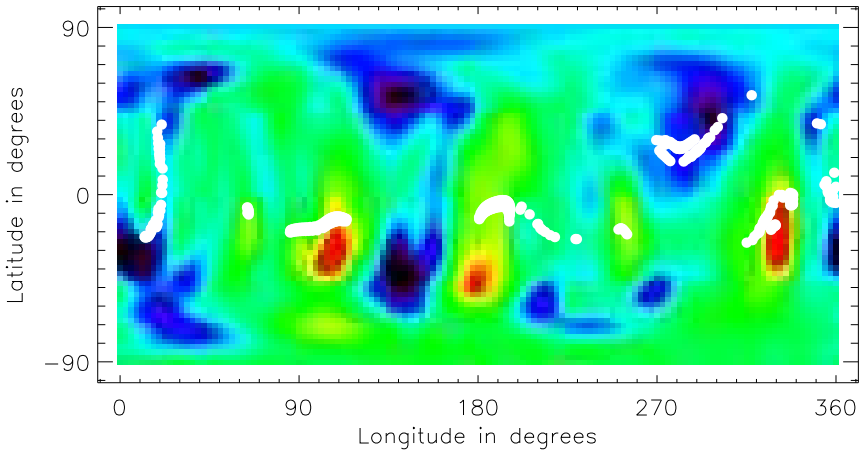

Figure 4.3: Surface magnetogram as used in Fig. 4.1 for the LQ Hya-like magnetic field, coloured to show the strength of the radial component of the field with red representing 1 kG and black −1 kG (Donati et al. 2003). White points are the accreting field line foot points and give an indication of the location of hot spots. Hot spots span a range of latitudes and longitudes; this is in contrast for accretion to a dipole field where the accreting field line foot points would be at high latitudes towards the poles. The accretion filling factor is about 2%.

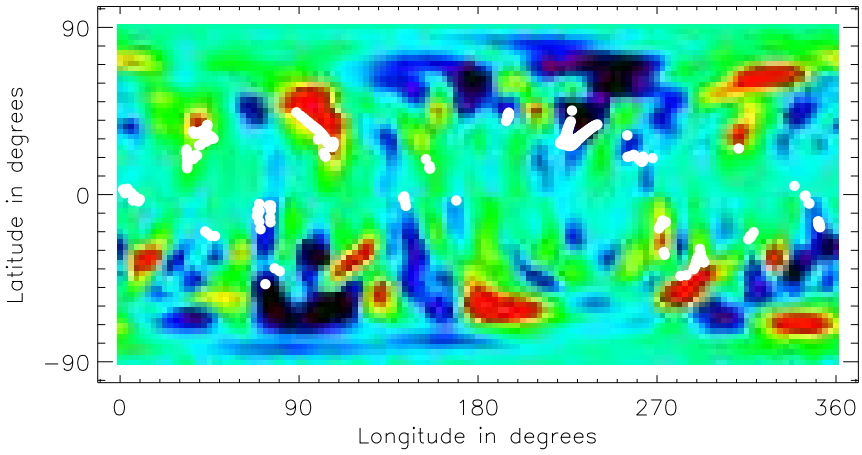

Figure 4.4: As Fig. 4.3 but for the surface magnetograms used in Fig. 4.2 for the AB Dor-like magnetic field. The accretion filling factor is about 2%.

model of a single hot spot at different latitudes dependent on the particular star. Such observations already suggest that low latitude hot spots may be a common feature of CTTs.

4.3.2 In-fall velocities

In Appendix A we discuss an analytic method for calculating the location of the critical radius. This allows us to determine which of the field lines from Figs. 4.1 and 4.2 have sonic points, and then to find a transonic velocity solution, where material leaves the disc at a low subsonic speed but arrives at the stellar surface with a large supersonic speed. The accreting field geometry obtained when considering complex magnetic fields is such that there are many field lines of different size and shape which are able to support accretion flows. This results in a distribution of in-fall speeds, rather than a discrete in-fall speed that would be expected for accretion along aligned dipole field lines. Figs. 4.5 and 4.6 show the distributions of in-fall velocities for our two accreting field geometries, and for each set of stellar parameters listed in Table 4.1, for an accretion flow temperature of 10^4 K and a coronal temperature of 10 MK. In both cases the in-fall speeds are large enough to produce hot spots on the stellar surface. Larger in-fall velocities are obtained when using the CY Tau parameters, which is a higher mass star, compared to the DF Tau parameters. Material accreting onto larger mass stars will experience a steeper gravitational potential than for accretion onto lower mass stars, and this combined with the larger corotation radii for the larger mass stars, naturally leads to greater in-fall speeds.

The accretion flow temperature has a negligible effect on the average in-fall velocity, for any magnetic field structure. The average in-fall speed remains almost constant as the accretion flow temperature is varied, changing by only a few kms^{-1}. As the temperature is increased the sonic point of the accretion flow is further from the disc, which reduces the final Mach number by which material is

arriving at the star. However this reduction in the final Mach number is caused almost exclusively by the increase in the sound speed at higher temperature, whilst the average in-fall velocity remains constant.

There is a broader distribution of in-fall velocities when considering the CY Tau stellar parameters compared to the narrow distribution for DF Tau, which is more strongly peaked about a single in-fall velocity (see Figs. 4.5 and 4.6). We calculate the natural radial extent of DF Tau's corona R_s to be larger than the corotation radius ($R_s = 2.5R_*$ for the AB Dor-like field and $2.7R_*$ for the LQ Hya-like field compared to $R_{co} = 2.47R_*$) and therefore accretion proceeds along a mixture of open and closed field lines which thread the disc at corotation. It can be seen from Fig. 4.1 that accretion occurs almost exclusively from the corotation radius with a small range of azimuths where there are neither open nor closed field lines threading the disc at corotation, and therefore the disc extends closer to the star. This effect is much greater for the CY Tau parameters as its corotation radius is beyond the natural extent of the corona ($R_s = 2.7R_*$ for the AB Dor-like field and $2.9R_*$ for the LQ Hya-like field compared to $R_{co} = 9.55R_*$). Most of the accretion occurs along radial field lines from corotation. However, at some azimuths there are no open field lines stretching out through the disc at corotation, and therefore the inner disc at those azimuths is much closer to the star, with accretion occurring along the closed field lines loops which constitute the star's corona. A more complete model would take account of the torques resulting from allowing accretion to occur from well within the corotation radius. We do not account for this in our model, however this only occurs for a very small number of field lines, with the bulk of accretion occuring from corotation. The number of field lines accreting at lower velocity from within corotation is small compared to those accreting from R_{co}, with the resulting distribution of in-fall speeds instead reflecting variations in the size and shape of field lines accreting from corotation.

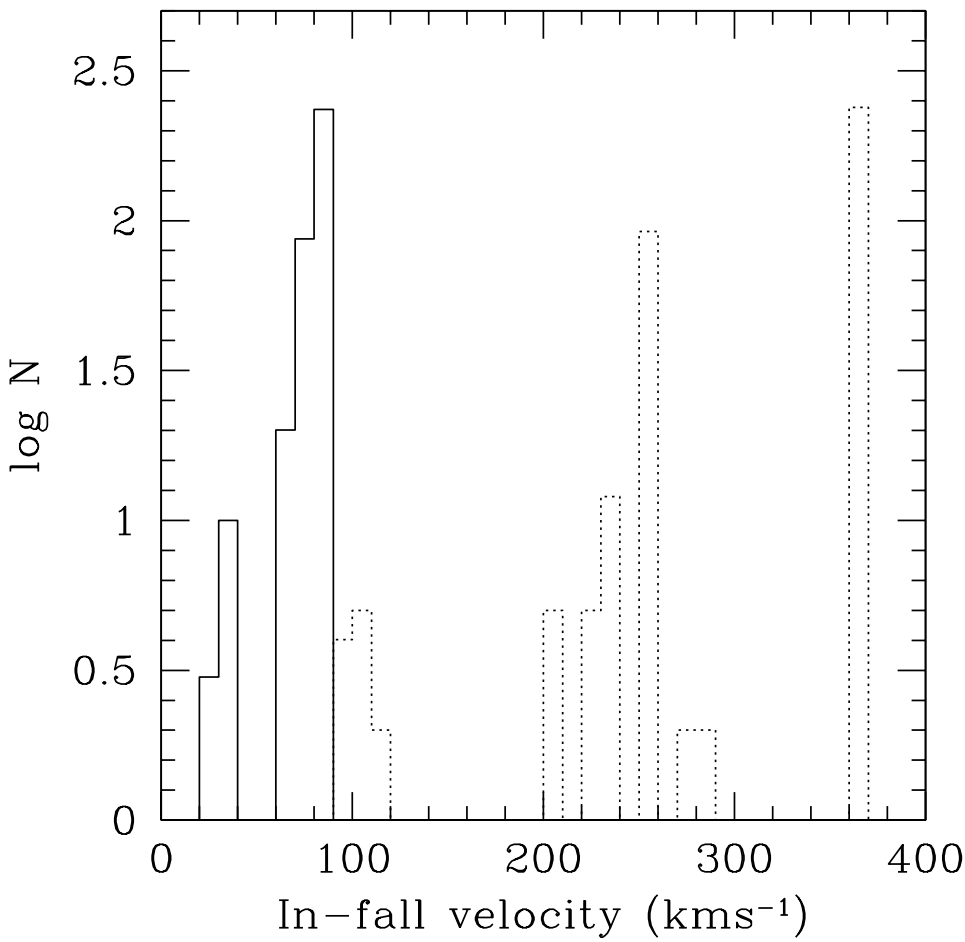

Figure 4.5: A histogram showing the distribution of in-fall velocities assuming steady state accretion flows at 10^4 K, using the field extrapolation in Fig. 4.1 corresponding to the LQ Hya-like field using the DF Tau (*solid*) and CY Tau (*dots*) stellar parameters listed in Table 4.1. For comparison the free-fall velocities are approximately 129 kms^{-1} for DF Tau and 397 kms^{-1} for CY Tau.

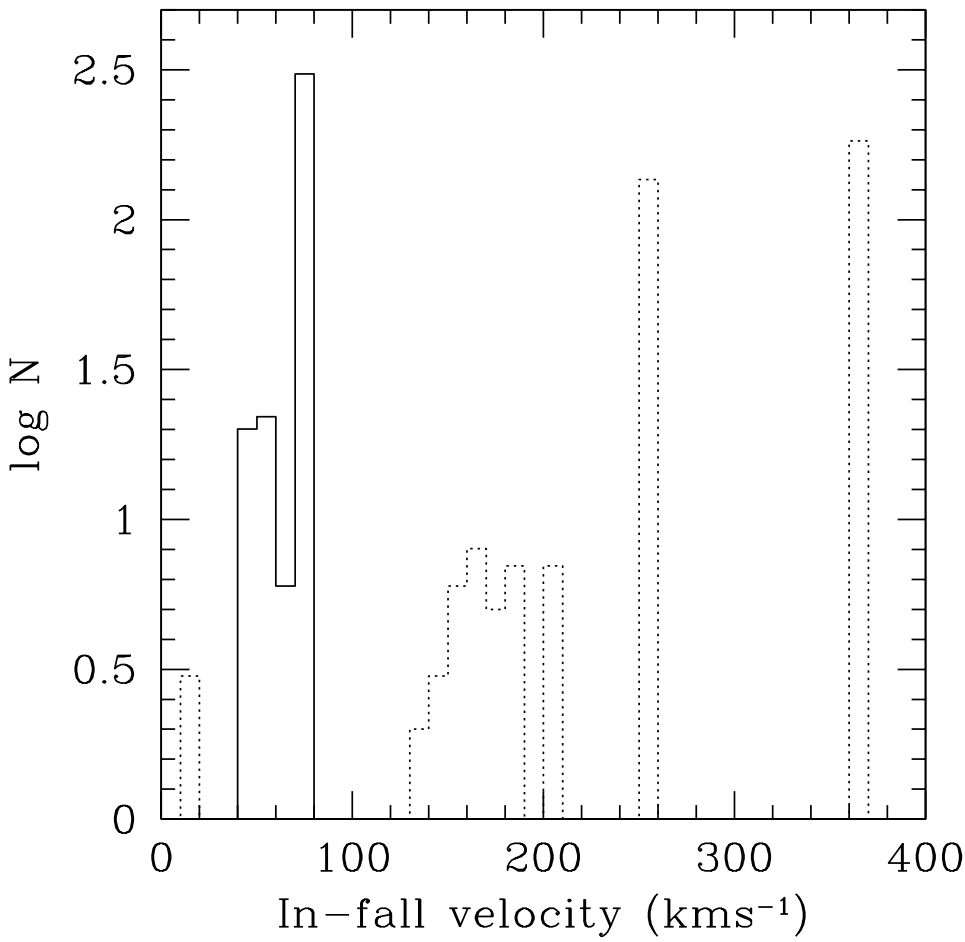

Figure 4.6: A histogram showing the distribution of in-fall velocities assuming steady state accretion flows at 10^4 K, using the field extrapolation in Fig. 4.2, corresponding to the AB Dor-like field using the DF Tau (*solid*) and CY Tau (*dots*) stellar parameters listed in Table 4.1.

We have found that the structure of the complex magnetic fields and more importantly the stellar parameters (mass, radius, rotation period, coronal temperature) are critical in controlling the distribution of in-fall velocities. Consequently this will affect mass accretion rates, which we discuss below, and also spectral line profiles, which will be the subject of future work.

4.3.3 Mass accretion rates and stellar mass

To investigate the correlation between mass accretion rate and stellar mass we require a large sample of accreting stars with estimates of stellar mass, radius, rotation period and coronal temperature. The X-ray emission from young stars in the Orion Nebula has been studied by COUP (The Chandra Orion Ultradeep Project), which provides a vast amount of data on accreting stars with estimates of all the parameters required by our model to calculate mass accretion rates. Getman et al. (2005) provides an overview of the observations and the COUP dataset[1].

Hillenbrand et al. (1992) first noted an apparent correlation between accretion rate and stellar mass. Rebull et al. (2000) then noticed an apparent increase in mass accretion rate with stellar mass and that the lack of low mass stars with high $\dot{M}$ was a real effect for stars in the Orion flanking fields. White & Ghez (2001) also noted an apparent $\dot{M} - M_*$ correlation for stars in Taurus-Auriga, with a large scatter in $\dot{M}$ values, with Rebull et al. (2002) reporting that the correlation also existed for stars in NGC 2264. The correlation was then found to extend across several orders of magnitude in mass with the detection of accretion in low mass T Tauri stars and brown dwarfs (White & Basri 2003) with Muzerolle et al. (2003) then suggesting that $\dot{M} \propto M_*^2$. Subsequent observations by Calvet et al. (2004) indicated that this correlation extended to the higher mass, intermediate mass T Tauri stars with several authors adding data at lower

[1]The COUP dataset is available from ftp://ftp.astro.psu.edu/pub/gkosta/COUP_PUBLIC/.

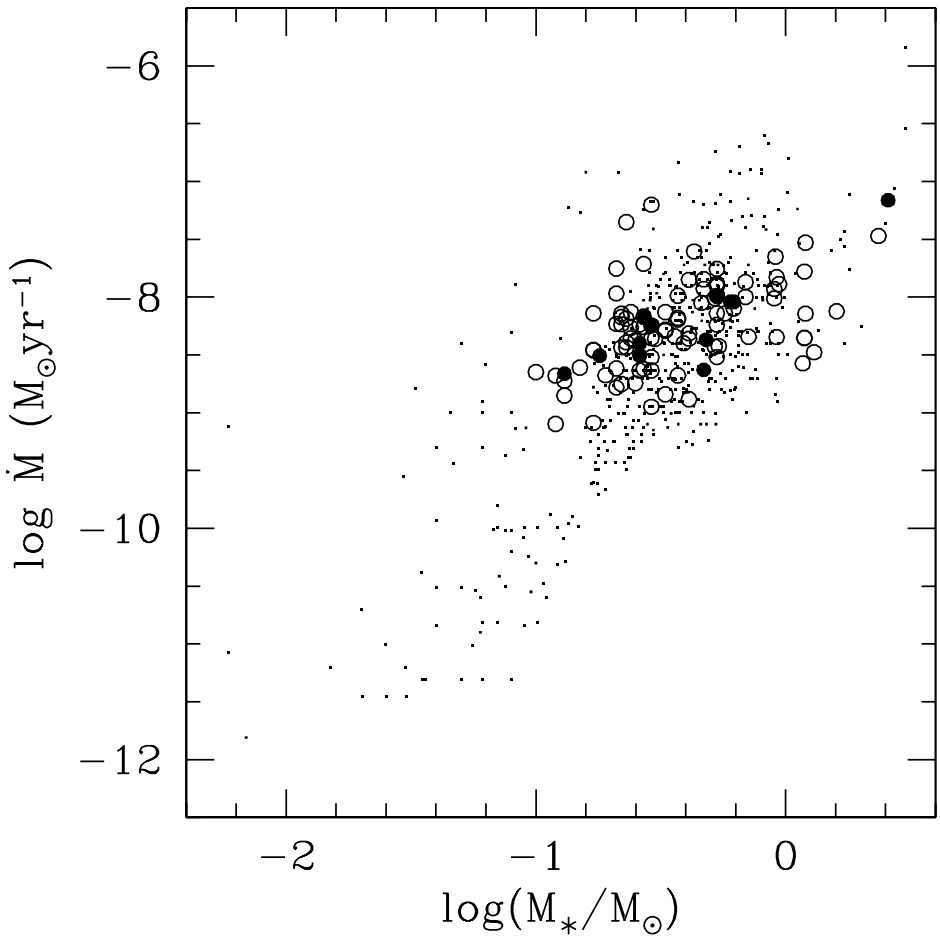

Figure 4.7: The correlation between $\dot{M}$ and M_*. Previously published values [*points*] are taken from Rebull et al. (2000); Rebull et al. (2002), Mohanty et al. (2005a), Natta et al. (2006) and Muzerolle et al. (2005) which is a collection of data from Gullbring et al. (1998), White & Ghez (2001), White & Basri (2003), Muzerolle et al. (2003), Calvet et al. (2004) and Natta et al. (2004). Using data from the COUP sample of accreting stars (Getman et al. 2005) our accretion model yields mass accretion rates [*large circles*] that are consistent within the observed scatter. *Open circles* are values calculated from COUP stars with estimates of the stellar parameters and a EW(CaII) measurement, whilst the *filled circles* are values calculated for stars which are regarded as strongly accreting with EW(CaII)< -1Å. All quantities have been calculated using the LQ Hya surface map and the higher coronal temperatures.

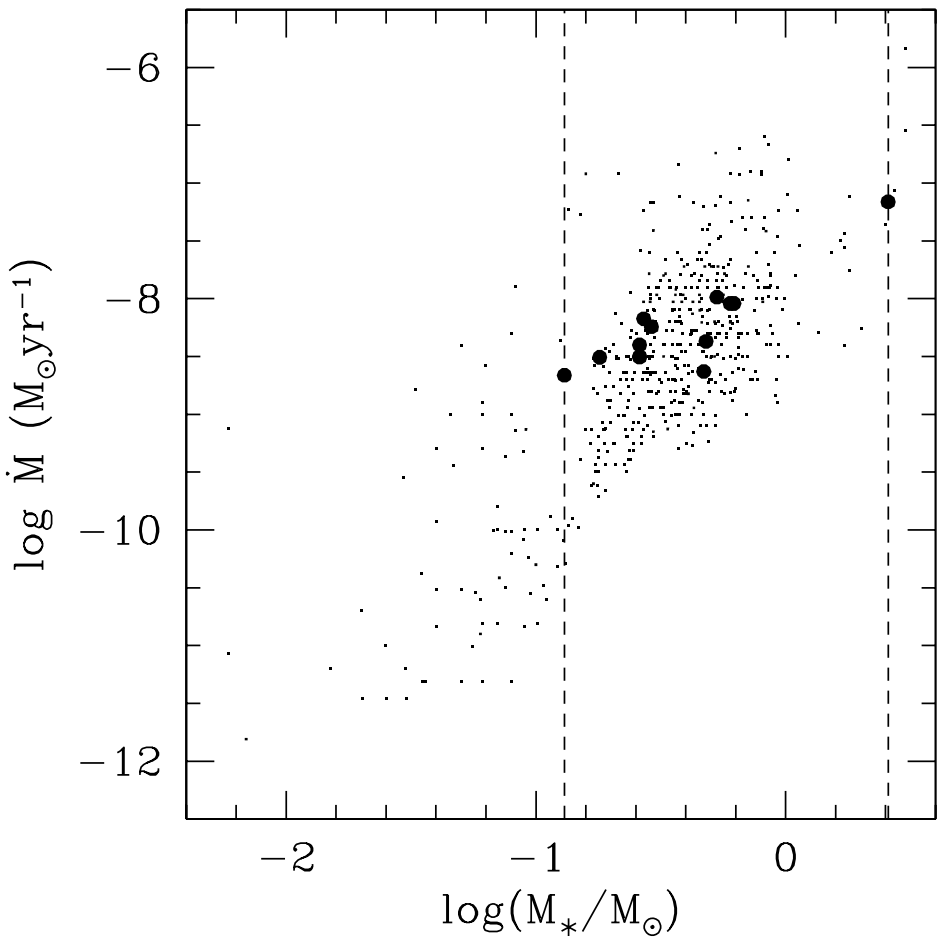

Figure 4.8: As Fig. 4.7 but only showing COUP stars which are regarded as strongly accreting (*filled circles*) with the *dashed lines* indicating the range in mass covered by such COUP stars. *Points* are previously published values.

masses from various star forming regions (Natta et al. 2004; Mohanty et al. 2005a; Muzerolle et al. 2005), with Natta et al. (2006) adding data from ρ-Ophiuchus. There can be as much as three orders of magnitude scatter in the measured mass accretion rate at any particular stellar mass. It should also be noted that mass accretion rate measurements for stars in the Trapezium cluster are not consistent with a correlation of the form $\dot{M} \propto M_*^2$. Robberto et al. (2004) report $\dot{M}$ values for the Trapezium cluster which are significantly lower than those obtained for stars in Taurus and the Orion flanking fields and suggest that the probable cause is that the discs of lower mass stars are being disrupted by UV radiation from the Trapezium OB stars, causing a large drop in mass accretion rates. Also, Calvet et al. (2004) point out that there is a strong bias against the detection of intermediate mass T Tauri stars ($M_* = 1.5 - 4\,\mathrm{M}_\odot$) with lower mass accretion rates, therefore the exponent of the $\dot{M} - M_*$ correlation may be less that 2. Further, Clarke & Pringle (2006) demonstrate that currently available data are perhaps limited by selection effects at high $\dot{M}$ values (whereby accretion rates cannot be determined when the accretion luminosity is greater than the stellar luminosity) and also by a lower bound defined by the upper limits of non-detections. Their work therefore suggests that the steep correlation between $\dot{M}$ and M_* is a natural consequence of detection/selection limitations, and that the true $\dot{M} - M_*$ correlation may be different.

Using the complex magnetic fields discussed above and assuming an accretion flow temperature of 10^4 K, we have calculated mass accretion rates and accretion filling factors for the COUP sample of stars which have estimates of M_*, R_*, P_{rot}, coronal temperature and measurements of the CaII 8542Å line. The lower coronal temperatures have been used, and, for those stars with spectra fitted with a two-temperature model, the higher coronal temperatures have also been considered. We have looked for a correlation between the mass accretion rate and stellar mass of the form $\dot{M} \propto M_*^\alpha$, where α is a constant. In Fig. 4.7 we have

plotted our calculated mass accretion rates from the COUP stars as a function of stellar mass, over-plotted on published values, for the LQ Hya-like magnetic field using the higher coronal temperatures. Preibisch et al. (2005) describe how the equivalent width of the CaII 8542Å line is used as an indicator of accretion for stars in the COUP dataset. They follow the classification discussed by Flaccomio et al. (2003a), who assume that stars are strongly accreting if the CaII line is seen in emission with EW(CaII)< -1Å. Stars with EW(CaII)>1Å are assumed to be either weak or non-accretors. However, it should be noted that many of the stars in the COUP dataset have EW(CaII)=0Å, and as such cannot be identified as either accreting or non-accreting. Stassun et al. (2006) discuss, with particular reference to the COUP, how some stars can show clear accretion signatures in Hα but without showing evidence for accretion in CaII. Therefore the sample of COUP stars considered in Fig. 4.7 may not be restricted to actively accreting CTTs and could also include other non-accreting young stars, such as weak line T Tauri stars, where the disc is rarefied or non-existent, and stars which are surrounded by discs but are not actively accreting at this time. However, we consider all of the available stellar parameters from the COUP dataset in order to demonstrate that our model produces a similar amount of scatter in calculated $\dot{M}$ values. In Fig. 4.8 we have only plotted those COUP stars which are regarded as strongly accreting based on the equivalent width of the CaII 8542Å line.

By fitting a line to the filled circles in Fig. 4.8 we find a correlation of the form $\dot{M} \propto M_*^{1.1}$ for COUP stars which are regarded as strong accretors, using the LQ Hya-like magnetic field. For the AB Dor-like field we find $\dot{M} \propto M_*^{1.2}$. Therefore our simple steady state isothermal accretion model produces an increase in mass accretion rate with stellar mass, and predicts $\dot{M}$ values which are consistent within the observed scatter, but it underestimates the exponent of 2 obtained from published values. We find similar results when considering both the lower and higher coronal temperatures. However, the strongly accreting COUP stars

only cover a small range of stellar mass, $M_* \approx 0.1 - 2.6\,\mathrm{M}_\odot$, and as such do not provide a large enough range in mass to test if our accretion model can reproduce the observed correlation. Therefore by only considering the observational data in the restricted range of mass provided by the COUP dataset (indicated by the vertical dashed lines in Fig. 4.8) then the exponent of the observed correlation is less than 2, with $\dot{M} \propto M_*^{1.4}$, and if higher mass stars do exist with lower mass accretion rates, could even be less than 1.4. Therefore our simple model, which Jardine et al. (2006) have used successfully to explain the observed correlation between X-ray emission measure and stellar mass, comes close to reproducing the stellar mass - mass accretion rate correlation. It is also worth noting that our model produces a correlation in agreement Clarke & Pringle (2006).

The accretion filling factors are typically around 2.5% for the sample of COUP stars (see Fig. 4.9), although it varies from less than 2% to greater than 4%. There is a slight trend for higher mass stars to have smaller filling factors, that is there is a slight trend for stars with larger corotation radii to have a smaller filling factors despite their larger mass accretion rates. For stars with smaller corotation radii (lower mass) there are many field lines threading the disc and able to support accretion, and therefore a large fraction of the stellar surface is covered in accreting field lines foot points, whereas for stars with larger corotation radii (higher mass) there are less accreting field lines and therefore smaller filling factors. However the higher mass stars are accreting at a larger velocity therefore producing larger mass accretion rates. The actual accretion filling factor depends on the magnetic field structure. For the AB Dor-like magnetic field the accretion filling factors are smaller at around 1.8%.

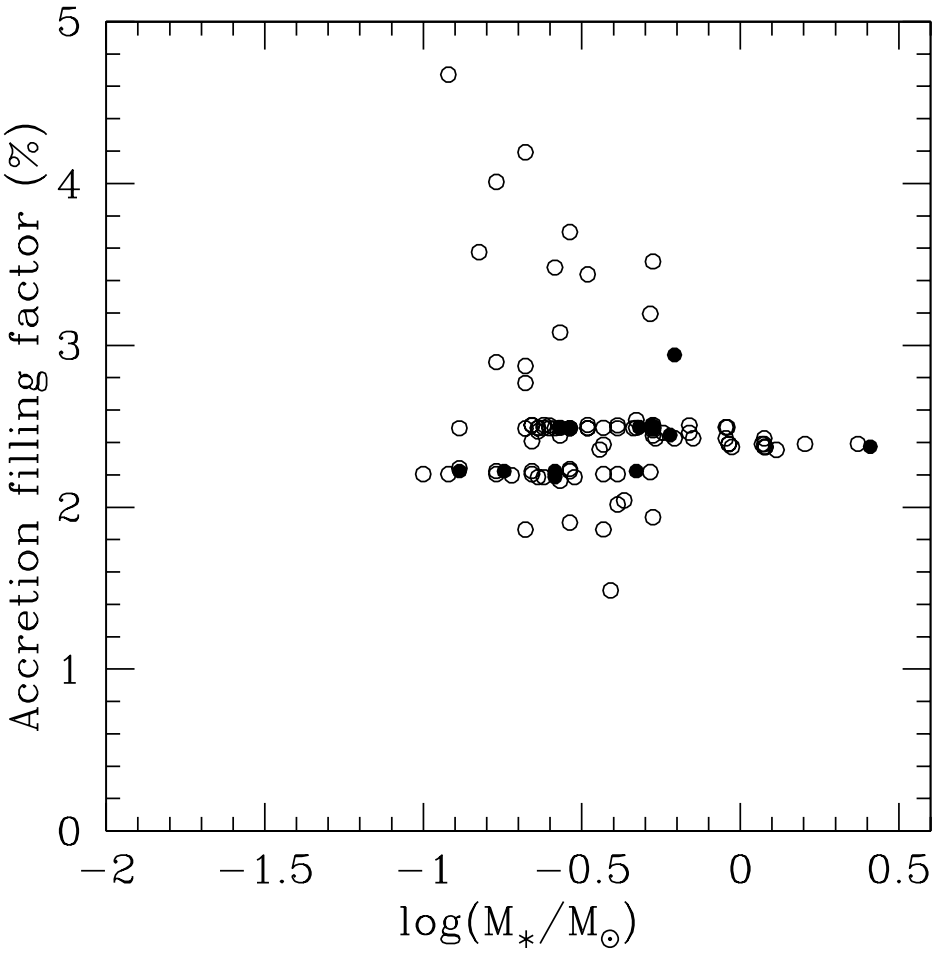

Figure 4.9: The accretion filling factors are small, and typically around 2.5% for the LQ Hya-like magnetic field. *Open* and *filled circles* represent the same set of stars as in Fig. 4.7.

4.4 Summary

The magnetic field geometry is crucial in controlling the location and distribution of hot spots on the stellar surface. For accretion to complex magnetic fields we find that hot spots can span a range of latitudes and longitudes, and are often at low latitudes towards the star's equator. We find that the accretion filling factors (the fractional surface area of a star covered in hot spots) are small and typically around 2.5%, but they can vary from less than 1% to over 4% and rarely to larger values. This is consistent with observations which suggest small accretion filling factors and the inference of hot spots at various latitudes (Valenti & Johns-Krull 2004).

For accretion with complex magnetic fields there is a distribution of in-fall speeds, which arises from variations in the size and shape of accreting field lines. The resulting effect that this will have on line profiles will be addressed in future work. In our model most of the accretion occurs from the corotation radius, but at some azimuths the disc extends closer to the star meaning that a small fraction of field lines are accreting material at lower velocity. Lower mass stars, with their lower surface gravities, typically have larger coronae which would extend out to corotation (Jardine et al. 2006). Therefore the lower mass stars are accreting along a mixture of open and closed field lines from the corotation radius. In contrast higher mass stars, with their higher surface gravities, have small compact coronae, and such stars actively accrete along mainly open field lines from the corotation radius. However, such open field lines do not thread the disc at all azimuths, with some accretion instead occuring along field lines which are much closer to the stellar surface. This gives rise to a small peak at low velocity in the in-fall velocity distribution. However, this represents only a small fraction of all accreting field lines which do not contribute significantly to the resulting mass accretion rate.

Finally we applied our accretion model to stars from the COUP dataset which have estimates of the stellar parameters and measurements of the equivalent width of the CaII 8542Å line, which is seen in emission for accreting stars. For the complex magnetic fields we calculated mass accretion rates and accretion filling factors as a function of stellar mass. The observed stellar mass - accretion rate correlation is $\dot{M} \propto M_*^2$ (Muzerolle et al. 2003; Calvet et al. 2004; Mohanty et al. 2005a; Muzerolle et al. 2005), however, this may be strongly influenced by detection/selection effects (Clarke & Pringle 2006). By only considering observational data across the range in mass provided by the COUP sample of accreting stars, the observed correlation becomes $\dot{M} \propto M_*^{1.4}$. Our steady state isothermal model gives an exponent of 1.1 for the LQ Hya-like magnetic field and 1.2 for the AB Dor-like field with similar results for both the high and low coronal temperatures, with the caveat that the observed correlation may be less than 1.4 due to a strong bias against the detection of higher mass stars with lower mass accretion rates (Calvet et al. 2004). It may be the case that an exponent of 1.2 compared to the observed 1.4, represents the best value that can be achieved with a steady state isothermal accretion model. Jardine et al. (2006) have used this model to reproduce the observed increase in X-ray emission measure with stellar mass (Preibisch et al. 2005). However, they find that when using the complex magnetic fields presented here (extrapolated from surface magnetograms of the young main-sequence stars AB Dor and LQ Hya) they slightly under estimate the emission measure-mass correlation. When they use dipolar magnetic fields, which represent the most extended stellar field, they slightly over estimated the correlation. This suggests that T Tauri stars have magnetic fields which are more extended than those of young main sequence stars, but are more compact than purely dipolar fields.

Also, our model has not been tested across a large enough range in mass to make the comparison with the observed correlation of $\dot{M} \propto M_*^2$. However, it

already compares well with the alternative suggestion of Clarke & Pringle (2006) that the $\dot{M} - M_*$ correlation is not as steep with $\dot{M} \propto M_*^{1.35}$. In future the model will be extended to consider accretion from the lowest mass brown dwarfs, up to intermediate mass T Tauri stars. This will require estimates of, in particular, rotation periods and coronal temperatures.

Our accretion model reproduces a similar amount of scatter in calculated $\dot{M}$ values compared with observations. This can be attributed to different sets of stellar parameters changing the structure of the accreting field. The stellar parameters control the location of the corotation radius, whilst it is the position of corotation relative to the natural coronal extent, which determines whether or not accretion occurs predominantly along the open field. However, for the moment we are restricted to using surface magnetograms of young main sequence stars which may not necessarily represent the true fields of T Tauri stars. It could be possible that variations in magnetic field geometry from star to star are responsible for the observed large scatter in mass accretion rate at any particular stellar mass. If there is a large difference in the structure of the accreting field from star to star this could lead to large variations in the mass accretion rate on to different stars. The spectropolarimeter at the Canada-France-Hawai'i telescope, ESPaDOnS: Echelle SpectroPolarimetric Device for the Observation of Stars (Petit et al. 2003; Donati 2004), will in the near future allow the reconstruction of the magnetic field topology of CTTs from Zeeman-Doppler imaging (Donati et al. 2007). This will allow a number of open questions to be addressed about the nature of the magnetic fields of T Tauri stars and allow us to test if our accretion model can indeed reproduce the stellar mass - accretion rate correlation.

Chapter 5

Rotationally Modulated X-ray Emission

This work has been published in Gregory, Jardine, Collier Cameron & Donati, 2006, MNRAS, 373, 827.

5.1 Introduction

One of the recent results from the Chandra Orion Ultradeep Project (COUP) was the detection of significant rotational modulation of X-ray emission from low mass pre-main sequence stars. The detection of such modulation suggests that the coronae of T Tauri stars are compact and clumpy, with emitting regions that are inhomogeneously distributed across the stellar surface, and confined within magnetic structures that do not extend out to much beyond a stellar radius (Flaccomio et al. 2005). There is also evidence for much larger magnetic loops, possibly due to the interaction with a surrounding circumstellar disc (Favata et al. 2005; Giardino et al. 2006). A model already exists for T Tauri coronae, where complex magnetic field structures contain X-ray emitting plasma close to

the stellar surface, whilst larger magnetic loops and open field lines are able to carry accretion flows (see Chapters 2-4).

In this Chapter I use surface magnetograms derived from Zeeman-Doppler imaging to extrapolate the coronae of T Tauri stars using stellar parameters taken from the COUP dataset (Getman et al. 2005). By considering isothermal coronae in hydrostatic equilibrium I obtain simulated X-ray light curves, for a range of stellar inclinations, and then X-ray periods using the Lomb Normalised Periodogram (LNP) method. I compare my results with those of Flaccomio et al. (2005), who demonstrate that those COUP stars which show clear evidence for rotationally modulated X-ray emission appear to have X-ray periods which are either equal to the optically determined rotation period ($P_X = P_{opt}$) or are half of it ($P_X = 0.5P_{opt}$).

5.2 Realistic magnetic fields

In order to model the coronae of T Tauri stars something must be assumed about the form of the magnetic field. Observations suggest it is compact and inhomogeneous and may vary not only with time on each star, but also from one star to the next. To capture this behaviour, we use as examples the field structures of two different main sequence stars, LQ Hya and AB Dor determined from Zeeman-Doppler imaging (Donati & Collier Cameron 1997; Donati et al. 1997; Donati 1999; Donati et al. 1999; Donati et al. 2003). By using both surface magnetograms, we can assess the degree to which variations in the detailed structure of a star's corona affects its X-ray emission. The method for extrapolating the field follows that employed by Jardine et al. (2002a). In Chapter 2 I dicussed in detail how to extrapolate stellar fields from surface magnetograms, and how X-ray emission measures from COUP are used to provide constraints on the extent of stellar coronae; I therefore do not repeat the details here. Figs. 5.1 and 5.2 show

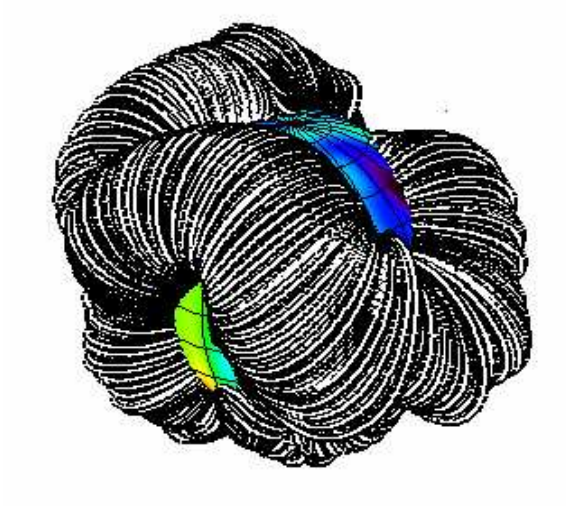

Figure 5.1: Closed coronal structures showing field lines which contain X-ray emitting plasma, extrapolated from a surface magnetogram of LQ Hya, for COUP source number 6 ($M_* = 0.23\,\mathrm{M}_\odot, R_* = 1.6\,\mathrm{R}_\odot, P_{rot} = 9.81\,\mathrm{d}$). The magnetic structures are compact and inhomogeneously distributed about the stellar surface.

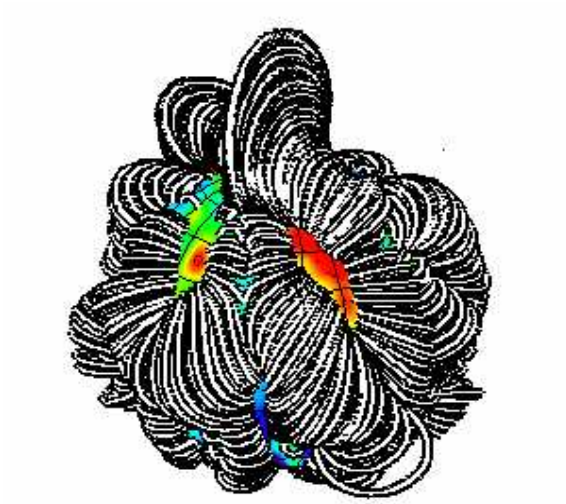

Figure 5.2: As Fig. 5.1 but extrapolated using a surface magnetogram of AB Dor.

examples of the complex magnetic field geometries which are considered.

The coronal field geometries considered in this work have been extrapolated from surface magnetograms of the young main sequence stars AB Dor and LQ Hya. In future it will be possible to use real T Tauri magnetograms derived from Zeeman-Doppler images obtained using the ESPaDOnS instrument at the Canada-France-Hawaii telescope. However, in the meantime, the example field geometries shown in Figs. 5.1 and 5.2 capture three essential features of T Tauri coronae. First, Jardine et al. (2006) have already demonstrated that the field structures which we consider here yield X-ray emission measures and mean coronal densities which are consistent with values obtained during the COUP - the largest available dataset of X-ray properties of young stellar objects (Getman et al. 2005). Second, the fact that rotational modulation of X-ray emission was at all detected during the COUP automatically led to the conclusion that the dominant X-ray emitting regions must be compact and unevenly distributed across the star (Flaccomio et al. 2005). It can be seen from Figs. 5.1 and 5.2 that the X-ray emitting closed coronal field lines do not extend out to much beyond the stellar surface (the coronae are compact) and that the emitting regions are inhomogeneously distributed about the star (the coronae are clumpy), in immediate agreement with the COUP results. Further, as we discuss below, the field geometries considered in this Chapter do give rise to significant rotational modulation of X-ray emission. It can also be seen from Figs. 5.1 and 5.2 that some regions of the stellar surface do not contain regions of closed field, and would therefore be dark in X-rays. Such regions contain wind bearing open field lines. Third, observations of various classical T Tauri stars by Valenti & Johns-Krull (2004) show the line-of-sight (longitudinal) magnetic field components measured using photospheric absorption lines, are often consistent with a net circular polarisation signal of zero. However, strong fields are detected from Zeeman broadening measurements. Such polarisation measurements trace the surface field structure

of T Tauri stars and immediately imply that such stars have complex and highly structured coronae. If the surface of the star is covered in many regions of opposite polarity this would give rise to a net polarisation signature of zero, with contributions to the overall signature from regions of opposite polarity cancelling out. Therefore the surface field must be highly complex and multipolar in nature, with many closed loops confining X-ray emitting plasma close to the surface of the star. However, it is also worth asking whether the coronal structure of classical T Tauri stars are likely to be fundamentally different from those of weak line T Tauri stars, a point which we discuss in §5.4.

Although we cannot be certain whether or not the magnetic field structures extrapolated from surface magnetograms of young main sequence stars in Figs. 5.1 and 5.2 do represent the magnetically confined coronae of T Tauri stars, they do satisfy the currently available observational constraints. They reproduce X-ray emission measures and coronal densities which are typical of T Tauri stars, and the field structures are complex, confining plasma within unevenly distributed magnetic structures close to the stellar surface. However, as such structures only represent a snap-shot in time of the coronal field geometry, we have chosen to consider two different field topologies. This allows us to model how much of an effect the field geometry has on the amplitude of modulation of X-ray emission and on resulting X-ray periods.

5.3 X-ray periods

5.3.1 X-ray light curves

Once the structure of the closed corona has been determined we calculate the density along the path of field line line loops as described in Chapter 2. From the density distribution we determine the X-ray emission measure ($EM = \int n^2 dV$).

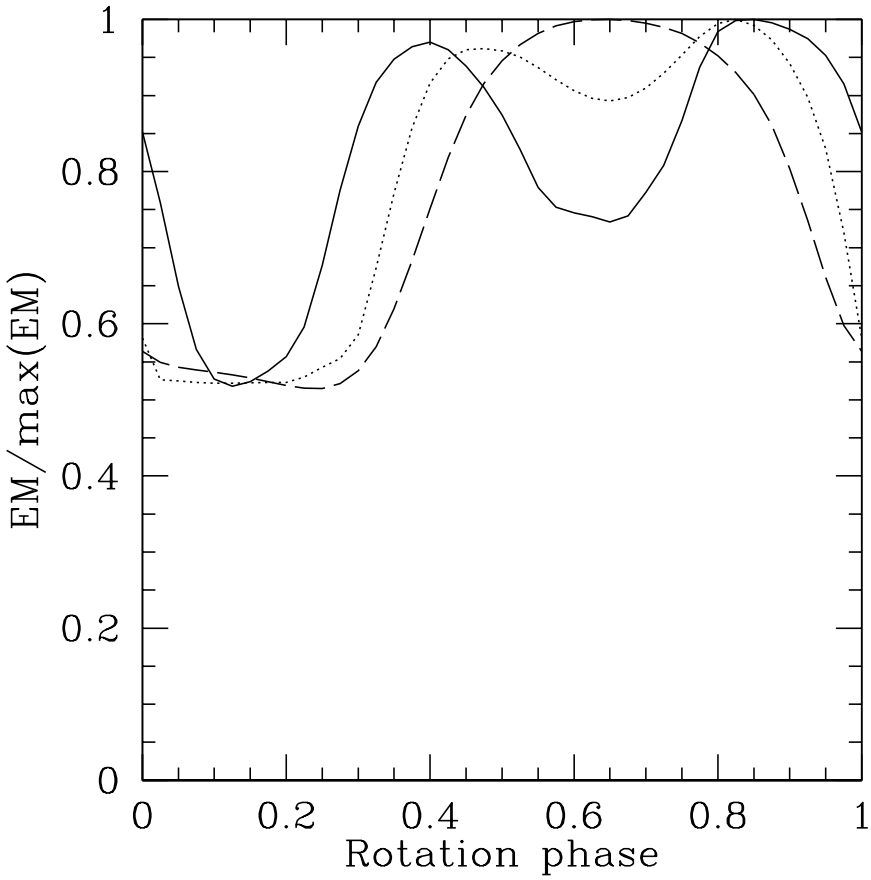

Figure 5.3: The variation in X-ray emission measure (EM) with rotation phase for the LQ Hya-like coronal structure shown in Fig. 5.1, for inclinations of the stellar rotation axis to the line-of-sight of 30 °(*dashed*), 60 °(*dotted*) and 90 °(*solid*). There is clear rotational modulation of X-ray emission.

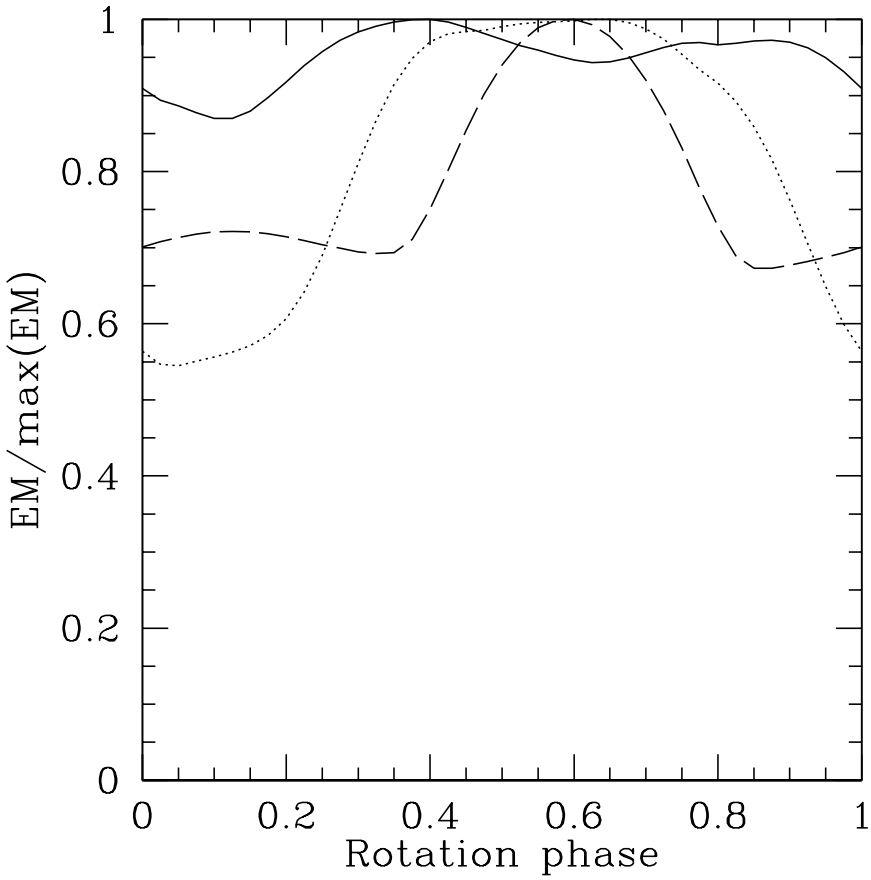

Figure 5.4: The variation in X-ray emission measure (EM) with rotation phase for the AB Dor-like coronal structure shown in Fig. 5.2, for inclinations of the stellar rotation axis to the line-of-sight of 30 °(*dashed*), 60 °(*dotted*) and 90 °(*solid*). There is clear rotational modulation of X-ray emission.

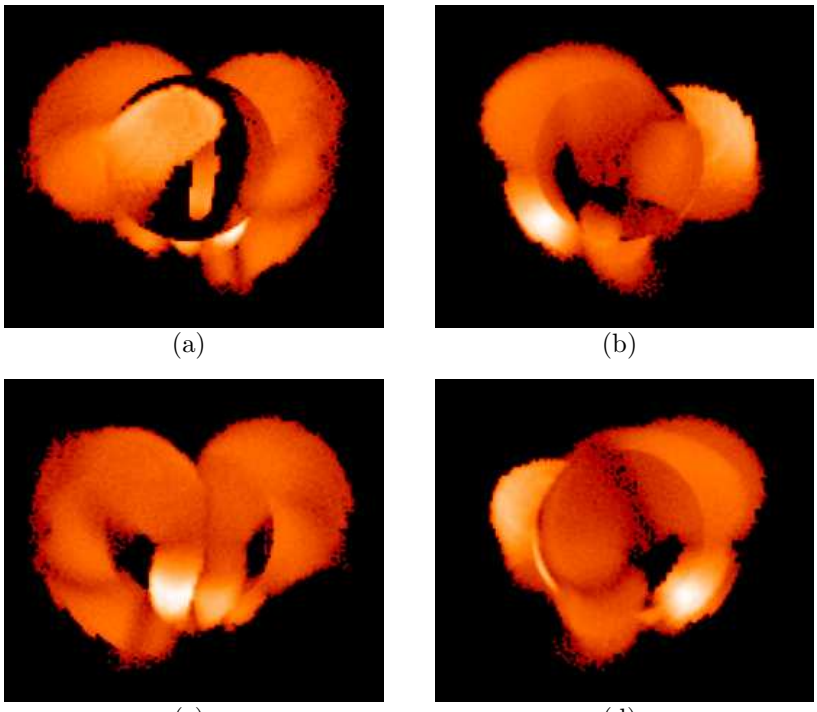

Figure 5.5: X-ray images obtained using the LQ Hya-like coronal structure from Fig. 5.1 for an inclination 90° (shown as the *solid line* in Fig. 5.3). Emitting regions are inhomogeneously distributed across the stellar surface and are confined within magnetic structures close to the star; some regions are, however, dark in X-rays. This particular surface map has two dominant emitting regions in opposite hemispheres, which at this inclination, go into eclipse as the star rotates giving rise to the two minima in Fig. 5.3 (*solid line*). Image (a) is for a rotational phase of 0.1, where the brightest of the two dominant emitting regions is in eclipse, (b) 0.4, where both of the dominant regions are visible, (c) 0.65, where the brightest emitting region is visible and the other is in eclipse and (d) 0.85, where once again both of the dominant regions can be seen.

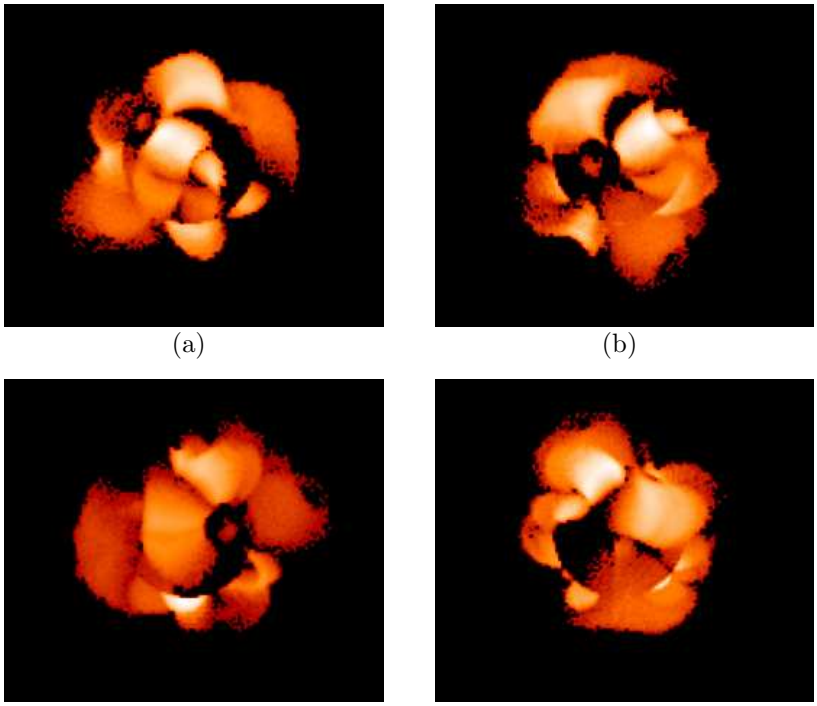

(a) (b) (c) (d)

Figure 5.6: As Fig. 5.5 but using the AB Dor-like coronal structure from Fig. 5.2 and for an inclination of 30 ° (shown as the dashed line in Fig. 5.4). Image (a) is for a rotational phase of 0.15, (b) 0.35, (c) 0.6, where the amount of X-ray emission is at a maximum due to the brightest emitting region (towards the bottom of the image) being visible and (d) 0.85. The coronal structure is more clumpy than the LQ Hya-like field, with many bright emitting regions across the stellar surface.

We calculate the contribution to the EM from each emitting region as projected onto an observer's line-of-sight and plot the ratio of EM to the maximum EM against rotational phase. Figs. 5.3 and 5.4 shows such plots using both the LQ Hya and AB Dor surface maps, for three inclinations. The corresponding X-ray images are shown in Figs. 5.5 and 5.6, from which it can be seen that emitting regions are compact and unevenly distributed across the stellar surface. However, some regions (which would contain open field lines) are dark in X-rays, in agreement with the conclusions of Flaccomio et al. (2005), that the saturation of activity cannot be due to the filling of the stellar surface with active regions[1].

For the LQ Hya-like coronal structure, although there are emitting regions across the stellar surface, there are two dominant emitting regions in opposite hemispheres, one of which is brighter in X-rays than the other. The effect of this is most apparent for large inclinations. For an inclination of $i = 30\,^\circ$ one minimum can be seen in the X-ray "light curve" (see Fig. 5.3), however as i is increased to $60\,^\circ$ a second minimum emerges, almost completely out of phase with the first. For $i = 90\,^\circ$ both of the dominant emitting regions go into eclipse as the star rotates, giving rise to the two distinct minima. As one of the dominant emitting regions is brighter in X-rays, however, the X-ray EM is further reduced when the brightest region goes into eclipse. The amplitude of the modulation is around 50%. For an inclination of $0\,^\circ$ there is no rotational modulation of X-ray emission, as expected.

The AB Dor-like coronal structure is more complex and, in contrast to the

[1]T Tauri stars are all in the saturated region of the rotation-activity relation (see e.g. Preibisch et al. 2005). One suggestion for the cause of saturated X-ray emission, whereby the X-ray luminosity relative to the stellar bolometric luminosity no longer increases with increasing rotation rate, is that the stellar surface is full of active regions. However, the detection of rotationally modulated X-ray emission suggests that regions of the stellar surface must be dark in X-rays. Therefore the saturation of X-ray emission cannot be due to the filling of the stellar surface with active regions.

LQ Hya-like coronal structure, there are many bright emitting regions (see Fig. 5.6). Fig. 5.4 shows the resulting X-ray light curves, and in this case we see little rotational modulation of the X-ray emission for $i = 90\,^{\circ}$, but see modulation of around 50% for smaller inclinations. It is already clear from the shapes of the X-ray light curves that the X-ray period depends on the stellar inclination.

5.3.2 Lomb Normalised Periodgram

The Lomb Normalised Periodgram (LNP) test was developed by Lomb (1976) who built upon earlier work by Barning (1963) and Vaníček (1971). The test has been further elaborated by Scargle (1982), Horne & Baliunas (1986) and Press & Rybicki (1989). For an evenly sampled dataset with a sampling interval Δ, whose reciprocal is the sampling rate,

$$h_n = h(n\Delta) \quad n = \ldots, -3, -2, -1, 0, 1, 2, 3, \ldots \tag{5.1}$$

The sampling theorem tell us that a data set like (5.1) contains complete information about all spectral components in a signal $h(t)$ up to a critical frequency called the Nyquist frequency, $f_c = 1/(2\Delta)$, and aliased information about any signal components at frequencies larger than the Nyquist frequency. However, for many astronomical applications we usually do not have an evenly sampled data set, and instead we must make do with unevenly sampled data obtained at discrete times t_i. The LNP test can be applied to search for periods within data sets with non-uniform sampling. It can be applied to data sets with missing data, e.g., when some observations have been lost due to poor weather or instrument problems. The COUP X-ray light curves have gaps where the Chandra satellite entered the van Allen belts. Although our simulated X-ray light curves do not contain gaps, we have chosen to search for X-ray periods using the LNP test to allow for the most direct comparison between our simulated results and the observations of Flaccomio et al. (2005).

Suppose that there are N data points $h_i = h(t_i), i = 1, \ldots, N$. The mean and variance of this data set are then,

$$\bar{h} = \frac{1}{N}\sum_{i=1}^{N} h_i \tag{5.2}$$

$$\sigma^2 = \frac{1}{N-1}\sum_{i=1}^{N}\left(h_i - \bar{h}\right)^2. \tag{5.3}$$

The LNP is then defined as,

$$P_N(\omega) = \frac{1}{2\sigma^2}\left\{\frac{\left[\Sigma_j(h_j - \bar{h})\cos\omega(t_j - \tau)\right]^2}{\Sigma_j \cos^2\omega(t_j - \tau)} + \frac{\left[\Sigma_j(h_j - \bar{h})\sin\omega(t_j - \tau)\right]^2}{\Sigma_j \sin^2\omega(t_j - \tau)}\right\}, \tag{5.4}$$

which is the spectral power as a function of angular frequency $\omega = 2\pi f > 0$, and τ is defined by,

$$\tan 2\omega\tau = \frac{\Sigma_j \sin 2\omega t_j}{\Sigma_j \cos 2\omega t_j}. \tag{5.5}$$

The constant τ is an offset that makes $P_N(\omega)$ completely independent of shifting all the t_i's by some constant. By expressing τ in the form of (5.5), Lomb (1976) demonstrated that equation (5.4) is identical to the equation which would result from estimating the harmonic content of a dataset by linear least squares fitting, at a given frequency ω,

$$h(t) = A\cos\omega t + B\sin\omega t. \tag{5.6}$$

It is also possible to calculate the significance of any peak in the spectrum $P_N(\omega)$. Scargle (1982) demonstrated that at any given ω and in the case of the null hypothesis that measured data points h_i are independent Gaussian random variables[2], the probability that $P_N(\omega)$ will be between $z(> 0)$ and $z+dz$ is $\exp(-z)dz$. Therefore if we consider M independent frequencies the probability that none give values larger than z is $(1-\mathrm{e}^{-z})^M$, and therefore the false alarm probability (FAP)

[2]Commonly measured data points h_i are the sum of a periodic signal and independent Gaussian noise.

of the null hypothesis[3] is,

$$P(> z) = 1 - \left(1 - \mathrm{e}^{-z}\right)^{M}. \tag{5.7}$$

The smaller the FAP the more significant is the periodic signal. To determine the FAP we need to know M, the number of independent frequencies. Horne & Baliunas (1986) discuss how M may be determined, however as we are only interested in peaks in the $P_N(\omega)$ distribution which have small FAPs, that is the region where the significance is a small number $<< 1$, then (5.7) may be written as,

$$P(> z) \approx M\mathrm{e}^{-z}. \tag{5.8}$$

The significance therefore scales with M. However, as is discussed in detail by Press et al. (1992), practical significance levels are e.g. 0.01, 0.001, etc. and therefore errors of even $\pm 50\%$ are acceptable since significance levels are typically spaced orders of magnitude apart. Therefore the estimate of M, the number of independent test frequencies, does not have to be accurate.

Fig. 5.7 is an example of the LNP test applied to a set of data taken at random times, reproduced from Press et al. (1992). There are 100 data points with a random Poisson distribution in time. If the points had been evenly spaced in time then the Nyquist frequency would have been $f_c = 0.5$. In this example it was assumed that $M = 2N$. Although the presence of any periodic variation in the data is not clear to the eye, the $P_N(\omega)$ distribution shows a clear peak at a frequency of $f = \omega/2\pi = 0.81$ with a FAP of less than 0.1%. This is the frequency of the sine wave present in the data. The significant peak is found above the Nyquist frequency and without significant aliasing down into the Nyquist interval. This would not be possible for evenly spaced data, but is possible here because the randomly spaced data has some points spaced much closer than the average sampling rate, removing ambiguity from any aliasing. Koen (2006) and

[3]The FAP is significance level of any given peak in the $P_N(\omega)$ distribution.

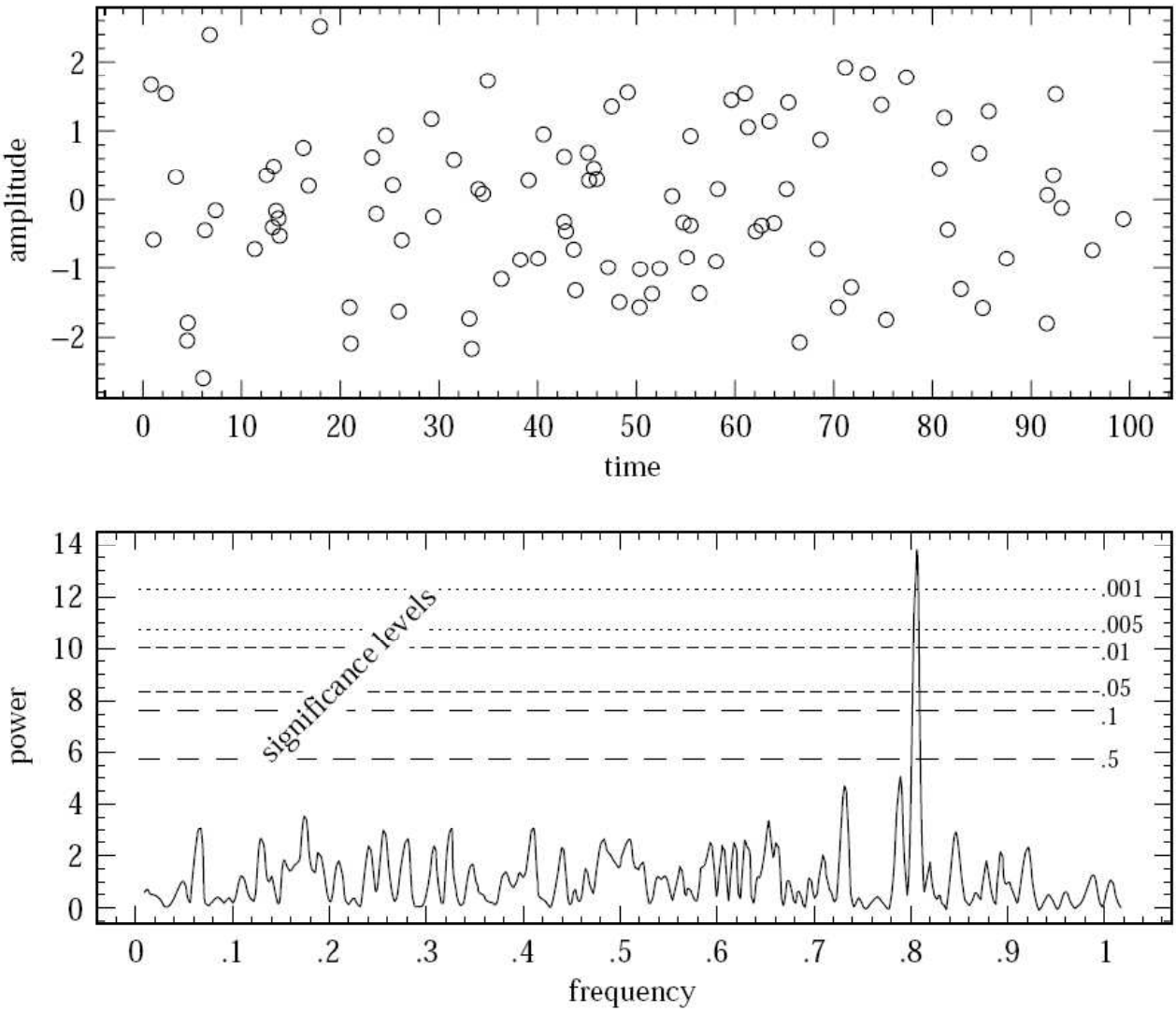

Figure 5.7: Example of the Lomb Normalised Periodogram, reproduced from Press et al. (1992). Although it is not obvious to the eye there is a sinusoidal variation within the data, with a frequency of 0.81. This shows up clearly as a large peak in the LNP power spectrum ($P_N(\omega)$) with a small FAP of less than 0.1%.

Eyer & Bartholdi (1999) provide further discussion about the relevance of the Nyquist frequency to irregularly spaced time series. The LNP test thus provides a powerful tool in determining periods present in noisy unevenly sampled data sets, and was therefore a key tool in the detection of rotationally modulated X-ray from young stellar objects as part of COUP (Flaccomio et al. 2005). In order to allow as consistent a comparison as possible between our simulated X-ray light curves and the observed light curves obtained during COUP, we also search for X-ray periods using the LNP test.

5.3.3 X-ray and optical periods

We consider the same 233 COUP sources used in the analysis of Flaccomio et al. (2005), however, as our model requires estimates of the stellar parameters (mass, radius, rotation period and measurements from which we can infer a coronal temperature) we have omitted those sources without estimates of these parameters. This leaves a total of 183 COUP sources with a lower coronal temperature and 141 where a higher temperature component is also given in the COUP dataset. For each COUP source we have generated an X-ray light curve (see Fig. 5.10 for three examples) using both the LQ Hya and AB Dor surface magnetograms, and for inclinations of $30\,^{\circ}$, $60\,^{\circ}$ and $90\,^{\circ}$. In the subsequent discussion we only consider the lower coronal temperatures. Our results for the higher coronal temperatures are similar and are discussed in §5.4. Each simulated light curve covers 13.2 days, to match the COUP observation time. COUP light curves also contain 5 gaps where the Chandra satellite passed through the van Allen belts. Therefore we have considered both continuous light curves (see Fig. 5.10), and light curves which have gaps at approximately the same observation times (and lasting for approximately the same duration) as the gaps in COUP X-ray light curves (see Fig. 5.11). We tried sampling our simulated X-ray light curves every 2000 s, 5000 s and $10,000$ s, to match the analysis of Flaccomio et al. (2005), but found

that our results were similar in all three cases. The results presented here refer only to a time sampling of $10,000\,\mathrm{s}$.

We have calculated X-ray periods using the Lomb Normalised Periodogram (LNP) method so that our analysis matches that of Flaccomio et al. (2005) as closely as possible. The observed X-ray light curves of COUP sources are contaminated with many flares, with a great variety of flaring behaviour, whereas our simulated light curves do not suffer from this problem. Therefore, when calculating X-ray periods, our false alarms probabilities (FAPs) indicating the significance of peaks found in the LNP power spectrum are vanishingly small, with $-40 < log_{10}[FAP(\%)] < -10$.

Figs. 5.8 and 5.9 are plots of our calculated X-ray periods against optically determined rotation periods from Flaccomio et al. (2005), which is collection of rotation periods taken mainly from Herbst et al. (2002). We have limited our search to X-ray periods of $P_X < 13\,\mathrm{d}$ and have chosen the scale of the axes to allow a direct comparison with similar plots in Flaccomio et al. (2005). For the LQ Hya-like coronal structure, at any given inclination, the ratio P_X/P_{opt} is independent of stellar mass and radius, except for stars with large P_{opt} (see the discussion below). We find that $P_X = P_{opt}$ for inclinations of $30\,^\circ$ and $60\,^\circ$, but that $P_X = 0.5P_{opt}$ for $i = 90\,^\circ$. Flaccomio et al. (2005) provide a qualitative argument that the X-ray period would equal the optical period if there was one dominant emitting region on the stellar surface. They also point out that if there were two dominant emitting regions in opposite hemispheres, separated by $180\,^\circ$ in longitude, then it should be expected that the X-ray period would be half of the optical period. Although we agree with this point of view, our LQ Hya-like field structure does have two dominant emitting regions in opposite hemispheres, which for high inclinations yields $P_X = 0.5P_{opt}$ but at low inclinations gives $P_X = P_{opt}$. Therefore the qualitative picture of having two dominant emitting regions in opposite hemispheres giving rise to $P_X = 0.5P_{opt}$ should come with the

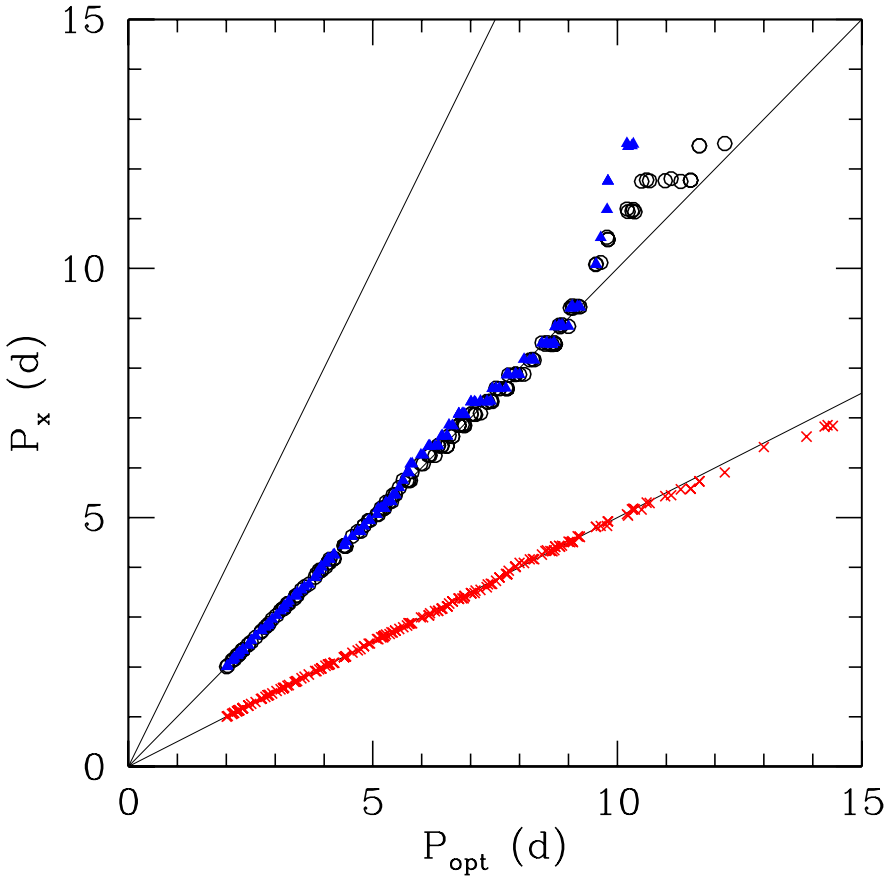

Figure 5.8: Comparison between X-ray periods P_X and optically determined periods P_{opt} for stars in the COUP dataset using the LQ Hya-like coronal structure shown in Fig. 5.1, for inclinations of 30 °(*black circles*), 60 °(*blue triangles*) and 90 °(*red crosses*). The *solid lines* represent $P_X = [0.5, 1, 2]P_{opt}$. The ratio P_X/P_{opt} is independent of stellar mass and radius.

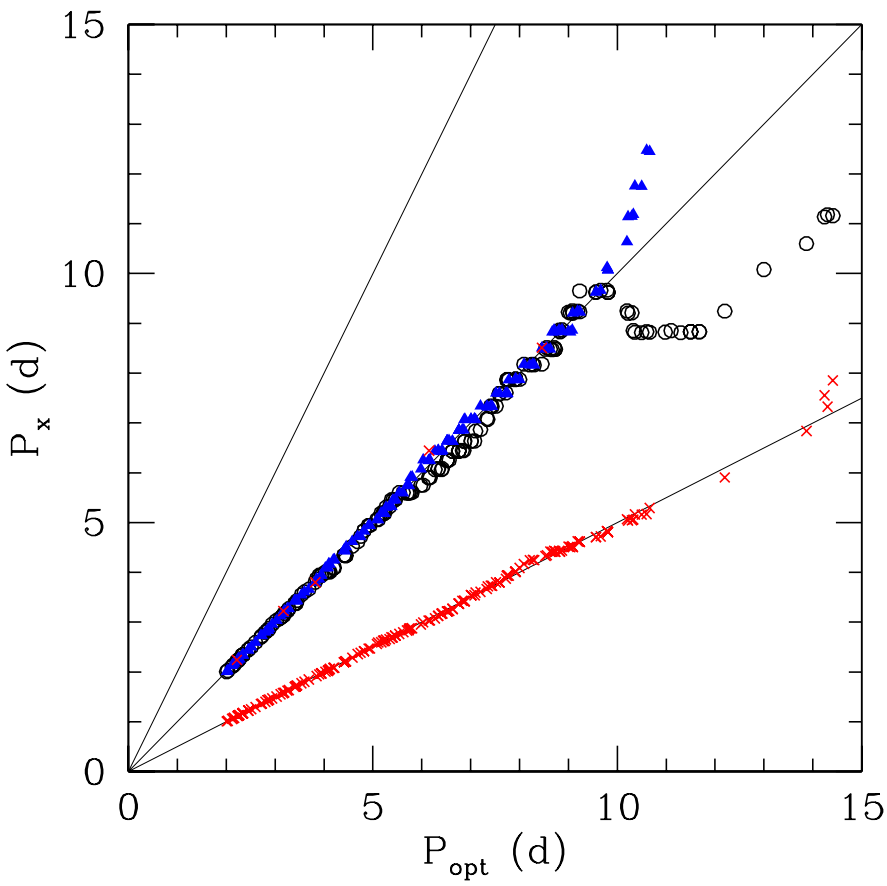

Figure 5.9: Comparison between X-ray periods P_X and optically determined periods P_{opt} for stars in the COUP dataset using the AB Dor-like coronal structure shown in Fig. 5.2, for inclinations of 30 °(*black circles*), 60 °(*blue triangles*) and 90 °(*red crosses*). The *solid lines* represent $P_X = [0.5, 1, 2]P_{opt}$. The ratio P_X/P_{opt} is independent of stellar mass and radius.

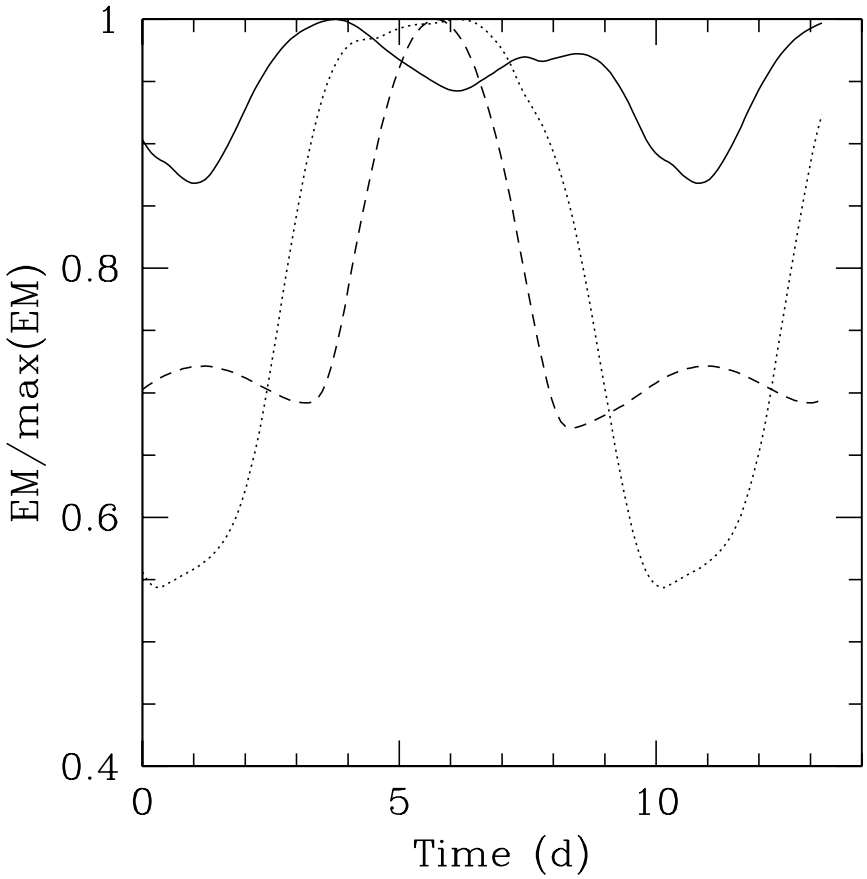

Figure 5.10: Simulated X-ray light curves without gaps corresponding to inclinations of 30° (*dashed*), 60° (*dotted*) and 90° (*solid*), for the coronal structure in Fig. 5.2.

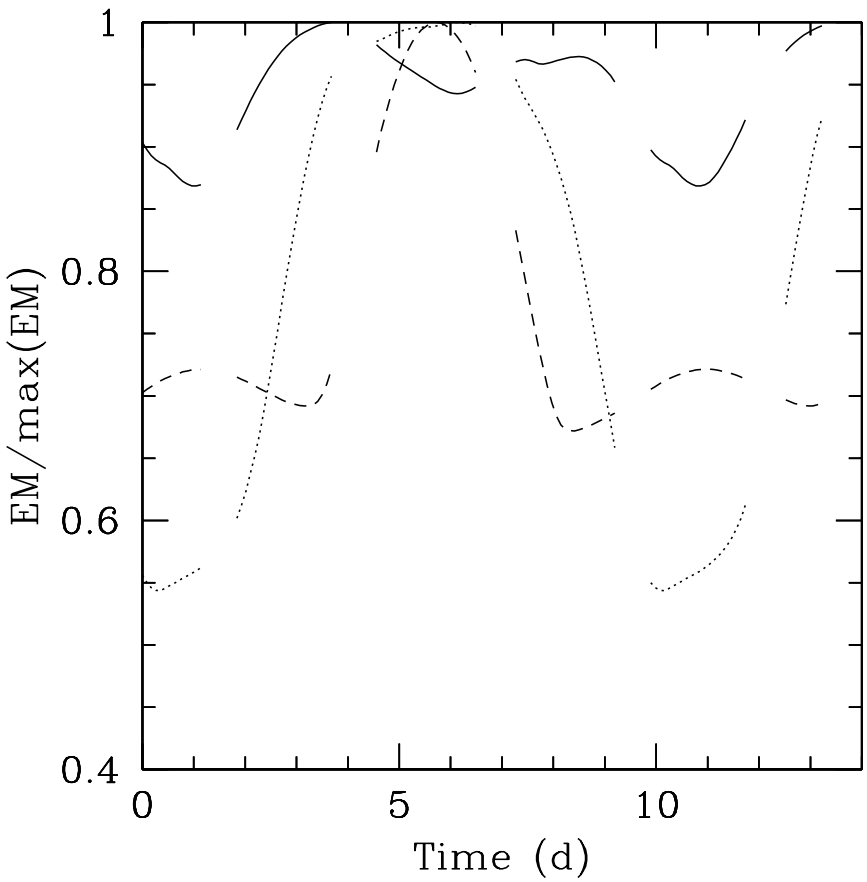

Figure 5.11: The same X-ray light curves as Fig. 5.10 but with gaps introduced to mimic the effect of missing data in COUP light curves when the Chandra satellite entered the van Allen belts

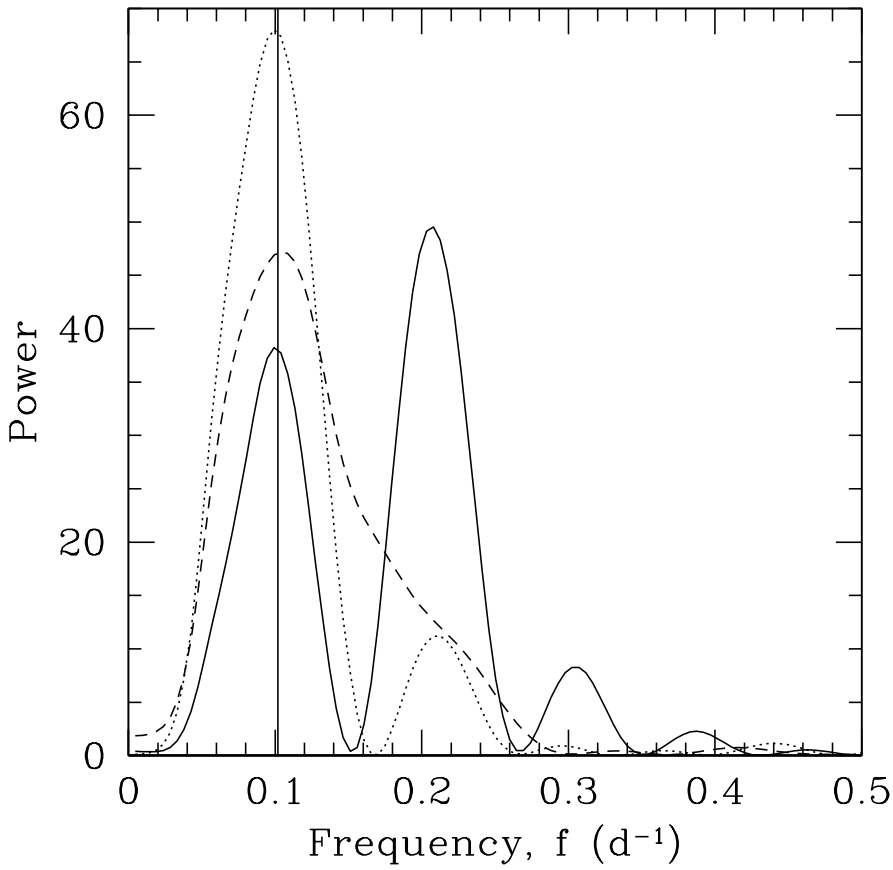

Figure 5.12: Lomb Normalised Periodograms corresponding to the light curves without gaps in Fig. 5.10, for inclinations of 30° (*dashed*), 60° (*dotted*) and 90° (*solid*), for the coronal structure in Fig. 5.2. There are two significant peaks for the $i = 90°$ case, one corresponding to P_{opt} and the other $0.5P_{opt}$. The *solid vertical line* is the frequency corresponding to the optical period.

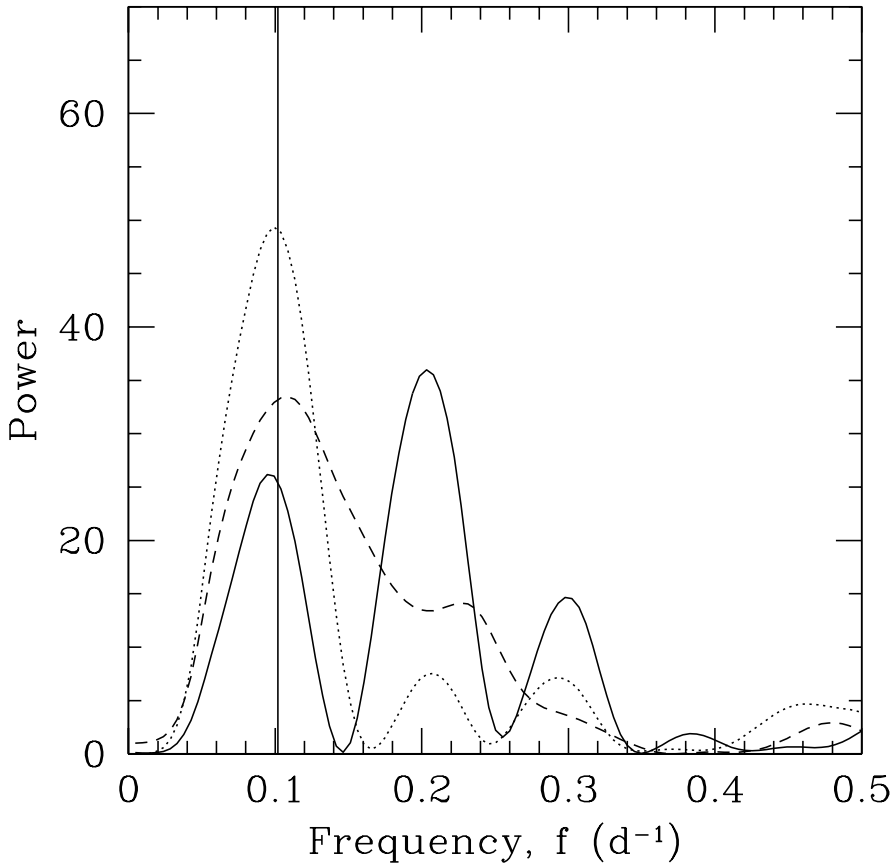

Figure 5.13: Lomb Normalised Periodograms corresponding to the light curves with gaps in Fig. 5.11, for inclinations of 30° (*dashed*), 60° (*dotted*) and 90° (*solid*), for the coronal structure in Fig. 5.2. There are two significant peaks for the $i = 90°$ case, one corresponding to P_{opt} and the other $0.5P_{opt}$. The *solid vertical line* is the frequency corresponding to the optical period. When gaps are introduced into the light curves we find that the most significant peak in the LNP power spectrum generates the same X-ray period as the light curve without gaps, albeit with lower significance.

(perhaps obvious) caveat that it depends on the inclination at which the star is viewed.

Results for the AB Dor-like coronal structure are similar (see Fig. 5.9). We again find that the ratio P_X/P_{opt} is independent of stellar mass and radius for the $i = 30\,^\circ$ and $60\,^\circ$ cases, provided that $P_{opt} < 10\,\mathrm{d}$. Stars with $P_{opt} > 10\,\mathrm{d}$, and in particular those which have optical periods longer than the COUP observing time (13.2 d), often do not have X-ray periods of either $0.5P_{opt}$ or P_{opt}. This is most noticeable for the AB Dor-like coronal structure in the $30\,^\circ$ case (see Fig. 5.9), where stars with the longest P_{opt} are found to have X-ray periods of $0.7P_{opt}$. This is a result of only considering the X-ray light curves over a duration equal to the COUP observing time. By extending our simulated X-ray light curves to cover twice the duration of the COUP observing time (so that ≈ 2 complete rotations of stars with the longest P_{opt} are covered by the light curves), we found that all X-ray periods in the $i = 30\,^\circ$ case clustered around $P_X = P_{opt}$. For the $i = 90\,^\circ$ case we find that most stars have $P_X = 0.5P_{opt}$, but five stars have $P_X = P_{opt}$. This is due to there being two significant peaks in the LNP power spectrum (see Fig. 5.12) and, depending on which peak is the larger, the X-ray period is either $0.5P_{opt}$ or P_{opt}. However, when the AB Dor-like coronal structure is viewed at an inclination of $90\,^\circ$, the amount of rotational modulation of X-ray emission is at its smallest (only 13%) of all the field structures and inclinations which we have considered; this can be seen from the light curve in Fig. 5.4. Therefore the $i = 90\,^\circ$ case for the AB Dor-like field is an interesting result. It shows that it is possible to have a highly structured corona, with emitting regions which are close to the stellar surface, with regions which are dark in X-rays, but when such a field structure is viewed at an unfavourable inclination, little rotational modulation of X-ray emission is detected, and it is difficult to recover an X-ray period. However, there is significant modulation detected for the $i = 30\,^\circ$ and $60\,^\circ$ cases with $P_X = P_{opt}$. Therefore the X-ray periods we have determined are

similar for both the AB Dor and LQ Hya-like coronal fields, and are dependent on the stellar inclination. The AB Dor field has many bright emitting regions making it difficult to qualitatively understand the exact shape of the resulting X-ray light curve. In the next section we further investigate the effects of inclination and the magnetic field structure on X-ray periods.

We have also considered how having gaps in our simulated X-ray light curves would affect the resulting X-ray period (see Figs. 5.11 and 5.13). We found that the values of P_X obtained from light curves with gaps were identical to those derived from continuous light curves, with the only difference being that the main peaks in the LNP power spectra were of lower significance.

5.3.4 Effect of inclination and coronal structure

In order to further investigate the effects of inclination and the structure of stellar coronae, we randomly assign an inclination of between $5\,^\circ$ and $90\,^\circ$ to each of the COUP sources before calculating an X-ray period. Inclinations of smaller than $\approx 5\,^\circ$ produce little or no rotational modulation of X-ray emission and so are not considered. The results are plotted in Fig. 5.14 for both the LQ Hya and AB Dor-like coronal structures. We again find that X-ray periods are either equal to P_{opt} or $0.5P_{opt}$, with a few exceptions.

Our simulations apparently highlight a well defined lower limit for X-ray periods of $P_X = 0.5P_{opt}$. It should be noted, however, that we are limited by the availability of magnetic surface maps; it could be the case that another surface magnetogram may yield X-ray periods which are lower that $0.5P_{opt}$. Flaccomio et al. (2005) find stars with reliably detected rotational modulation of X-ray emission with $P_X < 0.5P_{opt}$ but argue that such period detections may be spurious. In order to test if there is a well defined lower limit of $P_X = 0.5P_{opt}$ we generated a model coronal structure which had three emitting regions randomly positioned

around the stellar surface. In the case where all three emitting regions were evenly spaced in longitude, and at a fixed (low) latitude (e.g. the three emitting regions placed at equal increments about the star's equator) we found an X-ray period of $P_X = 0.333P_{opt}$. Therefore it is possible to have a coronal field where the dominant emitting regions are distributed such that $P_X < 0.5P_{opt}$. However, we find that such field structures are rare in comparison to those which yield $P_X = [0.5, 1]P_{opt}$.

Flaccomio et al. (2005) also find a few stars with evidence for rotationally modulated X-ray emission with X-ray periods which are larger than the optical period, however their further simulations appear to indicate that these period detections (in particular those with $P_X > 2P_{opt}$) are likely to be spurious. We could not create any model which led to a P_X value of much larger than P_{opt}.

The X-ray period depends on stellar inclination (see Fig. 5.15). At low inclinations for the LQ Hya field, $P_X = P_{opt}$. As the inclination is increased a second peak in the LNP power spectrum becomes stronger and eventually, for $i \approx 75\,^\circ$, both peaks are of almost equal significance. For $i > 75\,^\circ$, $P_X = 0.5P_{opt}$, with the secondary peak having become the most significant. This occurs when both of the dominant emitting regions enter eclipse at different times as the star rotates. At low inclinations the amplitude of modulation is small (see Fig. 5.16) for the LQ Hya field, but is almost constant for $i > 25\,^\circ$. Overall we find less modulation for the AB Dor field. This is consistent with our findings in §5.3.3. When the AB Dor field is viewed at both low ($i < 30\,^\circ$) and high ($i > 75\,^\circ$) inclinations there is little rotational modulation of X-ray emission. Thus, simply having compact emitting regions inhomogeneously distributed about the stellar surface is not enough to generate large modulation of X-ray emission - the amount of modulation depends strongly on the stellar inclination.

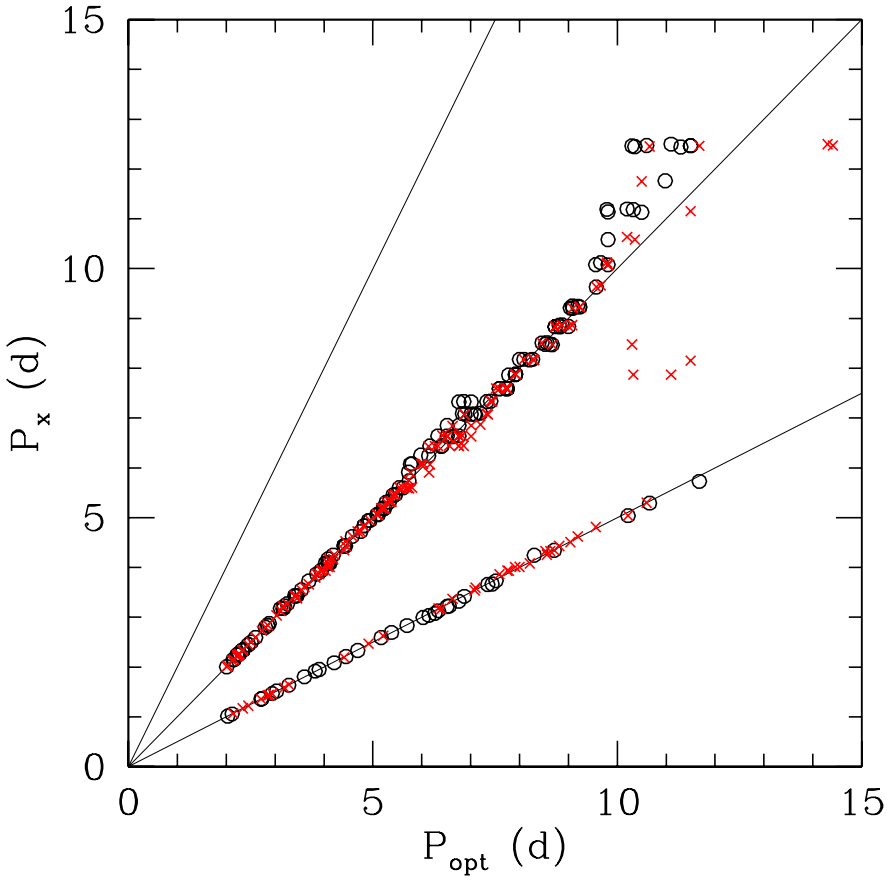

Figure 5.14: Comparison between our calculated X-ray periods and observed optical periods. X-ray periods have been calculated for COUP stars from Flaccomio et al. (2005) with randomly assigned inclinations. The lines represent $P_X = [0.5, 1, 2]P_{opt}$, with data for the LQ Hya-like (*black circles*) and AB Dor-like coronal structures (*red crosses*). There is little difference between the different coronal field geometries.

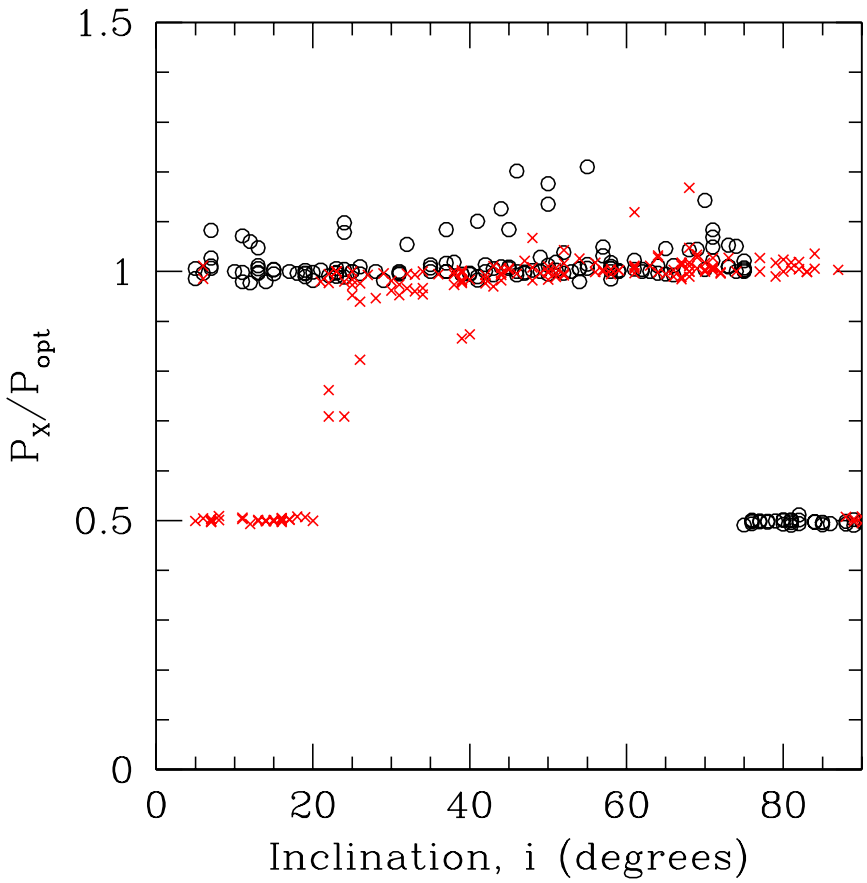

Figure 5.15: The variation in X-ray period as a fraction of the optical period with stellar inclination for the LQ Hya (*black circles*) and AB Dor (*red crosses*) coronal fields. Data represents the same stars as in Fig. 5.14 with the same randomly selected inclinations.

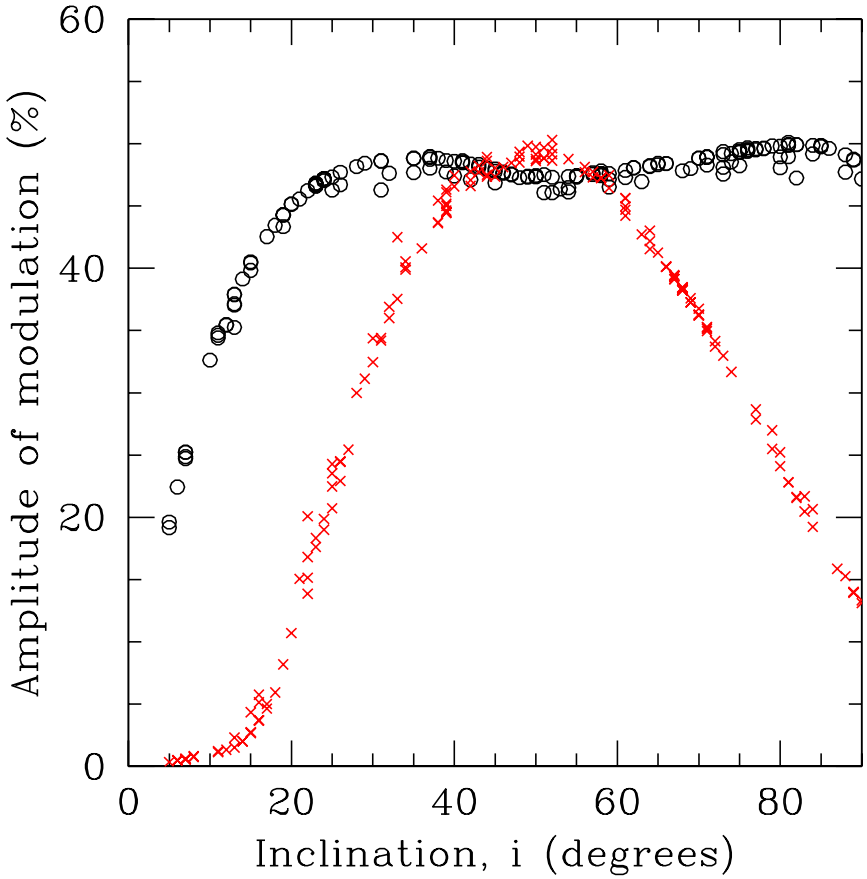

Figure 5.16: The variation in modulation amplitude with stellar inclination for the LQ Hya (*black circles*) and AB Dor (*red crosses*) coronal fields. Data represents the same stars as in Fig. 5.14 with the same randomly selected inclinations.

5.4 Summary and discussion

By extrapolating surface magnetograms of young main sequence stars we have shown that magnetic fields with a realistic degree of complexity reproduce the observed rotational modulation of X-ray emission from T Tauri stars (Flaccomio et al. 2005). This model has already been used to correctly predict X-ray EMs, mean coronal densities and the observed increase in X-ray EM with stellar mass (Jardine et al. 2006). We find that X-ray emitting regions are inhomogeneously distributed around the stellar surface and are typically compact ($\leq R_*$). This agrees with the findings of Flaccomio et al. (2005) who point out that in order to explain the amplitude of the modulation of X-ray emission which they detect, emitting regions must be compact in order to undergo eclipse.

We found that the ratio P_X/P_{opt} is independent of stellar mass and radius, but that X-ray periods are dependent on stellar inclination. For example, in the case where there are two dominant X-ray emitting regions in opposite hemispheres, we found that the X-ray period could be either $0.5P_{opt}$ or P_{opt} depending on how the star is inclined to the observer. In order words, the presence of two bright emitting regions in opposite hemispheres does not immediately imply that $P_X = 0.5P_{opt}$. Further, some coronal fields with compact emitting regions produce only small amplitude modulation of X-ray emission when viewed at unfavourable inclinations.

We do not find X-ray periods of $P_X > 2P_{opt}$, unlike Flaccomio et al. (2005). However, they argue that those period detections are likely to spurious, given the arduous task of removing flares from observed COUP X-ray light curves. Also the apparent lower limit of $P_X = 0.5P_{opt}$ may not be of true physical origin. We have demonstrated this by constructing a corona which resulted in $P_X = 0.333P_{opt}$; however this sort of field structure is perhaps uncommon. Instead the majority of X-ray periods cluster around $P_X = [0.5, 1]P_{opt}$. The majority of X-ray periods

are equal to the optical periods. This suggests that for complex magnetic fields, where there are many emitting regions distributed across the stellar surface, it becomes difficult to disentangle the contribution to the X-ray emission from any particular emitting region. Consequently, even though different stars are likely to have different coronal structures, the X-ray periods of T Tauri stars appear to cluster around P_{opt} and $0.5P_{opt}$. In other words, although different coronal structures give rise to different amounts of modulation at a fixed inclination, the X-ray period distribution for a given sample of stars is likely to be the same.

Throughout we have only considered the lower coronal temperatures derived from the COUP dataset. If instead we had used the higher coronal temperatures our results and conclusions remain the same. For a higher coronal temperature more field lines are unable to contain the coronal gas and are blown open to form a stellar wind, meaning that coronae are (slightly) more compact. This leads to small, but not important, differences in the resulting X-ray periods, however the amplitude of modulation is larger (typically 60% compared with 50% for the lower coronal temperatures). The amplitudes of modulation which we determine compare well with the observed values of Flaccomio et al. (2005) of 20-70%.

Although we have not considered it in this paper, the coronal structure of T Tauri stars may evolve on timescales that are comparable with the COUP observing time. For example a dominant X-ray emitting region may be lost due to a large coronal mass ejection which would open up a previously-closed region of field. This may then change the resulting X-ray period. However, it is still interesting that even with two different field structures such as those in Figs. 5.1 and 5.2, the X-ray periods are still typically equal to the optical period or are half of the optical period.

We have not considered how the presence of a circumstellar disc and active accretion influences the coronal structure, and their possible effects on the X-ray period/amplitude of modulation. A comprehensive and detailed discussion

of how accretion processes may influence X-ray emission from T Tauri stars is provided by Preibisch et al. (2005). The growing consensus, as was confirmed by COUP, is that X-ray emission from T Tauri stars does not depend upon the presence of a disc, but is influenced by active accretion. For example, Feigelson et al. (2002) found X-ray activity levels were the same for stars with and without discs[4]. However, Flaccomio et al. (2003a) found a difference in the X-ray activity levels of accreting and non-accreting stars. The process of accretion therefore influences the amount of X-ray emission detected, with stars that show evidence for accretion having observed X-ray luminosities which are a factor of 2-3 smaller than those stars without discs and those stars which show evidence for discs, but not for accretion (Preibisch et al. 2005).

Accretion may therefore affect the coronal structure of T Tauri stars, which in turn may have implications for rotational modulation of X-ray emission, and X-ray periods. It is important to note however that Flaccomio et al. (2005) have searched for correlations between observed modulation amplitudes and the Δ(I−K) excess, a disc indicator, and EW(CaII), an accretion indicator, but do not find any. Furthermore, Flaccomio et al. (2005) also search for dependencies on the X-ray period detection fraction with the indicators of discs and accretion, but again find none. This suggests that there is no difference in the spatial distribution of X-ray emitting regions in both classical and weak line T Tauri stars (with the former having both a disc and active accretion, and the latter neither). However, Flaccomio et al. (2005) did find a suggestion (but with a low significance of only about 1%) that stars with $P_X = 0.5P_{opt}$ are preferentially active accretors.

Jardine et al. (2006) have shown that stars (typically of lower mass) which

[4]It is important to remember that the presence of a disc does not immediately imply that accretion is taking place. Indeed many T Tauri stars show excess infrared emission, indicating the presence of a disc, but lack strong Hα or CaII emission, characteristic of active accretion (e.g. Lada et al. 2006).

have coronae that would naturally extend to beyond the corotation radius would have their outer corona stripped by the presence of a disc. In order to check if this would affect the resulting X-ray period we determined the coronal structure of all the stars considered previously assuming that they were surrounded by a disc. Any field line which passed through the disc at, or within the corotation radius was assumed to have the ability to carry an accretion flow and was therefore considered to be mass-loaded and set to be dark in X-rays - a process which is discussed in detail by Jardine et al. (2006) and Gregory et al. (2006a). We then calculated X-ray emission measures with rotational phase and determined the amplitude of modulation of X-ray emission and X-ray periods, using the same methods as before. We found no difference in the values of P_X and very little difference in the amplitudes of modulation. We therefore conclude, exactly as the observations suggest, that the presence of discs does not influence rotational modulation of X-ray emission. However, active accretion might.

We have yet to consider how accretion could influence rotational modulation of X-ray emission. As already discussed above stars which are actively accreting show lower levels of X-ray activity than those which are non-accretors. Again, the possible explanations for this are discussed by Preibisch et al. (2005), with the most likely being that magnetic reconnection events in the magnetosphere cannot heat the dense material within accretion columns to a high enough temperature to emit in X-rays. Some models suggest that accretion will distort magnetic field lines giving rise to instabilities and reconnection events (e.g. Romanova et al. 2004b). The energy liberated in such reconnection events may not be able to heat the high density material in accretion columns to a sufficiently high temperature in order to emit in X-rays. Thus accretion columns rotating across the line-of-sight to the star may be responsible for the observed reduction in X-ray emission in accreting T Tauri stars compared with the non-accretors. The effect of this on X-ray periods and modulation amplitudes will be considered in

future work. A detailed accretion flow model will have to be constructed in order to account for the attenuation of coronal X-rays by accretion columns rotating across the line-of-sight. Also, inner disc warps may have a similar effect at high stellar inclinations. This could change the shape of the X-ray variability curves shown in Figs. 5.3, 5.4, 5.10 and 5.11, with a reduction in X-ray emission at particular rotational phases, depending on the accretion flow geometry.

Our model may allow for the simultaneous confinement of X-ray emitting plasma in closed loops close to the stellar surface, but also for other field lines to stretch out into the inner disc and carry accretion flows. Gregory et al. (2006a) find that often open field lines can carry accretion flows, which may allow accretion to influence the magnetic field structure on the large scale, with field lines being mass-loaded with disc material, but leaving compact coronae relatively unaffected by the process of accretion. This model would allow for the existence of large extended magnetic structures, inferred to exist from the detection of large flaring loops by Favata et al. (2005), with the coexistence of compact coronae. However, work remains to be done here. Another new accretion model may offer insights into the connection between X-ray emission and accretion in T Tauri stars. An MHD model by von Rekowski & Piskunov (2006b) suggests that rather than material being loaded onto field lines at the inner edge of the disc, it flows onto the star only at times when, and into regions where, the accretion flow is able to overcome the stellar wind. In such a way this model predicts that accretion only occurs into regions of low field strength. It is also worth noting the observational results of Flaccomio et al. (2005) that indicate that rotational modulation of X-ray emission is not preferentially detected in either accreting or non-accreting T Tauri stars and that therefore the spatial structure of the X-ray emitting plasma is the same in both cases. Hence, although accretion does affect X-ray emission in accreting stars, and may distort the structure of stellar coronae, it may not affect the existence of rotational modulation.

Chapter 6

Large Flares

6.1 Introduction

The analysis of the brightest X-rays flares observed in the Chandra Orion Ultra-deep Project (COUP) has revealed that flaring plasma in young stellar objects (YSOs) can be contained within magnetic structures which extend out to well beyond a stellar radius (Favata et al. 2005). Further evidence for the existence of large magnetic structures in T Tauri stars has been found from radio VLBA observations of T Tau South (Loinard et al. 2005) and from XMM-Newton monitoring of HL Tau (Giardino et al. 2006). The largest events with reliable size estimates have flaring lengths $L \approx 5R_*$, but many may be even longer with $L \approx 10 - 20R_*$ (Favata et al. 2005). Before the COUP results flares on YSOs were found to be small and similar to those detected on older, more evolved stars - typically extending to only fractions of R_* (see e.g. Favata et al. 2001). Many such small flares were detected during COUP, whilst for YSOs with circumstellar discs, small flares appear to coexist with the larger magnetic structures (Favata et al. 2005).

As Favata et al. (2005) discuss, large magnetic structures extending to several

stellar radii would be torn open by the centrifugal force if their foot points were anchored solely on the star. Therefore the large flares detected by COUP are likely to occur inside magnetic structures which link the star to a circumstellar disc. Indeed, the lengths of such structures are comparable to typical corotation radii of T Tauri stars, suggesting that they could be magnetic flux tubes which carry accretion flows from the disc to the star as predicted by magnetospheric accretion models (Königl 1991; Shu et al. 1994a). However, there is other evidence from COUP which suggests that the coronae of T Tauri stars are compact and clumpy, with X-ray emitting plasma being confined within magnetic structures which do not extend out to much beyond a stellar radius (Flaccomio et al. 2005). Compact emitting regions are required to explain the rotational modulation of X-ray emission detected in a number of COUP stars (Flaccomio et al. 2005 and Chapter 5). It is therefore important that models take account of the COUP results, namely that the coronae of T Tauri stars are likely to be compact, but are also capable of supporting large magnetic structures linking the star to the disc.

In this Chapter I argue that our new model which takes account of the complexity of T Tauri star magnetic fields provides a natural mechanism of supporting the large flares detected by COUP, whilst also allowing for the coexistence of compact coronae (Chapters 2-5). In this model magnetic fields are extrapolated from surface magnetograms derived from Zeeman-Doppler imaging. Some field lines contain X-ray emitting plasma close to the stellar surface, whilst others thread the circumstellar disc. In contrast to purely dipolar accretion models, realistic magnetic fields allow accretion to proceed along a mixture of open and closed field lines (Chapters 2 and 4). It was found that (typically) lower mass stars from the COUP dataset, with their lower surface gravities and therefore large pressure scale heights, have large coronae which extend out to the corotation radius (see Fig. 2.6). Accretion may then proceed along both closed and

open field lines threading the disc at corotation. In contrast, higher mass stars with their larger surface gravities and smaller pressure scale heights, typically have compact coronae which do not extend to the corotation radius. Therefore accretion occurs predominantly along open field lines threading the disc. In the following work we demonstrate that the COUP stars for which large flares have been detected are ones which have open field lines extending out into the disc, and are predominantly accreting along the open field. We therefore suggest that the extended magnetic structures which contain large flares observed during COUP are a result of the reconnection of open field lines within the disc. It is also worth noting that, Favata et al. (2005) do suggest that long flares occur in non-accreting structures which connect the star and the disc, and that accretion may inhibit the production of large flares in extended magnetic structures.

6.2 Reale's solar loop model

Flares occur when the magnetic energy which has built up in the stellar atmosphere is suddenly released in a violent magnetic reconnection event. On the Sun we can resolve the detailed temporal and spatial evolution of individual flares, however on other stars all that is observed is an intense variation in brightness. The flaring events detected on T Tauri stars are time and space averages across a complex and dynamical corona, although stellar astronomers are not limited by only considering a single star. Fig. 6.1 is an example of a flaring event detected in a Chandra X-ray light curve for a source in the ONC (Favata et al. 2005). Using properties which can be estimated from such X-ray light curves it is possible to derive the lengths of flaring loops. We assume that flares occur inside magnetic structures which are of length L, where L is the distance from the loop foot point on the star to the loop apex. Reale et al. (1997) developed a model to estimate the lengths of flaring loops on the Sun, which was then applied to the analysis of

stellar flares by Reale & Micela (1998).

The behaviour of flares seen on T Tauri stars is similar to what we see on the Sun. Characteristic flaring behaviour is a rapid initial rise in hard X-ray emission, refered to as the impulsive stage, followed by a slower decay stage where the temperature and X-ray luminosity decay away more slowly. This behaviour can be seen in Fig. 6.1. The impulsive energy release of stored magnetic energy causes plasma to fill the loop rapidly increasing the X-ray luminosity. During the decay phase the luminosity and the temperature decay through radiative loses and thermal conduction back to the photosphere. In order to determine the length of a flaring loop the decay time of the flare is estimated from an X-ray light curve. If we assume that the plasma in the flaring loop cools uniformly, that is without any additional heating, then the two cooling processes of thermal conduction and radiative loses have characteristic 1/e decay timescales (see Favata et al. 2005 and Serio et al. 1991) of,

$$\tau_{cond} \approx \frac{3nk_BL^2}{\kappa T^{5/2}} \tag{6.1}$$

$$\tau_{rad} \approx \frac{3nk_BT}{n^2P(T)}, \tag{6.2}$$

where n is the plasma density, κ the thermal conductivity and $P(T)$ is the plasma emissivity per unit emission measure. Both of these timescales depend on the length of the flaring loop (for τ_{rad} the length enters through the density n). Combining these timescales a total decay time for the plasma in the loop, τ, can be estimated,

$$\frac{1}{\tau} \approx \frac{1}{\tau_{rad}} + \frac{1}{\tau_{cond}}. \tag{6.3}$$

Serio et al. (1991) then demonstrated that this decay time could be directly related to the length of a flaring loop. If the loop length L is measured in units of 10^9 cm, the peak temperature of the flaring plasma T_{pk} in 10^7 K and the decay time τ in seconds then,

$$L = \frac{\tau\sqrt{T_{pk}}}{3.7 \times 10^{-4}}. \tag{6.4}$$

However, in the 1990s it was demonstrated that heating of the plasma within the loop continued into the decay phase. This sustained heating must be accounted for when estimating the loop length. In other words the sustained heating is competing with thermodynamic cooling, increasing the decay time of the flaring event. As a result the measured flare decay time τ from X-ray light curves is an overestimate the true decay time τ_{lc}, and must be corrected before deriving flaring loop lengths. Reale et al. (1997) demonstrated that the gradient of the time evolution of the flare on a plot of $\log T$ vs $\log n$ was a measure of the sustained heating. The lower the gradient the more heating is present. In practice density measurements are not available for stellar coronae so instead the gradient ζ on plots of $\log T$ vs $\log EM^{1/2}$ is used. It was shown by Reale et al. (1997) that the ratio of the true flare decay time could be related to the measured decay time via,

$$\frac{\tau_{lc}}{\tau} = f(\zeta), \tag{6.5}$$

with the functional form of $f(\zeta)$ dependent upon particular properties of the X-ray detector used to observe the flare. Combining equations (6.4) and (6.5) we obtain an expression for the length of a flaring loop,

$$L = \frac{\tau_{lc}\sqrt{T_{pk}}}{3.7 \times 10^{-4} f(\zeta)}. \tag{6.6}$$

Using Reale's solar loop model, Favata et al. (2005) obtain the lengths of the brightest flaring loops observed during COUP. Many have lengths which are comparable to the flaring loops that are commonly detected on the Sun and other stars, with L values ranging from a few tenths of a stellar radius to around a stellar radius at most. However, some of the flares detected by Favata et al. (2005) have lengths well in excess of the typical flaring loop lengths, out to 5 or 10, and perhaps as much as 20, times the stellar radius. It is also worth noting that the ACIS camera on Chandra used during COUP is only sensitive to photon energies corresponding to a temperature of up to 100 MK. Many of the peak

flare temperatures exceeded this value, and as from equation (6.6) $L \propto \sqrt{T_{pk}}$, then many of the flaring loop lengths may be underestimated. Such large flares have thus been interpreted as occuring inside extended magnetic structures which connect stars to their circumstellar discs.

6.3 Coronal extent and open field accretion

We have discussed in Chapter 2 how magnetic fields are extrapolated from surface magnetograms. We assume that at field line footpoints the gas pressure scales with the magnetic pressure, $p_0 = KB_0^2$. The constant of proportionality is determined by comparing calculated X-ray emission measures with observed emission measures from the COUP dataset. In this Chapter we consider the LQ Hya surface magnetogram using the values of K given in Chapter 2. We note that we make a conservative estimate of the location of the source surface by calculating the largest radial distance at which a dipole field line would remain closed, with the same average field strength. Figs. 6.2 and 6.3 show examples of the complex magnetic field geometries which we consider.

Our model requires estimates of stellar mass and radius, rotation period, and data from which an estimate of the coronal temperature can be derived. For many stars in the COUP dataset it is possible to derive both a lower and a higher coronal temperature, and we consider both where possible in this work. We select stars from COUP which have estimates of these parameters and for each calculate the natural extent of their coronae R_S (see Fig. 6.4). Some stars, typically those of lower mass, have large extended coronae which would naturally extend to beyond the corotation radius R_{co}. If such stars are then surrounded by a disc, those field lines threading the disc beyond corotation are quickly wrapped up and blown open, allowing the disc to extend in to R_{co}. Therefore the coronal extent of such stars is limited by the presence of a disc, which suppresses the X-

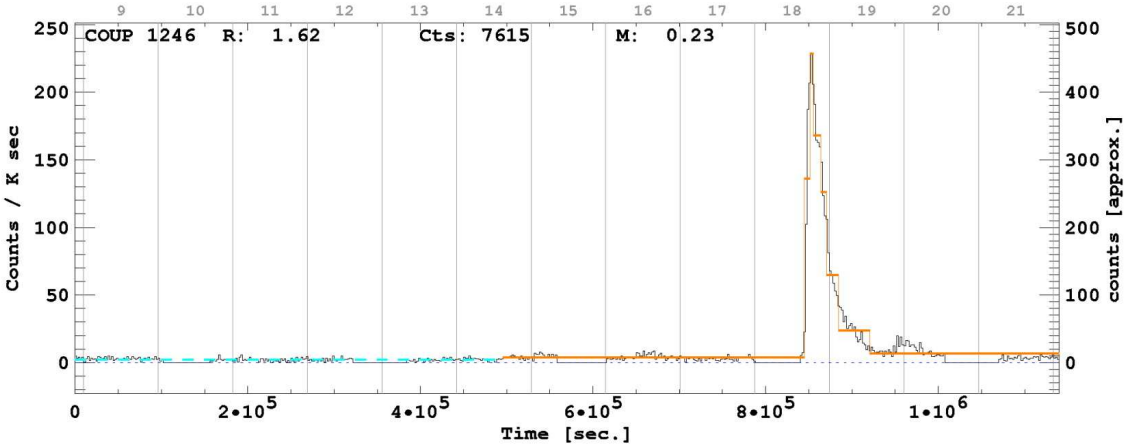

Figure 6.1: A COUP X-ray light curve showing a flaring event. The fast rise of the impulsive phase can be clearly seen as the rapid increase in X-ray counts, followed by a slower decay. Reproduced with permission from Favata et al. (2005).

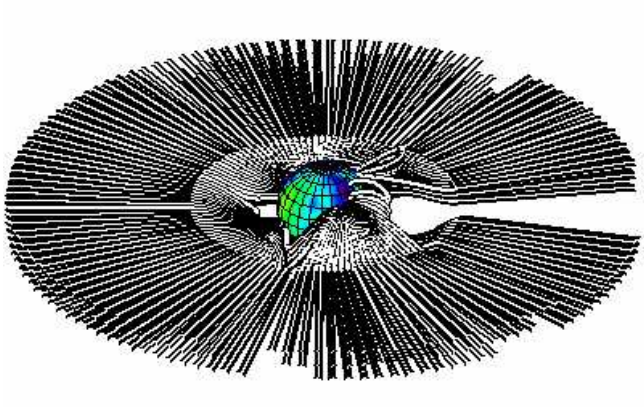

Figure 6.2: Magnetic field extrapolated from a surface magnetogram showing field lines which thread the circumstellar disc drawn from the corotation radius. The parameters for COUP 223 have been used which has a coronal extent of $R_S = 2.6R_*$ (at the higher coronal temperature) which is within the corotation radius of $R_{co} = 6.6R_*$. Therefore the inner disc is sitting in a reservoir of open field lines, the reconnection of which within the disc could provide large magnetic structures able to contain the large flares detected during the COUP.

ray emission. This effect has been detailed in Chapter 2 and by by Jardine et al. (2006) who show that it is partially responsible for the observed increase in X-ray emission measure with stellar mass (Preibisch et al. 2005). Higher mass stars (typically) have more compact coronae and so are less affected by the presence of a disc. For such stars accretion occurs along open field lines which connect the star to the disc (see Chapter 4). Reconnection of these open field lines within the disc could provide magnetic structures capable of containing the large flares detected during COUP (Favata et al. 2005).

We consider the stars from the COUP dataset where large flares have been detected (see Table 1 of Favata et al. 2005). However, of the 32 stars considered by Favata et al. (2005), only 8 have estimates of all of the parameters which we require, namely COUP 28, COUP 90, COUP 223, COUP 454, COUP 1246, COUP 1384, COUP 1410 and COUP 1608. Flaccomio et al. (2005) have added further rotation period estimates to the COUP dataset allowing COUP 891 to also be considered, but only at the lower coronal temperature[1]. The squares in Fig. 6.4 show that these COUP stars, apart from COUP 90, have compact coronae which would not extend to the corotation radius ($R_S/R_{co} < 1$). In other words, the closed field in such stars is only able to contain the coronal gas out to a radius which is within corotation. For such COUP stars, the inner disc is sitting in a reservoir of open field, suggesting an intimate link between the open field lines threading the disc and the large flares detected by COUP. Table 6.1 is a summary of the ratio of coronal extent to the corotation radius calculated at both the lower and higher coronal temperatures, with the lengths of the flaring structures detected on such stars as derived by Favata et al. (2005). At the higher coronal temperature only COUP 90 has $R_S/R_{co} > 1$ and therefore has a mixture of open and closed field lines threading the disc at corotation, rather

[1]A rotation period for COUP 1040 is also provided by Flaccomio et al. (2005) but this star lacks estimates of stellar mass and radius, and therefore cannot be considered.

than predominantly open field. COUP 90 therefore has a large extended coronae. However, the flare detected in COUP 90 only has a length of $0.4R_*$, as derived by Favata et al. (2005), which is similar to the small flares commonly detected on T Tauri stars, rather than the large flares occuring in the long extended magnetic structures which connect the star to the disc.

The ratio R_S/R_{co} is smaller for the higher coronal temperatures (see Table 6.1). For higher temperatures more field lines are blown open by the gas pressure exceeding the magnetic pressure, reducing the maximum radial extent of the corona R_S. A large flare extending to $3R_*$ was detected on COUP 1384 (Favata et al. 2005). At the higher coronal temperature we find that COUP 1384 is accreting along open field lines, consistent with our argument that large flares occur in stars where the inner disc is truncated in regions of open field. However, at the lower coronal temperature we find that COUP 1384 would have a corona which would naturally extend to beyond R_{co} (see Table 6.1). This does not agree with our model for the existence of large flares, and therefore COUP 1384 may be an exception. However, there is considerable uncertainty involved, both in the determination of the lengths of flaring structures, and in calculating the corotation radius (due to uncertainties in the assumed stellar mass, radius and rotation period).

There are many more stars in the COUP dataset where large flares have been detected, but which lack estimates of the parameters required by our model. A further 13 stars (COUP 7, COUP 43, COUP 141, COUP 262, COUP 597, COUP 649, COUP 669, COUP 752, COUP 848, COUP 960, COUP 971, COUP 976 and COUP 1568) from the table of flare parameters in Favata et al. (2005) have estimates of all the parameters required by our model, except for rotation periods. In order to determine the coronal structure of such stars, and whether or not it is open field which is threading the disc at corotation, we have estimated P_{rot} values for these 13 stars. Fig. 6.5 is the distribution of known rotation periods for stars

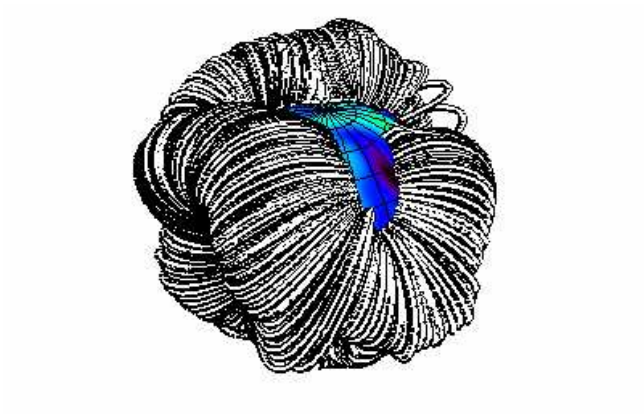

Figure 6.3: As Fig. 6.2 but showing only the closed coronal field lines which contain X-ray emitting plasma.

Table 6.1: Flare parameters from Favata et al. (2005) for COUP sources with estimates of P_{rot}, M_*, R_* and coronal temperatures, with our estimates of the length of the flare relative to the coronal extent R_S and estimates of coronal extent relative to the corotation radius R_{co} for the lower (kT_1) coronal temperature. The coronal extent relative to corotation is shown for the higher (kT_2) coronal temperature for comparison.

COUP Source	L/R_*	L/R_S	R_S/R_{co} (kT_1)	R_S/R_{co} (kT_2)
28	1.9	0.71	0.78	0.67
90	0.4	0.16	1.87	1.54
223	2.5	0.94	0.54	0.40
454	10.1	3.78	0.58	0.48
891	5.1	2.01	0.73	-
1246	3.8	1.50	0.65	0.53
1384	3.0	1.18	1.12	0.92
1410	55.0	20.60	0.16	0.13
1608	6.7	2.51	0.64	0.55

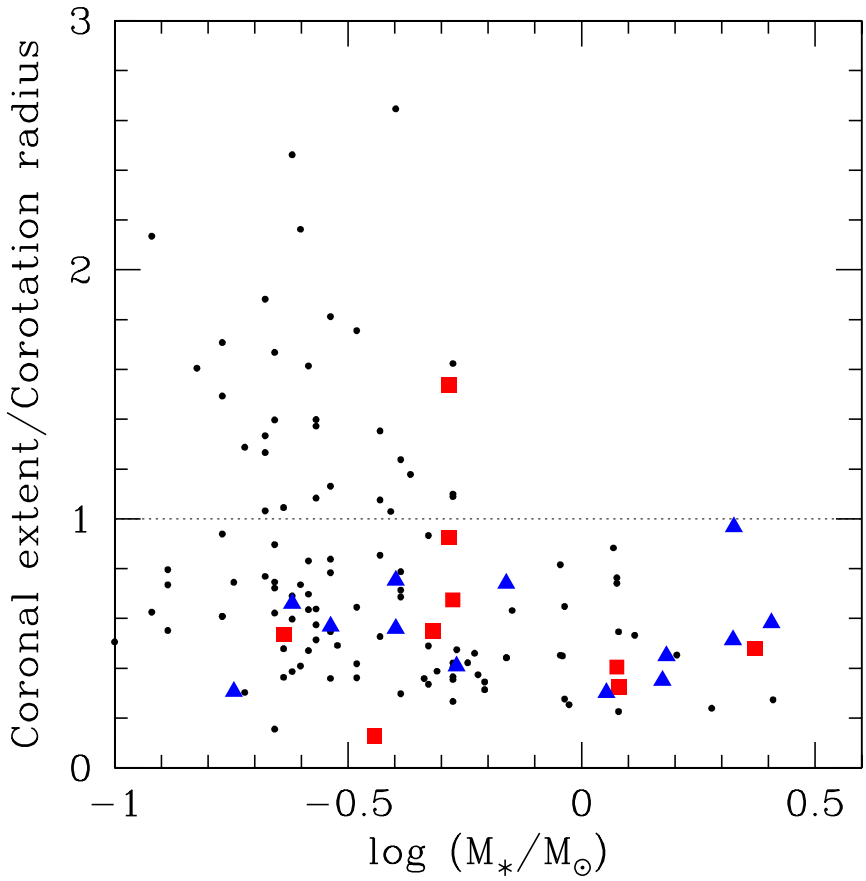

Figure 6.4: Coronal extent R_S, in units of the corotation radius R_{co}, as a function of stellar mass for stars in the COUP sample (*points*). The higher coronal temperatures have been used. The squares represent stars from Table 1 of Favata et al. (2005) and which have estimates of R_*, M_*, P_{rot} and coronal temperature. The triangles are also from Table 1 of Favata et al. (2005) but for which we have assumed a rotation period of 5.72 d, the mean value for stars in the COUP dataset with estimates of P_{rot}. Stars below the line have compact coronae and have open field lines threading the disc at corotation.

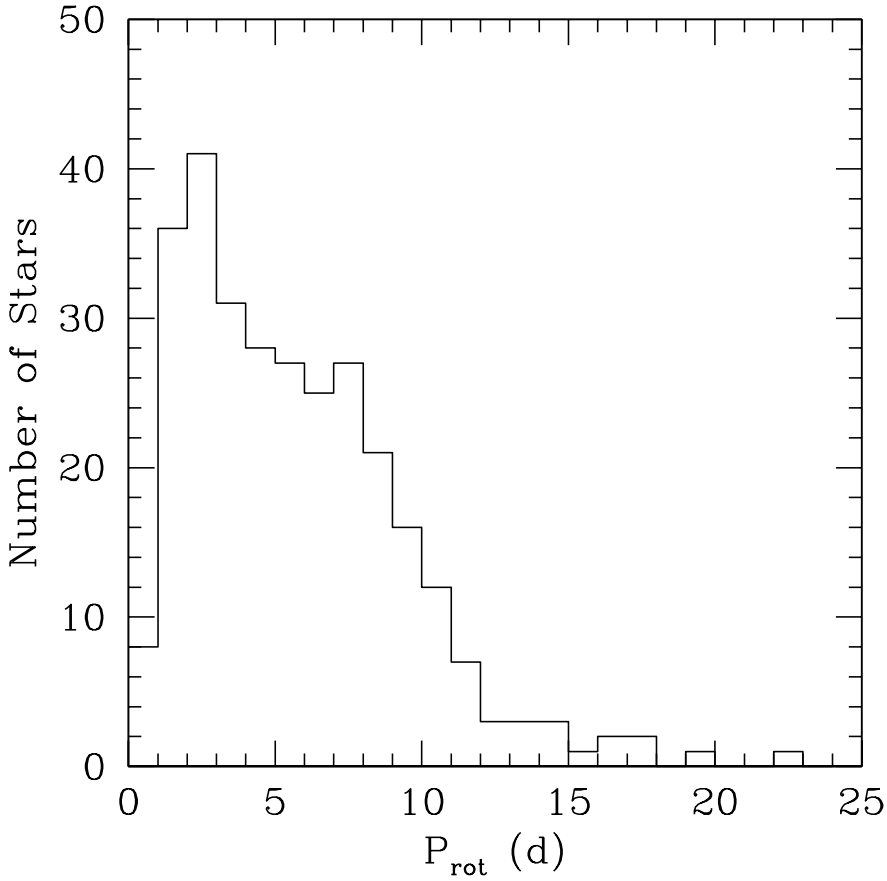

Figure 6.5: The distribution of rotation periods for the 295 COUP sources with P_{rot} estimates complied by Flaccomio et al. (2005). The median and mean rotation periods are 5.17 d and 5.72 d respectively, with $\approx 80\%$ of the stars having periods between 2 and 12 d.

in the COUP dataset, constructed using the 295 P_{rot} values compiled from various sources by Flaccomio et al. (2005). The median and mean values of P_{rot} are 5.17 d and 5.72 d respectively, with $\approx 80\%$ of stars having rotation periods of between 2 and 12 d. Assuming that these 13 COUP stars have rotation periods equal to the mean P_{rot} value of 5.72 d, we find that all have $R_S/R_{co} < 1$ (the triangles in Fig. 6.4), and are therefore accreting along open field lines from corotation. Of course the value of R_S/R_{co} depends on the assumed rotation period for each star. However, as $R_{co} \propto \omega^{-2/3} \propto P_{rot}^{2/3}$, then the longer the rotation period the larger the corotation radius. Therefore the ratio R_S/R_{co} is smaller for larger values of P_{rot}. Given that T Tauri stars which are surrounded by discs are typically slower rotators than weak line T Tauri stars (were the disc has dispersed), it is likely that the 13 COUP stars with unknown P_{rot} values, but which show evidence for large flares that must be anchored to both the star and a disc, probably have rotation periods which are toward the larger values in the rotation period histogram (see Fig. 6.5). Therefore these stars are likely to have compact coronae which do not extend to corotation, with open field lines threading the disc. If some of these stars have faster rotation periods, well below the mean value of 5.72 d, then some will have $R_S/R_{co} > 1$ and therefore large coronae, reducing the significance of having predominantly open field threading the disc. Although, this does not matter for COUP 7, COUP 141, COUP 960 and COUP 1568, where the flaring loop lengths reported by Favata et al. (2005) are all less than a stellar radius. However without estimates of true rotation periods we are limited to considering the 8 COUP stars (9 at the lower coronal temperature) where large flares have been detected and have estimates of the parameters required by our model.

With such few stars to work with it is difficult to do a meaningful statistical analysis to compare the differences between stars where large flares have been detected and those where none have been seen. However, we can still (partially) address the issue over whether the stars with large flares represent a different

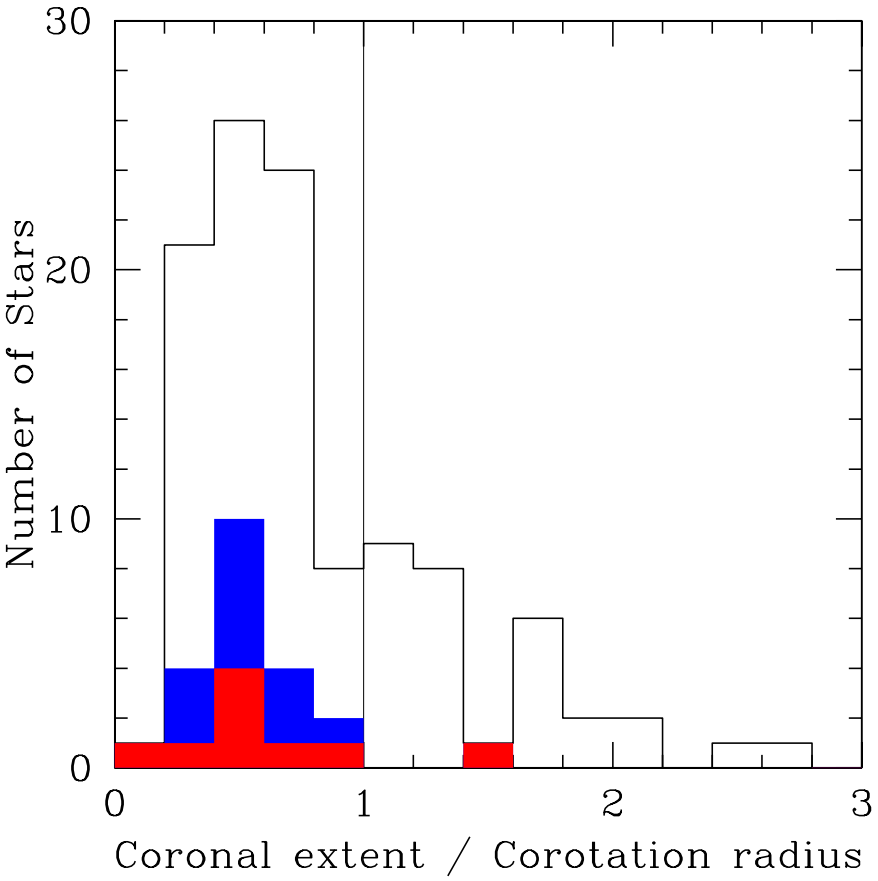

Figure 6.6: Histograms showing the number of stars in bins of the ratio of coronal extent to corotation radius, from the data plotted in Fig. 6.4. The solid black line indicates stars from COUP which have estimates of the parameters required by our model. The red histogram is all stars with the brightest detected flares, and which have estimates of all of the stellar parameters, from Favata et al. (2005). The blue histogram is again data from Favata et al. (2005) where we have assumed a rotation period, equal to the mean P_{rot} value from the whole COUP dataset, for stars without P_{rot} estimates.

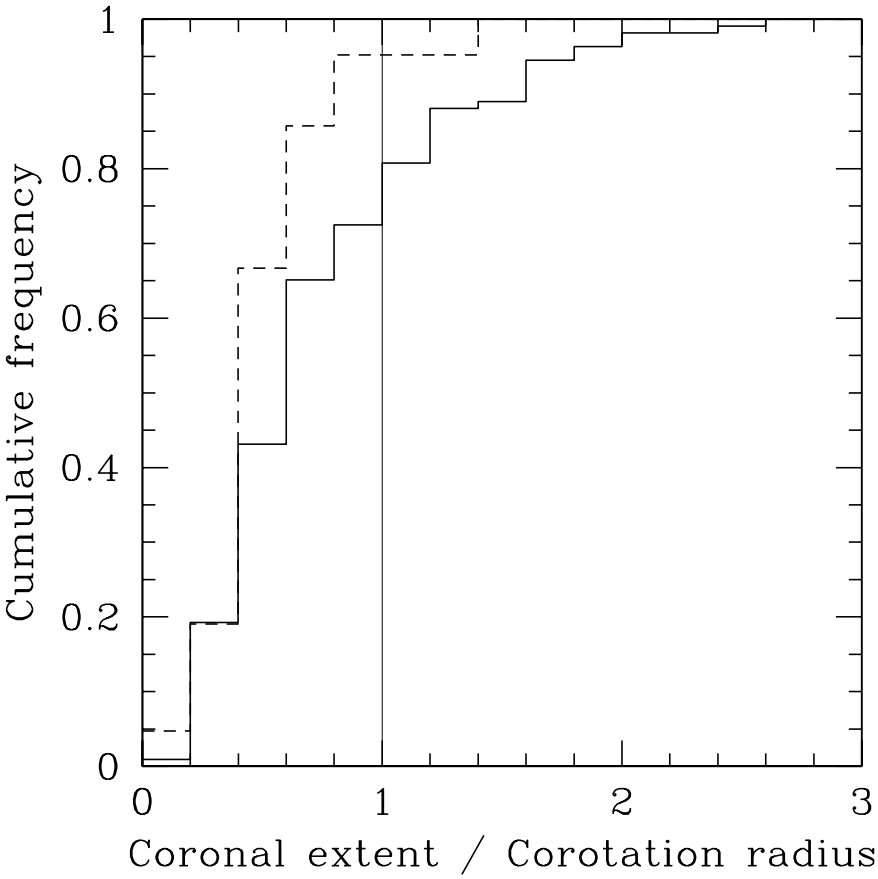

Figure 6.7: Cumulative distribution of the ratio of coronal extent to corotation radii generated from Fig. 6.6. The solid line is all of the data, whilst the dashed line is from the blue histogram.

underlying distribution in mass than the rest of the stars from the COUP data set. In other words, if we consider Fig. 6.4, are the large flare data distributed in mass in such a way that they have been picked from the same underlying distribution defined by all of the data from the COUP stars. The distribution of all of the COUP data is shown for comparison with the data for which large flares have been detected in Fig. 6.6. To check this we produce cumulative distribution functions of the ratio of coronal extent to corotation radius using the data plotted in Fig. 6.4, and run a Kolomogorov-Smirnov (KS) test to determine the significance of any difference between those cumulative distributions (see Fig. 6.7). A KS probability of 100% would indicate that the distributions were identical, in other words, that large flare stars had been drawn from the same distribution defined by the COUP sources as a whole. If this was the case then the only reason we are seeing the large flare stars in the region where open field lines are threading the disc is because we only have a very small sample of large flare stars. More data for stars with large flares would then more uniformly fill the $R_S/R_{co} - M_*$ plane. If the KS probability was 0% then the large flares stars would represent a distinct distribution which is different from the distribution defined by all of the COUP data. By only considering all stars with detected large flares and rotation period estimates, the KS probability is 74%. However, by also including those stars which are assumed to have rotation periods equal to the mean P_{rot} value of stars from COUP, the KS probability becomes 18%. Furthermore, by including the stellar parameters for HL Tau, another star where a large flare has been detected by Giardino et al. (2006), then the KS probabilities drop to 53% and 16% respectively. The initial results are therefore not that promising, however, it is interesting to note that by considering more stars with large flares and assumed rotation periods, the likelihood of the large flare stars been drawn from a different underlying distribution is greater. In future more data should be able to confirm whether or not this is true.

6.4 Discussion and future work

We have found hints that the largest flares detected on T Tauri stars only occur in stars where the inner disc is threaded by open field lines. It could be the case that the reconnection of large extended open field lines within the disc can explain the existence of large flaring loops. However, more large flare detections on stars which also have stellar parameter estimates will be required in future to test our model more fully. The preliminary results from DROXO (the Deep ρ-Ophiuchi XMM Observation) already show evidence for large flaring loops (Flaccomio et al. 2007). It may be possible that some of the stars where the large flares have been detected will have estimates of the stellar parameters. However, the ρ-Oph star forming region is poorly studied photometrically (to determine rotation periods) and spectroscopically (to determine spectral types and therefore radii and masses) due to the high levels of extinction related to its comparatively young age. However, some of the DROXO large flare data may be use for our purposes in future. Further, the DROXO results may provide additional clues as to whether large flares occur only in stars which have evidence for circumstellar discs, supporting the conclusions of Favata et al. (2005) that such large events can only occur inside magnetic loops which connect the star to the disc. It would also be interesting to note if large flares occured in stars which simultaneously showed evidence for accretion.

We are currently developing models of large flaring loops, with particular emphasis on the difference between closed field lines and open field lines which thread the disc. It is likely that such large flares do occur inside magnetic structures which connect the star to the disc. If their footpoints were anchored solely on the stellar surface they would be quickly be torn open by the centrifugal force (Jardine & Unruh 1999). However, if such field lines were threading the disc at corotation then it is difficult to imagine how large flares could occur. In order to explain the energy release required to generate such large flaring events it seems

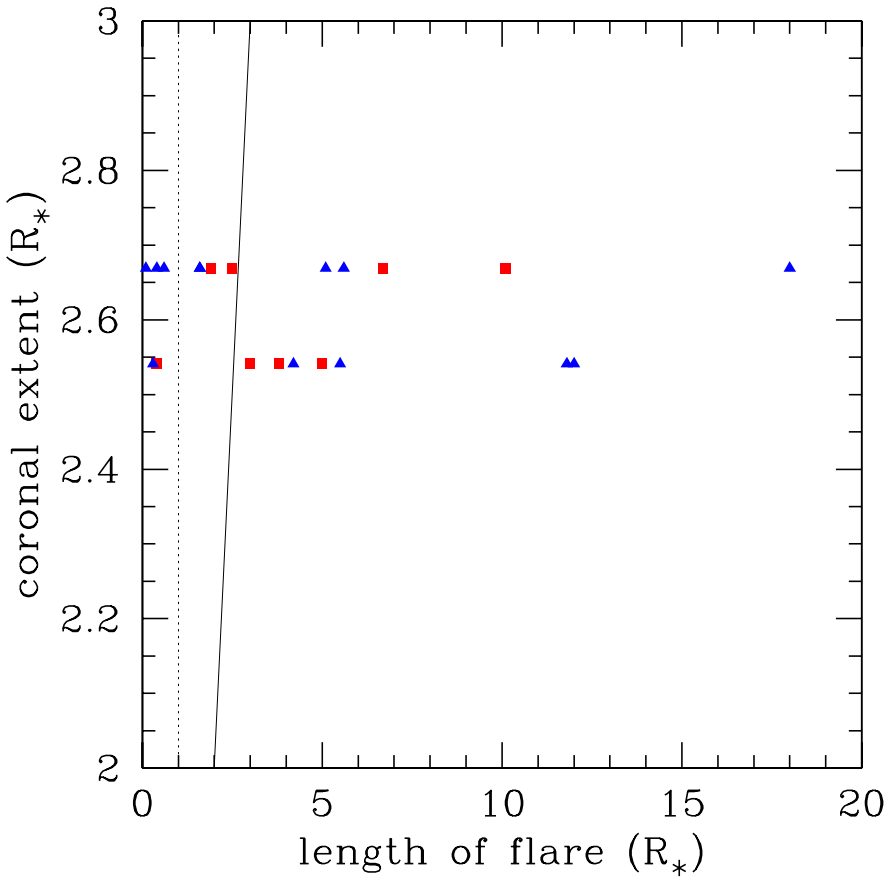

Figure 6.8: Comparison between the lengths of flaring loops and the coronal extent. Any data point on the solid line would have a length equal to the coronal extent, which represents the maximum radial extent of the closed field line region. Any flares with lengths greater than the coronal extent, below the solid line, are occuring inside magnetic structures which extend out to the open field region. Any data points to the left of the dotted line are flaring loops with a length of less than a stellar radius, and are therefore not large flares. The squares are stars from Favata et al. (2005) which have rotation period estimates, and the triangles are those for which we assume a rotation period. The majority of flaring loops extend into the open field region.

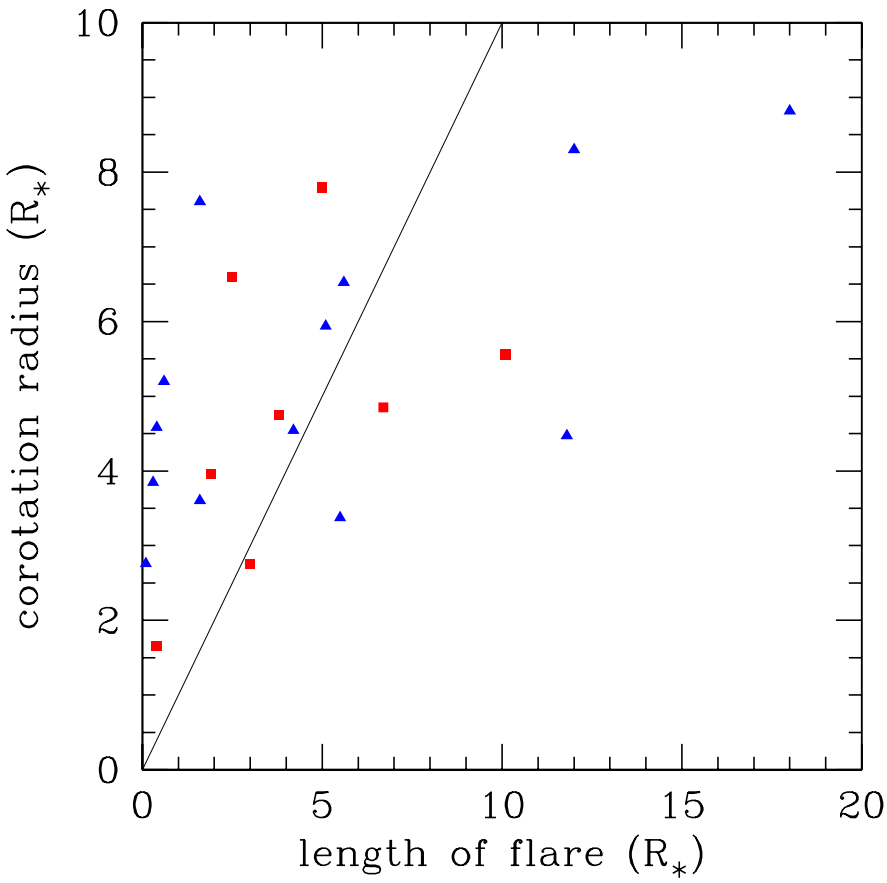

Figure 6.9: As Fig. 6.8, but comparing the lengths of flaring loops to the location of corotation. Any data point on the solid line represents a flare occuring inside a magnetic structure which extends to the corotation radius. This suggests that the position of corotation is irrelevant in the production of large flares, which instead appear to occur inside magnetic structures which are likely to be stressed due to rotation in the disc.

reasonable that field lines must be distorted by the differential rotation between the star and the disc (see Figs. 6.8 and 6.9). Field lines threading the disc inside, or outside, of corotation would quickly be wrapped up and torn open (e.g. Lovelace et al. 1995). Models of these large flaring events will have to address this problem; can the magnetic structures fill with X-ray emitting plasma before they are torn open? This may be evidence that discs are not disrupted at the corotation radius as is assumed by many magnetospheric accretion models (e.g. Ostriker & Shu 1995); perhaps the inner disc extends closer to the stellar surface (Safier 1998; Matt & Pudritz 2005a,b). There are other remaining questions, for example, why are large flares not detected more often? The COUP results suggest two large flares per week per star. It is also worth remembering that small flares coexist with the largest flaring loops, suggesting a solar-like corona is responsible for the small flaring loops whilst other physical mechanisms produce the largest flares.

Chapter 7

Conclusions and Future Work

I have taken the first steps in developing a new magnetospheric accretion model that takes account of the true complexity of T Tauri magnetic fields, and models the effects of a stellar corona. Magnetic fields are extrapolated from surface magnetograms derived from Zeeman-Doppler imaging. Field lines close to the stellar surface contain the X-ray emitting corona, with field lines at larger radii interacting with the disc and carrying accretion flows. By considering stellar parameters from the Chandra Orion Ultradeep Project dataset I have demonstrated that my model reproduces several of the X-ray observations of T Tauri stars, and makes new predictions about the accretion process. Jardine et al. (2006) demonstrated that complex magnetic fields are required to explain observed X-ray emission measures and coronal densities, with rotationally modulated X-ray emission arising from the dominant emitting regions entering eclipse as the star rotates (Gregory et al. 2006b). Lower mass stars typically have more extended coronae and are therefore more affected by a disc than higher mass stars. The outer coronae of some lower mass T Tauri stars may be stripped away via the interaction with a disc. Further, I have made several new predictions about the accretion process. For the higher mass stars the bulk of accretion may occur along large open field lines, and in contrast to dipolar accretion models, discrete hot spots are found

to span a range of latitudes and longitudes (Gregory et al. 2005, 2006a). I have also discussed the possibility that large flares may be naturally explained by the interaction between the disc and open field lines. Below I summarise these conclusions in more detail, emphasise the limitations of the model, and discuss ways in which it will be improved. I also discuss some of the current observational puzzles and suggest possible avenues for exploration in the future.

7.1 Conclusions

7.1.1 Mass accretion

By extrapolating from surface magnetograms we have considered how magnetic fields with a realistic degree of complexity would effect the accretion process. We assumed that the fields are potential (current-free) and that the field is static in time. We also assumed that at the base of field line foot points the gas pressure scaled with the magnetic pressure. This technique has been used successfully to explain the observed X-ray emission measures of the Sun and other main sequence stars (e.g. Jardine et al. 2002a,b). From surface magnetograms the field strength varies across the stellar surface which means that the gas pressure will also vary across the surface of the star. The proportionality constant K from $p_0 \propto B_0^2$ is therefore crucial in controlling the coronal extent. Small values of K lead to a large extended corona, with large values resulting in a compact corona. Before considering the influence of a circumstellar disc on the coronal structure we calculated the maximum radial extent that field lines in the coronae could have before the gas pressure overcame the magnetic pressure. As a dipole represents the most extended closed field structure we made a conservative estimate of the coronal extent by calculating the maximum radial extent that a dipolar field line could have before being blown open. This was done for each star in the COUP dataset with estimates of the input parameters required by our model, namely stellar

mass, radius, rotation period, coronal temperature and X-ray emission measure. For a given surface magnetogram we calculated the value of K which resulted in the best fit between our calculated emission measures and those derived from the X-ray spectra taken during COUP. Jardine et al. (2006) then demonstrated that complex fields were required to reproduce the observed emission measures and coronal densities inferred from the modelling of individual flares.

We considered the distribution of the ratio of coronal extent to the corotation radius with stellar mass for stars from COUP. There is a large variation in the sizes of T Tauri coronae at any particular mass. Considering the sample as a whole, however, higher mass stars typically have coronae that are well within the corotation radius. There are two contributing effects which can explain this. Higher mass stars naturally have larger corotation radii $R_{co} \propto M_*^{1/3}$, but more importantly their higher surface gravities and therefore small pressure scale heights lead to more compact coronae. It is only the lower mass stars which can have large extended coronae that would naturally extend to beyond the corotation radius. Lower mass stars have lower surface gravities and large pressure scale heights and therefore tend to have larger coronae than higher mass stars. Stars which have coronae that extend to well beyond corotation are more likely to be affected by the presence of a disc. The coronal extent is the limit of the closed field regions. Beyond this all the field lines are open, and in the absence of a disc they would carry a stellar wind. For the stars with coronae that extend to beyond the corotation radius, the closed field lines threading the disc are quickly wrapped up and torn open. Thus the disc extends in to the corotation radius. This coronal stripping process converts closed field line loops, which would have coronal plasma trapped along their length, into open field lines. For such stars the amount of X-ray emission is reduced. In contrast to this are the higher mass stars which have compact coronae. For such objects the inner disc is instead threaded by open field lines.

This model was extended to consider steady state isothermal accretion flows. We considered transonic accretion solutions were material leaves the disc at a low subsonic speed but arrives at the star with a large supersonic speed. Our in-fall velocities are consistent with the widths of the large redshifted absorption components of inverse P-Cygni profiles (e.g. Edwards et al. 1994). We initially considered a dipolar magnetic field, with a source surface. The source surface represents the maximum possible coronal extent, that is the radius at which the field is no longer strong enough to contain the coronal gas. The modified dipole magnetic field comprises of closed field lines with open field closer to the poles. By tilting the dipole field a mixture of open and closed field lines interact with the inner disc. Whether or not the open field lines could support transonic accretion depended strongly on the accretion flow temperature, with an increase in mass accretion rate when both the open and closed field lines were able to carry accreting material.

Open field accretion is also important when considering realistic magnetic fields extrapolated from surface magnetograms. We found that the location and distribution of hot spots was strongly dependent upon the geometry of the magnetic field. Discrete hot spots, which arise at the base of accretion columns, were found to span a range of latitudes and longitudes. Often low latitude hot spots were found. This is consistent with the predictions of many new, and independently developed, accretion models (von Rekowski & Piskunov 2006b; Long et al. 2007; Mohanty & Shu 2007). In dipolar accretion models the hot spots are often at high latitudes towards the poles. Further, the accretion filling factors predicted by dipolar accretion models are often too large. The filling factors derived for complex field accretion are of order 1% in agreement with observationally inferred values (e.g. Valenti & Johns-Krull 2004).

The paths followed by accreting material onto stars with complex magnetic fields led to a distribution of in-fall velocities. The majority of field lines carry

material at close to the free-fall speed, however there are regions where the disc extends closer to the stellar surface. In-falling material from within corotation reaches the stellar surface at a lower velocity, leading to a distribution of in-fall speeds. There is observational evidence that the inner disc radius is non-uniform. The observed near-IR variability detected in some CTTs has been attributed to either variations in the disc accretion rate, a non-uniform radius inner disc rim, or a combination of both (Carpenter, Hillenbrand & Skrutskie 2001; Eiroa et al. 2002; Colavita et al. 2003). The basic idea is that at the azimuths corresponding to the location of hot spots on the star, the increased stellar luminosity due to the spot increases the temperature at that particular section of the inner disc. This increases the dust sublimation radius and pushes the inner disc rim further from the star. Therefore the inner disc rim is no-longer uniform in radius. The idea that sections of the inner disc rim may move back and forth in time agrees with the interfermotric observations of Colavita et al. (2003) of DG Tau. Further, Fernández & Eiroa (2007) have found that large near-IR variabilities shown by some stars from a study by Carpenter et al. (2001) are well fitted by model in which the inner disc radius varies in azimuth. Our model predicts that such behaviour would lead to a distribution of in-fall velocities, rather than the discrete in-fall velocity predicted by dipolar accretion models (e.g. Hartmann et al. (1994)).

The mass accretion rates supported by complex magnetic fields can reproduce the observed correlation with stellar mass. Over the restricted mass range provided by data from COUP our model yields a correlation of $\dot{M} \propto M_*^{1.2}$ compared to the observed $\dot{M} \propto M_*^{1.4}$. In future our model should be tested across a greater range in mass to determine if it can reproduce the full correlation of $\dot{M} \propto M_*^2$. However, it should be noted that this correlation may be nothing more than an observational artifact, a product of detection and selection effects (Clarke & Pringle 2006). The lower limit of the correlation corresponds to the

upper limit of non-detections, and the upper bound appears to correspond to the condition that the stellar luminosity equals the accretion luminosity. This is a little suspicious (Clarke & Pringle 2006).

7.1.2 X-ray emission

Complex magnetic fields reproduce the observed rotational modulation of X-ray emission. The dominant X-ray emitting regions are confined within magnetic structures which are compact and unevenly distributed about the star. Some regions of the stellar surface are dark in X-rays. As the star rotates emitting regions are eclipsed, giving rise to modulated X-ray emission. We used the Lomb Normalised periodogram (LNP) method to determine X-ray periods from simulated X-ray light curves. For each star in the COUP dataset considered by Flaccomio et al. (2005) and which had estimates of the stellar parameters, we generated X-ray light curves that matched the duration of the COUP observations, for different magnetic field geometries. Our calculated X-ray periods were compared to optically determined rotation periods for direct comparison with Flaccomio et al. (2005). It was found observationally that those stars which had reliably detected modulated X-ray emission had X-ray periods which were equal to, or were half of, the optical period. It was argued that stars would have $P_X = P_{opt}$ if there was a single (or at least a single dominant) X-ray emitting region on the stellar surface. If however there were two dominant X-ray bright regions roughly separated by 180° in longitude, then $P_X = 0.5P_{opt}$. The X-ray periods determined from our simulated X-ray light curves confirmed this conclusion, with the additional conclusion that the X-ray period depends on how the star is inclined to an observer's line-of-sight. Stars with two dominant X-ray bright regions are found to have either $P_X = P_{opt}$ or $P_X = 0.5P_{opt}$ depending on the stellar inclination. Once there were more that two dominant X-ray bright regions on the star then it became difficult to look at the shape of the X-ray light curve and

determine the contribution from any particular emitting region. In such cases the LNP test typically only returned an X-ray period that was equal to the optical period. At some inclinations, particular surface field structures were found to be unfavourable to giving rise to large modulations in X-ray emission. Also the ratio of P_X/P_{opt} was found to be independent of stellar mass and radius.

Our accretion/X-ray emission model allows for the confinement of X-ray emitting plasma close to the stellar surface, while larger field line loops and open field lines, stretch out to the inner disc and carry accretion flows. We have found some preliminary evidence that large flares [which occur inside magnetic loops with lengths that are comparable to typical corotation radii for CTTs (Favata et al. 2005)] only occur in stars where the inner disc is threaded by a reservoir of open field lines. Further observational data from, for example, the DROXO project, will help to confirm if this hypothesis is true (Flaccomio et al. 2007). Thus the reconnection of open field lines within the disc may provide the large magnetic structures required for the production of large flares. We are currently developing models of large flares to determine if such magnetic structures can remain stable for a long enough time to fill with plasma before being torn open by the differential rotation between the star and the disc.

7.1.3 Model limitations

In the model presented so far I have assumed a constant value of the disc mid-plane density ρ_d. An improvement would be to allow this value to adjust self-consistently so that the mass accretion rate onto the star equals that which can be supplied by the outer disc. In such a way the system would be in a steady state. If the mass accretion rate was too large then the inner disc would be cleared out by accretion onto the star, whereas if it was too small, then material would pile up at the inner disc rim. Most magnetospheric accretion models which have been developed to date consider full disc models, but usually assume

a simple dipolar stellar field. Our model attacks the problem from the opposite direction and considers realistic stellar fields with a corona but with a simplistic approximation to a true circumstellar disc. The eventual goal will be to merge both approaches and combine multipolar magnetic fields with a disc model. The isothermal assumption for the accretion flows should be dropped and a more realistic flow model developed. Further, our model makes no account of how material is actually loaded onto the stellar field lines, assuming that as long the field lines thread the disc at, or interior to, the corotation radius then they will accrete. This point will addressed in future work.

Also, do the field extrapolations capture the true nature of T Tauri magnetic fields? Certainly they represent only a snap-shot in time, but the field structures which I have presented here satisfy currently available observational constraints. They reproduce X-ray emission measures and coronal densities, explain the observed rotational modulation of X-ray emission, explain the increase of X-ray emission measure with stellar mass (Jardine et al. 2006) and may provide a natural mechanism to explain large flaring loops. However, in future it will be possible to determine if the field geometries extrapolated from surface magnetograms are an accurate representation of true stellar fields. In the next section I discuss how comparisons can be made between our model and independently obtained polarisation measurements. Additional tests will be carried out based on observed line profiles. By extrapolating the newly obtained surface magnetograms of CTTs (Donati et al. 2007) we can use our model to predict the location of accretion hot spots on the stellar surface and the in-fall velocities of accreting material. The predicted locations of hot spots can be compared to the observationally inferred locations obtained from the rotational variation of line profiles such as the He I 5876Å emission line. However, the problem of the unobservable hemisphere remains. Zeeman-Doppler imaging only allows one hemisphere and a small section of the other to be mapped. Therefore something has to be assumed about the

form of the field in the other hemisphere. Various things can be attempted, for example, mirroring the other hemisphere, or mirroring the upper hemisphere rotated through some angle. We will simulate line profiles by combining our models with 3D radiative transfer codes, as is described in the next section.

Our prediction that many higher mass stars will be accreting along open field lines can be extended to study implications for the torque balance between the star and the disc. I discuss this in the next section. However, another intriguing possibility is that T Tauri stars have K-coronae. We can be fairly sure from the detection of modulated X-ray emission and the small lengths of the majority of flaring loops, that the X-ray emitting coronae of T Tauri stars are compact. The X-ray emitting plasma is confined within magnetic structure close to the stellar surface. However, during a solar eclipse we can see the Sun's K-corona, which is more extended than the X-ray emitting coronae. Perhaps, therefore, T Tauri stars do have larger closed field line loops which are not X-ray bright. This possibility should be explored.

The X-ray corona of a CTTs is likely to evolve in time. This time evolution could affect the observed modulation of X-ray emission and therefore the X-ray period. It has been found that the presence of a disc alone does not affect the level of X-ray emission but that active accretion does. Although we can model the effects of a disc on the coronal structure, we have yet to consider how the dense material in accretion columns could affect the level of detected X-ray emission; I discuss this point further in the next section. Also, we have not yet considered how a stellar wind, a disc wind or even a disc field could disrupt the coronal structure. These are areas which will be addressed as the model is developed.

7.2 Future work

The first ever magnetic surface maps of accreting T Tauri stars have now been obtained (Fig. 2; Donati et al. 2007). Zeeman-Doppler images of V2129 Oph and BP Tau were taken using the ESPaDOnS instrument on the Canada-France-Hawai'i Telescope (CFHT; Donati et al. 2007). By extrapolating their magnetic fields we have found that V2129 Oph has a complex field structure, but that BP Tau has a large scale field structure that is (surprising) similar to a tilted dipole, with much of the accretion occurring into a single magnetic spot (this result is still preliminary). This is consistent with the findings of Johns-Krull et al. (1999a) and Valenti & Johns-Krull (2004), who detected strong polarisation in the HeI 5876Å emission line, and determined that the variation of the longitudinal (line-of-sight) field component (B_z) with rotational phase was consistent with a simple model of a single accreting magnetic spot. In order to test the accuracy of field structures which are extrapolated from surface magnetograms of T Tauri stars new simultaneous observations should be obtained of CTTs. For example both the ESPaDOnS instrument at the CFHT, and another polarimeter such as the Zeeman-Analyzer at the Harlan J. Smith Telescope, McDonald Observatory could be used. From the ESPaDOnS surface magnetogram the accreting field structure of the CTTs could be determined using the techniques discussed in Chapters 2 and 4. My accretion model could then be used to predict the variation in B_z with rotational phase, and directly compared with the independently obtained B_z measurements from the McDonald Observatory. Thus it could be determined whether or not the extrapolated magnetic fields obtained from Zeeman-Doppler imaging capture the true magnetic field geometry of T Tauri stars.

It is still poorly understood why stars with discs are observed to be slower rotators than stars where the disc has dispersed. In traditional accretion models high angular momentum material is accreted onto the star whilst other magnetic links between the star and the disc provide a spin-down torque, driving the star

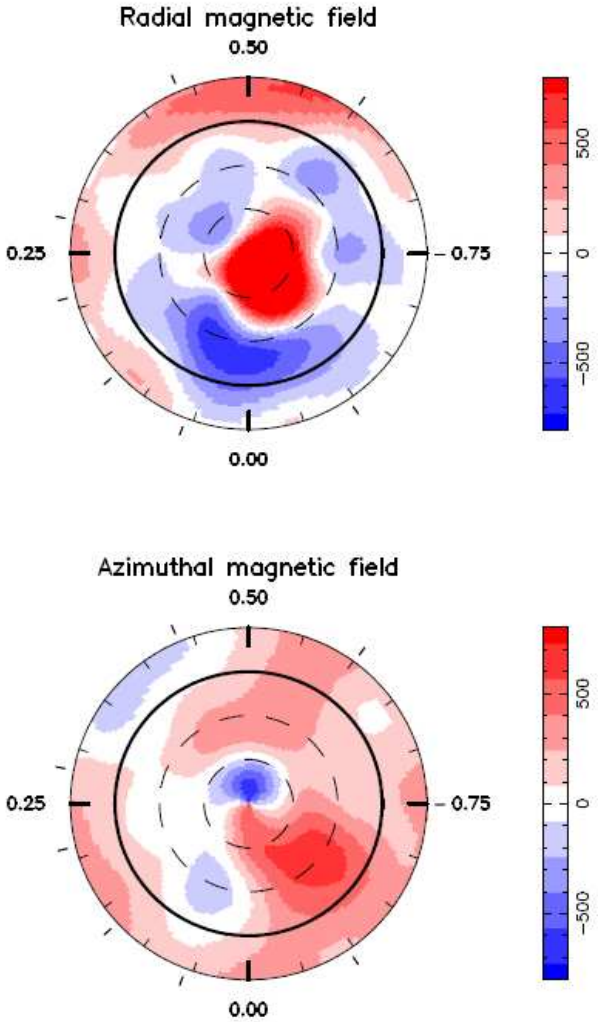

Figure 7.1: The radial and azimuthal magnetic field components at the surface of the classical T Tauri star V2129 Oph as derived from Zeeman-Doppler imaging (Donati et al. 2007). The star is shown in flattened polar projection down to latitudes of -30° with the equator depicted as a bold circle and parallels as dotted circles. Radial ticks around each plot indicate the phases of observation. Field flux values are in G. This accreting T Tauri star clearly has a complex, non-dipolar, surface magnetic field.

towards spin equilibrium (e.g. Königl 1991; Collier Cameron & Campbell 1993). Disc-locking models require field strengths of a few kG, and such strong average fields have been found on a number of T Tauri stars (Johns-Krull et al. 1999b, 2004; Yang et al. 2005; Johns-Krull 2007). Models assume that T Tauri stars have dipolar magnetic fields, however, current observations have shown that the dipole magnetic field component is at least a factor of 10 weaker than such models require (Valenti & Johns-Krull 2004; Daou et al. 2006; Yang et al. 2007). As a result it is unclear whether the real magnetic field geometries of T Tauri stars can enforce disc-locking, an issue which I will address in future work. Magnetic surface maps of T Tauri stars are now available (Donati et al. 2007) allowing the geometry of the magnetic field to be fully considered in explaining why accreting T Tauri stars remain slow rotators. Large data sets will provide constraints on stellar rotation rates as a function of stellar mass in various clusters (e.g. Rebull, Wolff & Strom 2004; Cieza & Baliber 2006). Such datasets will provide invaluable observational guidance in studying the magnetic braking of young stellar objects. Disc-locking models should be reconsidered in light of the new data, and compared with non-disc locking models. The field extrapolation code which I use assumes that the stellar field rotates as a solid body, however, it has recently been updated by Adriaan van Ballegooijen to allow for the shearing of field lines. I will adapt this new approach to model the shearing of field lines interacting with the inner disc. I will determine whether or not this process can inject enough stresses into the field to allow a significant spin down torque to be applied to the star. Also, using the realistic magnetic field geometries, I will determine if there is enough stellar field connected to the disc to allow for the slowing of stellar rotation rates.

Brown dwarfs are likely to be accreting material in much the same way as T Tauri stars, and have been observed to have flares, broad Hα emission lines, discs, and unsteady accretion (e.g. Scholz & Jayawardhana 2006). Recently a new technique has been developed which in future could allow the direct detection of

magnetic fields on brown dwarfs by measuring the broadening of molecular lines of FeH (Johns-Krull & Valenti 2005; Reiners & Basri 2006). There are likely to be fundamental differences between the accretion process in brown dwarfs compared to the higher mass T Tauri stars. Mohanty et al. (2005a) have found that a derived correlation between the flux in the CaII 8662Å line, an indicator of accretion, and mass accretion rate is different when considering brown dwarfs and T Tauri stars. One possible explanation for this difference is that the formation region (accretion shock or in-falling gas) is different in brown dwarfs compared to T Tauri stars. In future it should be determined if current magnetospheric accretion models can be directly adapted to model accretion onto substellar objects.

Flares occurring in magnetic loops of length $< R_*$ are commonly observed on T Tauri stars (e.g. Favata et al. 2001). However, some very large flares (superflares) have been detected and are thought to occur inside magnetic structures which extend to several stellar radii, $\sim 5 - 20R_*$ (see Chapter 6 and Favata et al. 2005; Giardino et al. 2006). Such large magnetic loops would be torn open by the centrifugal force if their foot points were anchored solely on the star, and have thus been interpreted as direct evidence for a magnetic link between the star and the disc. Intriguingly I have found that superflares appear to occur only in stars where the magnetic geometry is such that open field lines are interacting with the inner disc. This suggests that the reconnection of open field lines within the disc provides a natural mechanism for the production of superflares. In future I will explore the physical mechanisms which lead to the production of large flares.

Superflares may also influence the formation of rocky planets within the discs of T Tauri stars. The coronal structure of T Tauri stars is complex with X-ray emitting plasma confined within compact magnetic structures which are unevenly distributed about the star (Chapter 5 and Flaccomio et al. 2005). Higher mass stars are more active in X-rays than lower mass stars (Preibisch et al. 2005; Güdel et al. 2007a), and thus X-ray irradiation may increase the ionisation in

the outer layers of the discs of higher mass stars. This would lead to a more efficient magnetorotational instability and consequently a larger mass accretion rate (Glassgold et al. 2005). Radiative transfer codes could be used to determine the amount of X-ray ionisation in the disc as a function of radius and azimuth, and the resulting effects on the mass accretion rate through the disc. It has also been suggested that violent magnetic reconnection flares could influence rocky planet formation, with protoplanetary discs being irradiated by X-rays from superflares, creating turbulence which halts the inward migration of proto-Earths (Wolk et al. 2005). The physical mechanisms which lead to the production of superflares should be investigated as to how they may aid the formation of rocky planets.

The models of stellar coronae that I have discussed throughout can be used to model the behaviour of flaring loops emerging from rotational eclipse. The motivation for this project is that a number of stellar flares display a mysterious slow rise over a timescale of hours (e.g. Imanishi, Tsujimoto & Koyama 2002; Grosso et al. 2004). This seems to be inconsistent with the impulsive phase model in which hard X-ray emission increases rapidly over a timescale of a few minutes. This suggests geometric effects are active, e.g. the emergence of a flaring loop from rotational eclipse. I will apply my models of T Tauri magnetospheres to interpret these events.

It is still not understood why CTTs are observed to be less luminous in X-rays than non-accreting T Tauri stars. It has been proposed that magnetic reconnection events within the magnetosphere cannot heat the dense material within accretion columns to a high enough temperature to emit in X-rays (Preibisch et al. 2005). Thus accretion columns rotating across the line-of-sight to the star may be responsible for the observed reduction in X-ray emission in accreting T Tauri stars compared with the non-accretors (e.g. Flaccomio et al. 2006). I will develop a full accretion flow model, by modifying my existing code, using complex magnetic fields derived from surface maps of T Tauri stars. Existing radiative

transfer codes could then be used to account for the attenuation of coronal X-rays by the dense material in accretion columns. This will determine whether or not absorption of X-rays by accretion columns is the mechanism responsible for the suppression of X-ray emission in accreting stars. Indeed, the initial results indicate that this is the case (Gregory et al. 2007).

Further, I am currently working on combining my accretion model with existing radiative transfer codes. The distribution of in-fall velocities and accretion flow densities predicted by my model are being used to synthesise hydrogen line profiles (Paβ and Brγ) for direct comparison with observations (see Symington et al. 2005b). This is the first time that a radiative transfer code has been produced which takes account of the true complexity of pre-main sequence star magnetic fields.

It remains unclear exactly how the stellar magnetic field couples to and interacts with the inner disc. The 3D MHD simulations of Romanova et al. (2003) suggest that the process is more complex than initially imagined with inner disc warps and other obscuration effects arising from the tendency of material to corotate with the star in the magnetospheric cavity. The new models of von Rekowski & Piskunov (2006b) point to a complex interaction which does not involve material being loaded onto field lines. Instead in their model accreting material is in constant competition with the stellar wind. Accretion only occurs at times, and onto locations where, the accreting material can overcome the out-flowing wind. Indeed many accretion models suggest that the inclusion and consideration of outflows is an essential ingredient to explain the slow rotation of CTTs (Shu et al. 1994a; Ferreira et al. 2000, 2006; Matt & Pudritz 2005a,b). The different models differ by how the stellar field interacts with the disc, the origin of winds which carry away excess angular momentum and the location of the inner disc.

High resolution X-ray spectroscopic observations have been obtained for a handful of CTTs, and show evidence for soft X-ray emission from accretion shocks

that is distinguishable from the harder coronal X-ray emission (e.g. from BP Tau by Schmitt et al. 2005). However, the bulk of X-ray emission from CTTs is likely to be coronal in nature. For example, if X-rays from accretion shocks were the dominant origin of X-rays from CTTs, we would expect to see a correlation between optical and X-ray variability as the hot spots rotated across the stellar disc. However, Stassun et al. (2006) found only 5% of stars, from a sample of 800, showed any evidence for such a correlation. By developing accretion shock models we can study the interplay between the soft X-ray emission from accretion shocks and the harder X-ray emission from the corona. In future years the XEUS (The X-Ray Evolving Universe Spectrometer) satellite may allow for the disentangling of modulated X-ray emission from accretion shocks and coronal structures. XEUS will be 100 times more sensitive than XMM-Newton, however, stellar observing (other than compact objects) does not even feature on the instruments science goals.

A further research area that will develop on longer time scales is the search for T Tauri star magnetic cycles. This will require various long term observations. Long term spectroscopic and photometric observations of AA Tau appear to show some evidence for a magnetic cycle (Bouvier et al. 2007a). Zeeman-Doppler images of particular T Tauri stars taken at consistent time intervals over a period of perhaps many years will be required to search for magnetic cycles. Once enough Zeeman-Doopler maps have been obtained the existence, or non-existence, of such cycles can be established (at least on particular stars). Such a cycle may also produce cyclic changes in mass accretion rate.

Another project, which can be carried out immediately, is to search for a correlation between X-ray luminosity and mass accretion rate. Initially it may seem obvious that such a correlation should exist, as there are well established correlations between X-ray luminosity and stellar mass and between mass accretion rate and stellar mass. However, in both cases there is a large scatter in values at any

particular stellar mass. By comparing X-ray luminosities from COUP with the mass accretion rates for stars in the ONC obtained by Robberto et al. (2004) no correlation is found. However, mass accretion rates (and potentially also X-ray luminosities) are highly time variable. Furthermore, the accretion rates in the core of the ONC are often well below typical values for most CTTs. This is a result of the UV radiation field generated by the massive ONC OB-type stars. This excess UV radiation disrupts the discs of forming low mass stars, causing a drop in accretion rates. Therefore the core of the ONC is not the ideal location to search for any correlation between L_X and $\dot{M}$. The XEST project has combined literature values of accretion rates with XMM-Newton X-ray data (Güdel et al. 2007a). However, again no correlation between X-ray luminosity and accretion rate is apparent. However, it cannot be stressed enough that the search for such a correlation requires simultaneous observations at X-ray and optical wave bands. Simply combining observations in one wave band with literature values of observations in other wave band, will not be sufficient due to the highly time variable nature of mass accretion.

Appendix A: Algorithm for finding a sonic point and the initial Mach number required for a smooth transonic solution

In order to determine the initial Mach number which results in a transonic accretion flow we need to understand exactly what the different solutions in Fig. 3.3 represent. These curves are obtained from the pressure solutions plotted in Fig. 3.2 using equation (3.14). These pressure profiles track how the roots of (3.13) change as the flow moves along a field line. The pressure function (3.13) can be written in the form,

$$f\left(\frac{p}{p_d}\right) = \ln\left(\frac{p}{p_d}\right) + a\left(\frac{p_d}{p}\right)^2 + b = 0, \tag{7.1}$$

where a and b are constants at any fixed point along a field line with,

$$a = \frac{1}{2}\mathcal{M}^2\left(\frac{B}{B_d}\right)^2, \tag{7.2}$$

$$b = -\frac{1}{2}\mathcal{M}^2 - \frac{1}{c_s^2}\int \boldsymbol{g}_{eff}\cdot\hat{\boldsymbol{s}}ds. \tag{7.3}$$

For a Mach number prescribed to a flow leaving the disc, the pressure function has two roots, which consequently yield two velocities. One of the roots represents the true physical solution, and the other is a mathematical solution of no physical significance. The branches in Fig. 3.3 occur in pairs, with an individual branch tracking how one of the pressure roots change as the flow travels along the field line. For example, suppose we had chosen an initial (subsonic) Mach number which resulted in a purely subsonic flow from the disc to the star (curve A in Fig. 3.3). Then one of the roots, the one which gives a subsonic solution everywhere along the flow, is the true physical one. The second root of (A1) produces a supersonic solution (curve B), which is of mathematical interest, but has no physical meaning. Conversely, had we chosen the initial Mach number

which corresponded to the same supersonic branch, then this purely supersonic branch is the one with physical meaning, with the other root then generating the purely subsonic branch, the mathematical artifact. Thus the purely subsonic and supersonic solutions exist provided our pressure function (7.1) has two real roots when evaluated at each point along a field line.

At small values of p/p_d the second $(p/p_d)^{-2}$ term in (7.1) dominates with $f(p/p_d) \to \infty$ as $p/p_d \to 0$. At larger values of p/p_d the logarithmic term dominates. Thus (7.1) has a minimum which occurs when,

$$\frac{p}{p_d} = \mathcal{M}\frac{B}{B_d}. \tag{7.4}$$

For this value of p/p_d the pressure function reduces to,

$$f_c(r) = \ln\left(\mathcal{M}\frac{B}{B_d}\right) + \frac{1}{2} - \frac{1}{2}\mathcal{M}^2 - \frac{1}{c_s^2}\int \boldsymbol{g}_{eff} \cdot \hat{\boldsymbol{s}} ds, \tag{7.5}$$

which we will refer to as the critical function, f_c. In order for two real roots to exist at some point r along a field line then $f_c(r) < 0$ must hold. Thus for purely subsonic/supersonic solutions to exist then $f_c < 0$ at each point along a field line, with f_c reaching its highest value at the critical radius (where the two roots of the pressure function, and therefore the velocity roots, are closest together). Another pair of solutions are the discontinuous ones labelled C and D in Fig. 3.3. For these solutions $f_c < 0$ for $r_1 < r \leq R_d$ and $R_* \leq r < r_2$. However for the domain $r_2 < r < r_1$, $f_c > 0$, and therefore the pressure function has no real roots, and we cannot satisfy (3.13); hence there are no velocity solutions for these values of r. For $r = r_1$ and $r = r_2$, $f_c = 0$, and at these points the pressure function has a single repeated root that coincides with the pressure function minimum.

The final pair of solutions are the transonic ones labelled E and F in Fig. 3.3. Here $f_c < 0$ for all r, except at the sonic point where $r = r_c$ and $f_c = 0$. Hence, for a transonic solution the maximum value of the critical function f_c is zero at the critical radius r_c, but less than zero at all other points along the field line.

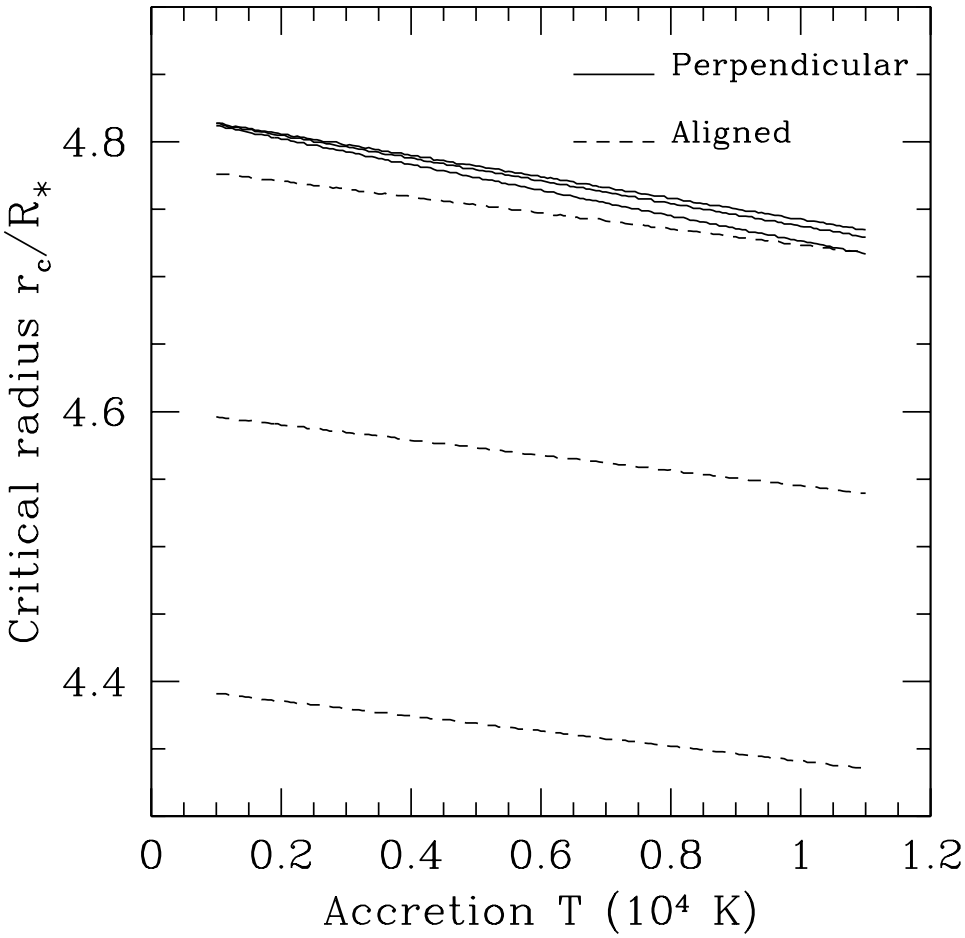

Figure 7.2: The location of the critical radius r_c as a function of accretion flow temperature T_{acc} for starting radii R_d about the corotation radius (upper line, $R_d = 7.0R_*$, middle line $R_d = 6.0R_* \approx R_{co}$ and lower line $R_d = 5.0R_*$). At lower temperatures r_c is closer to the inner edge of the disc, and the difference between the aligned and perpendicular dipoles is larger. Variation of the starting radius has little effect for the perpendicular dipole, and is of minor significance for the aligned dipole.

This then gives us a robust method for finding both the critical radius and the initial Mach number required for a smooth transonic solution (provided such a solution exists).

At the critical radius the minimum of our pressure function is at its highest value; that is f_c has a maximum turning point. Hence to determine if a transonic solution exists we select any initial Mach number $\mathcal{M}$ and calculate how f_c varies as we move along a field line from the disc to the star. If a sonic point exists on that field line, f_c will have a distinct maximum at some point. The advantage of this method is that it is possible to recover the initial Mach number that would result in a smooth transonic flow, simply by varying $\mathcal{M}$ until $f_c = 0$ at r_c; that is we change $\mathcal{M}$ until the maximum value of f_c occurs at zero. This algorithm is an efficient method for quickly determining both the critical radius and the initial Mach number which results in a transonic accretion flow. Of course, not all field lines have a sonic point as the critical radius may either be interior to the star or exterior to the starting radius. This algorithm may be applied to accretion flows along field lines of any size, shape and inclination, even in the absence of analytic descriptions of the magnetic field and effective gravity.

The location of the critical radius (or the sonic point for a transonic solution) determines the velocity with which material impacts the stellar photosphere. We have found the critical radius from the maximum value of f_c for both the perpendicular and aligned dipoles for a CTTs with a mass of $0.5\,\mathrm{M}_\odot$, radius $2\,\mathrm{R}_\odot$ and a rotation period of 7 d. For our two dipole cases the B/B_d and $\boldsymbol{g}_{eff} \cdot \hat{\boldsymbol{s}}$ terms that contribute to (7.5), have analytic forms given respectively by (3.5) and either (3.15) for the perpendicular dipole, or (3.19) for the aligned dipole; in both cases $\hat{\boldsymbol{s}} = \boldsymbol{B}/B$. The location of r_c therefore changes as we vary both the starting radius R_d and also the temperature (which enters through the sound speed). It should be noted, however, that for certain choices of parameters sometimes f_c has no distinct maximum turning point, indicating that either the critical radius

is interior to the star ($r_c \leq R_*$), or is beyond the starting radius ($r_c > R_d$). For such cases flows leaving the disc at a subsonic speed remain subsonic all the way to the star, and likewise supersonic flows remain supersonic at all points along a field line.

Fig. 7.2 shows how the critical radius varies for a range of temperatures and starting radii for both the perpendicular and aligned dipoles. In both cases, the critical radius moves towards the inner edge of the disc with decreasing temperature. In other words as the accretion flow temperature decreases the sonic point moves along the field line away from the star, closer to where the flow leaves the disc. It is straight forward to explain why this should happen by considering a transonic flow which would leave the disc at a subsonic speed. As the temperature drops the sound speed decreases ($c_s \propto \sqrt{T}$); therefore a flow leaving the disc does not have to accelerate for as long to reach its own sound speed and becomes supersonic sooner. Thus r_c moves closer to R_d with decreasing temperature; and for a high enough temperature the critical radius is interior to the star, and conversely for a low enough temperature the critical radius is beyond the starting radius. However, at least for this particular set of stellar parameters, the actual change in critical radius location with temperature is small.

We also found that as the critical radius moved towards the inner edge of the disc, the Mach number with which the flow arrived at the star increased. This would be expected however as the critical radius moves away from the star due to the sound speed decrease, which would naturally increase the flow Mach number at the star (for transonic and purely supersonic flows).

It can be seen from Fig. 7.2 that for the perpendicular dipole varying the starting radius of the flow, R_d, has little effect on the location of the critical radius. Therefore changing the size of equatorial field lines has a negligible effect on the velocity with which accretion flows (along the field) reach the star. For the aligned dipole changing where the field lines thread the disc does have an effect on

the critical radius location and therefore on the final velocity with which material impacts the star. However, due to the overall small change in the critical radius location evident in Fig. 7.2 the in-fall velocity only varies by around 6 kms^{-1}. It therefore appears that the physical size of field lines, in a dipole accretion model, is of little importance for poloidal field lines (aligned north-south in the star's meridional plane), and is negligible for equatorial field lines (aligned east-west in the star's equatorial plane).

The effect of the field orientation is also of little importance for closed dipolar field lines. For a closed field line in the equatorial plane, with a maximum radial extent R_d, changing the inclination of that field line so that it now lies in the meridional plane, has an effect on the critical radius location (see Fig. 7.2). The only major difference between the two cases enters through the effective gravity, which only has a radial component in the equatorial plane, but both r and θ components in the meridional plane. However, the difference in in-fall velocities is again very small, at only a few kms^{-1}. This suggests that for accretion along closed dipolar field lines, where material is leaving the disc at a fixed radius, the field geometry has little effect on in-fall velocities; however, as discussed in Chapter 4, this result does not hold when considering more complicated multi-polar fields.

References

Adams F. C., Shu F. H., 1986, ApJ, 308, 836

Agapitou V., Papaloizou J. C. B., 2000, MNRAS, 317, 273

Alcalá J. M., Covino E., Torres G., Sterzik M. F., Pfeiffer M. J., Neuhäuser R., 2000, A&A, 353, 186

Alencar S. H. P., Basri G., 2000, AJ, 119, 1881

Alencar S. H. P., Basri G., Hartmann L., Calvet N., 2005, A&A, 440, 595

Alencar S. H. P., Batalha C., 2002, ApJ, 571, 378

Alencar S. H. P., Johns-Krull C. M., Basri G., 2001, AJ, 122, 3335

Alexander R. D., Armitage P. J., 2006, ApJL, 639, L83

Altschuler M. D., Newkirk G., 1969, SoPh, 9, 131

Aly J. J., Kuijpers J., 1990, A&A, 227, 473

Andrews S. M., Williams J. P., 2005, ApJ, 631, 1134

Ardila D. R., Basri G., 2000, ApJ, 539, 834

Ardila D. R., Basri G., Walter F. M., Valenti J. A., Johns-Krull C. M., 2002, ApJ, 567, 1013

Armitage P. J., Clarke C. J., 1996, MNRAS, 280, 458

Balbus S. A., Hawley J. F., 1991, ApJ, 376, 214

Bardou A., Heyvaerts J., 1996, A&A, 307, 1009

Barning F. J. M., 1963, Bull. astr. Inst. Nether., 17, 22

Basri G., Marcy G. W., Valenti J. A., 1992, ApJ, 390, 622

Batalha C., Batalha N. M., Alencar S. H. P., Lopes D. F., Duarte E. S., 2002, ApJ, 580, 343

Berdyugina S. V., 2005, Living Reviews in Solar Physics, 2, 8

Beristain G., Edwards S., Kwan J., 2001, ApJ, 551, 1037

Bertout C., Basri G., Bouvier J., 1988, ApJ, 330, 350

Bondi H., 1952, MNRAS, 112, 195

Boss A. P., 1996, ApJ, 469, 906

Bouvier J., 1990, AJ, 99, 946

Bouvier J., Alencar S. H. P., Harries T. J., Johns-Krull C. M., Romanova M. M., 2007a, in Reipurth B., Jewitt D., Keil K., eds, Protostars and Planets V Magnetospheric Accretion in Classical T Tauri Stars. pp 479–494

Bouvier J., Bertout C., 1989, A&A, 211, 99

Bouvier J., Cabrit S., Fernandez M., Martin E. L., Matthews J. M., 1993, A&A, 272, 176

Bouvier J., Covino E., Kovo O., Martin E. L., Matthews J. M., Terranegra L., Beck S. C., 1995, A&A, 299, 89

Bouvier J., et al. 1999, A&A, 349, 619

Bouvier J., et al. 2003, A&A, 409, 169

Bouvier J., et al. 2007b, A&A, 463, 1017

Briceño C., Luhman K. L., Hartmann L., Stauffer J. R., Kirkpatrick J. D., 2002, ApJ, 580, 317

Briggs K. R., et al. 2007, A&A, in press (astro-ph/0701422)

Brown S. F., Donati J.-F., Rees D. E., Semel M., 1991, A&A, 250, 463

Burrows C. J., et al. 1996, ApJ, 473, 437

Calvet N., Gullbring E., 1998, ApJ, 509, 802

Calvet N., Hartmann L., Strom S. E., 2000, in Mannings V., Boss A. P., Russell S. S., eds, Protostars and Planets IV, University of Arizona Press, Tucson, p. 377

Calvet N., Muzerolle J., Briceño C., Hernández J., Hartmann L., Saucedo J. L., Gordon K. D., 2004, AJ, 128, 1294

Camenzind M., 1990, in Klare G., ed., Reviews in Modern Astronomy, p. 234

Carpenter J. M., Hillenbrand L. A., Skrutskie M. F., 2001, AJ, 121, 3160

Casanova S., Montmerle T., Feigelson E. D., Andre P., 1995, ApJ, 439, 752

Chelli A., Carrasco L., Mújica R., Recillas E., Bouvier J., 1999, A&A, 345, L9

Cieza L., Baliber N., 2006, ApJ, 649, 862

Clarke C. J., Pringle J. E., 2006, MNRAS, 370, L10

Colavita M., et al. 2003, ApJL, 592, L83

Collier Cameron A., Campbell C. G., 1993, A&A, 274, 309

Damiani F., Micela G., 1995, ApJ, 446, 341

Daou A. G., Johns-Krull C. M., Valenti J. A., 2006, AJ, 131, 520

Donati J.-F., 1999, MNRAS, 302, 457

Donati J. F., 2004, in Combes F., Barret D., Contini F., Meynadier F., Pagani L., eds, SF2A-2004: Semaine de l'Astrophysique Francaise, EdP-Sciences, Paris, p. 217

Donati J.-F., Brown S. F., 1997, A&A, 326, 1135

Donati J.-F., Collier Cameron A., 1997, MNRAS, 291, 1

Donati J.-F., Collier Cameron A., Hussain G. A. J., Semel M., 1999, MNRAS, 302, 437

Donati J.-F., et al. 2003, MNRAS, 345, 1145

Donati J.-F., et al. 2006b, MNRAS, 370, 629

Donati J.-F., et al. 2007, MNRAS, submitted.

Donati J.-F., Forveille T., Cameron A. C., Barnes J. R., Delfosse X., Jardine M. M., Valenti J. A., 2006a, Science, 311, 633

Donati J.-F., Semel M., Carter B. D., Rees D. E., Collier Cameron A., 1997, MNRAS, 291, 658

Donati J.-F., Semel M., Praderie F., 1989, A&A, 225, 467

Donati J.-F., Semel M., Rees D. E., 1992, A&A, 265, 669

Dullemond C. P., Natta A., Testi L., 2006, ApJL, 645, L69

Edwards S., Hartigan P., Ghandour L., Andrulis C., 1994, AJ, 108, 1056

Eiroa C., et al. 2002, A&A, 384, 1038

Eyer L., Bartholdi P., 1999, A&AS, 135, 1

Favata F., Flaccomio E., Reale F., Micela G., Sciortino S., Shang H., Stassun K. G., Feigelson E. D., 2005, ApJS, 160, 469

Favata F., Giardino G., Micela G., Sciortino S., Damiani F., 2003, A&A, 403, 187

Favata F., Micela G., 2003, Space Sci. Rev., 108, 577

Favata F., Micela G., Reale F., 2001, A&A, 375, 485

Feigelson E. D., Broos P., Gaffney III J. A., Garmire G., Hillenbrand L. A., Pravdo S. H., Townsley L., Tsuboi Y., 2002, ApJ, 574, 258

Feigelson E. D., Casanova S., Montmerle T., Guibert J., 1993, ApJ, 416, 623

Feigelson E. D., Gaffney III J. A., Garmire G., Hillenbrand L. A., Townsley L., 2003, ApJ, 584, 911

Feigelson E. D., Lawson W. A., 2004, ApJ, 614, 267

Fernández M., Eiroa C., 2007, in preparation

Ferreira J., 1997, A&A, 319, 340

Ferreira J., Dougados C., Cabrit S., 2006, A&A, 453, 785

Ferreira J., Pelletier G., Appl S., 2000, MNRAS, 312, 387

Flaccomio E., Damiani F., Micela G., Sciortino S., Harnden Jr. F. R., Murray S. S., Wolk S. J., 2003a, ApJ, 582, 398

Flaccomio E., Micela G., Sciortino S., 2003b, A&A, 397, 611

Flaccomio E., Micela G., Sciortino S., 2006, A&A, 455, 903

Flaccomio E., Micela G., Sciortino S., Damiani F., Favata F., Harnden Jr. F. R., Schachter J., 2000, A&A, 355, 651

Flaccomio E., Micela G., Sciortino S., Feigelson E. D., Herbst W., Favata F., Harnden Jr. F. R., Vrtilek S. D., 2005, ApJS, 160, 450

Flaccomio E., Stelzer B., Pillitteri I., Micela G., Reale F., Sciortino S., 2007, A&A, in preparation

Folha D. F. M., Emerson J. P., 2001, A&A, 365, 90

Gagne M., Caillault J.-P., 1994, ApJ, 437, 361

Gagne M., Caillault J.-P., Stauffer J. R., 1995, ApJ, 445, 280

Gammie C. F., 1996, ApJ, 457, 355

Garcia Lopez R., Natta A., Testi L., Habart E., 2006, A&A, 459, 837

Gatti T., Testi L., Natta A., Randich S., Muzerolle J., 2006, A&A, 460, 547

Getman K. V., et al. 2005, ApJS, 160, 319

Getman K. V., Feigelson E. D., Townsley L., Bally J., Lada C. J., Reipurth B., 2002, ApJ, 575, 354

Ghosh P., Lamb F. K., 1979a, ApJ, 232, 259

Ghosh P., Lamb F. K., 1979b, ApJ, 234, 296

Ghosh P., Pethick C. J., Lamb F. K., 1977, ApJ, 217, 578

Giardino G., Favata F., Silva B., Micela G., Reale F., Sciortino S., 2006, A&A, 453, 241

Glassgold A. E., Feigelson E. D., Montmerle T., Wolk S., 2005, in Krot A. N., Scott E. R. D., Reipurth B., eds, ASP Conf. Ser. 341: Chondrites and the Protoplanetary Disk, p. 165

Glassgold A. E., Najita J., Igea J., 1997, ApJ, 480, 344

Goodson A. P., Böhm K.-H., Winglee R. M., 1999, ApJ, 524, 142

Goodson A. P., Winglee R. M., 1999, ApJ, 524, 159

Goodson A. P., Winglee R. M., Böhm K.-H., 1997, ApJ, 489, 199

Grankin K. N., Melnikov S. Y., Bouvier J., Herbst W., Shevchenko V. S., 2007, A&A, 461, 183

Gregory S. G., Jardine M., Cameron A. C., Donati J.-F., 2006b, MNRAS, 373, 827

Gregory S. G., Jardine M., Collier Cameron A., Donati J.-F., 2005, in Favata F., Hussain G. A. J., B. B., eds, Proceedings of the 13th Cambridge Workshop on Cool Stars, Stellar Systems and the Sun, ESA SP-560 Vol. 1, p. 191

Gregory S. G., Jardine M., Simpson I., Donati J.-F., 2006a, MNRAS, 371, 999

Gregory S. G., Wood K., Jardine M., 2007, MNRAS, in press (astro-ph/0704.2958)

Grosso N., Audard M., Bouvier J., Briggs K. R., Güdel M., 2007, A&A, in press, astro-ph/0609027

Grosso N., Montmerle T., Bontemps S., André P., Feigelson E. D., 2000, A&A, 359, 113

Grosso N., Montmerle T., Feigelson E. D., Forbes T. G., 2004, A&A, 419, 653

Güdel M., et al. 2007a, A&A, in press, astro-ph/0609160

Güdel M., Telleschi A., Audard M., Skinner S. L., Briggs K. R., Palla F., Dougados C., 2007b, A&A, in press (astro-ph/0609182)

Guenther E. W., Lehmann H., Emerson J. P., Staude J., 1999, A&A, 341, 768

Gullbring E., Calvet N., Muzerolle J., Hartmann L., 2000, ApJ, 544, 927

Gullbring E., Hartmann L., Briceño C., Calvet N., 1998, ApJ, 492, 323

Günther H. M., Liefke C., Schmitt J. H. M. M., Robrade J., Ness J.-U., 2006, A&A, 459, L29

Günther H. M., Schmitt J. H. M. M., Robrade J., Liefke C., 2007, A&A, 466, 1111

Hartigan P., Edwards S., Ghandour L., 1995, ApJ, 452, 736

Hartigan P., Kenyon S. J., Hartmann L., Strom S. E., Edwards S., Welty A. D., Stauffer J., 1991, ApJ, 382, 617

Hartmann L., 2002, ApJ, 578, 914

Hartmann L., Calvet N., Gullbring E., D'Alessio P., 1998, ApJ, 495, 385

Hartmann L., D'Alessio P., Calvet N., Muzerolle J., 2006, ApJ, 648, 484

Hartmann L., Hewett R., Calvet N., 1994, ApJ, 426, 669

Hayashi M. R., Shibata K., Matsumoto R., 1996, ApJL, 468, L37+

Herbig G. H., Bell K. R., 1988, Catalog of emission line stars of the orion population : 3 : 1988. Lick Observatory Bulletin, Santa Cruz: Lick Observatory, —c1988

Herbst W., Bailer-Jones C. A. L., Mundt R., Meisenheimer K., Wackermann R., 2002, A&A, 396, 513

Herbst W., Dhital S., Francis A., Lin L., Tresser N., Williams E., 2006, PASP, 118, 828

Herbst W., Eislöffel J., Mundt R., Scholz A., 2007, in Reipurth B., Jewitt D., Keil K., eds, Protostars and Planets V The Rotation of Young Low-Mass Stars and Brown Dwarfs. pp 297–311

Herbst W., et al. 1986, ApJL, 310, L71

Herbst W., Rhode K. L., Hillenbrand L. A., Curran G., 2000, AJ, 119, 261

Hillenbrand L. A., Strom S. E., Vrba F. J., Keene J., 1992, ApJ, 397, 613

Hirose S., Uchida Y., Shibata K., Matsumoto R., 1997, PASJ, 49, 193

Horne J. H., Baliunas S. L., 1986, ApJ, 302, 757

Hueso R., Guillot T., 2005, A&A, 442, 703

Hussain G. A. J., 1999, PhD thesis, University of St Andrews

Hussain G. A. J., Donati J.-F., Collier Cameron A., Barnes J. R., 2000, MNRAS, 318, 961

Hussain G. A. J., Jardine M., Collier Cameron A., 2001, MNRAS, 322, 681

Hussain G. A. J., van Ballegooijen A. A., Jardine M., Collier Cameron A., 2002, ApJ, 575, 1078

Imanishi K., Koyama K., Tsuboi Y., 2001, ApJ, 557, 747

Imanishi K., Tsujimoto M., Koyama K., 2002, ApJ, 572, 300

Isobe H., Shibata K., Yokoyama T., Imanishi K., 2003, PASJ, 55, 967

Jardine M., Cameron A. C., Donati J.-F., Gregory S. G., Wood K., 2006, MNRAS, 367, 917

Jardine M., Collier Cameron A., Donati J.-F., 2002a, MNRAS, 333, 339

Jardine M., Unruh Y. C., 1999, A&A, 346, 883

Jardine M., Wood K., Collier Cameron A., Donati J.-F., Mackay D. H., 2002b, MNRAS, 336, 1364

Johns C. M., Basri G., 1995, ApJ, 449, 341

Johns-Krull C. M., Gafford A. D., 2002, ApJ, 573, 685

Johns-Krull C. M., Hatzes A. P., 1997, ApJ, 487, 896

Johns-Krull C. M., Valenti J. A., 2001, ApJ, 561, 1060

Johns-Krull C. M., Valenti J. A., 2005, in Favata F., Hussain G. A. J., B. B., eds, Proceedings of the 13th Cambridge Workshop on Cool Stars, Stellar Systems and the Sun, ESA-SP 560 Vol. 1, p. 261

Johns-Krull C. M., Valenti J. A., Hatzes A. P., Kanaan A., 1999a, ApJL, 510, L41

Johns-Krull C. M., Valenti J. A., Koresko C., 1999b, ApJ, 516, 900

Johns-Krull C. M., Valenti J. A., Linsky J. L., 2000, ApJ, 539, 815

Johns-Krull C. M., Valenti J. A., Saar S. H., 2004, ApJ, 617, 1204

Johns-Krull C. M., 2007, ApJ, in press (astro-ph/0704.2923)

Joy A. H., 1945, ApJ, 102, 168

Kastner J. H., Huenemoerder D. P., Schulz N. S., Canizares C. R., Weintraub D. A., 2002, ApJ, 567, 434

Kenyon S. J., Gomez M., Marzke R. O., Hartmann L., 1994, AJ, 108, 251

Koen C., 2006, MNRAS, 371, 1390

Koldoba A. V., Lovelace R. V. E., Ustyugova G. V., Romanova M. M., 2002a, AJ, 123, 2019

Koldoba A. V., Romanova M. M., Ustyugova G. V., Lovelace R. V. E., 2002b, ApJL, 576, L53

Königl A., 1991, ApJL, 370, L39

Kurosawa R., Harries T. J., Symington N. H., 2006, MNRAS, 370, 580

Lada C. J., et al. 2006, AJ, 131, 1574

Lamzin S. A., 1995, A&A, 295, L20

Lamzin S. A., Bisnovatyi-Kogan G. S., Errico L., Giovannelli F., Katysheva N. A., Rossi C., Vittone A. A., 1996, A&A, 306, 877

Landé A., 1923, Zeitschrift für Physik, 15, 189

Lawson W. A., Feigelson E. D., Huenemoerder D. P., 1996, MNRAS, 280, 1071

Li J., Wickramasinghe D. T., Ruediger G., 1996, ApJ, 469, 765

Li J., Wilson G., 1999, ApJ, 527, 910

Littlefair S. P., Naylor T., Harries T. J., Retter A., O'Toole S., 2004, MNRAS, 347, 937

Loinard L., Mioduszewski A. J., Rodríguez L. F., González R. A., Rodríguez M. I., Torres R. M., 2005, ApJL, 619, L179

Lomb N. R., 1976, Ap&SS, 39, 447

Long M., Romanova M. M., Lovelace R. V. E., 2005, ApJ, 634, 1214

Long M., Romanova M. M., Lovelace R. V. E., 2007, MNRAS, 374, 436

Lovelace R. V. E., Romanova M. M., Bisnovatyi-Kogan G. S., 1995, MNRAS, 275, 244

Lynden-Bell D., Boily C., 1994, MNRAS, 267, 146

Lynden-Bell D., Pringle J. E., 1974, MNRAS, 168, 603

Mahdavi A., Kenyon S. J., 1998, ApJ, 497, 342

Martin S. C., 1996, ApJ, 470, 537

Mathys G., 1988, A&A, 189, 179

Mathys G., 1991, A&AS, 89, 121

Matt S., Goodson A. P., Winglee R. M., Böhm K.-H., 2002, ApJ, 574, 232

Matt S., Pudritz R. E., 2004, ApJL, 607, L43

Matt S., Pudritz R. E., 2005b, ApJL, 632, L135

Matt S., Pudritz R. E., 2005a, MNRAS, 356, 167

McCaughrean M. J., O'dell C. R., 1996, AJ, 111, 1977

McIvor T., Jardine M., Cameron A. C., Wood K., Donati J.-F., 2003, MNRAS, 345, 601

McIvor T., Jardine M., Cameron A. C., Wood K., Donati J.-F., 2004, MNRAS, 355, 1066

Ménard F., Bertout C., 1999, in Lada C. J., Kylafis N. D., eds, NATO ASIC Proc. 540: The Origin of Stars and Planetary Systems, p. 341

Ménard F., Bouvier J., Dougados C., Mel'nikov S. Y., Grankin K. N., 2003, A&A, 409, 163

Miller K. A., Stone J. M., 1997, ApJ, 489, 890

Mohanty S., Basri G., Jayawardhana R., 2005b, Astron. Nachr., 326, 891

Mohanty S., Jayawardhana R., Basri G., 2005a, ApJ, 626, 498

Mohanty S., Shu F., 2007, in preparation

Mokler F., Stelzer B., 2002, A&A, 391, 1025

Montmerle T., Grosso N., Tsuboi Y., Koyama K., 2000, ApJ, 532, 1097

Muzerolle J., Calvet N., Hartmann L., 1998, ApJ, 492, 743

Muzerolle J., Calvet N., Hartmann L., 2001, ApJ, 550, 944

Muzerolle J., Hillenbrand L., Calvet N., Briceño C., Hartmann L., 2003, ApJ, 592, 266

Muzerolle J., Luhman K. L., Briceño C., Hartmann L., Calvet N., 2005, ApJ, 625, 906

Najita J. R., Shu F. H., 1994, ApJ, 429, 808

Natta A., Testi L., Muzerolle J., Randich S., Comerón F., Persi P., 2004, A&A, 424, 603

Natta A., Testi L., Randich S., 2006, A&A, 452, 245

Neuhäuser R., 1997, Science, 276, 1363

Neuhäuser R., Sterzik M. F., Schmitt J. H. M. M., Wichmann R., Krautter J., 1995, A&A, 297, 391

Oliveira J. M., Foing B. H., van Loon J. T., Unruh Y. C., 2000, A&A, 362, 615

Ostriker E. C., Shu F. H., 1995, ApJ, 447, 813

O'Sullivan M., Truss M., Walker C., Wood K., Matthews O., Whitney B., Bjorkman J. E., 2005, MNRAS, 358, 632

Ozawa H., Grosso N., Montmerle T., 2005, A&A, 429, 963

Paatz G., Camenzind M., 1996, A&A, 308, 77

Padoan P., Kritsuk A., Norman M. L., Nordlund Å., 2005, ApJL, 622, L61

Petit P., Donati J.-F., The Espadons Project Team 2003, in Arnaud J., Meunier N., eds, EAS Publications Series, Toulouse, p. 97

Petrov P. P., Gahm G. F., Gameiro J. F., Duemmler R., Ilyin I. V., Laakkonen T., Lago M. T. V. T., Tuominen I., 2001, A&A, 369, 993

Petrov P. P., Gullbring E., Ilyin I., Gahm G. F., Tuominen I., Hackman T., Loden K., 1996, A&A, 314, 821

Pinte C., Ménard F., 2005, in Adamson A., Aspin C., Davis C., Fujiyoshi T., eds, ASP Conf. Ser. 343: Astronomical Polarimetry: Current Status and Future Directions, p. 201

Piskunov N., Kochukhov O., 2002, A&A, 381, 736

Preibisch T., 1997, A&A, 320, 525

Preibisch T., 2004, A&A, 428, 569

Preibisch T., et al. 2005, ApJS, 160, 401

Preibisch T., Zinnecker H., 2002, AJ, 123, 1613

Press W. H., Rybicki G. B., 1989, ApJ, 338, 277

Press W. H., Teukolsky S. A., Vetterling W. T., Flannery B. P., 1992, Numerical recipes in FORTRAN. The art of scientific computing. Cambridge: University Press, —c1992, 2nd ed.

Pringle J. E., 1981, ARA&A, 19, 137

Reale F., Betta R., Peres G., Serio S., McTiernan J., 1997, A&A, 325, 782

Reale F., Micela G., 1998, A&A, 334, 1028

Rebull L. M., et al. 2002, AJ, 123, 1528

Rebull L. M., Hillenbrand L. A., Strom S. E., Duncan D. K., Patten B. M., Pavlovsky C. M., Makidon R., Adams M. T., 2000, AJ, 119, 3026

Rebull L. M., Stauffer J. R., Ramirez S. V., Flaccomio E., Sciortino S., Micela G., Strom S. E., Wolff S. C., 2006, AJ, 131, 2934

Rebull L. M., Wolff S. C., Strom S. E., 2004, AJ, 127, 1029

Reiners A., Basri G., 2006, ApJ, 644, 497

Robberto M., Song J., Mora Carrillo G., Beckwith S. V. W., Makidon R. B., Panagia N., 2004, ApJ, 606, 952

Robinson Jr. R. D., 1980, ApJ, 239, 961

Robitaille T. P., Whitney B. A., Indebetouw R., Wood K., 2007, ApJS, 169, 328

Robitaille T. P., Whitney B. A., Indebetouw R., Wood K., Denzmore P., 2006, ApJS, 167, 256

Rodgers B. M., 2001, Ph.D. Thesis, University of Washington

Romaniello M., Robberto M., Panagia N., 2004, ApJ, 608, 220

Romanova M. M., Ustyugova G. V., Koldoba A. V., Lovelace R. V. E., 2002, ApJ, 578, 420

Romanova M. M., Ustyugova G. V., Koldoba A. V., Lovelace R. V. E., 2004b, ApJL, 616, L151

Romanova M. M., Ustyugova G. V., Koldoba A. V., Lovelace R. V. E., 2004a, ApJ, 610, 920

Romanova M. M., Ustyugova G. V., Koldoba A. V., Lovelace R. V. E., 2005, ApJL, 635, L165

Romanova M. M., Ustyugova G. V., Koldoba A. V., Wick J. V., Lovelace R. V. E., 2003, ApJ, 595, 1009

Rydgren A. E., Vrba F. J., 1983, ApJ, 267, 191

Safier P. N., 1998, ApJ, 494, 336

Scargle J. D., 1982, ApJ, 263, 835

Schmitt J. H. M. M., Robrade J., Ness J.-U., Favata F., Stelzer B., 2005, A&A, 432, L35

Scholz A., Jayawardhana R., 2006, ApJ, 638, 1056

Sciortino S., et al. 2006, in Wilson A., ed., ESA SP-604: The X-ray Universe 2005, p. 111

Semel M., 1989, A&A, 225, 456

Semel M., Donati J.-F., Rees D. E., 1993, A&A, 278, 231

Semel M., Li J., 1996, SoPh, 164, 417

Serio S., Reale F., Jakimiec J., Sylwester B., Sylwester J., 1991, A&A, 241, 197

Shakura N. I., Sunyaev R. A., 1973, A&A, 24, 337

Shu F., Najita J., Ostriker E., Wilkin F., Ruden S., Lizano S., 1994a, ApJ, 429, 781

Shu F. H., Najita J., Ostriker E. C., Shang H., 1995, ApJL, 455, L155+

Shu F. H., Najita J., Ruden S. P., Lizano S., 1994b, ApJ, 429, 797

Sicilia-Aguilar A., Hartmann L. W., Briceño C., Muzerolle J., Calvet N., 2004, AJ, 128, 805

Sicilia-Aguilar A., Hartmann L. W., Fürész G., Henning T., Dullemond C., Brandner W., 2006, AJ, 132, 2135

Siess L., Forestini M., Bertout C., 1999, A&A, 342, 480

Smith K., Pestalozzi M., Güdel M., Conway J., Benz A. O., 2003, A&A, 406, 957

Stahler S. W., Palla F., 2005, The Formation of Stars, Wiley-VCH

Stassun K. G., Ardila D. R., Barsony M., Basri G., Mathieu R. D., 2004a, AJ, 127, 3537

Stassun K. G., Mathieu R. D., Mazeh T., Vrba F. J., 1999, AJ, 117, 2941

Stassun K. G., Mathieu R. D., Vaz L. P. R., Stroud N., Vrba F. J., 2004b, ApJS, 151, 357

Stassun K. G., van den Berg M., Feigelson E., Flaccomio E., 2006, ApJ, 649, 914

Stelzer B., Neuhäuser R., 2001, A&A, 377, 538

Stelzer B., Neuhäuser R., Hambaryan V., 2000, A&A, 356, 949

Stelzer B., Schmitt J. H. M. M., 2004, A&A, 418, 687

Stempels H. C., Piskunov N., 2002, A&A, 391, 595

Symington N. H., Harries T. J., Kurosawa R., 2005a, MNRAS, 356, 1489

Symington N. H., Harries T. J., Kurosawa R., Naylor T., 2005b, MNRAS, 358, 977

Telleschi A., Güdel M., Briggs K. R., Audard M., Palla F., 2007a, A&A, in press (astro-ph/0612338)

Telleschi A., Güdel M., Briggs K. R., Audard M., Scelsi L., 2007b, A&A, in press (astro-ph/0611024)

Terquem C., Papaloizou J. C. B., 2000, A&A, 360, 1031

Tinbergen J., 1996, Astronomical Polarimetry, Cambrige University Press

Tsujimoto M., Koyama K., Tsuboi Y., Goto M., Kobayashi N., 2002, ApJ, 566, 974

Uchida Y., Shibata K., 1984, PASJ, 36, 105

Unruh Y. C., Collier Cameron A., Guenther E., 1998, MNRAS, 295, 781

Valenti J. A., Basri G., Johns C. M., 1993, AJ, 106, 2024

Valenti J. A., Johns-Krull C. M., 2004, Ap&SS, 292, 619

Valenti J. A., Marcy G. W., Basri G., 1995, ApJ, 439, 939

van Ballegooijen A. A., 1994, Space Sci. Rev., 68, 299

van Ballegooijen A. A., Cartledge N. P., Priest E. R., 1998, ApJ, 501, 866

Vaníček P., 1971, Ap&SS, 12, 10

Vasconcelos M. J., Jatenco-Pereira V., Opher R., 2002, ApJ, 574, 847

von Rekowski B., Brandenburg A., 2004a, A&A, 420, 17

von Rekowski B., Brandenburg A., 2006a, Astron. Nachr., 327, 53

von Rekowski B., Brandenburg A., Dobler W., Shukurov A., 2004b, Ap&SS, 292, 493

von Rekowski B., Piskunov N., 2006b, Astron. Nachr., 327, 340

Vrba F. J., Chugainov P. F., Weaver W. B., Stauffer J. S., 1993, AJ, 106, 1608

White R. J., Basri G., 2003, ApJ, 582, 1109

White R. J., Ghez A. M., 2001, ApJ, 556, 265

White R. J., Hillenbrand L. A., 2004, ApJ, 616, 998

Wichmann R., et al. 2000, A&A, 359, 181

Wolk S. J., Harnden Jr. F. R., Flaccomio E., Micela G., Favata F., Shang H., Feigelson E. D., 2005, ApJS, 160, 423

Wood K., Kenyon S. J., Whitney B. A., Bjorkman J. E., 1996, ApJL, 458, L79+

Yang H., Johns-Krull C. M., Valenti J. A., 2005, ApJ, 635, 466

Yang H., Johns-Krull C. M., Valenti J. A., 2007, AJ, 133, 73